AN ABSTRACT OF THE THESIS OF

WALTER WILLIAM LAITY (Name of student) for the DOCTOR OF PHILOSOPHY (Degree)

in Mechanical Engineering (Major department) presented on October 20, 1976 (Date)

Title: Temperature Profiles, Thermal Diffusion Factors, and Molecular Diffusion Coefficients for Flow-Coupled Diffusion in a Two-Dimensional Flow Field

Abstract approved: Redacted for Privacy

Dr. R. J. Zaworski

The results of an experimental and analytical investigation of temperature fields associated with flow-coupled, binary gaseous diffusion are presented. Attention is restricted to steady, laminar flow of a gas mixture through a circular duct along which a steep axial concentration gradient is maintained, with no net flow of the lighter gas in the region of the concentration gradient. Associated with the changes in concentration are temperature changes that occur due to the diffusion-thermo effect.

A novel apparatus is described in which gas A (the heavier gas) flows upward through a vertically oriented diffusion tube and gas B (the lighter gas) is injected against the bulk flow. Both gases enter the diffusion tube at the same temperature. The injection plane through which

gas B is introduced is formed by the outlets of 25 small-diameter tubes located over a cross section through the diffusion tube. The concentration of gas A, X_{A_o}, at the injection plane may be adjusted arbitrarily and then held constant.

If the velocity of gas A is sufficiently small, gas B will diffuse against the flow and both gases will be present in the region upstream of the injection plane. In this region mass is transported by both convection and diffusion. The relative magnitudes of these two transport processes may be expressed in terms of a mass Peclet number (denoted as Pe and defined as the average velocity times the tube diameter divided by the molecular diffusion coefficient). For values of Pe less than 2.0, diffusion is the controlling process. For values of Pe greater than 10.0, convection becomes controlling to the extent that diffusion against the bulk flow is essentially eliminated.

Experimentally determined axial and radial temperature profiles for helium-nitrogen mixtures are reported for flow conditions corresponding to Pe = 1.9, X_{A_o} = 0.5; Pe = 3.8, X_{A_o} = 0.5; Pe = 3.8, X_{A_o} = 0.7; and Pe = 5.9, X_{A_o} = 0.7. The temperature effects associated with flow-coupled diffusion are shown to become much more pronounced with increasing values of Pe.

Thermal diffusion factors and molecular diffusion coefficients based on data taken in the above mentioned

apparatus are presented as a function of gas composition. These transport coefficients were computed from the temperature distributions measured in this investigation combined with velocity and concentration distributions measured previously under the same flow conditions. The results, which are for helium-nitrogen mixtures corresponding to mole fractions of nitrogen in the range between 0.65 and 0.95, are consistent with theoretical predictions and with results reported by other investigators.

A model is discussed that was developed for use in predicting the radial and axial temperature distributions associated with flow-coupled diffusion. The model, which is programmed for numerical solution, is in the form of a second order, elliptic partial differential equation, in two dimensions. It allows for both radial and axial variations in the velocity and concentration fields, which must be specified in order to solve for the temperature distribution corresponding to a given set of flow conditions. Temperature profiles predicted with this model are reported for the four sets of flow conditions under which experimental measurements were taken. The predicted and experimental profiles are found to be in general agreement.

Temperature Profiles, Thermal Diffusion Factors, and Molecular Diffusion Coefficients for Flow-Coupled Diffusion in a Two-Dimensional Flow Field

by

Walter William Laity

A THESIS

submitted to

Oregon State University

in partial fulfillment of
the requirements for the
degree of

Doctor of Philosophy

Commencement June 1977

APPROVED:

Redacted for Privacy

Professor of Mechanical Engineering

Redacted for Privacy

Head of Department of Mechanical Engineering

Redacted for Privacy

Dean of Graduate School

Date thesis is presented October 20, 1976

Typed by Corrine Wilkerson and Wilma Laity for
Walter William Laity

ACKNOWLEDGMENTS

I wish to express my sincere gratitude to Dr. Robert J. Zaworski for serving as my major professor for this project. The successful development of the diffusion apparatus discussed in this thesis is due in large part to his informed guidance. I am also grateful to Dr. James R. Welty, who served as my major professor for my M.S. degree and who has been a valuable source of advice and guidance throughout my graduate program, and to Mr. Jack Kellogg, who provided considerable assistance and advice in the fabrication of the experimental apparatus.

In addition, I wish to acknowledge the assistance I received from Dr. David E. Stock, who is currently a member of the faculty in the Mechanical Engineering Department at Washington State University. My research is an extension of the research performed by Dr. Stock when he was a Ph.D. candidate working under the direction of Dr. Zaworski at Oregon State University. Dr. Stock has maintained an active interest in flow-coupled diffusion, and he played a significant (but unofficial) role as an advisor for my research. He also provided the data for the concentration and velocity distributions used in computing the temperature distributions discussed in Chapter IV of this thesis and the transport coefficients discussed in Chapter VII.

Dr. David C. Junge, Mrs. Franny Junge, and their

children, Amy and Steve, deserve special acknowledgment for the invaluable assistance they provided to me and my wife when severe illness struck within our family not long after the birth of our daughter. At the time, Dave and I were both engaged in graduate studies at Oregon State University. On their own initiative, the members of the Junge family took over the primary care of our daughter for a period of several months. My wife and I will never forget their sensitivity to our plight and the competent assistance that they willingly and cheerfully provided.

I wish to express my thanks to Dr. Anthony M. Sutey, manager of the Energy Systems Engineering Section at Battelle, Pacific Northwest Laboratories, for permitting me to have time off to prepare this manuscript, and for maintaining patience during the period that this manuscript was in preparation. Mrs. Corrine Wilkerson, a secretary at Battelle-Northwest, deserves special thanks for long hours that she spent typing major portions of this manuscript during evenings and weekends.

I am deeply grateful to my wife, Wilma, for her understanding, support, encouragement, and patience during the course of my graduate work. Only she knows the true cost of this effort. She contributed materially to the preparation of this thesis by typing the last two chapters and substantial portions of the appendices, and by preparing virtually all the figures in final form. While these and other activities related to work on this thesis were

underway, our daughter, Kirsten, helped in her own way by showing exceptional patience and by engaging in non-interferring activities, which included preparation of her own "thesis" (in color!).

I am indebted to the Oregon State University Department of Mechanical Engineering for providing equipment and supplies; to the Oregon State University Computer Center for providing the computer time necessary for this work; and to the Society of the Sigma Xi for providing a Grant-in-Aid of Research that was applied toward the purchase of the diffusion tube thermocouple instrumentation.

Finally, I wish to acknowledge my heartfelt gratitude to my parents, Professor W. Clifford Laity and Mrs. Lila I. Laity, for their encouragement and support in my academic endeavors.

TABLE OF CONTENTS

LIST OF FIGURES

LIST OF TABLES

TEMPERATURE PROFILES, THERMAL DIFFUSION FACTORS, AND MOLECULAR DIFFUSION COEFFICIENTS FOR FLOW-COUPLED DIFFUSION IN A TWO-DIMENSIONAL FLOW FIELD

I. INTRODUCTION

1.1. Description of Problem

Temperature changes due to the diffusion-thermo effect were investigated analytically and experimentally for conditions occurring when a binary gas mixture of helium and nitrogen flows through a cylindrical duct along which a steep axial concentration gradient is maintained. Within the region of the concentration gradient, mass is transported by both convection and diffusion. The relative magnitudes of these two transport phenomena may be expressed in terms of a mass Peclet number (defined as the average velocity times the tube diameter divided by the molecular diffusion coefficient). This work is a continuation of research reported by Stock (1972) which was initiated at Oregon State University to investigate velocity, concentration, and temperature fields associated with flow-coupled binary diffusion in the Peclet number range of 2.0 to 6.0.

Attention was restricted in this investigation to steady laminar flow of the gas mixture with no net axial flow of the lighter gas. In the diffusion tube developed for this investigation, which is shown diagrammatically in

Figure 1.1, gas A (the heavier gas) enters at a far upstream location and gas B (the lighter gas) is introduced at the injection plane. The concentration of gas A at the injection plane is held constant. If the average velocity of gas A is sufficiently low (corresponding to Peclet numbers less than approximately 10), gas B will diffuse against the flow and both gases will be present in the region immediately upstream of the injection plane.

Previous investigations of binary gaseous diffusion in cylindrical ducts (e.g. Yang (1966), Wyatt (1968)) were conducted under conditions such that diffusion was the dominant process of mass transport in the flow field (Peclet numbers less than 2.5). For the flow conditions considered in this investigation, convection is the dominant process of mass transport.

1.2. Objectives of Research

Objectives established for the research discussed in this thesis are as follows:

1. To measure radial and axial temperature profiles that exist for flow-coupled diffusion in the Peclet number range between 2.0 and 6.0.
2. To compute thermal diffusion factors and molecular diffusion coefficients from the combined results of

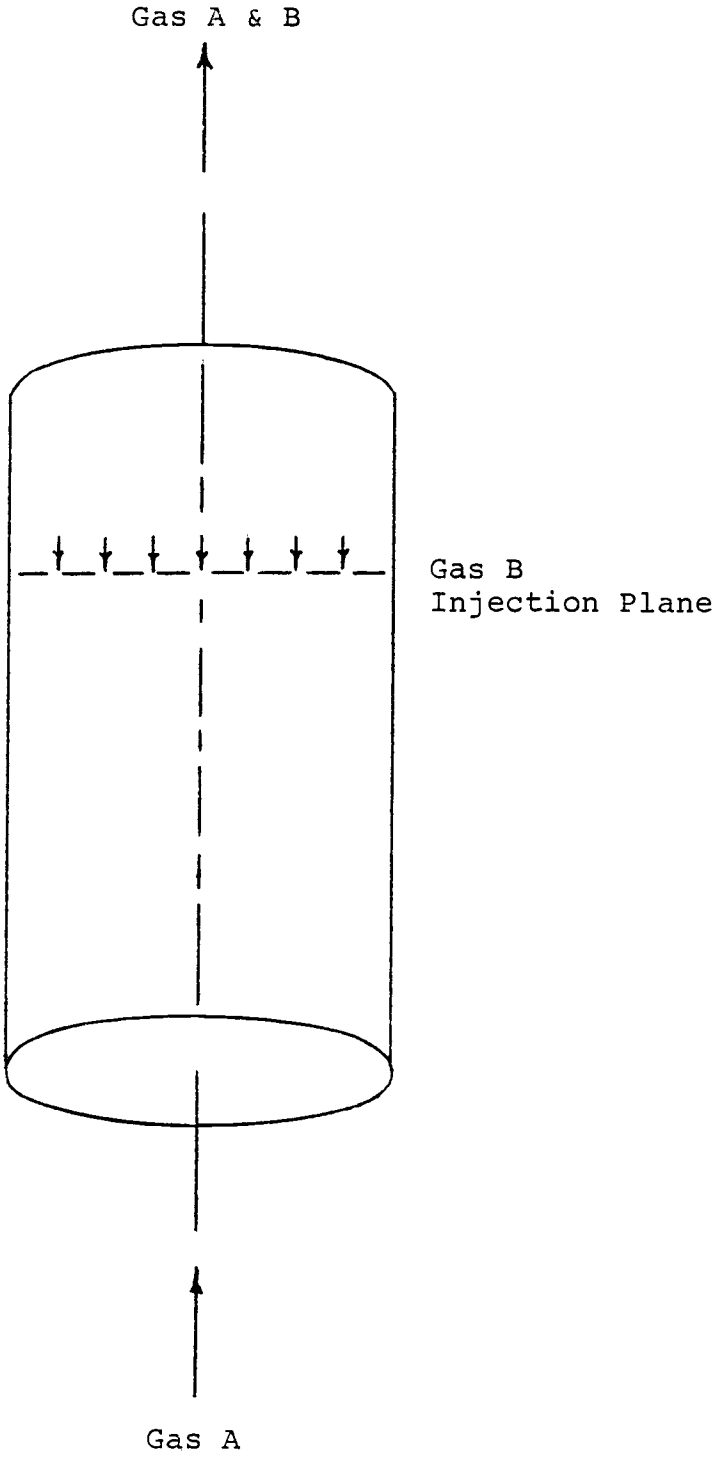

Figure 1.1. Schematic Diagram of Tube for Investigation of Flow-Coupled Diffusion

temperature distributions measured as part of this research and velocity and concentration distributions measured under the same conditions by Stock (1972).

3. To develop an analytical model for use in predicting the temperature field for a given set of flow conditions, assuming that the velocity and concentration fields are known.

II. BACKGROUND

2.1. Diffusion Phenomena

To simplify the discussion that follows, attention is generally restricted to binary mixtures of nonreacting gases. The kinetic theory referred to in this discussion is applicable only to dilute gases (having densities sufficiently low so that three-body collisions may be ignored, but sufficiently high so that fluid properties are continuous), due to the assumptions on which the theory is based.

Of primary interest for the research discussed in this thesis is the phenomenon known as the diffusion-thermo effect, or Dufour effect, which refers to energy transport associated with the existence of a concentration gradient in a mixture. The effect is observed as a temperature gradient that develops when, for example, two gases initially at the same temperature are allowed to interdiffuse.

According to the theories of the thermodynamics of irreversible processes, the diffusion-thermo effect is interrelated with another phenomenon, thermal diffusion or the Soret effect, in such a way that the same transport coefficient is used in quantitative descriptions of both phenomena. Thermal diffusion is observed as a concentration gradient that develops in a mixture initially of uniform

composition when a temperature gradient is imposed on the mixture. Due to the interrelationship between the two phenomena, experimental studies involving either the thermal diffusion effect or the diffusion-thermo effect provide independent but complementary means to gain information regarding the coefficient of thermal diffusion used in describing both phenomena.

Also of interest for the research described in this thesis is the diffusion that occurs as a direct result of a concentration gradient. Nonuniformities of composition in a mixture result in relative motion of the constituents, each down its concentration gradient, so that the mixture tends ultimately to become uniform. Using experimental data from the apparatus described in Chapter V, molecular diffusion coefficients associated with diffusion resulting from a concentration gradient may be determined together with thermal diffusion coefficients associated with the diffusion-thermo effect.

As discussed in more detail in section 2.2, diffusion effects may occur simultaneously in ways that tend to counteract each other. For example, when a temperature gradient is imposed on a gas mixture initially of uniform composition, a partial separation of the constituents occurs. Concentration gradients that develop as a result of this separation act as driving forces for diffusion

tending to restore homogeneity in the mixture. Hence, a steady state is possible in which the separating effect of thermal diffusion is balanced by the remixing effect of concentration diffusion.

2.2. Relationships between Driving Forces and Fluxes in Gas Mixtures

Much of the research discussed in this thesis involves relationships between fluxes of momentum, energy, and mass and gradients of velocity, temperature, and concentration. In the kinetic theory developed to model the physical phenomena, the fluxes are related to their corresponding driving forces in terms of transport coefficients. Books in which relationships between fluxes and their corresponding forces are discussed include those by Bird, et al. (1960) and Hirschfelder, et al. (1954). The following is a brief summary of the discussions presented in those two references.

Fluxes and forces are related as shown in Table 2.1. Theories from the thermodynamics of irreversible processes provide insights into the relationships between these fluxes and forces. As a postulate of the thermodynamics of irreversible processes it is assumed that, for conditions not too far removed from equilibrium, fluxes J_i are linear

functions of forces X_j according to the relationship

$$J_i = \sum_j \alpha_{ij} X_j . \qquad (2.1)$$

Table 2.1. Driving Forces, Fluxes, and Associated Transport Coefficients

Driving Force	Flux	Associated Transport Coefficient
1. Velocity gradient	a. momentum	viscosity
2. Temperature gradient	a. energy	thermal conductivity
	b. mass (Soret effect)	coefficient of thermal diffusion
3. Concentration gradient	a. mass	molecular diffusion coefficient
	b. energy (Dufour effect)	coefficient of thermal diffusion

Note: Mass fluxes associated with pressure gradients and external forces are not included in this table.

The coupling of flux-force pairs indicated by equation 2.1 is illustrated in the relationships summarized in Table 2.1. In a system having both a concentration gradient and a temperature gradient, there are four effects: direct effects, illustrated in Table 2.1 by fluxes 2a and 3a, of energy transport due to a temperature gradient and mass transport due to a concentration gradient, and

coupled effects, illustrated by fluxes 2b and 3b, of mass transport due to a temperature gradient and energy transport due to a concentration gradient.

The theory of the thermodynamics of irreversible processes includes a fundamental theorem developed by Onsager (1931), which indicates that the matrix of phenomenological coefficients α_{ij} in equation 2.1, above, is symmetric provided that the fluxes and forces meet certain criteria. This theorem may be expressed in the following form, commonly referred to as the Onsager reciprocal relations:

$$\alpha_{ij} = \alpha_{ji} \qquad j \neq i. \tag{2.2}$$

As a consequence of the Onsager reciprocal relations, only one transport coefficient, the coefficient of thermal diffusion, is needed for quantitative descriptions of the Dufour and Soret effects referred to in Table 2.1.

2.3. Coefficients Used in Mathematical Formulations for Thermal Diffusion Phenomena

A variety of coefficients, all closely related, are referred to in the literature on thermal diffusion phenomena. The more commonly used coefficients and their interrelationships are discussed in this section.

For a binary mixture subject to no external forces and in which the pressure, but not the temperature, is

uniform, the equation for difffusion may be written as follows (Grew and Ibbs (1952)):

$$\vec{V}_{D_A} - \vec{V}_{D_B} = -\frac{1}{X_A X_B}\left[D_{AB}\vec{\nabla}X_A + D_T\vec{\nabla}(\ln T)\right] \qquad (2.3)$$

where:

Gas A is the heavier gas.

$\vec{V}_{D_A}$ and $\vec{V}_{D_B}$ are the diffusion velocities of gases A and B relative to the mass average velocity of the gas mixture.

X_A and X_B are the mole fractions of gases A and B.

D_{AB} is the molecular diffusion coefficient (associated with diffusion resulting from a concentration gradient). For a binary mixture, $D_{AB} = D_{BA}$.

D_T is the coefficient of thermal diffusion. The general convention on sign for this coefficient is that D_T is positive if the heavier gas concentrates in the colder region.

Both D_{AB} and D_T are functions of the relative quantities and physical characteristics of the two gases, and the nature of the forces between the molecules of the gases. The coefficient of thermal diffusion is particularly sensitive to intermolecular forces; for a given sign convention, it can be positive, negative, or zero depending on the conditions and the types of gases under consideration (Mason, et al. (1966)).

Equation 2.3 may be rewritten in the following form:

$$\vec{V}_{D_A} - \vec{V}_{D_B} = -\frac{D_{AB}}{X_A X_B}\left[\vec{\nabla}X_A + k_T\vec{\nabla}(\ln T)\right] \tag{2.4}$$

where k_T, the thermal diffusion ratio, is defined as $k_T = D_T/D_{AB}$. The thermal diffusion ratio is a measure of the relative importance of thermal and concentration diffusion.

One reason for writing the diffusion equation in the latter form is that a convenient relationship for use in experimental studies of k_T may be obtained under the condition that $\vec{V}_{D_A} - \vec{V}_{D_B}$ is zero. Applying this condition to equation 2.4, the following relationship is obtained between nonuniformities of composition and nonuniformities of temperature:

$$\vec{\nabla}X_A = -k_T\vec{\nabla}(\ln T) \tag{2.5}$$

Equation 2.5 may be integrated to yield the following, assuming k_T is a constant (Grew and Ibbs (1952)):

$$k_T = \frac{X_A - X_A'}{\ln(T'/T)} \tag{2.6}$$

In equation 2.6, X_A' is the mole fraction of gas A where the temperature of the mixture is T', and X_A is the mole fraction of gas A where the temperature is T.

As discussed by Grew and Ibbs (1952), the theoretical expression for k_T based on kinetic theory includes the

product of X_A and X_B as one factor, and therefore k_T is a strong function of composition. A related quantity which is a less sensitive function of composition is the thermal diffusion factor α_T, defined by

$$\alpha_T = \frac{k_T}{X_A X_B} \tag{2.7}$$

The latter quantity is frequently used rather than k_T in formulations for modeling thermal diffusion phenomena. Due to its importance, a considerable amount of research has been directed toward gaining a better understanding of the behavior of α_T.

2.4. Comments on Simplified Theories for Thermal Diffusion Phenomena

Although the Chapman-Enskog theory (discussed in Chapter III) has proven to be successful for quantitative modeling of transport phenomena in gases, including thermal diffusion phenomena, its mathematical complexity is such that it has not been so useful as a basis for simplified quantitative theories of such phenomena. Attempts to develop simplified theories of thermal diffusion on the basis of other approaches have either been deficient in essential aspects or else almost as complicated as the Chapman-Enskog theory (Mason, et al. (1966)). Only recently (Monchick and Mason (1967)) has a theory been

developed that provides a rigorous means for modeling thermal diffusion on the basis of an elementary (single collision) mean-free-path theory.

A principal reason for the difficulty in developing simplified theories of thermal diffusion is discussed by Chapman (1962) with further elaboration by Mason, et al. (1966). As explained in those references, thermal diffusion depends strongly on the nature of molecular interactions, while other transport phenomena depend primarily on the occurrence of molecular interactions and only secondarily on their nature. Consequently, as demonstrated by Monchick and Mason (1967) in their development of a "free-flight" theory of gas mixtures, thermal diffusion is much more difficult to account for than the other transport phenomena when formulating rigorous phenomenological theories (i.e., those based on physical models of the phenomena involved).

2.5. Importance of Research Involving Thermal Diffusion Phenomena

Results of research involving the thermal diffusion and diffusion-thermo effects are useful for both practical applications and for refining theories of transport processes. Incentives for performing such research include the following:

1. Thermal diffusion phenomena are very sensitive to and strongly dependent upon forces between unlike molecules (Mason, et al. (1966)). Consequently, experimental studies of thermal diffusion phenomena provide valuable information for relating physical measurements to theoretical models of intermolecular forces.

2. Thermal diffusion can be utilized to separate the components of a gas mixture. As discussed by Grew and Ibbs (1952) in a chapter devoted to this application, Clusius and Dickel stimulated considerable interest in developing techniques for component separation by their announcement in 1938 that they had applied thermal diffusion to achieve a partial separation of the isotopes of chlorine. The separation column developed by Clusius and Dickel has been refined to the point where almost complete separation of isotopic mixtures can be performed. Grew and Ibbs (1952) provide citations for references regarding extension of the technique to liquid mixtures.

3. In studies of boundary layers containing unlike gases, large discrepancies can occur between predicted and measured transport phenomena unless provision is made in the analytical formulations for

the thermal diffusion and diffusion-thermo effects. Until recently, thermal diffusion phenomena have been neglected in analytical treatments of binary boundary layers (Sparrow, et al. (1964)). Experimental investigations involving transpiration cooled boundary layers containing unlike gases, however, produced results which differed considerably from predictions based on theories formulated without taking into consideration thermal diffusion phenomena. For example, in measurements of local heat transfer by free convection around a porous cylinder through which helium was injected into the boundary layer, Tewfik and Yang (1962) found that the adiabatic wall temperature was considerably higher than the free-stream air temperature, with the temperature difference dependent upon the helium injection rate and the location around the cylinder. These observed temperature differences were attributed to the diffusion-thermo effect.

4. As discussed by Chapman (1958 and 1962), thermal diffusion effects can be of importance in a number of natural phenomena, such as transport phenomena associated with flames, planetary atmospheres, stellar interiors, and nebulae. One of the examples mentioned in the preceding references is a

phenomenon that is well known but perhaps not generally recognized as a special case of thermal diffusion: namely, the distribution of dust spots on walls near heaters and hot pipes. For a mixture consisting of a dilute suspension of dust particles in a gas, the thermal diffusion factor is approximately 10^6 times larger than that observed for mixtures in which the particle sizes are not so dissimilar (Chapman (1962)). A small temperature gradient in such a mixture is sufficient to cause considerable separation of the dust from the gas, with the result that dust diffuses from the region around a hot body and tends to deposit on cooler surfaces.

III. LITERATURE REVIEW

3.1. Introductory Comments

Included in the literature on thermal diffusion phenomena is a wealth of information regarding the broad spectrum of research activities devoted to obtaining a better understanding of the phenomena and to developing techniques for utilizing the phenomena in practical applications. Only a few of the topics discussed in the literature are reviewed in this section. Attention is focused on research performed to investigate the magnitude and behavior of the thermal diffusion factor, α_T, and related coefficients discussed in section 2.3 of Chapter II.

As discussed in section 2.3, the thermal diffusion factor, α_T, is less sensitive to variations in composition of a gas mixture than related coefficients appearing in mathematical formulations of thermal diffusion phenomena. Consequently, α_T has generally been the coefficient chosen for study in the more recent experimental and theoretical investigations of such phenomena. The related coefficient k_T (defined in section 2.3) has also received considerable attention, particularly in the time period immediately following the development of the Chapman-Enskog kinetic theory in 1917.

3.2. General References

Among the numerous references that contain discussions of transport phenomena in gases, those listed below are particularly recommended for readers interested in detailed treatments of the phenomena described in this thesis. Complete citations for these references are included in the bibliography. The references are listed in chronological order as follows, together with brief descriptions of their contents:

1. Grew and Ibbs (1952) for a comprehensive review of experimental and theoretical investigations performed prior to about 1950 to study thermal diffusion phenomena. This book is a recommended starting point for those interested in commencing a study of thermal diffusion.

2. Hirschfelder, et al. (1954) for a unified and extensive treatment of the theoretical, computational, and experimental developments in the studies of properties of gases and liquids prior to about 1952. This book is an excellent reference for discussions of transport phenomena as well as for detailed mathematical treatments of transport phenomena.

3. Mason, et al. (1966) for a detailed review of research associated with thermal diffusion in gases

up to about 1965. Included in the review is an extensive bibliography of references available in the literature.

4. Chapman and Cowling (1970) for an advanced treatment of the kinetic theory of transport phenomena in nonuniform gases. This book (including its earlier editions), perhaps more than any other, is cited frequently in papers appearing in the literature regarding transport phenomena in gases. Included in the 1970 edition are references to papers in the literature for recently completed research involving the kinetic theory and its applications.

3.3. Historical Summary - 1856 to Present

The history of research involving thermal diffusion phenomena is discussed in the references cited in section 3.2, as well as in other references on the kinetic theory of gases. Accordingly, the summary that follows is limited to comments on only a few of the major developments that contributed to present-day understanding of such phenomena. Except where noted, this summary is based on historical background information presented by Grew and Ibbs (1952), and by Ferziger and Kaper (1972). The original papers describing each of the following events are cited in the preceding references.

Date	Event
1856	The existence of thermal diffusion was discovered in liquids, by Ludwig, who found differences of concentration in samples of sodium sulfate solutions taken from different parts of a vessel that was unequally heated. It is of interest to note that the analogous effect in gases was not detected experimentally until 1917, after its prediction in the Chapman-Enskog kinetic theory.
1859 to 1867	Maxwell published his theory on the distribution of molecular velocities for a uniform gas in equilibrium (known as the Maxwellian velocity distribution). In addition, he formulated the equations of transfer and transport coefficients for a gas in which the molecules act as point centers of repulsion interacting with forces inversely proportional to the fifth power of their separation (called Maxwellian molecules). Terms involving thermal diffusion do not appear in formulations based on the conditions modeled by Maxwell.
1872	By means of his H-Theorem, Boltzmann demonstrated that a gas having any initial distribution of molecular positions and velocities will most probably evolve into an equilibrium state, in which the velocities are distributed according to the

Maxwellian velocity distribution. Boltzmann also derived an integro-differential equation for the velocity distribution function in terms of space and time, and showed that the solution of the equation for a gas of Maxwellian molecules yields formulae for the various transport coefficients which agree with those developed by Maxwell. This integro-differential equation is now known as Boltzmann's equation.

1873 Dufour published results of experiments showing that the diffusion of one gas into another initially at the same temperature results in a temperature gradient. His discovery of what has come to be called the diffusion-thermo effect predated the formulation of the Chapman-Enskog kinetic theory which accounts for such an effect, and apparently no further interest was shown in experimental investigations of this effect until the work by Waldmann in the 1940's.

1879 to 1881 Thermal diffusion in liquids was investigated more thoroughly by Soret, who measured changes in concentration of salt solutions exposed to a temperature gradient in a vertical tube. Attempts to formulate a theoretical explanation for the phenomenon were unsuccessful.

1911 to 1917 Chapman and Enskog, working independently, developed a general kinetic theory of nonuniform gases based on solutions to the fundamental equations that originated with Maxwell and Boltzmann. Using Maxwell's equations of transfer in an extended way, Chapman derived equations showing that "...diffusion is produced by (1) a concentration gradient, or variation in the relative proportion of the constituent gases; (2) by external forces acting unequally per unit of mass on the two sets of molecules, and by variations in (3) the total pressure, or (4) temperature of the component gas." (Chapman (1916) pg. 9).

Enskog developed a series solution to Boltzmann's equation for the velocity distribution function, and arrived at results identical to those of Chapman for the transport coefficients. The Chapman-Enskog kinetic theory, discussed in detail by Chapman and Cowling (1970), is based primarily on Enskog's approach.

1917 Using a mixture of hydrogen and carbon dioxide in an apparatus consisting of two bulbs connected by a tube, Chapman and Dootson (1917) demonstrated experimentally that diffusion in a gas mixture occurs

under the influence of a temperature gradient (the thermal diffusion effect).

1938 Clusius and Dickel demonstrated that thermal diffusion can be utilized to almost completely separate the components of a mixture. The separation column that they developed has since been refined and used extensively, particularly for separation of isotopes.

1943 to 1950 Waldmann investigated the diffusion-thermo effect both analytically and experimentally. As part of his work he developed methods of measuring the effect at various temperatures and pressures, and from the results he determined values of the thermal diffusion factor for a variety of gas mixtures. In addition to Waldmann's publications, two of which are cited in section 3.4, an excellent source of information regarding his work is the chapter by Grew and Ibbs (1952) devoted to a discussion of the diffusion-thermo effect.

1965 The existence of the diffusion-thermo effect in a liquid mixture was detected experimentally by Rostigi and Madan (1965), who used benzene and chlorobenzene in their apparatus. They were the first to report success in verifying that the effect exists in liquids.

3.4. Experimental Methods for Investigating Thermal Diffusion Phenomena

Experiments involving either the thermal diffusion effect or the diffusion-thermo effect may be used to investigate the magnitude and behavior of the thermal diffusion factor, α_T, and related coefficients discussed in section 2.3. Both approaches have received extensive attention in the literature. A comprehensive list of the various binary mixtures for which thermal diffusion measurements have been reported is given by Mason, et al. (1966).

Much of the research performed to investigate agreement between theoretical predictions and experimental results has been conducted using mixtures of inert gases, for the assumptions on which the Chapman-Enskog kinetic theory is based correspond more closely with interactions between molecules of the inert gases than for interactions between molecules of other gases.

3.4.1. Experimental Methods: Thermal Diffusion

Experimental investigations of thermal diffusion have generally been performed using one of three types of equipment: the two-bulb apparatus, the swing separator, or the thermal diffusion column (Mason, et al. (1966)). Each type of equipment has advantages over the others for certain

applications, which are discussed in detail in the preceding reference. Beginning with the first reported experiment (by Chapman and Dootson (1917)) that confirmed the existence of thermal diffusion in gases, the two-bulb apparatus (in a variety of designs) has been used extensively for experimental investigations of the behavior of thermal diffusion coefficients. Accordingly, a brief description of the manner in which such an apparatus is used is given in the following paragraphs. Readers interested in a discussion of the other types of apparatus used to study thermal diffusion are referred to Mason, et al. (1966) and Grew and Ibbs (1952).

When measuring thermal diffusion phenomena with an apparatus of the two-bulb type, each of the bulbs is held at a different temperature so that a temperature gradient is established along a tube of relatively small diameter joining the bulbs. Under the influence of the temperature gradient, a concentration gradient develops within the gas mixture. When a steady-state is achieved, an analysis of the mixture in each bulb indicates the extent of the separation of the gases. (The separation is defined as the difference in mole fractions of one of the two constituents corresponding to the temperature difference between the two bulbs.)

From the measurements of compcsition and temperature in the two bulbs, the thermal diffusion ratio, k_T, may be computed using equation 2.6. An alternate approach is to plot values of the separation as a function of the natural log of the temperature difference, holding one of the temperatures, say T_1, constant; it may be shown from equation 2.5 that k_T at any temperature T_2 is the slope of the curve at the point corresponding to T_2. By replacing k_T in equation 2.5 with the equivalent expression for α_T, similar approaches may be followed for computing α_T from experimental data.

As an aid in following the course of thermal diffusion in apparatus of the two-bulb type as well as in other types of diffusion apparatus, radioactive isotopes have proven to be very useful, particularly when it is desired to form a mixture with one component present in only a vanishingly small quantity. Generally the mixture is limited to two components, with a radioactive tracer as one of the components. One advantage of this technique is that uncertainties of interpretation are avoided which might otherwise arise due to the variation of thermal diffusion coefficients as a function of the relative proportions of the gases forming a mixture. In addition, such a technique leads to simplifications in the theoretical analyses necessary to obtain information regarding intermolecular

forces, for the interactions of the trace molecules with themselves can be neglected with respect to the total number of collisions (Heymann and Kistemaker (1959)). Finally, the partial pressure of a component present as a trace quantity in a gas mixture is very low, and therefore the temperature at which condensation begins to occur in a gas mixture can be reduced by substituting a radioactive tracer for the component with the highest condensation point.

3.4.2. Experimental Methods: Diffusion-Thermo Effect

Following the experiment described by Dufour in 1873 which illustrated what has since come to be called the diffusion-thermo effect, no further experimental investigations of the phenomenon were conducted until the decade beginning in 1940, even though the possibility of such an effect is contained in the Chapman-Enskog kinetic theory (Grew and Ibbs (1952)). During the period from 1943 to 1950, Waldmann published the results of extensive experimental and theoretical investigations which he conducted to study the phenomenon, and he is recognized (Grew and Ibbs (1952), Chapman and Cowling (1970)) as the principal contributor to the literature on the phenomenon.

Waldmann's work followed two approaches. The first involved a study of the transient temperature changes that take place under conditions occurring when two vertical

cylinders containing different gases are placed end-to-end (for example, see Waldmann (1947)). The second involved a study of the temperature effects associated with flow of two gases through parallel tubes joined by a gauze-covered slot across which diffusion occurs (for example, see Waldmann (1949)). In the latter approach, a steady temperature difference develops between corresponding points on either side of the slot, and Waldmann used platinum wires, one in each tube oriented parallel to the slot, as resistance thermometers to measure the mean axial temperature difference due to diffusion across the slot.

From experimental measurements of the diffusion-thermo effect, the thermal diffusion factor, α_T, may be determined by performing an energy balance over an appropriate control volume. A formulation of this type is included later in this thesis. The thermal conductivity of the gas mixture must be known, which is a disadvantage of this approach since for many gas mixtures no experimental values of the thermal conductivity are available. Therefore the thermal conductivity must generally be estimated, using an approximate formula, from the values for the pure gases in the mixture.

Experimental techniques that have been developed more recently to investigate the diffusion-thermo effect

associated with flow-coupled diffusion in a circular tube are discussed in section 3.6.

3.5. Experimental Investigations of Thermal Diffusion Phenomena

3.5.1. Temperature Dependence of Thermal Diffusion Coefficients

Using equipment of the two-bulb type, Ibbs and Grew (1931), Grew and Atkins (1936), and Grew (1946) were among the investigators who examined variations in the thermal diffusion ratio, k_T, as a function of temperature. They also examined the behavior of the thermal separation ratio, R_T, defined as follows (Ibbs and Grew (1931)):

$$R_T = \frac{k_T(\text{exp})}{k_T(\text{res})}$$

where $k_T(\text{exp})$ is the thermal diffusion ratio computed from experimental data for a given binary mixture, and $k_T(\text{res})$ is the corresponding value of k_T predicted from theory assuming that the molecules behave as rigid elastic spheres. An incentive for studying the behavior of R_T is that, if the molecules are considered to interact as point centers of repulsion with the force between any given pair varying inversely as the nth power of their separation, then R_T may be regarded as an approximate measure of the exponent n (Ibbs and Grew (1931)).

The investigation by Ibbs and Grew involved thermal diffusion measurements with one bulb of the apparatus at +15° C and the other bulb at temperatures down to -190° C. Results of their investigation indicate that k_T tends to decrease at low temperatures, and that the variation in k_T differs widely depending on the characteristics of the individual gases. Ibbs and Grew concluded that k_T may be regarded as practically constant for any given gas mixture over a considerable range of temperatures.

In the investigation by Grew and Atkins (1936), the molecular fields of hydrogen and deuterium (which have different molecular masses but the same electronic structure), and helium and deuterium (which have the same molecular mass but different electronic structures), were compared by examining thermal separations in a series of hydrogen-nitrogen, deuterium-nitrogen, and helium-nitrogen mixtures with one bulb of the apparatus at room temperature and the other bulb at temperatures ranging from -190° C to +100° C. The thermal separation ratio, R_T, was found to be the same for hydrogen-nitrogen and deuterium-nitrogen mixtures throughout the entire temperature range, and Grew and Atkins therefore concluded that the fields of force of hydrogen and deuterium molecules are similar. Their results also indicated that the fields of force of deuterium and helium differ appreciably.

The investigation by Grew (1946) involved a systematic examination of all the binary combinations of helium, neon, argon, krypton, and xenon, except for krypton-xenon mixtures. Temperatures at which measurements were taken varied from -180° C to 400° C. His results indicate that, in general, the magnitude of the thermal separation ratio, R_T, increases with temperature in the lower temperature ranges and becomes constant at high temperatures. Although the temperature at which R_T first becomes constant was found to vary widely from mixture-to-mixture of the inert gases, the constant value was found to be nearly the same for all mixtures, with a value of approximately 0.64.

The variation of α_T as a function of temperature was investigated by Waldmann (1949) as part of his experiments involving the diffusion-thermo effect. With the exception of the anomalous behavior exhibited by argon-carbon dioxide mixtures, Waldmann's results confirm the finding by other investigators that the value of α_T diminishes with decreasing temperature.

Waldmann also found a change in sign of α_T at low temperatures. Prior to his experiments, a change in sign of α_T had been observed only for isotopic thermal diffusion in ammonia (by Watson and Woernley in 1943, as discussed in Grew and Ibbs (1952)). Binary mixtures for which Waldmann

found a change in sign of α_T include nitrogen-argon (at -155° C), oxygen-argon (at -131° C), and nitrogen-carbon dioxide (at -68° C).

Grew, et al. (1954), using a two-bulb apparatus for thermal diffusion experiments, confirmed the occurrence of the change in sign of α_T in the three mixtures mentioned in the preceding paragraph, but observed no change in sign of α_T for mixtures of three different noble gas pairs. They found good agreement between their results and those of Waldmann (1949) for the gas pairs common to the two investigations, which provides further experimental evidence that transport coefficients determined from experiments involving the diffusion-thermo effect are consistent with those determined from experiments involving thermal diffusion.

The behavior of α_T noted by Waldmann (1949) for argon-carbon dioxide mixtures is anomalous in the sense that the value of α_T decreased with increasing temperature in a temperature range where it would be expected to increase. This behavior has also been found to exist for several other gas pairs. As discussed by Mason, et al. (1966), no satisfactory explanation for this behavior has been found which is consistent with what is known about molecular structure and intermolecular forces.

3.5.2. Composition Dependence of Thermal Diffusion Coefficients

Lonsdale and Mason (1957) and Saxena and Mason (1959) used radioactive tracers in an apparatus of the two-bulb type to observe both the steady state separation of gas mixtures under the influence of a temperature gradient and the rate of approach to the steady state. Values of the thermal diffusion factor, α_T, were computed from measurements of the steady state separations, and values of the binary diffusion coefficient, D_{AB}, were computed from measurements of the rate of approach to the steady state. In the former investigation, measurements were taken using mixtures of H_2-CO_2 and He-CO_2 with $^{14}CO_2$ as the radioactive tracer. After refining the apparatus, measurements were taken in the latter investigation using mixtures of He-Ar, He-CO_2, H_2-CO_2, and D_2-CO_2 with $^{14}CO_2$ and ^{37}Ar as the radioactive tracers.

Based in part on data from the investigations described in the preceding paragraph, Mason, et al. (1964) published experimental confirmation of a theory by Laranjeira (1960) that the inverse of the thermal diffusion factor ($1/\alpha_T$) is a linear function of mole fraction in a binary mixture. Thermal diffusion measurements described in the preceding paragraph, which involved only the heavier components as radioactive tracers, were supplemented by Mason and his co-workers with additional measurements for

mixtures in which a hydrogen isotope (tritium) was the radioactive tracer. These measurements were combined with measurements by other investigators for less dilute mixtures, and for each binary mixture that was examined the linear relationship of $1/\alpha_T$ as a function of mole fraction was found to hold within experimental error over the entire range of mole fractions of either component.

3.5.3. Pressure Dependence of Thermal Diffusion Coefficients

On the basis of the Chapman-Enskog kinetic theory, the magnitude of the thermal diffusion factor is independent of pressure in the pressure range for which only binary collisions are important (Mason, et al. (1966)). Results of experimental investigations conducted with apparatus of the two-bulb type have confirmed this prediction in the pressure range of approximately 0.3 to 2 atmospheres (Grew and Ibbs (1952)).

More recently, Walther and Drickamer (1958) used a two-bulb apparatus to measure separations due to thermal diffusion in a series of binary mixtures of gases at pressures up to 1000 atm. They found that the effect of pressure on α_T is small when the average temperature of the apparatus is far above the critical temperature of either of the gases. Their measurements show, however, that when the average temperature of the apparatus is near the critical temperature of one of the gases, the value of α_T,

which is usually positive near atmospheric pressure, changes sign as the pressure increases. Furthermore, after passing through a minimum at a pressure at which the mixture is apparently in the neighborhood of the critical point, the value of α_T increases with an increase of pressure, and usually becomes positive again within the pressure range utilized for their experimental measurements. A satisfactory theoretical explanation for this observed behavior is not known (Walther and Drickamer (1958), Mason, et al. (1966)).

3.6. Experimental Investigations of Flow-Coupled Diffusion

Zaworski (1966), Yang (1966), Wyatt (1968), and Stock (1972) investigated diffusion phenomena that occur when a steady-state flow field is established for a binary gas mixture in a cylindrical duct along which a steep axial concentration gradient is maintained. Zaworski obtained calorimetric measurements of energy effects associated with diffusion of hydrogen into nitrogen. Yang and Wyatt each measured transport phenomena for helium-nitrogen mixtures in flow fields for which the Peclet numbers were less than 2.5. Stock obtained velocity and concentration distributions for helium-nitrogen mixtures flowing under the same conditions as those established for measuring the temperature distributions discussed in Chapter VII of this thesis.

Transport coefficients computed by Yang and by Wyatt from their experimental data are compared in Chapter VII

with transport coefficients computed from the data measured by Stock combined with the data measured in the experimental investigation reported in this thesis. The apparatus used to obtain the latter data is described in Chapter V. A brief description of the type of apparatus used by Yang and by Wyatt is as follows.

The latter investigators each used an apparatus in which the lighter of two gases flows downward through a vertically oriented, cylindrical diffusion tube and is swept away at the bottom end of the tube by a heavier gas flowing through a horizontal duct to which the tube is attached. Under these flow conditions, axial concentration gradients develop due to diffusion of the heavier gas against the flow of the lighter gas. The concentration distribution in the diffusion tube is dependent on the specific flow conditions established in the apparatus. Wyatt used a larger diameter diffusion tube than the one used by Yang.

IV. PREDICTED TEMPERATURE DISTRIBUTIONS IN DIFFUSION FLOW FIELD

To provide additional insight into the phenomena that were investigated for this thesis, a model was developed for predicting the radial and axial temperature distributions within the diffusion flow field. The model is in the form of a second order, elliptic partial differential equation, which was solved numerically to obtain predicted temperature distributions for each of the four test conditions under which experimental measurements were taken.

In order to solve the differential equation for the temperature distribution corresponding to a given set of flow conditions, velocity and concentration distributions must be known. Velocity and concentration data measured by Stock (1972) were used in solving for the predicted temperature distributions corresponding to the test conditions discussed in this thesis. An alternate approach, and one recommended in Chapter VIII under suggestions for further work, would be to incorporate the differential equation developed in this chapter into a system of coupled equations that could be solved simultaneously for the velocity, concentration, and temperature distributions.

4.1. Model for Predicting Temperature Distributions

The analysis that follows is for flow-coupled diffusion of a binary gas mixture within a vertically oriented, cylindrical tube. As shown in Figure 4.1, gas A (designated as the primary gas) is introduced into the tube at a location far upstream of the injection plane for gas B (the secondary gas). If the average velocity of a gas A is sufficiently small, gas B will diffuse against the flow and both gases will be present in the region immediately upstream of the injection plane. The net axial flow of gas B at any cross section in this region is zero.

Under these flow conditions, mass is transported by both convection and diffusion within the region immediately upstream of the injection plane. This combined transport is referred to as flow-coupled diffusion. As discussed in Chapter I, the relative magnitudes of these two transport processes may be expressed in terms of the mass Peclet number for the flow. Upper and lower bounds on the Peclet numbers for flow-coupled diffusion are defined as follows (Stock and Zaworski (1973)): For flows with Peclet numbers greater than 10, mass transport by convection is dominant to the extent that diffusion against the flow is essentially eliminated. For flows

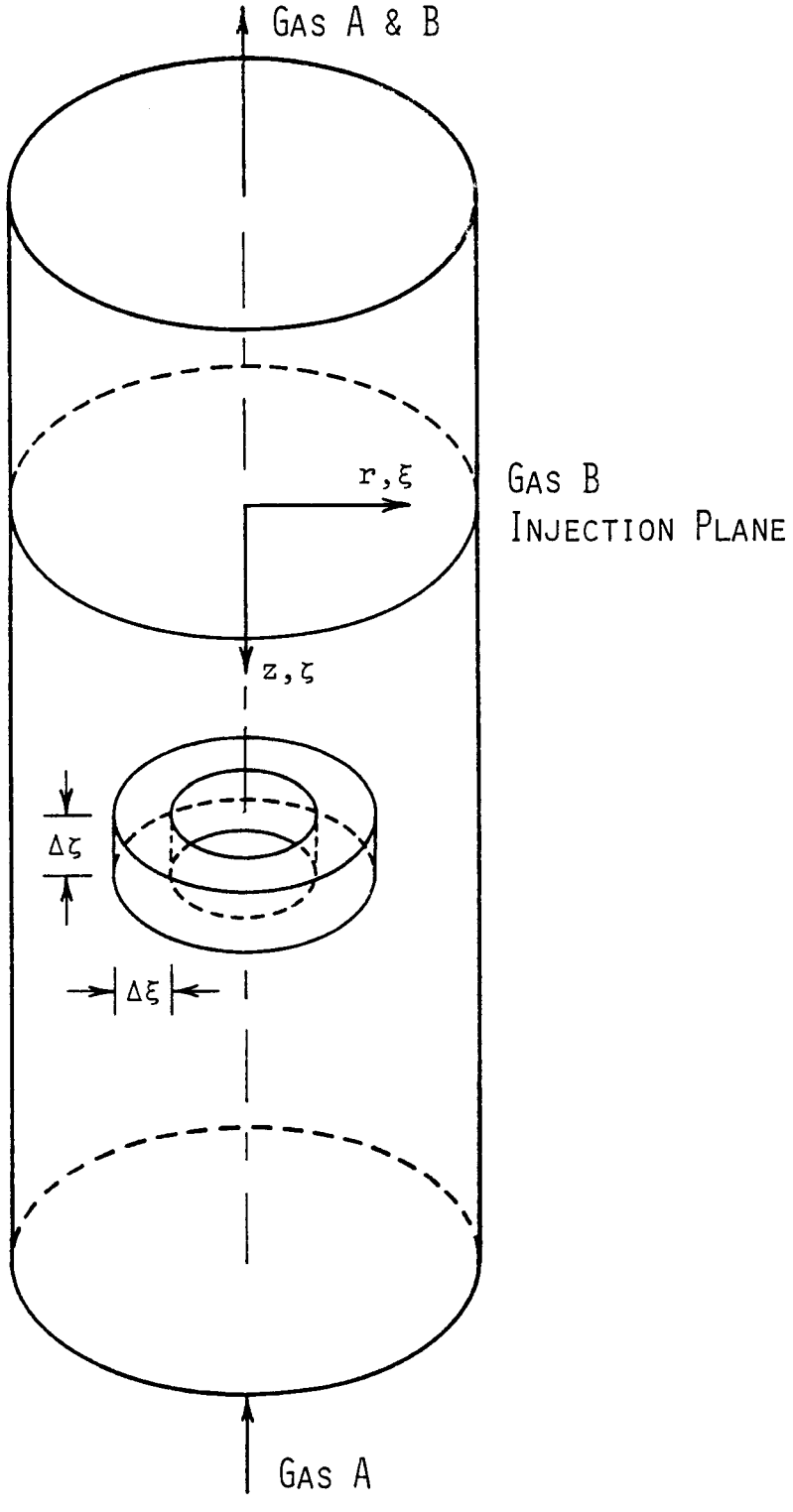

Figure 4.1. Control Volume and Coordinate System for Modeling Temperature Fields

with Peclet numbers less than 2, diffusion is the dominant mass transport process.

Attention is restricted to an analysis of the temperature fields associated with flow-coupled diffusion of a binary gas mixture in the region upstream of the injection plane shown in Figure 4.1. The assumptions for the analysis are as follows:

1. Concentration, velocity, and temperature distributions within the flow field are axisymmetric.
2. The bulk flow is steady and laminar.
3. The components of the gas mixture are ideal and nonreacting.
4. Throughout the flow field, the pressure is constant.
5. The gas mixture is dilute in the sense that only two-body collisions are likely to occur.
6. Gravity is the only force field acting on the components of the gas mixture.
7. Viscous dissipation, which tends to increase the internal energy of the fluid as a result of interactions that are dependent upon fluid viscosity and shear-strain rates, is negligible.

8. Energy interchanges in the gas mixture are essentially unaffected by the kinetic energy associated with the bulk fluid motion. (The energy interchanges are strongly dependent, however, on the internal energy of the gas mixture; this includes the energy associated with the random translational and internal motions of the molecules and the energy of interactions between the molecules.)

9. Radiant energy transfer within the gas mixture and between the gas mixture and its surroundings is negligible.

4.1.1. Energy Equation in Terms of Energy Flux $\vec{e}$

Although an energy equation for the diffusion flow field could be formulated on the basis of an energy balance over the control volume shown in Figure 4.1, it is unnecessary to commence the analysis in that way. Energy equations of considerable generality are readily available in the literature, and it is convenient to select an appropriate equation and then simplify it in accordance with the assumptions for the flow conditions under consideration. The latter approach is followed for this analysis.

An equation of energy for multicomponent systems in which energy interchanges are essentially unaffected by the kinetic energy of the bulk fluid motion is as follows (Bird, et al. (1960); equation (D), page 562):

$$\rho\frac{D\hat{E}}{Dt} = -(\vec{\nabla}\cdot\vec{q}) - (\vec{\pi}:\vec{\nabla}\vec{v}) + \sum_i \vec{j}_i\cdot\vec{g}_i. \qquad (4.1)$$

The symbols used in the preceeding equation represent the following:

$\hat{E}$ is the internal energy per unit mass.

$\vec{q}$ is the multicomponent energy flux relative to the mass average velocity $\vec{v}$.

$\vec{\pi}$, the pressure tensor, is related to the shear stress $\vec{\tau}$ and the static pressure p by the equation $\vec{\pi} = \vec{\tau} + p\vec{\delta}$, where $\vec{\delta}$ is the unit tensor.

$\vec{v}$, the mass average velocity, is defined by the equation $\vec{v} = \frac{1}{\rho}\sum_i \rho_i \vec{v}_i$, where $\vec{v}_i$ is the velocity of the ith constituent of the fluid relative to stationary coordinates and ρ_i is the mass concentration (mass per unit volume) of constituent i.

$\vec{j}_i$, the mass flux of constituent i of the fluid relative to the mass average velocity, is defined by the equation $\vec{j}_i = \rho_i(\vec{v}_i - \vec{v})$.

$\vec{g}_i$ is an external force per unit mass acting on constituent i of the fluid.

Additional information on the nomenclature is given in Appendix A.

For convenience in analyzing the transport of energy relative to a coordinate system fixed in space, equation 4.1 may be rewritten in the following form:

$$\frac{\partial}{\partial t}(\rho\hat{E}) = -(\vec{\nabla}\cdot\rho\hat{E}\vec{v}) - (\vec{\nabla}\cdot\vec{q}) - (\vec{\pi}:\vec{\nabla}\vec{v}) + \sum_i \vec{j}_i\cdot\vec{g}_i . \tag{4.2}$$

The third term on the right hand side may be expanded as follows (Bird, et al. (1960)):

$$\vec{\pi}:\vec{\nabla}\vec{v} = \vec{\nabla}\cdot(\vec{\pi}\cdot\vec{v}) - \vec{v}\cdot(\vec{\nabla}\cdot\vec{\pi}) .$$

Substituting $\vec{\tau} + p\vec{\delta}$ for $\vec{\pi}$ and carrying out the operations indicated in the preceding equation,

$$\vec{\pi}:\vec{\nabla}\vec{v} = \left[\vec{\nabla}\cdot(\vec{\tau}\cdot\vec{v}) - \vec{v}\cdot(\vec{\nabla}\cdot\vec{\tau})\right] + \vec{\nabla}\cdot(pv) - \vec{v}\cdot(\vec{\nabla}p)$$

or

$$\vec{\pi}:\vec{\nabla}\vec{v} = \vec{\tau}:\vec{\nabla}\vec{v} + \vec{\nabla}\cdot(p\vec{v}) - \vec{v}\cdot(\vec{\nabla}p) .$$

After substituting these terms into equation 4.2 and rearranging, the energy equation becomes

$$\frac{\partial}{\partial t}(\rho\hat{E}) = -\left[\vec{\nabla}\cdot(\rho\hat{E}\vec{v} + \vec{q} + p\vec{v})\right] - (\vec{\tau}:\vec{\nabla}\vec{v}) + \vec{v}\cdot(\vec{\nabla}p) + \sum_i \vec{j}_i\cdot\vec{g}_i . \tag{4.3}$$

On the basis of the assumptions for this analysis, equation 4.3 may be simplified as follows:

- For steady-state conditions, $\frac{\partial}{\partial t}(\rho\hat{E}) = 0$.
- For constant pressure throughout the flow field, $\vec{\nabla}p = 0$.
- Under conditions for which viscous dissipation is negligible, $\vec{\tau}:\vec{\nabla}\vec{v} = 0$. (This term represents the rate of internal energy increase per unit volume by viscous dissipation, as discussed on page 314 of Bird, et al. (1960).)
- If the only external force field acting on the constituents of the gas mixture is gravity,

$$\sum_i \vec{j}_i \cdot \vec{g}_i = \sum_i \vec{j}_i \cdot \vec{g} = (\vec{j}_A + \vec{j}_B) \cdot \vec{g} = 0$$

since

$$\vec{j}_A + \vec{j}_B = \rho_A(\vec{v}_A - \vec{v}) + \rho_B(\vec{v}_B - \vec{v}) = 0.$$

With these simplifications, equation 4.3 reduces to the following:

$$\vec{\nabla} \cdot (\vec{q} + \rho\hat{E}\vec{v} + p\vec{v}) = 0. \qquad (4.4)$$

The second and third terms within the brackets in equation 4.4 may be combined as follows:

$$\rho\hat{E}\vec{v} + p\vec{v} = \rho\left(\hat{E} + \frac{p}{\rho}\right)\vec{v}.$$

Noting that $1/\rho$ is the specific volume and that $\hat{E}$ is the internal energy per unit mass,

$$\hat{E} + \frac{p}{\rho} = \hat{H}$$

where $\hat{H}$ is the enthalpy per unit mass. Further,

$$\rho\hat{H} = \rho_A\hat{H}_A + \rho_B\hat{H}_B = C_AM_A\hat{H}_A + C_BM_B\hat{H}_B$$

or

$$\rho\hat{H} = C_AH_A + C_BH_B,$$

where C_i is the molar concentration (moles per unit volume), M_i is the molecular weight, and H_i is the partial molal enthalpy of constituent i. With these changes, equation 4.4 becomes

$$\vec{\nabla}\cdot\left[\vec{q} + (C_AH_A + C_BH_B)\vec{v}\right] = 0$$

or

$$\vec{\nabla}\cdot\vec{e} = 0 \qquad (4.5)$$

where

$$\vec{e} = \vec{q} + (C_AH_A + C_BH_B)\vec{v}. \qquad (4.6)$$

4.1.2. Multicomponent Energy Flux, $\vec{q}$, Relative to Mass Average Velocity

In equation 4.6, $\vec{q}$ is the multicomponent energy flux relative to the mass average velocity $\vec{v}$. An equation for $\vec{q}$ that is applicable for a dilute, nonreacting binary gas mixture is as follows (Chapman and Cowling (1970); Hirschfelder, et. al (1954)):

$$\vec{q} = -\lambda\vec{\nabla}T + (n_A h_A \vec{V}_{D_A} + n_B h_B \vec{V}_{D_B}) + knTX_A X_B \alpha_T (\vec{V}_{D_A} - \vec{V}_{D_B}). \quad (4.7)$$

Symbols used in equation 4.7 represent the following:

λ is the thermal conductivity of the gas mixture.

n_A, n_B, and n are, respectively, the molecules per unit volume of gas A, gas B, and the gas mixture.

h_A and h_B are the enthalpies per molecule of gases A and B.

$\vec{V}_{D_A}$ and $\vec{V}_{D_B}$ are the diffusion velocities of gases A and B relative to the mass average velocity of the gas mixture, i.e.,

$$\vec{V}_{D_i} = \vec{v}_i - \vec{v}.$$

X_A and X_B are the mole fractions of gases A and B.

α_T is the thermal diffusion factor for the gas mixture.

k is the Boltzmann constant.

The terms grouped on the right hand side of equation 4.7 represent the following three components of the energy flux: transport by conduction due to inequalities of temperature in the gas mixture; transport associated with the molecules of gases A and B moving relative to the mass average velocity of the gas mixture, and transport due to the diffusion-thermo effect.

4.1.3. Energy Equation in Terms of Temperature

A differential equation for the temperature distribution in the diffusion flow field may be developed using equations 4.5, 4.6, and 4.7. After substituting for $\vec{q}$ in equation 4.6 using the terms given in equation 4.7, the divergence of equation 4.6 is taken in accordance with equation 4.5. Details of the derivation are given in Appendix B. After performing the mathematical operations, the following equation is obtained:

$$\lambda\frac{\partial^2 T}{\partial r^2} + \lambda\frac{\partial^2 T}{\partial z^2} + \left[\frac{\partial\lambda}{\partial r} + \frac{\lambda}{r} - \rho_A\left(\frac{C_{p_A}}{M_A} - \frac{C_{p_B}}{M_B} + \frac{M\tilde{R}\alpha_T}{M_A M_B}\right)v_{A_r} - \left(\rho\frac{C_{p_B}}{M_B} - 2\frac{M\tilde{R}\rho_A\alpha_T}{M_A M_B}\right)v_r\right]\frac{\partial T}{\partial r}$$

$$+\left[\frac{\partial\lambda}{\partial z} - \rho_A\left(\frac{C_{p_A}}{M_A} - \frac{C_{p_B}}{M_B} + \frac{M\tilde{R}\alpha_T}{M_A M_B}\right)v_{A_z} - \left(\rho\frac{C_{p_B}}{M_B}\right.\right.$$

$$\left.\left. - 2\frac{M\tilde{R}\rho_A\alpha_T}{M_A M_B}\right)v_z\right]\frac{\partial T}{\partial z} - \frac{\tilde{R}}{M_A M_B}\left[\rho_A\left(v_{A_r}\frac{\partial(\alpha_T M)}{\partial r}\right.\right.$$

$$\left. + v_{A_z}\frac{\partial(\alpha_T M)}{\partial z}\right) - M\left(v_r\frac{\partial(\alpha_T\rho_A)}{\partial r}\right.$$

$$\left.\left. + v_z\frac{\partial(\alpha_T\rho_A)}{\partial z}\right)\right]T = 0. \qquad (4.8)$$

4.1.3.1. Nondimensional Variables

Equation 4.8 may be placed in nondimensional form by introducing the following variables:

$$\zeta = \frac{z}{R},\ \xi = \frac{r}{R},\ \beta = \frac{\rho}{\rho_{A_o}},\ U = \frac{v_r}{|\bar{v}_{A_o}|},$$

$$V = \frac{v_z}{|\bar{v}_{A_o}|},\ \theta = \frac{T-T_o}{T_o}.$$

In these variables, r and z are coordinates shown in Figure 4.1; R is the radius of the diffusion tube; ρ_{A_o} and $\bar{v}_{A_o}$ are, respectively, the density and the average of gas A at large values of z where only gas A is present; T_o is the reference temperature, which is taken as the temperature of gas A at the entrance to the diffusion tube; ρ and T are, respectively, the density and temperature of the gas mixture at location (r,z), and v_r

and v_z are the components of the mass average velocity of the gas mixture in the r and z directions.

Density and velocity terms that apply only to constituent A of the gas mixture are identified by subscript A.

In terms of the preceding variables,

$$\frac{\partial T}{\partial r} = \frac{\partial}{\partial \xi}(T_o(\theta+1))\frac{\partial \xi}{\partial r} = \frac{T_o}{R}\frac{\partial \theta}{\partial \xi}.$$

It is a straightforward but somewhat lengthy task to proceed in this manner to incorporate the nondimensional variables into all of the terms in equation 4.8. After carrying out the substitutions and rearranging, equation 4.8 may be expressed as follows in nondimensional form:

$$\frac{\partial^2 \theta}{\partial \xi^2} + \frac{\partial^2 \theta}{\partial \zeta^2} + J\frac{\partial \theta}{\partial \xi} + K\frac{\partial \theta}{\partial \zeta} + L(\theta+1) = 0. \qquad (4.9)$$

The coefficients J, K, and L are as follows:

$$J = \frac{1}{\lambda}\frac{\partial \lambda}{\partial \xi} + \frac{1}{\xi} + FU_A + GU$$

$$K = \frac{1}{\lambda}\frac{\partial \lambda}{\partial \zeta} + FV_A + GV$$

$$L = -\frac{\tilde{R}}{\lambda M_A M_B}(\rho_{A_o}|\bar{V}_{A_o}|R)\left[\beta_A\left(U_A\frac{\partial(\alpha_T M)}{\partial \xi} + V_A\frac{\partial(\alpha_T M)}{\partial \zeta}\right)\right.$$

$$\left. - M\left(U\frac{\partial(\alpha_T \beta_A)}{\partial \xi} + V\frac{\partial(\alpha_T \beta_A)}{\partial \zeta}\right)\right]$$

where

$$F = -(\rho_{A_o}|\bar{V}_{A_o}|R)\beta_A\left(\frac{(C_{p_A}/M_A) - (C_{p_B}/M_B)}{\lambda} + \frac{\tilde{R}M\alpha_T}{\lambda M_A M_B}\right)$$

$$G = -(\rho_{A_o}|\bar{V}_{A_o}|R)\left(\beta\frac{(C_{p_B}/M_B)}{\lambda} - 2\beta_A\alpha_T\frac{\tilde{R}M}{\lambda M_A M_B}\right).$$

The coefficients of equation 4.9 may also be written as follows:

$$J = \frac{1}{\lambda}\frac{\partial\lambda}{\partial\xi} + \frac{1}{\xi} + Pe(YU_A + ZU)$$

$$K = \frac{1}{\lambda}\frac{\partial\lambda}{\partial\zeta} + Pe(YV_A + ZV)$$

$$L = -\frac{Pe}{2Sc_A}\frac{\mu_A\tilde{R}}{\lambda M_A}\left[\frac{1}{M_B}\left(U_A\frac{\partial(\alpha_T M)}{\partial\xi} + V_A\frac{\partial(\alpha_T M)}{\partial\zeta}\right) - \frac{1}{\beta_A}\frac{M}{M_B}\left(U\frac{\partial(\alpha_T\beta_A)}{\partial\xi} + V\frac{\partial(\alpha_T\beta_A)}{\partial\zeta}\right)\right]$$

where

$$Y = -\frac{1}{2Sc_A}\left[\frac{\mu_A(\hat{C}_{p_A} - \hat{C}_{p_B})}{\lambda} + \frac{\mu_A\tilde{R}}{\lambda M_A}\frac{M}{M_B}\alpha_T\right]$$

$$Z = -\frac{1}{2Sc}\frac{\mu\hat{C}_{p_B}}{\lambda} + \frac{1}{Sc_A}\frac{\mu_A\tilde{R}}{\lambda M_A}\frac{M}{M_B}\alpha_T.$$

In the preceding equations, $Pe = ReSc = \frac{(2R)|\bar{V}_{A_o}|}{D_{AB}}$; $Sc = \frac{\mu}{\rho D_{AB}}$; $Sc_A = \frac{\mu_A}{\rho_A D_{AB}}$; $\hat{C}_{p_i} = \frac{C_{p_i}}{M_i}$ = the specific heat per unit mass of constituent i; μ and μ_i are, respectively,

viscosities of the mixture and of constituent i, and D_{AB} is the molecular diffusion coefficient for the binary mixture.

Equation 4.9 is a second order, elliptic, partial differential equation for the radial and axial temperature distributions within the diffusion flow field. With the assumption that the temperature dependence of the coefficients may be neglected, the equation is linear.

4.1.3.2. Boundary Conditions

Four boundary conditions are required for a solution of equation 4.9. The boundary conditions that were selected for computations of the temperature distributions presented later in this chapter are as follows:

1. For axial symmetry of the temperature profiles, $\frac{\partial T}{\partial r} = 0$ at $r = 0$. In terms of nondimensional variables, $\frac{\partial \theta}{\partial \xi} = 0$ at $\xi = 0$.
2. At locations sufficiently far upstream of the gas B injection plane, the temperature is the same as the temperature of gas A entering the diffusion tube. Thus,

$$T = T_o \text{ at } z \geq z_u$$

or $\theta = 0$ at $\zeta \geq \zeta_u$.

3. It is convenient to consider the diffusion tube wall as either an isothermal or an adiabatic boundary. Since the thermal conductivity of the wall is considerably greater than that of the gas mixture, an isothermal boundary condition would be expected to be a better approximation than an adiabatic one. Either option may be selected in the computer program used to solve equation 4.9.

   a. For an isothermal wall,

   $$T = T_o \text{ at } r = R$$

   or $\theta = 0$ at $\xi = 1$.

   b. For an adiabatic wall,

   $$\frac{\partial T}{\partial r} = 0 \text{ at } r = R$$

   or $$\frac{\partial \theta}{\partial \xi} = 0 \text{ at } \xi = 1.$$

4. As shown in the experimental results presented in Chapter VII, the temperature of the gas mixture at the gas B injection plane tends to approach the temperature at which the two gases are maintained in their flow circuits upstream of the diffusion tube.

Accordingly, the following boundary condition is a reasonable approximation for conditions existing at the injection plane:

$$T = T_o \text{ at } x = 0$$

or $\theta = 0$ at $\zeta = 0$.

The fourth of the boundary conditions listed above proved to be a difficult one to select. Due to the presence of the tubing needed to inject gas B into the flow field, an abrupt change in flow conditions occurs at the injection plane. To avoid having to account for flow conditions downstream of the injection plane, it is necessary to specify a boundary condition at that plane. It is not clear, however, either from the assumptions for the analysis or from intuition regarding the diffusion phenomena, what an appropriate boundary condition on temperature at that plane would be. Accordingly, the boundary condition at the injection plane was specified on the basis of the experimental results presented in Chapter VII.

4.2. Method of Solution

Program TFIELD, a copy of which is included in Appendix C, was written for use in solving equation 4.9 numerically. A Gauss-Seidel iteration scheme with over-relaxation is used in the program.

After replacing the derivatives of the dimensionless temperature in equation 4.9 with central difference approximations and then rearranging terms, the equation for θ in the form programmed for solution is as follows:

$$\theta_{j,k} = \frac{1}{\left[\frac{2}{(\Delta\xi)^2} + \frac{2}{(\Delta\zeta)^2} - L_{j,k}\right]} \left[\frac{\theta_{j+1,k} + \theta_{j-1,k}}{(\Delta\xi)^2} + \frac{\theta_{j,k+1} + \theta_{j,k-1}}{(\Delta\zeta)^2} + J_{j,k}\left(\frac{\theta_{j+1,k} - \theta_{j-1,k}}{2\Delta\xi}\right) + K_{j,k}\left(\frac{\theta_{j,k+1} - \theta_{j,k-1}}{2\Delta\zeta}\right) + L_{j,k}\right] . \qquad (4.10)$$

Boundaries for the finite difference scheme are located at the tube centerline, the tube wall, the gas B injection plane, and a location upstream of the injection plane where only gas A is present. Two extra columns of nodes, one located on the opposite side of the tube centerline from the rest of the grid system and the other located one node radially outward from the inside surface of the tube wall, are used for computations of derivatives associated with zero-slope boundary conditions at the centerline and the wall. The axial length of the grid system may be varied as necessary to accommodate changes in the length of the diffusion flow field as a function of the flow conditions.

4.2.1. Use of Experimental Data to Compute Coefficients

Coefficients J, K, and L of equation 4.9 are computed from experimental data for the concentration and velocity distributions in the diffusion flow field. Because of their dependence on the velocity and concentration distributions, these coefficients vary as a function of position in the flow field. The temperature dependence of these coefficients is assumed to be negligible, and therefore at any given position they are constants in the iteration scheme for the dimensionless temperature θ. They are computed in subroutine READY of program TFIELD using the equations immediately following equation 4.9.

To compute derivatives that appear in coefficients J, K, and L, five-point differentiation formulas are used. As discussed in Wylie (1966), the five-point formulas are written on the basis of fitting a parabola to successive sets of five data points by the method of least squares, and then taking derivatives of the parabola. The smoothing provided by these formulas tends to reduce irregularities in the data that would otherwise be magnified when taking derivatives of the data.

To illustrate the manner in which the variables in the coefficients are computed, the derivatives in the

radial direction of M, the mean molecular weight of the mixture, will be considered. Noting that $M = X_A M_A + X_B M_B$ and that $X_A + X_B = 1$ (Bird, et al. (1960)),

$$M = X_A(M_A - M_B) + M_B$$

and

$$\frac{\partial M}{\partial \xi} = \frac{\partial M}{\partial X_A} \frac{\partial X_A}{\partial \xi} = (M_A - M_B) \frac{\partial X_A}{\partial \xi}$$

where M_A and M_B are the molecular weights of gases A and B. The following five-point formulas may be used to compute the derivatives (Wylie (1966), Scheid (1968)):

For the central node of five nodes,

$$\frac{\Delta X_A(j,k)}{\Delta \xi} =$$

$$\frac{-2X_A(j-2,k)-X_A(j-1,k)+X_A(j+1,k)+2X_A(j+2,k)}{10(\Delta \xi)} .$$

For the wall boundary nodes and those located one node into the flow field from the boundary, respectively,

$$\frac{\Delta X_A(j,k)}{\Delta \xi} =$$

$$\frac{54X_A(j,k)-13X_A(j-1,k)-40X_A(j-2,k)-27X_A(j-3,k)+26X_A(j-4,k)}{70(\Delta \xi)}$$

and

$$\frac{\Delta X_A(j,k)}{\Delta \xi} =$$

$$\frac{34X_A(j+1,k)-3X_A(j,k)-20X_A(j-1,k)-17X_A(j-2,k)+6X_A(j-3,k)}{70(\Delta \xi)} .$$

Similar formulas apply for derivatives in the axial direction.

Noting that $\rho_A = C_A/M_A$, $C = C_A + C_B$, and $X_A = C_A/C$ (Bird, et al. (1960)), the term $\beta_A = \rho_A/\rho_{A_o}$ that appears in coefficient L of equation 4.9 may be replaced with the following:

$$\beta_A = \frac{\rho_A}{\rho_{A_o}} = \frac{C_A M_A}{C_{A_o} M_A} \simeq \frac{C_A}{C} = X_A.$$

The substitution of X_A for β_A is not strictly applicable unless C, the molar density of the mixture, is constant throughout the flow field. As shown in Appendix B, C is inversely proportional to the absolute temperature of the gas. This variation of C amounts to less than 1.5%, however, corresponding to the largest variation in temperature (4° C) measured experimentally for the various flow conditions considered in this thesis. (The experimental results are presented in Chapter VII.) Therefore, this variation of C is disregarded in accordance with the assumption that the temperature dependence of the coef-

ficients of equation 4.9 is negligible in comparison with their dependence on the velocity and concentration distributions in the flow field.

4.2.2. Equations for Calculating Velocity Components

Radial and axial components of both the mass average velocity and the velocity of gas A are needed for computations of coefficients J, K, and L in equation 4.9. If the concentration distribution and the axial mass average velocity components are known for a given set of flow conditions, the remaining velocity components may be computed using the equations discussed in the following paragraphs.

4.2.2.1. Radial Components of the Mass Average Velocity

In accordance with the continuity equation for steady flow conditions, $\vec{\nabla}\cdot(\rho\vec{v}) = 0$. If the flow is axisymmetric, the continuity equation may be written in cylindrical coordinates as

$$\frac{1}{r}\frac{\partial}{\partial r}\left[r(\rho v_r)\right] + \frac{\partial}{\partial z}(\rho v_z) = 0.$$

Noting that $\rho = CM$, where C is assumed to be a constant for reasons discussed in section 4.2.1, and incorporating the nondimensional variables

$$U = \frac{v_r}{|\bar{V}_{A_o}|}, \quad V = \frac{v_z}{|\bar{V}_{A_o}|}, \quad \xi = \frac{r}{R}, \text{ and } \zeta = \frac{z}{R},$$

the continuity equation becomes

$$\frac{\partial}{\partial \xi} (\xi MU) = -\xi \frac{\partial}{\partial \zeta} (MV).$$

Integrating the preceding equation between the tube centerline and any arbitrary radial location ξ_s,

$$(\xi MU)_{\xi_s} = -\int_o^{\xi_s} \xi \frac{\partial}{\partial \zeta} (MV) d\xi.$$

Solving for U, the equation in nondimensional form for the radial velocity component of the mass average velocity at any position (ξ_s, ζ) in the diffusion flow field is as follows:

$$U(\xi_s, \zeta) = -\frac{1}{\xi_s M(\xi_s, \zeta)} \int_o^{\xi_s} \xi \frac{\partial}{\partial \zeta} \left[M(\xi, \zeta) V(\xi, \zeta) \right] d\xi. \quad (4.11)$$

The notation (ξ, ζ) is included to designate the variables that are functions of both the radial and axial coordinates.

As noted in section 4.2.1, the mean molecular weight M of the mixture is related to X_A, the mole fraction of gas A, by the equation $M = X_A(M_A - M_B) + M_B$. Thus, values of M on the right hand side of equation 4.11 may be computed as a function of position in the

diffusion flow field on the basis of the concentration distribution of gas A in the flow field.

Program VELOCITY, a copy of which is included in Appendix C, is used to solve equation 4.11 for the radial components of the mass average velocity corresponding to a given set of flow conditions. The radial velocity components are computed from experimental data for the concentration and axial mass average velocity distributions.

As indicated on the right hand side of equation 4.11, the computations involve both integration and differentiation. Integration is performed using the trapezoid rule, since that rule is applicable for either an even or an odd number of subintervals and it is an acceptably accurate approximation for use with the experimental data. In accordance with the trapezoid rule, the integral on the right hand side of equation 4.11 may be written as follows for node $j = j_s$ corresponding to an arbitrary radial location ξ_s:

$$\int_0^{\xi_s} \xi \frac{\partial}{\partial \zeta} (MV)\, d\xi = \frac{\Delta \xi}{2} \left[\cancel{\left(\xi \frac{\partial}{\partial \zeta} (MV) \right)_{\xi=0}} \to 0 + 2 \sum_{j}^{j_s-1} \left(\xi \frac{\partial}{\partial \zeta} (MV) \right)_j + \left(\xi \frac{\partial}{\partial \zeta} (MV) \right)_{\xi=\xi_s} \right]$$

The derivatives in the preceding equation are computed using five-point differentiation formulas similar to those discussed in section 4.2.1.

4.2.2.2. Axial Components of the Velocity of Gas A

The mass flux of constituent A relative to the mass average velocity of a mixture is defined as $\vec{j}_A = \rho_A(\vec{v}_A - \vec{v})$. In accordance with Fick's first law of diffusion, $\vec{j}_A$ is related to the mass fraction of constituent A, defined as $\omega_A = \rho_A/\rho$, in the following way (Bird, et al. (1960), Table 16.2-1):

$$\vec{j}_A = -\rho D_{AB} \vec{\nabla} \omega_A .$$

Considering only the mass flux in the axial direction, and using the former equation to substitute for $\vec{j}_A$ in the latter, the following equation is obtained:

$$\rho_A(v_{A_z} - v_z) = -\rho D_{AB} \frac{\partial \omega_A}{\partial z} .$$

With the use of the relationships $M = \rho/C$ and $\frac{\partial \omega_A}{\partial z} = \frac{M_A M_B}{M^2} \frac{\partial X_A}{\partial z}$ (Bird, et al. (1960), Table 16.1.1), and after some rearranging, the preceding equation may be rewritten as follows:

$$v_{A_z} = v_z - \frac{C^2}{\rho \rho_A} M_A M_B D_{AB} \frac{\partial X_A}{\partial z} .$$

Finally, noting that $C_A = \rho_A/M_A$, $C = \rho/M$, and $X_A = C_A/C$, the equation for the axial velocity component of gas A relative to stationary coordinates is

$$v_{A_z} = v_z - \frac{1}{X_A} \frac{M_B}{M} D_{AB} \frac{\partial X_A}{\partial z} .$$

After incorporating the nondimensional variables $\zeta = \frac{z}{R}$, $V_A = \frac{v_{A_z}}{|\bar{V}_{A_o}|}$, $V = \frac{v_z}{|\bar{V}_{A_o}|}$, and $Pe = \frac{2R|\bar{V}_{A_o}|}{D_{AB}}$, the equation in nondimensional form for the axial velocity component of gas A at any position (ξ,ζ) in the diffusion flow field is

$$V_A(\xi,\zeta) = V(\xi,\zeta) - \frac{2}{X_A(\xi,\zeta)} \frac{M_B}{M(\xi,\zeta)Pe} \frac{\partial X_A(\xi,\zeta)}{\partial \zeta} . \quad (4.12)$$

As in equation 4.11, the notation (ξ,ζ) is included to designate the variables that are functions of both the radial and axial coordinates.

Solutions to equation 4.12 are obtained using program VELOCITY and experimental data for the concentration and velocity distributions. As in the programming for equation 4.11, five-point formulas similar to those discussed in section 4.2.1 are used for computing derivatives of X_A.

4.2.2.3. Radial Components of the Velocity of Gas A

The continuity equation for steady flow of constituent A of a nonreacting mixture is $\vec{\nabla}\cdot(\rho_A\vec{v}_A) = 0$. If the flow is axisymmetric, the continuity equation in cylindrical coordinates becomes

$$\frac{1}{r}\frac{\partial}{\partial r}\left[r(\rho_A v_{A_r})\right] + \frac{\partial}{\partial z}(\rho_A v_{A_z}) = 0.$$

The preceding equation may be expressed in terms of X_A rather than ρ_A, noting that $\rho_A = C_A M_A$ and that $C_A = CX_A$. After making these substitutions and then proceeding in the same manner used to formulate equation 4.11, the following equation in nondimensional form is obtained for the radial velocity component of gas A at any position (ξ_s,ζ) in the flow field:

$$U_A(\xi_s,\zeta) = -\frac{1}{\xi_s X_A(\xi_s,\zeta)}\int_o^{\xi_s} \xi\frac{\partial}{\partial\zeta}\left[X_A(\xi,\zeta)V_A(\xi,\zeta)\right]d\xi \quad . \quad (4.13)$$

Solutions to equation 4.13 are obtained using program VELOCITY. The computational methods used are similar to those described for equation 4.11.

4.2.3. Flow Charts for Computer Programs

Abbreviated flow charts for programs VELOCITY and TFIELD are shown in Figures 4.2 and 4.3. Program VELOCITY

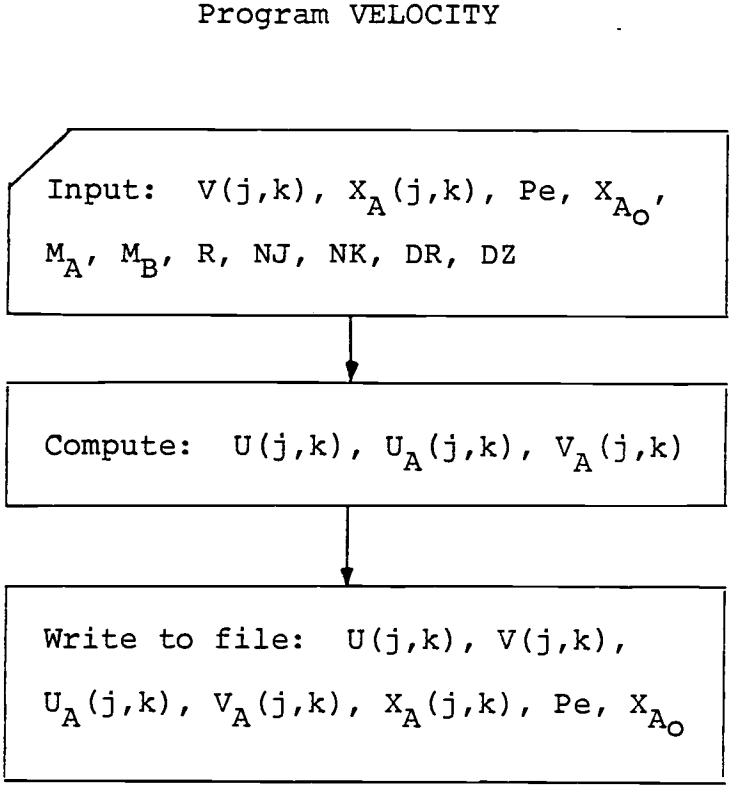

Figure 4.2. Flow Chart for Program VELOCITY

Program TFIELD

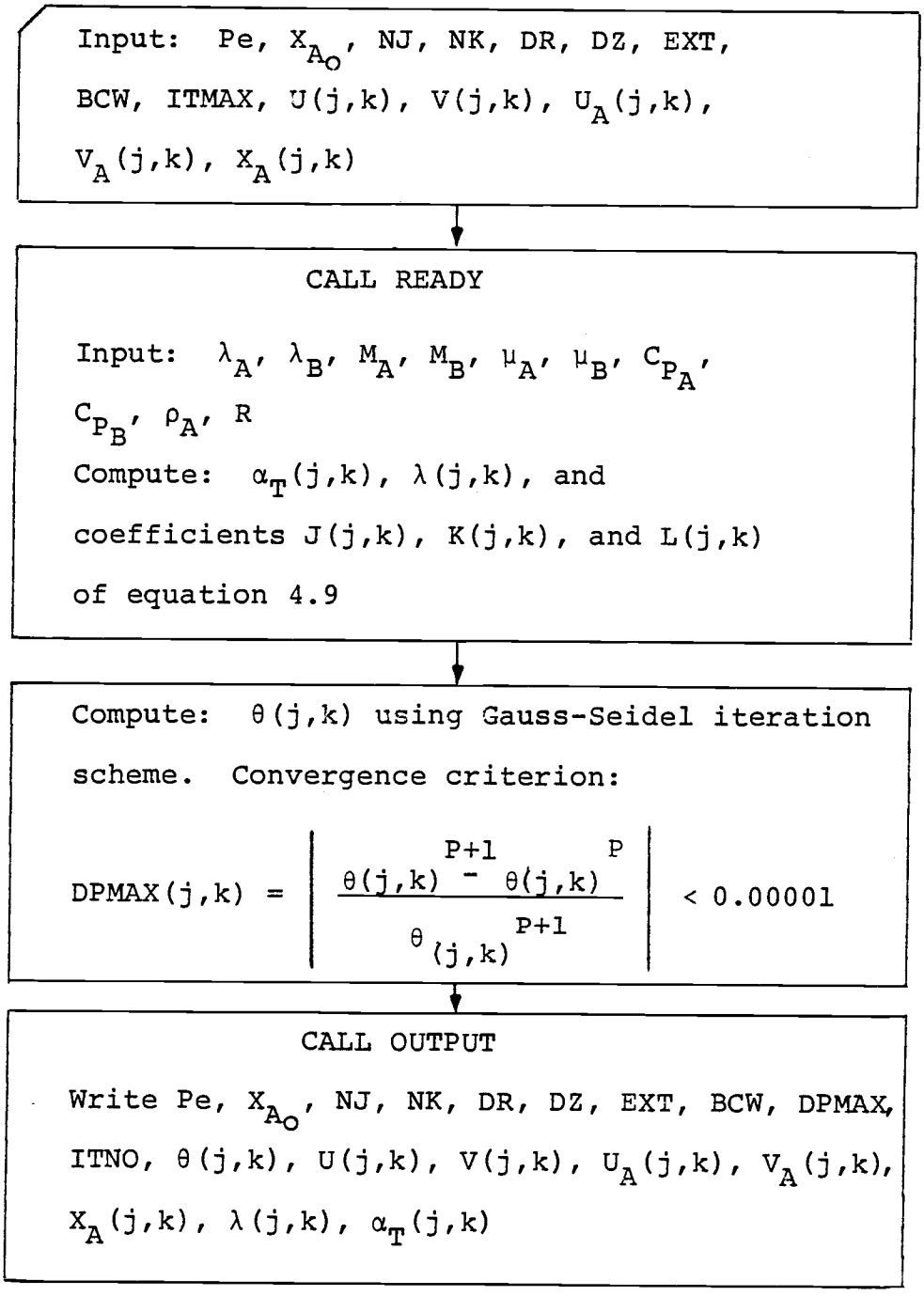

Figure 4.3. Flow Chart for Program TFIELD

is used to compute velocity components needed in program TFIELD for computations of the temperature distributions.

4.3. Data Used for Computing the Temperature Distributions

Fluid properties and related data used in computing the temperature distributions for the flow conditions discussed in section 4.4.1 are summarized in Table 4.1, together with citations for the references from which the data were obtained.

The specific volume of nitrogen at atmospheric pressure is one of the fluid properties listed in Table 4.1. To obtain the corresponding value at the diffusion tube pressure assumed for computing the temperature distributions, Boyle's law was used.

For most gases at pressures below 10 atmospheres, values of the viscosity and the thermal conductivity are essentially invariant as a function of pressure (Bird, et al. (1960)). Accordingly, these transport properties were assumed to be independent of pressure in the computations for the temperature distributions.

4.3.1. Formula Used for Computing Thermal Conductivities of Helium-Nitrogen Mixtures

The thermal conductivities listed in Table 4.1 are those for pure helium and pure nitrogen. Thermal conduc-

Table 4.1. Fluid Properties and Related Data

Notes:

1. All energy values are expressed in terms of the thermochemical calorie, which is defined by the National Bureau of Standards as follows: 1 cal = 4.1840 joules (N.B.S. TN 270-3, January, 1968).

2. Molecular weights are based on the atomic mass of $^{12}C = 12$ exactly.

3. Complete citations for the references are given in the bibliography.

Fluid Property	Gas A Nitrogen	Gas B Helium	Source of Data
Molecular Weight, gm/mol	28.0134	4.0026	N.B.S. TN 270-3, January, 1968
Specific Heat, cal/(gm° K)	0.2485	1.2412	Touloukian and Makita, 1970
Specific Volume @ 294.26° K and 1 atm, cm^3/gm	761.493	not needed	N.B.S. TN 129, January, 1962
Thermal Conductivity @ 294.26° K, cal/(cm sec °K)	6.109×10^{-5}	3.540×10^{-4}	Touloukian, Liley, and Saxena, 1970
Viscosity @ 294.26° K and 1.13 atm, μ poise	176.16	197.01	Kestin, Paykoc, and Sengers, 1971

Related Data (from N.B.S. TN 270-3, January 1968)

$\tilde{R}$ = gas constant = 1.98717 cal/(mol °K)

0° C = 273.15° K

tivities of helium-nitrogen mixtures are required for computations of the temperature distributions. Since the required values are not readily available in the literature, they were estimated from the values for the pure gases.

A formula developed by Mason and Saxena (1958) was used for estimating the thermal conductivities of the gas mixtures. Comparisons of computed and experimental results performed by Mason and Saxena for a number of monatomic and polyatomic gas mixtures indicate that the formula is accurate to within approximately four percent for mixtures containing nonpolar gases. In terms of the notation used in this thesis, the formula is as follows:

$$\lambda(j,k) = \frac{\lambda_A}{1 + \phi_{AB} \frac{X_B(j,k)}{X_A(j,k)}} + \frac{\lambda_B}{1 + \phi_{BA} \frac{X_A(j,k)}{X_B(j,k)}} \qquad (4.14)$$

where

$$\phi_{AB} = \frac{\frac{1.065}{2\sqrt{2}}\left[1 + \left(\frac{\mu_A}{\mu_B}\right)^{1/2}\left(\frac{M_B}{M_A}\right)^{1/4}\right]^2}{\left(1 + \frac{M_A}{M_B}\right)^2}$$

and the expression for ϕ_{BA} is obtained by interchanging subscripts in the expression for ϕ_{AB}.

The (j,k) notation is included in equation (4.14) for convenience in relating the thermal conductivities to the nodes in the finite difference grid used for computa-

tions of the temperature distributions. As seen from equation 4.14, the thermal conductivity at node (j,k) is a function of the mole fractions X_A and X_B of the two gases at the node. The relative proportions of the two gases vary as a function of position in the diffusion tube, and therefore the thermal conductivity varies from node to node in the finite difference grid. An array of thermal conductivities must be specified over the entire grid in order to compute the temperature distributions for a given set of flow conditions.

4.3.2. Thermal Diffusion Factors

A second transport property that must be specified at each node in the finite difference grid is the thermal diffusion factor.

Several investigators (e.g. Ibbs and Grew (1931), Yang (1966), and Wyatt (1968)) have performed experimental investigations from which values of the thermal diffusion factor were obtained for helium-nitrogen mixtures. As discussed in section 7.2 of Chapter VII, the experimental results reported by these investigators are not consistent. Furthermore, the experimental results are for a range of mole fractions of the two component gases that only partially overlaps the range of mole fractions in the gas mixtures under consideration in this thesis. Thermal

diffusion factors predicted on the basis of the kinetic theory of gases were, therefore, used in the computations for the temperature distributions.

General equations for the transport coefficients that have been formulated as part of the rigorous kinetic theory of gases (the Chapman-Enskog theory) are very complex. Chapman and Cowling (1970) have devised a method involving the use of successive approximations to obtain approximate solutions to the equations. An alternate method has been devised by Kihara (1953) and extended by Mason (1957). The approximations developed for the thermal diffusion factor are much more complicated than those for the other transport coefficients.

Even the first approximations obtained by these methods require a great deal of computational effort to produce numerical results. Higher approximations for the thermal diffusion factor are so complicated that they are very difficult to use (Mason, et al. (1964)), and therefore their use is generally restricted to investigations requiring the highest accuracy attainable (such as investigations involving thermal diffusion to study intermolecular forces).

Thermal diffusion factors for helium-nitrogen mixtures have been computed by Yang (1966) using first approximations for the Chapman-Cowling and the Kihara methods. With each method, Yang considered two inter-

molecular potential energy functions: the Lennard-Jones (12-6) potential, and the modified Buckingham (exp-6) potential. Both of these potential energy functions are in common use for computing properties of gases, and they are defined in most references on kinetic theory (e.g. Hirschfelder, et al. (1954); Chapman and Cowling (1970)).

The thermal diffusion factors computed by Yang are plotted in Figure 4.4 as a function of the mole fraction of nitrogen. As shown in this figure, the computed values are strongly influenced by the type of potential energy function chosen to model the molecular interactions, and they are influenced to a lesser extent by the type of approximation (Chapman-Cowling or Kihara) used to perform the computations.

On the basis of comparisons of computed and experimental values for a variety of mixtures containing monatomic and polyatomic gases, Mason, et al. (1964) concluded that neither of the first approximations obtained by the Chapman-Cowling and Kihara methods is generally superior to the other for computing thermal diffusion factors.

Saxena and Mathur (1965) concluded from a critical review of thermal diffusion data for noble gases that for binary gas mixtures containing helium as a component, use of the Lennard-Jones (12-6) potential in computations of

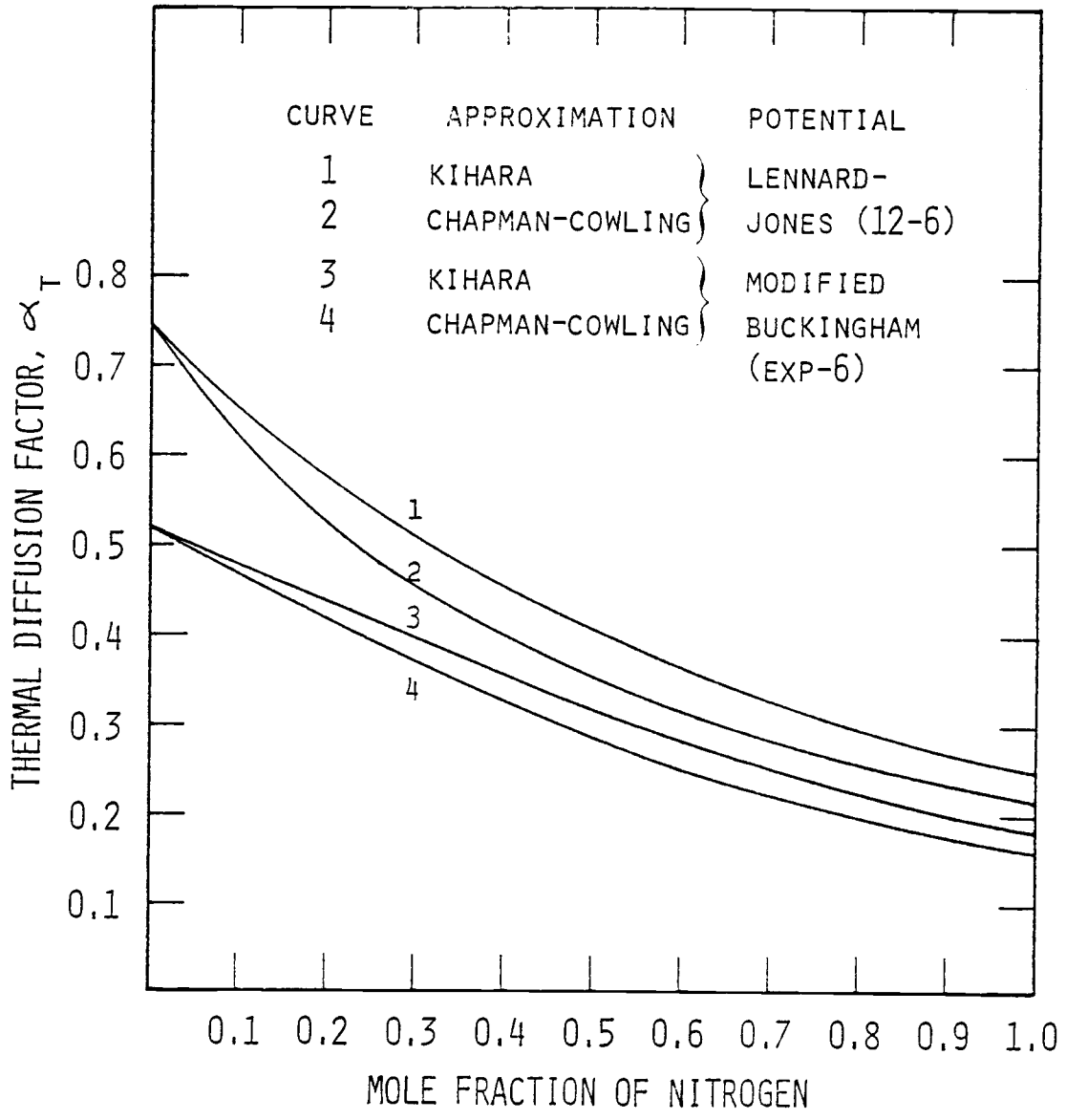

Figure 4.4. Composition Dependence of the Thermal Diffusion Factor for Helium-Nitrogen Mixtures*

* Computed by Yang (1966)

thermal diffusion factors leads to values that are systematically higher than those measured experimentally. They attributed this discrepancy to the use of the power 12 for the repulsive force index in the potential, and stated that a lower power would be more suitable. They also concluded that the modified Buckingham (exp-6) potential is a satisfactory model for representing molecular interactions in such mixtures.

The thermal diffusion factors used in program TFIELD are those computed by Yang (1966) with the Chapman-Cowling first approximation and the modified Buckingham (exp-6) potential. For convenience in programming Yang's results, a regression curve was fitted to the values of the thermal diffusion factor corresponding to increments of 0.05 in the mole fraction of nitrogen over the range of 0.0 to 1.0. The regression equation is as follows:

$$\alpha_T(j,k) = 0.52030 - 0.57230\, X_A(j,k) + 0.21043[X_A(j,k)]^2. \qquad (4.15)$$

This equation fits Yang's results with a coefficient of determination, R^2, of 0.9998. (As discussed in standard references on regression analysis (e.g. Draper and Smith (1966)), the coefficient of determination is a measure of the amount of variation that is accounted for by the regression equation.)

4.4. Computed Temperature Distributions

4.4.1. Flow Conditions Modeled

Using programs VELOCITY and TFIELD, temperature distributions were computed for flow-coupled diffusion occurring within the vertically oriented, cylindrical tube illustrated in Figure 4.1. The flow conditions that were modeled are the same as those investigated experimentally using the apparatus discussed in chapter V. These flow conditions are as follows:

Pe = 1.9, X_{A_o} = 0.5,

Pe = 3.8, X_{A_o} = 0.5,

Pe = 3.8, X_{A_o} = 0.7, and

Pe = 5.9, X_{A_o} = 0.7.

For each set of flow conditions, the value of X_{A_o} is the mole fraction of gas A (nitrogen) at the gas B (helium) injection plane.

In keeping with the size of the diffusion tube used in the experimental apparatus and the conditions under which it was operated, the following data were used in modeling the flow conditions:

Diffusion tube radius, R: 0.96 cm.

Diffusion tube pressure, p: 86 cm Hg.

Temperature of each gas entering the diffusion tube, T_o: 21.1° C.

Velocity and concentration distributions used in the computations are tabulated in Appendix H.

The diffusion tube wall was modeled in two ways: as an adiabatic boundary, and as an isothermal boundary. For solutions in which the wall was treated as an isothermal boundary, the wall temperature was fixed at the same temperature, T_o, specified for the two gases entering the diffusion tube.

The latter boundary condition is a better approximation than the former for modeling the thermal characteristics of the wall of the diffusion tube used in the experimental apparatus. As discussed in Chapter V, the diffusion tube used for the experimental work is housed together with the flow circuits for the two gases within an enclosure in which the temperature is essentially constant. Since the thermal conductivity of the diffusion tube wall is considerably higher than that of either the air surrounding the diffusion tube or the gas mixture confined within it, the wall tends to have the characteristics of an isothermal boundary.

For all computations, a grid spacing of 0.1 was used in the radial ($\Delta\xi = \Delta r/R$) and axial ($\Delta\zeta = \Delta z/R$) directions. The axial length of the grid system was

varied as necessary to accommodate the changes in length of the diffusion flow field as a function of the flow conditions.

Computed values for the temperature distributions discussed in this chapter are contained in Appendix D.

4.4.2. Examples of Computer Times Required to Achieve Solutions

As would be expected, the computer time required to solve for the temperature distribution corresponding to a given set of flow conditions was found to depend upon the size of the grid system, the wall boundary condition (adiabatic or isothermal) chosen for the solution, and the level of convergence specified for terminating the solution. For example, with 744 nodes in the finite difference grid, an overrelaxation factor of 1.25, and the isothermal wall boundary condition, 66 iterations were required to solve for the temperature field corresponding to Pe = 3.8, $X_{A_o} = 0.5$. Under the same conditions except for the use of 806 nodes and the adiabatic wall boundary condition, 148 iterations were required. Running times on the C.D.C. 3300 computer at Oregon State University were 72 seconds and 134 seconds, respectively, for these cases.

The maximum relative error at any node (defined as $\left|\frac{\theta^{P+1} - \theta^{P}}{\theta^{P+1}}\right|$, where θ is the dimensionless temperature at the node and P is the iteration number) was limited to

1×10^{-5} for the solutions described above. With the maximum relative error at any node limited to 1×10^{-7}, 84 iterations and 101 seconds were required to achieve a solution for the isothermal wall case.

4.4.3. Centerline Temperature Profiles

Shown in Figures 4.5 through 4.8 are centerline temperature profiles plotted from the temperature distributions that were computed for the flow conditions discussed in section 4.4.1. Also shown in these figures are centerline concentration and temperature profiles that were measured experimentally. The concentration profiles were measured by Stock (1972).

As illustrated in Figure 4.1, axial positions within the diffusion tube are measured upstream of and relative to the gas B (helium) injection plane. Accordingly, in Figures 4.5 through 4.8 the helium injection plane is located at the origin of the axial coordinate, and this coordinate ($\zeta = z/R$) extends in a direction opposite to the direction of bulk flow through the diffusion tube.

Gas A (nitrogen) flows upward through the diffusion tube and gas B (helium) diffuses against the flow, as discussed in section 4.1. The gas mixture flows past the helium injection plane to the diffusion tube outlet.

Along the direction of flow, the proportion of helium contained in the gas mixture increases from zero at locations far upstream of the helium injection plane to a value that can be varied arbitrarily at the injection plane. As shown in Figures 4.5 through 4.8, the axial concentration gradients vary as a function of the Peclet number for the flow field and the relative proportions of the two gases entering the diffusion tube.

Associated with the concentration gradients are temperature gradients resulting from the transport of energy due to the diffusion-thermo effect. As illustrated in Figures 4.5 through 4.8, the temperature of the gas mixture along the direction of flow decreases from the reference temperature of the incoming gases to a minimum value that varies in magnitude and axial position with the flow conditions. Downstream of this minimum the temperature increases on a steep gradient toward the reference temperature of the helium at the helium injection plane.

Within most interdiffusing gas mixtures, the temperature rises where the lighter gas is in excess and falls where the heavier gas is in excess (Grew and Ibbs (1952)). The temperature profiles shown in Figures 4.5 through 4.8 are consistent with this observation, for the heavier gas (nitrogen) is the dominant gas in the flow field at all locations upstream of the helium injection

plane, and the temperature effects in this region are negative relative to the reference temperature of the incoming gases.

In the following paragraphs, comparisons are made between the temperature profiles computed on the basis of the isothermal and adiabatic boundary conditions at the diffusion tube wall. Comparisons are also made between the computed and experimental temperature profiles. The experimental results are discussed in more detail in Chapter VII.

4.4.3.1. Effects of Boundary Condition at the Diffusion Tube Wall

For the flow field with the lowest Peclet number considered in the calculations, temperatures along the diffusion tube centerline are very sensitive to the boundary condition at the tube wall. As shown in Figure 4.5, the centerline temperature profiles computed for $Pe = 1.9$, $X_{A_o} = 0.5$ on the basis of the adiabatic and isothermal wall boundary conditions are similar in shape, and each profile has a minimum at the same axial location. The minimum temperature corresponding to the adiabatic wall boundary condition, however, is over 1.8 times lower relative to the temperature of the gases entering the diffusion tube than the minimum temperature corresponding to the isothermal wall boundary condition.

As shown in Figures 4.6 and 4.7, the centerline temperature profiles computed for Pe = 3.8, X_{A_o} = 0.5 and Pe = 3.8, X_{A_o} = 0.7 are less sensitive to the boundary condition at the diffusion tube wall than those computed for Pe = 1.9. For Pe = 5.9, which is the highest Peclet number considered in the calculations, the centerline temperature profiles computed on the basis of the adiabatic and isothermal wall boundary conditions are virtually indistinguishable from each other, as shown in Figure 4.8.

The apparent relationship between the Peclet number for the flow field and the sensitivity of the centerline temperatures to the boundary condition at the diffusion tube wall may be attributed to changes in the relative magnitudes of the mass transport processes that occur as a function of the Peclet number. As discussed in section 4.1, diffusion is the dominant mass transport process in flow fields with Peclet numbers less than two. Convection becomes dominant to an increasingly greater extent in flow fields with Peclet numbers greater than two. Thus, for increasing values of the Peclet number, the energy of the molecules transported by convection becomes an increasingly significant component of the total energy flux within the diffusion flow field, and the energy transported by conduction through the diffusion tube wall becomes a less significant component of the

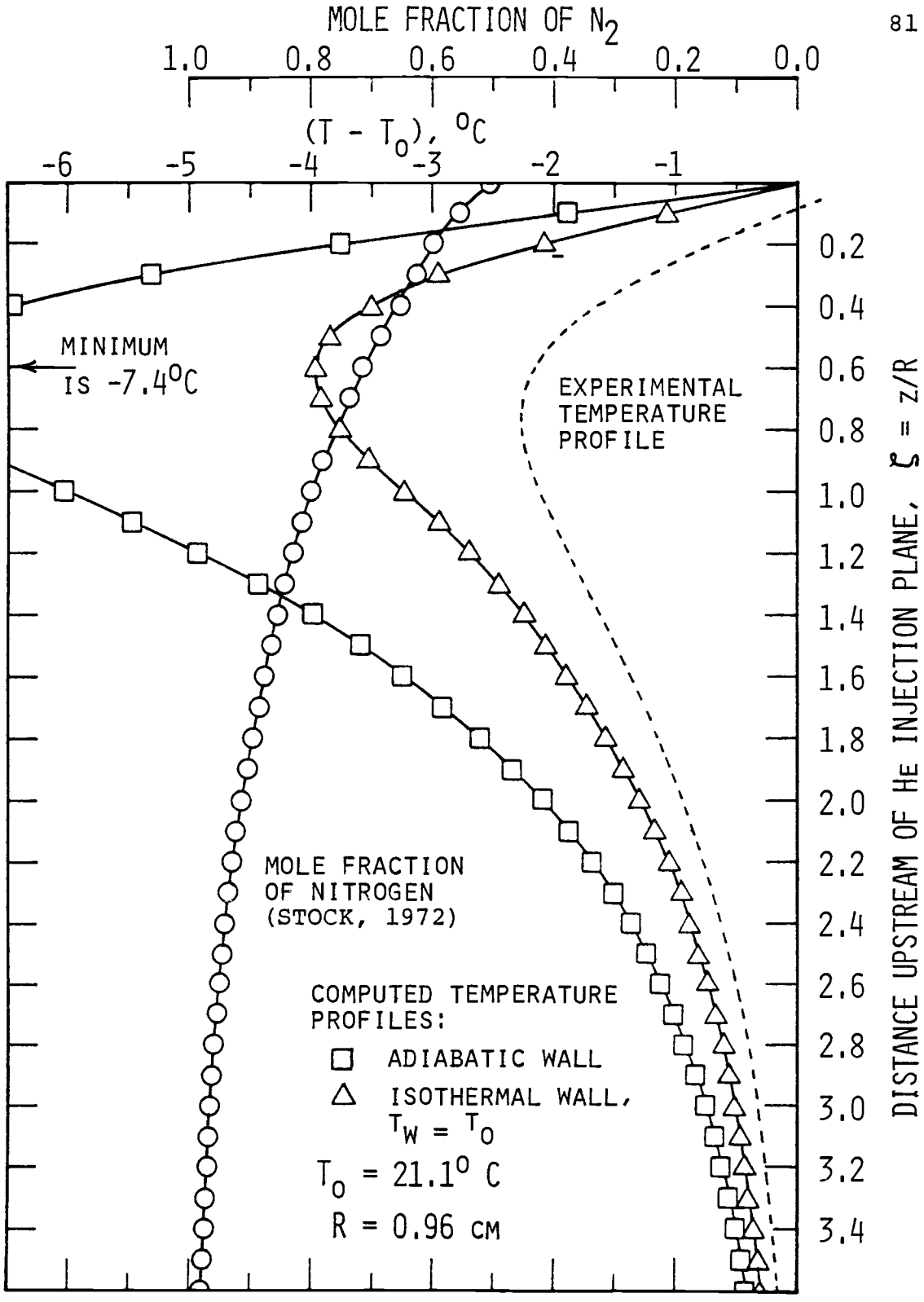

Figure 4.5. Experimental and Theoretical Centerline Temperature Profiles for Pe = 1.9, $X_{A_o} = 0.5$

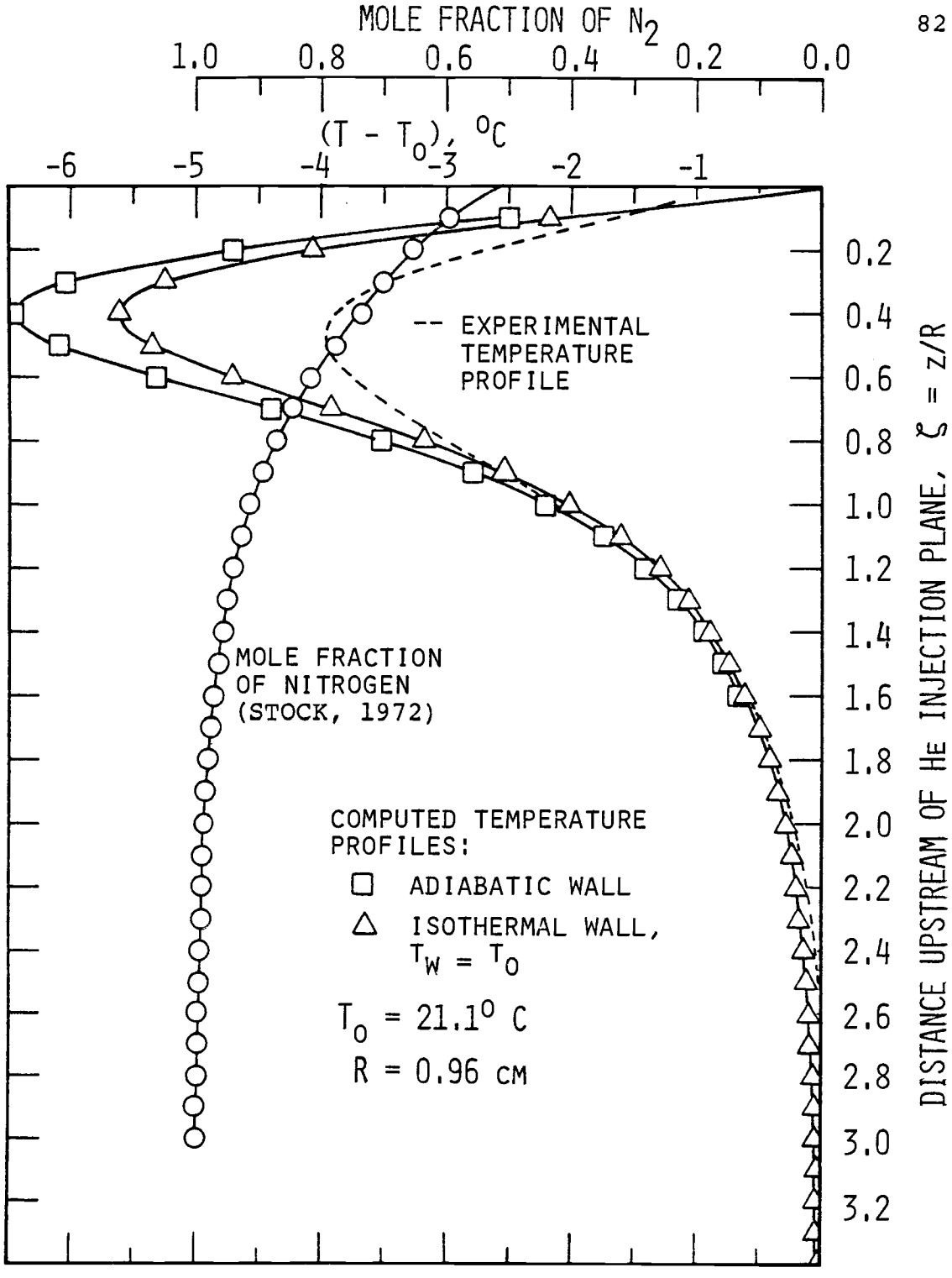

Figure 4.6. Experimental and Theoretical Centerline Temperature Profiles for Pe = 3.8, $X_{A_o} = 0.5$

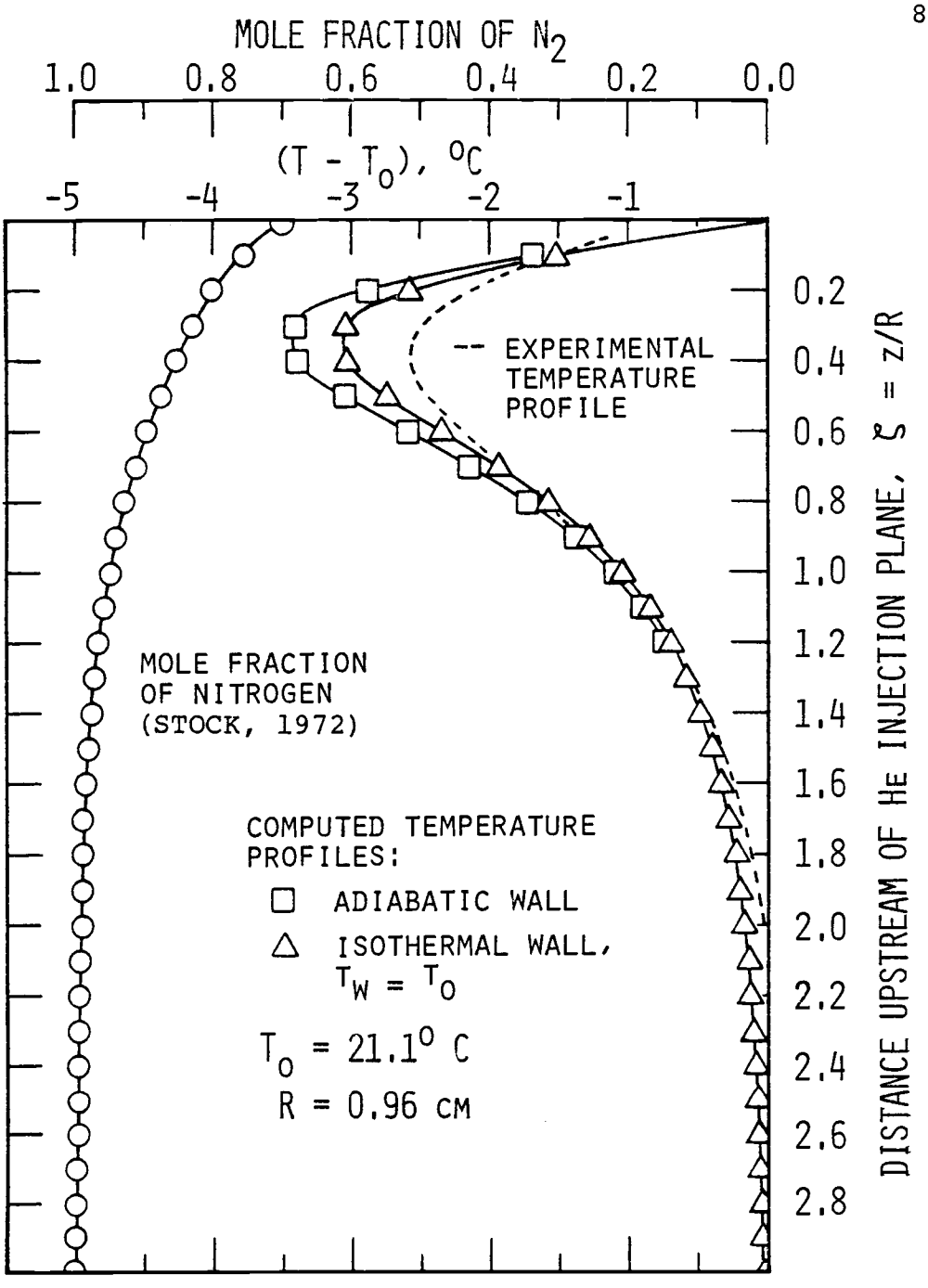

Figure 4.7. Experimental and Theoretical Centerline Temperature Profiles for Pe = 3.8, X_{A_o} = 0.7

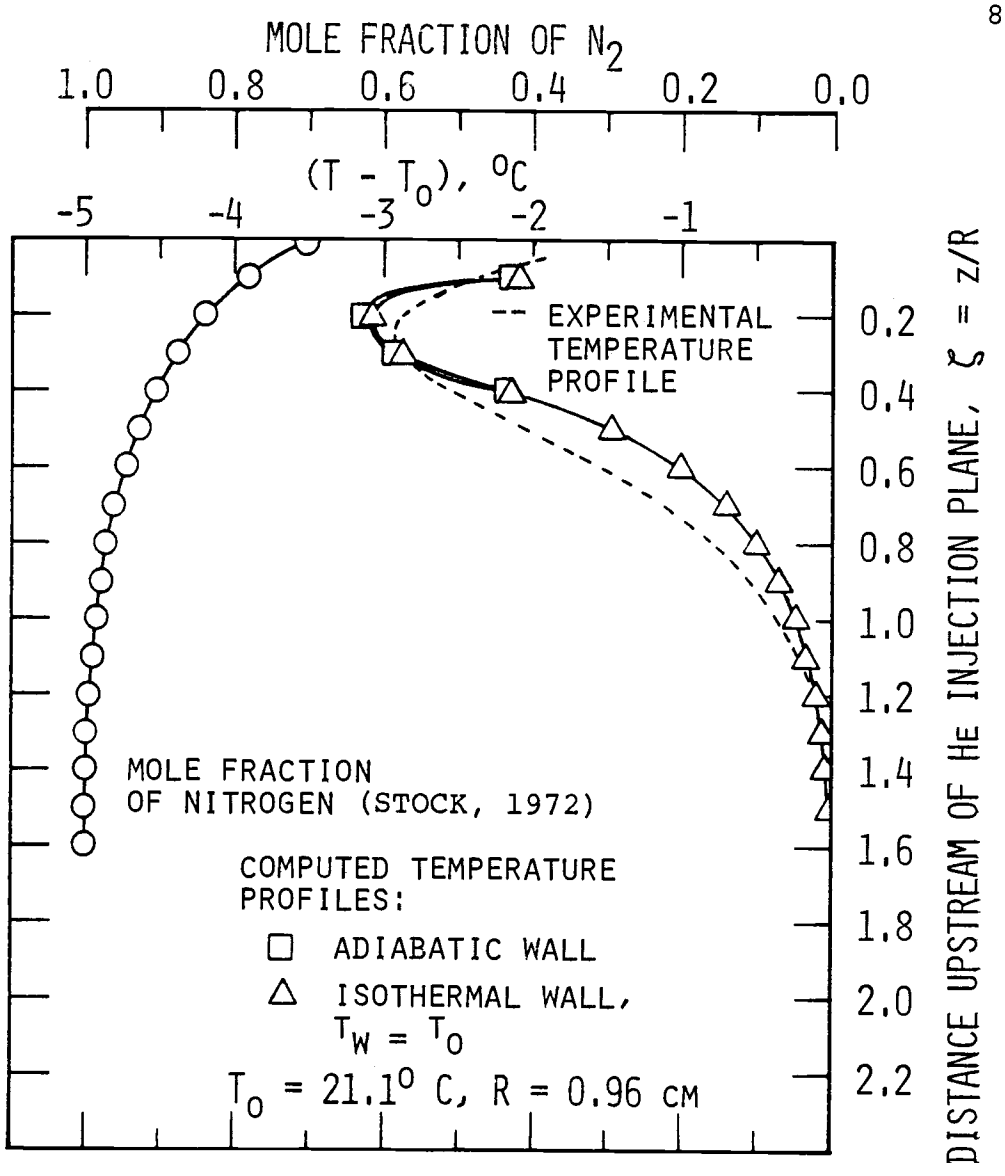

Figure 4.8. Experimental and Theoretical Centerline Temperature Profiles for Pe = 5.9, $X_{A_o} = 0.7$

total energy flux. The centerline temperatures are therefore less sensitive to the boundary condition at the diffusion tube wall for high Peclet numbers than for low Peclet numbers.

4.4.3.2. Comparisons of Computed and Measured Temperature Profiles

In the discussion that follows, temperature profiles computed on the basis of the isothermal boundary condition at the diffusion tube wall are compared with those measured experimentally. Attention is restricted to the isothermal wall boundary condition for the computed temperature profiles because it is a closer approximation than the adiabatic boundary condition to the conditions under which the temperature profiles were measured experimentally, as discussed in section 4.4.1.

As shown in Figures 4.5 through 4.8, the centerline temperature profiles computed for the four sets of flow conditions are similar in shape to those measured experimentally. The axial positions of the minimum values of the computed temperature profiles are in close agreement with those of the measured temperature profiles. There is also close agreement between the distances that

the computed and measured temperature effects of flow-coupled diffusion extend upstream of the secondary gas injection plane.

Depending on the flow conditions, however, the values of the computed centerline temperatures differ considerably from the corresponding values measured experimentally. Discrepancies between the computed temperatures and the measured temperatures are most pronounced for the flow field corresponding to the lowest Peclet number considered in the calculations. As shown in Figure 4.5, the minimum value of the centerline temperature profile computed for Pe = 1.9, X_{A_O} = 0.5, with the isothermal wall boundary condition, is approximately 1.7 times lower relative to the reference temperature than the minimum value measured experimentally under the same flow conditions. The discrepancies between the computed and measured temperature profiles are less pronounced for the flow conditions corresponding to Pe = 3.8, X_{A_O} = 0.5 and Pe = 3.8, X_{A_O} = 0.7 as shown in Figures 4.6 and 4.7, and, as shown in Figure 4.8, the computed and measured temperature profiles are in good agreement for Pe = 5.9, X_{A_O} = 0.7.

These comparisons indicate that the differences between corresponding values of the computed temperatures and the measured temperatures are strongly influenced by the relative magnitude of convection as a transport pro-

cess within the diffusion flow field. As the energy of the molecules transported by convection becomes an increasingly significant component of the total energy flux, the boundary conditions used for the computations and the errors introduced in the temperature measurements by the presence of instrumentation in the diffusion flow field become less significant in their influence on the differences between the computed and the measured centerline temperature profiles.

4.4.4. Radial Temperature Profiles

Attention is restricted in the discussion that follows to radial temperature profiles plotted from temperature fields that were computed with the diffusion tube wall treated as an isothermal boundary. As discussed in section 4.4.1, the isothermal wall boundary condition is a closer approximation than the adiabatic wall boundary condition to the conditions under which the temperature profiles were measured experimentally.

Shown in Figure 4.9 are radial temperature profiles computed with the isothermal wall boundary condition for flow conditions corresponding to Pe = 1.9, X_{A_o} = 0.5. These profiles are also representative of the radial profiles for the other flow conditions considered in the analysis.

As shown in Figure 4.9, a common characteristic of the radial temperature profiles is that they are essentially parabolic in shape. The temperature profiles tend to be relatively flat, however, in the center core of the diffusion flow field at axial positions near the helium injection plane (where $\zeta = 0$). This is illustrated in the radial profile for $\zeta = 0.6$ plotted in Figure 4.9.

The flattening of the radial temperature profiles at axial positions near the helium injection plane may be attributed to the dependence of the temperature distributions on the velocity and concentration distributions. Radial velocity profiles measured by Stock (1972), which are discussed in Chapter VII together with the other experimental results, tend to be relatively flat in the center core of the diffusion flow field at axial positions near the helium injection plane. Concentration profiles measured by Stock have relatively small radial gradients throughout the flow field. At the positions where the radial velocity and concentration profiles are both relatively flat, the driving forces for radial energy transport are smaller than at other locations in the flow field. Accordingly, the radial temperature gradients are small at these locations.

Radial temperature profiles measured experimentally are similar in shape to the computed temperature profiles

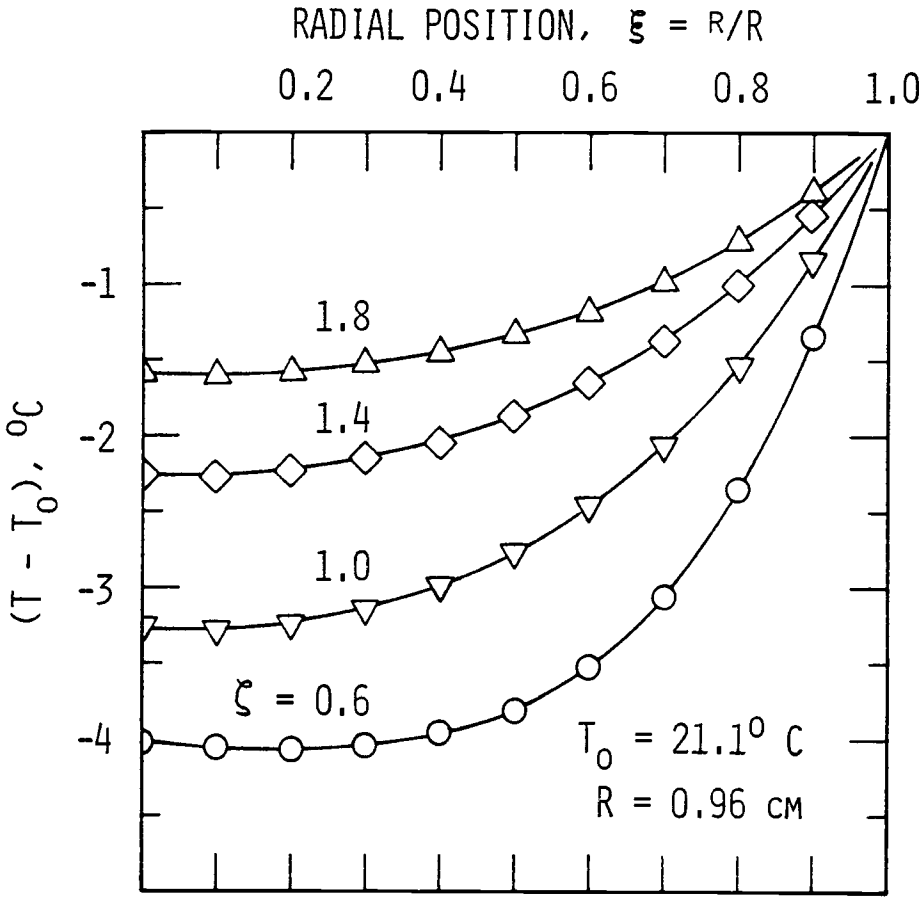

Figure 4.9. Theoretical Radial Temperature Profiles for Pe = 1.9, X_{A_o} = 0.5, Isothermal Wall

shown in Figure 4.9. The experimental measurements are discussed in Chapter VII.

4.4.5. Sources of Error in the Computed Temperature Distributions

The largest source of error in the temperature distributions computed for the four sets of flow conditions is probably that associated with the use of experimental data for the concentration and velocity distributions needed for the computations. As discussed in sections 4.2.1 and 4.2.2, the computations involved both differentiation and integration of the experimental data. Even small errors in experimental data are likely to be magnified to troublesome size when derivatives of the data are taken (Scheid (1968)). Although the five-point differentiation formulas discussed in section 4.2.1 were used to reduce the consequence of irregularities in the data, the derivatives computed with those formulas are, nevertheless, only estimates subject to substantial error.

A second source of error in the computed temperature distributions is that associated with the discrepancies between the boundary conditions chosen for the analysis and the phenomena that the boundary conditions are intended to represent. It is not strictly accurate, for example, to model the diffusion tube wall as either an adiabatic or an isothermal boundary, because the diffusion

tube used in the experimental apparatus is neither perfectly insulated nor maintained at constant temperature. The isothermal wall boundary condition is, however, a reasonable approximation for the temperature along the diffusion tube wall.

As discussed in section 4.1.3.2, the most difficult boundary to model is the one at the gas B injection plane (where $\zeta = 0$). The boundary condition chosen for that plane is a reasonable approximation for the temperatures measured experimentally, but it is not in complete agreement with the experimental results.

Another source of error in the computed temperature distributions is that associated with inaccuracies in the equations used to compute transport properties for the gas mixtures. At each node point in the finite difference grid used for computing the temperature distributions, the thermal conductivity and the thermal diffusion factor must be specified. Both of these transport properties vary as functions of the relative proportions of the two gases. Since experimental values for the transport properties of helium-nitrogen mixtures are not readily available in the literature, they were estimated using the equations and data discussed in section 4.3.

Additional sources of error include those associated with the numerical scheme used for solving the

differential equation (equation 4.9) for the temperature distributions, and those associated with the limitations of the kinetic theory used to model the flow field. These latter sources of error are inherently less severe, however, than the other sources of error discussed in the preceding paragraphs.

V. EXPERIMENTAL APPARATUS

The experimental apparatus used in this investigation is a modified version of the diffusion test facility developed by D. E. Stock and R. J. Zaworski at Oregon State University. As discussed by Stock (1972), the test facility was originally designed for use in investigations of velocity and concentration fields associated with flow-coupled binary gaseous diffusion in the Peclet number range of 2.0 to 8.0. For the investigation discussed in this thesis, the apparatus was modified to incorporate temperature instrumentation, mechanical devices for radial and axial positioning of the temperature probes, thermal shielding, and other changes that would facilitate taking measurements of temperature profiles within diffusion flow fields.

Two oblique views of the test facility and instrumentation, one from the front and one from the back, are shown in Figures 5.1 and 5.2. The principal components and flow systems in the apparatus are described in the following paragraphs.

5.1. Diffusion Cell

A view of the diffusion test facility as it appeared before the thermal shielding and diffusion tube instrumentation were installed is shown in Figure 5.3. In the

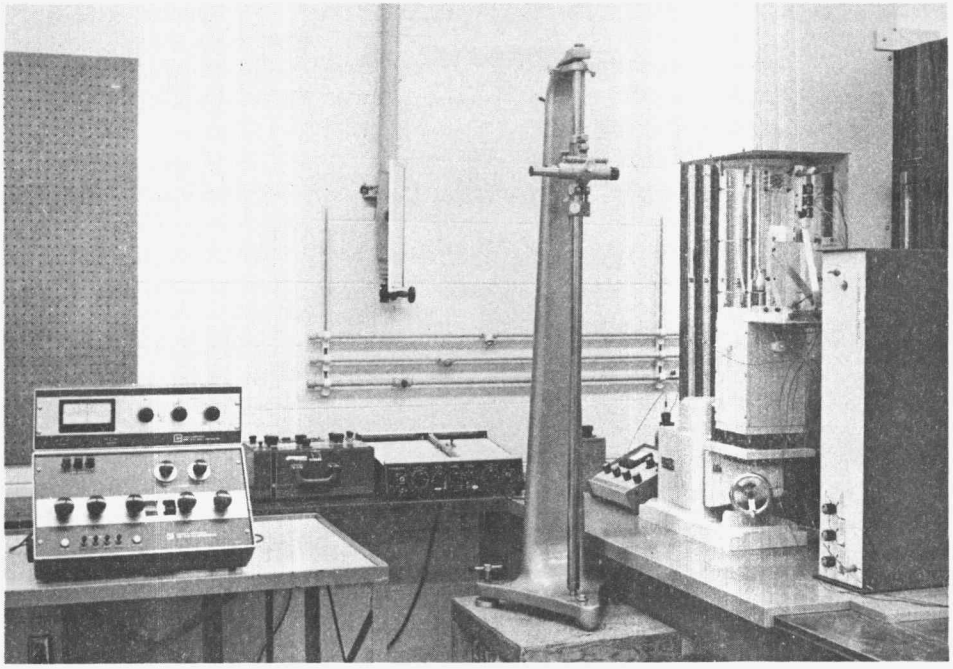

Figure 5.1. Front View of Diffusion Test Facility

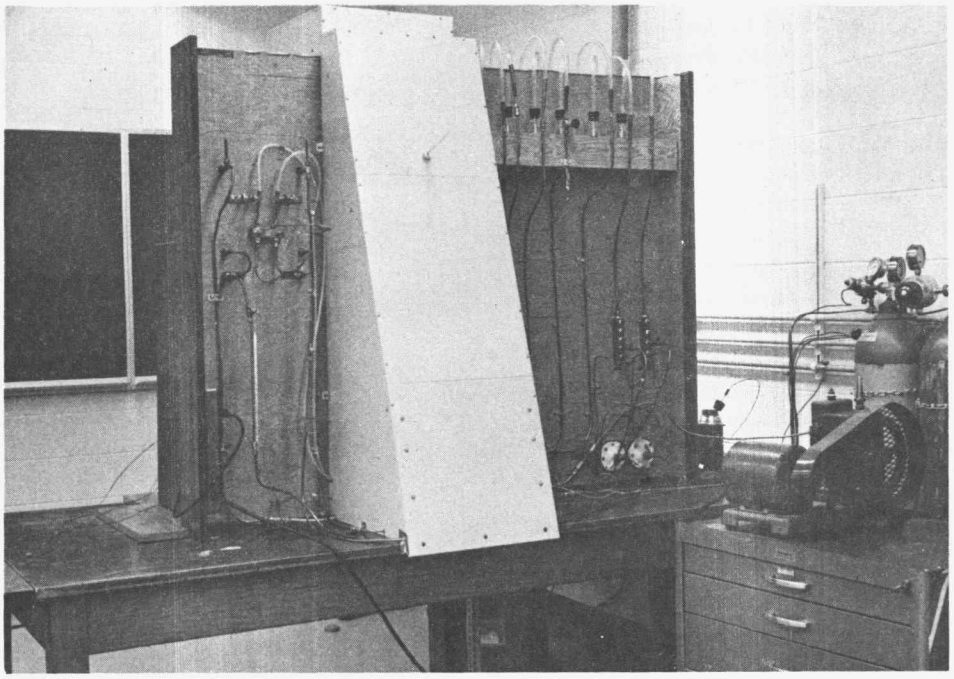

Figure 5.2. Rear View of Diffusion Test Facility

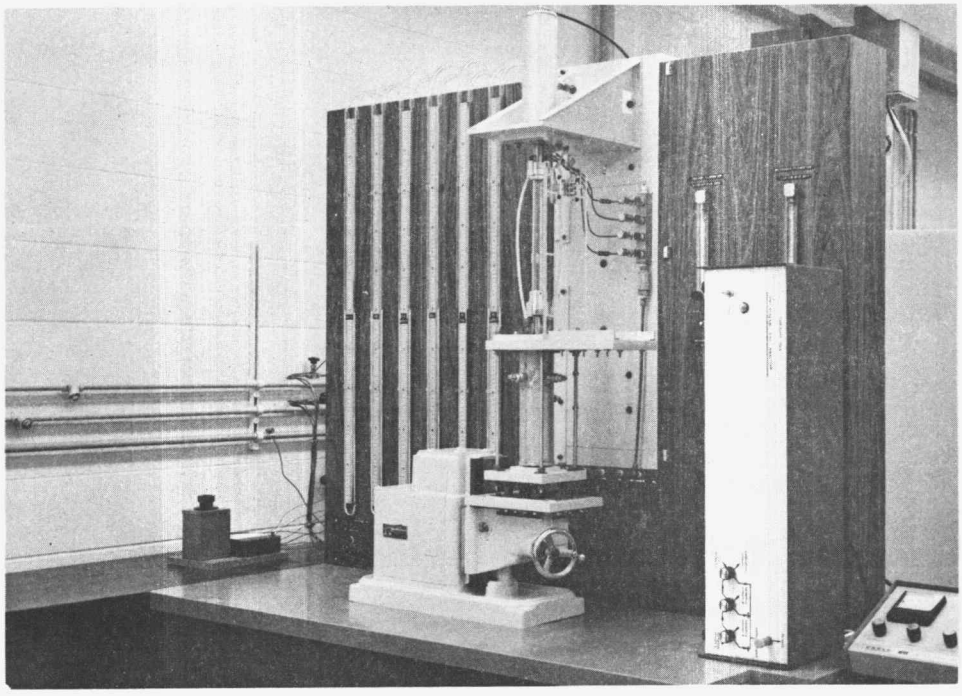

Figure 5.3. Test Facility Without Thermal Shielding and Diffusion Tube Instrumentation

absence of the thermal shielding, the principal components of the diffusion cell are exposed. These include the vertically oriented, plexiglass diffusion tube, the lower and upper plenum chambers, and a set of four capillary needle valves.

As shown in Figure 5.3, the diffusion tube assembly and the lower plenum chamber are mounted on a vertical carriage. The upper plenum chamber and components within it are mounted on a steel frame consisting of a horizontal tapered beam attached to a vertical channel. To allow for rotational as well as axial movement of the diffusion tube assembly relative to the stationary upper plenum chamber, a ball-thrust bearing is used to connect the plate clamped on the carriage to the frame for the lower plenum chamber and diffusion tube assembly. These arrangements facilitate the positioning of instrumentation used for taking data in the diffusion flow field.

All of the components of the apparatus are easily accessible for maintenance, and individual components can be removed with minimal disruption to the rest of the apparatus. The panels for the diffusion cell cover shown in Figures 5.1 and 5.2 are assembled with screws rather than with nails or glue, so that individual panels can be readily removed for access to the components underneath them.

5.1.1. Flow Paths

As shown schematically in Figure 5.4, the primary gas is supplied to the diffusion tube through the lower plenum chamber and the secondary gas is introduced through small diameter injection tubes mounted in the upper plenum chamber. For the work discussed in this thesis, prepurified nitrogen was used as the primary gas and zero gas helium as the secondary gas. The mixture of the two gases flows past the injection tubes through the upper plenum chamber to a vent line.

The 25 tubes through which the secondary gas is injected are mounted symmetrically in the flow cross-section, as shown in Figure 5.4. Each injection tube is made of stainless steel, with an outside diameter of 0.079 cm (1/32 inch) and an inside diameter of 0.028 cm (0.011 inch). The tubes are arranged in three concentric circles with one tube in the center. Twelve tubes are located in the outer circle, and six tubes are located in each of the inner circles.

The secondary gas is supplied to the injection tubes through four headers, one for the center tube and one for each of the three circular banks of tubes. To balance the flow to the tubes supplied from a common header, an equal length of flow resistance tubing is

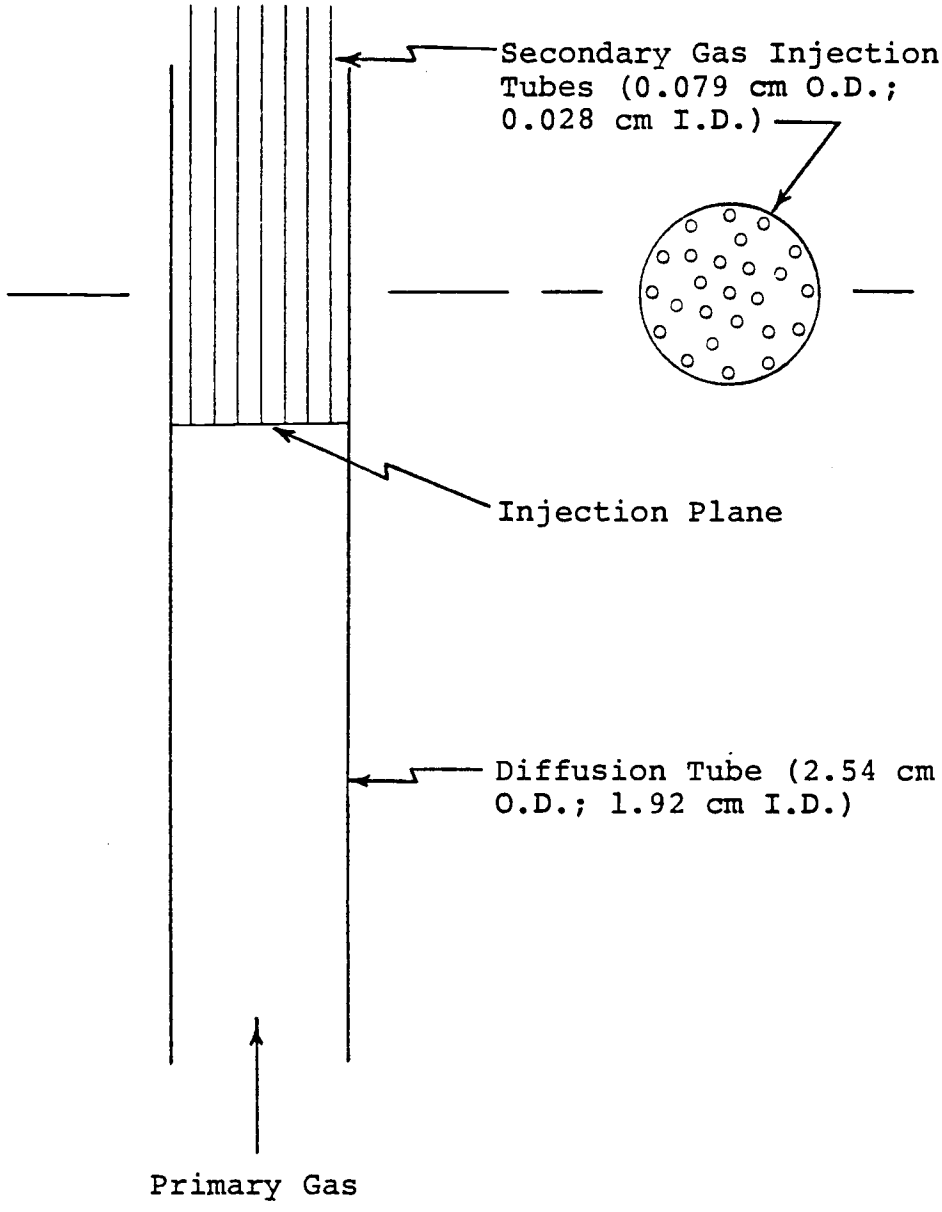

Figure 5.4. Schematic Diagram of Diffusion Cell

installed between the header and each of the tubes in its flow circuit. The headers and associated tubing are located within the upper plenum chamber.

Four Matheson capillary needle valves, one for each header, are used to regulate the distribution of the secondary gas to the separate banks of injection tubes. The four valves are shown in Figure 5.3 to the right of the diffusion tube. To protect the valves and other small diameter passages in the event that particulate material enters the flow system, a filter is located in the supply line upstream of the valves.

5.1.2. Diffusion Tube

A full-scale layout of the upper portion of the diffusion tube is shown in Figure 5.5. The diffusion tube is made of plexiglass, with an outer diameter of 2.54 cm, an inner diameter of 1.92 cm, and a length of 28 cm.

Three ports are provided through which probes can be inserted radially through the wall of the diffusion tube. At the entrance of each port is a Swagelok fitting, which is sized to form a pressure-tight seal around tubing of the diameter (0.159 cm) used for the outer housings of the probe assemblies. (The design of the probe assemblies is discussed in section 5.4.1.) The shoulder in each Swagelok fitting was removed so that the tubing can pass through it,

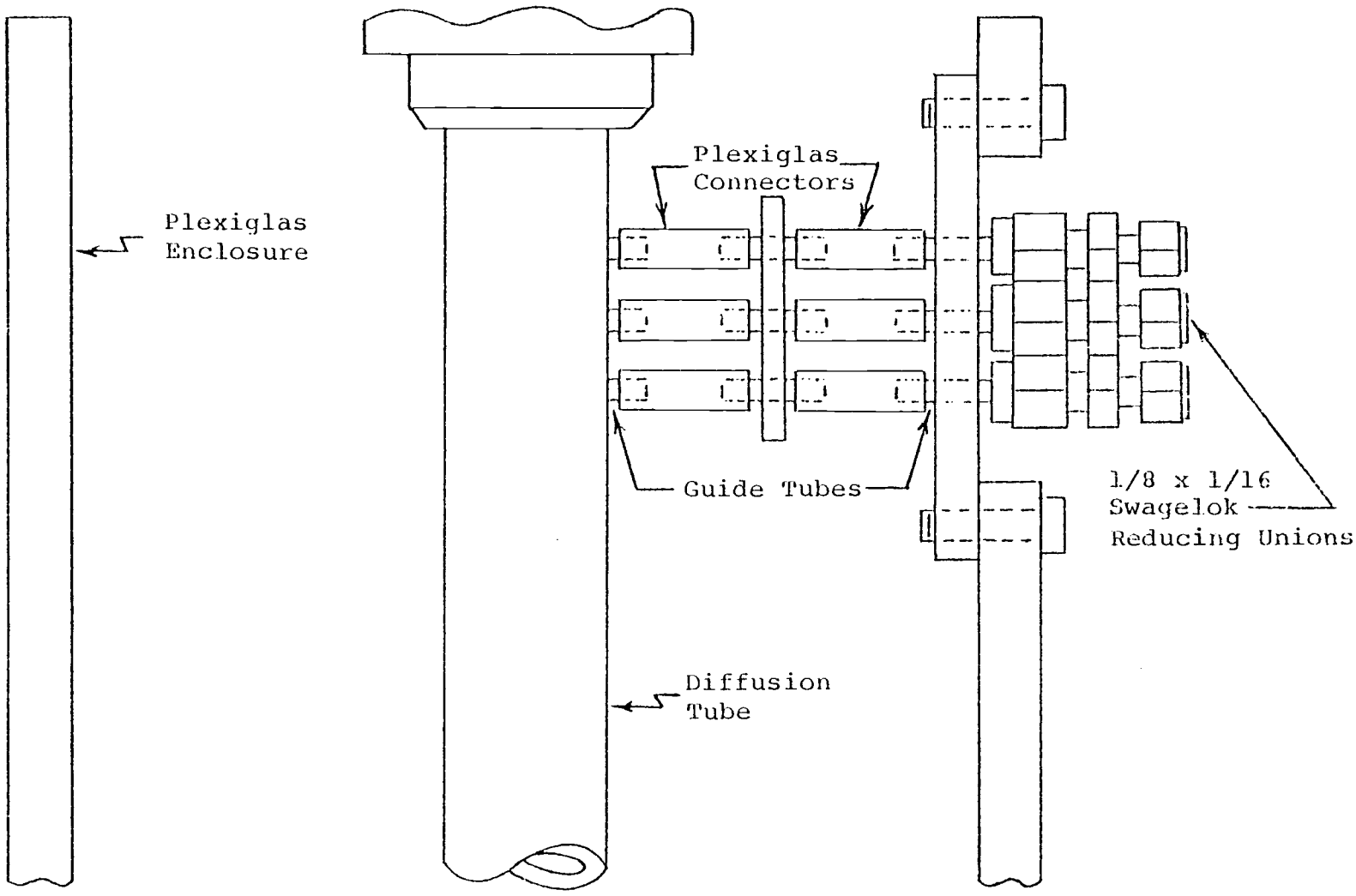

Figure 5.5. Layout of Ports for Diffusion Tube Instrumentation

and each fitting is equipped with nylon ferrels so that a leak-tight seal can be attained without deforming the tubing.

Along the length of approximately 9.3 cm between the entrance of each port and the interior surface of the diffusion tube, three carefully aligned guides are provided so that a probe inserted through the port is constrained to move radially into the diffusion tube. The material used for two of the three guides is hard temper, stainless steel tubing, with an inside diameter of 0.178 cm. This results in a nominal diametral clearance of approximately 0.02 cm between the guides and the probe assembly. The third guide, which is embedded part way into the diffusion tube wall, is made of glass rather than stainless steel, since the thermal resistance of glass more closely matches the thermal resistance of the diffusion tube wall. The guides are coupled with plexiglass tubing and the assemblies are sealed with epoxy cement.

Between the Swagelok fittings and the diffusion tube are two spacer blocks for the stainless steel guide tubes. The outer spacer block is sized to fill the opening cut in the plexiglass panel bolted to it. This arrangement allows for easy removal of the panel without interference from the guide tubes and the Swagelok fittings.

5.2. Gas Supply Circuits, Instrumentation, and Controls

5.2.1. Flow Circuits

Flow circuits for the test facility are shown schematically in Figure 5.6. The system proved to be very stable. After the flow controls were adjusted for a given set of test conditions, generally no additional adjustments were necessary during a typical data collection run of six to eight hours.

Gases for the diffusion apparatus are supplied from high-pressure cylinders equipped with two-stage regulators. Due to the relatively low gas flow rates required under the test conditions considered in this investigation, none of the cylinders had to be refilled during the period of operation necessary to take the data discussed in Chapter VII of this thesis.

To dampen out fluctuations in gas temperatures that might occur in response to small fluctuations in laboratory temperature, and to equalize the temperatures of the two gases before they enter the diffusion tube, a solid aluminum cylinder that serves the same purpose as a constant temperature bath is included in the flow circuit of each gas. Each cylinder is approximately 8.9 cm in diameter and 31 cm long. Tightly clamped to the surface of each cylinder is a coil of copper tubing, which is 0.32 cm in

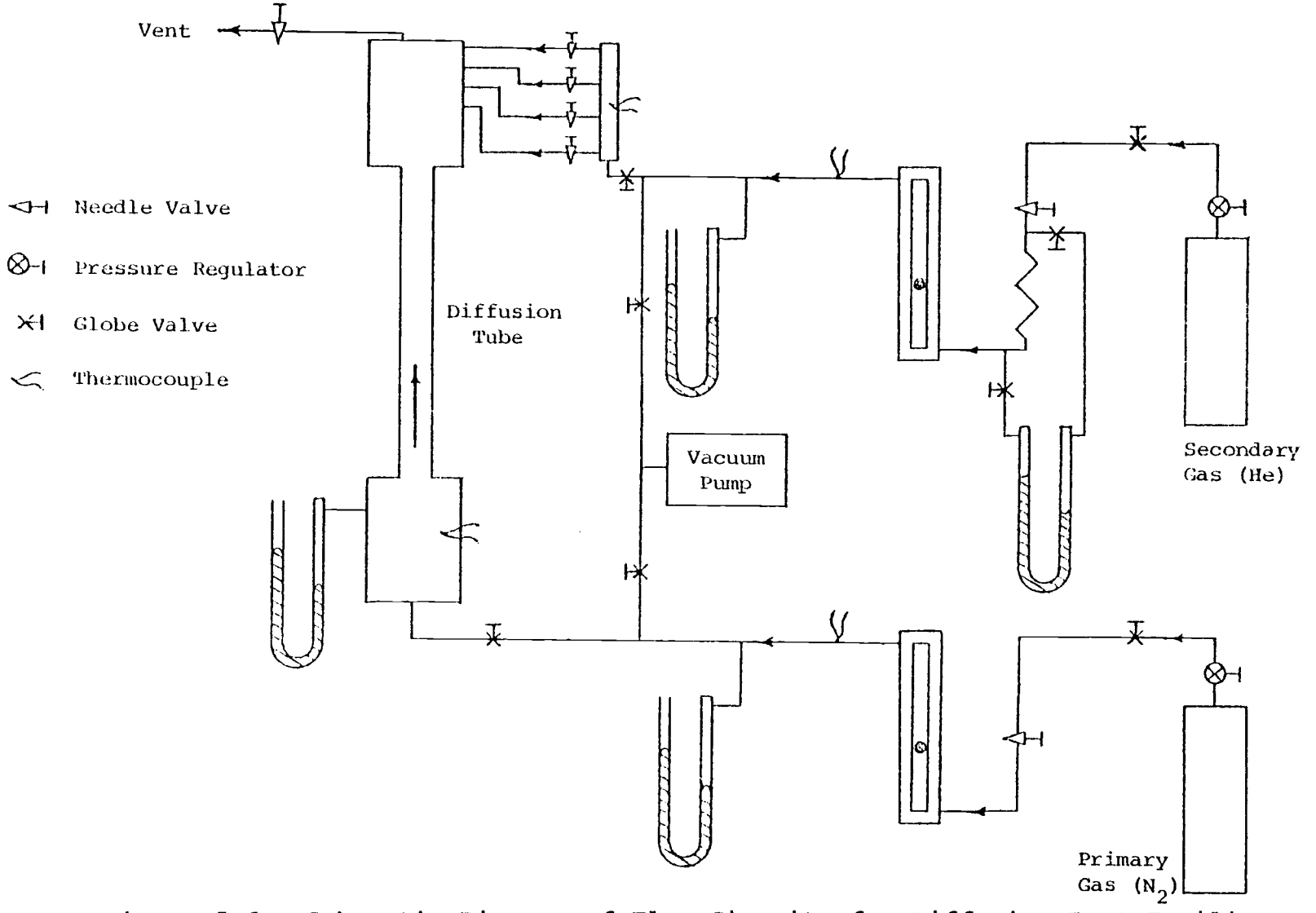

Figure 5.6. Schematic Diagram of Flow Circuits for Diffusion Test Facility

diameter and 762 cm long. The cylinders are mounted together under the cover that is installed over the back of the diffusion apparatus as shown in Figure 5.2, and are therefore shielded from fluctuations in laboratory temperature.

Either of the flow circuits shown in Figure 5.6, together with the diffusion tube, can be evacuated to simplify removal of unwanted gases from the apparatus prior to the start of tests. The vacuum pump shown in Figure 5.2 is used for this purpose. All components in the flow circuits, including the manometers, are designed to withstand a full vacuum without failure.

The vent line at the outlet of the diffusion cell is equipped with a needle valve for use in adjusting the pressure within the diffusion cell. To prevent over-pressurization of the system in the event of equipment malfunction or operator error, the vent line is also equipped with a pressure relief valve at a location upstream of the needle valve. The outlet of the vent line is located in the discharge duct of a laboratory hood, to accommodate the possible use of dangerous gases (such as carbon monoxide) in the diffusion apparatus.

5.2.2. Flow Instrumentation

Manometers and flow meters shown schematically in Figure 5.6 are mounted on a common panel together with the framework for the stationary components of the diffusion cell. As shown in Figure 5.3, the manometers are located to the left and the ball-and-tube flowmeters to the right of the diffusion cell.

All manometers are filled with mercury except the one used to measure the pressure drop across the capillary tube flowmeter in the secondary gas supply line. The latter manometer is filled with water and fitted with shut-off valves, which are closed when measurements are taken in the diffusion flow field. Traces of water vapor that might otherwise enter the diffusion tube during data taking would constitute a source of error in the experimental results.

The flow meters in the secondary gas supply line are used only to provide a relative indication of the secondary gas flow rate when desired test conditions are being established. Final adjustments in the secondary gas flow rate are made using a concentration detector to measure the portion of the secondary gas in the exhaust mixture leaving the upper plenum chamber.

In the primary gas supply line the ball-and-tube flowmeter is used to set the flow rate. This flowmeter was calibrated in place at operating temperature and pressure using a bubble flowmeter and a stopwatch. The results of the calibration are included in Appendix E.

5.2.3. System Temperature Instrumentation

Copper-constantan thermocouples are used to monitor the room temperature, temperatures under the cover shown in Figures 5.1 and 5.2 for components of the diffusion cell, and the temperatures in the flow circuits at locations shown in Figure 5.6. Outputs of the thermocouples are measured relative to an ice-bath reference using a Leeds and Northrup millivolt potentiometer. This thermocouple system is independent of the instrumentation described in section 5.3 that is used to measure temperatures in the diffusion flow field.

Two additional thermocouples, one in the secondary gas supply line and the other in the primary gas supply line, are provided for detecting small differences that might exist between the temperatures of the two gases immediately upstream of the diffusion tube. These two thermocouples are incorporated into a single circuit, the output voltage of which is zero when they are at the same

temperature. The Leeds and Northrup K-4 potentiometer discussed in section 5.3.4 is used to monitor the output voltage of this circuit.

In addition to the system thermocouples, two thermometers are installed on the apparatus, one for use in measuring room temperature and the other for measuring the temperature within the cover over the diffusion cell.

The system thermocouples were calibrated using the Hewlett-Packard quartz thermometer and the variable temperature bath described in section 5.3.5. Results of the calibrations are included in Appendix E.

5.2.4. Concentration Detector

Stock (1972) found that the composition of the diffusion cell vent gas is in close agreement with the gas composition within the diffusion cell at the plane formed by the outlets of the secondary gas injection tubes. In his work and in the work reported in this thesis, the composition of the vent gas was therefore used as the basis for adjusting the flow rate of the secondary gas (helium) entering the diffusion cell.

Gas mixtures are analyzed with a Carle model 1161 Micro-Detector in conjunction with a Hewlett-Packard model 7001AM X-Y recorder. The principal components of the detector are a thermal conductivity cell, a bridge circuit,

and a power supply consisting of eight mercury batteries. A particularly advantageous feature of the detector is that the gas sample flow rate required for an analysis is on the order of only one cc/min.

Valves, flow circuits, and the thermal conductivity cell for the concentration analyzing system are housed in the relatively large, rectangular enclosure shown to the right of the diffusion cell in Figures 5.1 and 5.3. The X-Y recorder and the bridge circuit are located to the left of the diffusion cell as shown in Figure 5.1.

5.2.4.1. Thermal Conductivity Cell Assembly

Within the thermal conductivity cell there are two thermistors, each of which is in a separate flow passage as illustrated in Figure 5.7. One flow passage is for the gas to be analyzed; the second is for a reference gas. The two thermistors are incorporated into a bridge circuit through which an electric current flows, and which is balanced when the reference gas is passed over both thermistors. When a gas of different composition is passed over one of the thermistors, the dissimilarity in thermal conductivity between it and the reference gas results in a change in the temperature of the thermistor with a corresponding change in its resistance. This causes an imbalance of the bridge, which is sensed as a voltage and read out on the X-Y recorder.

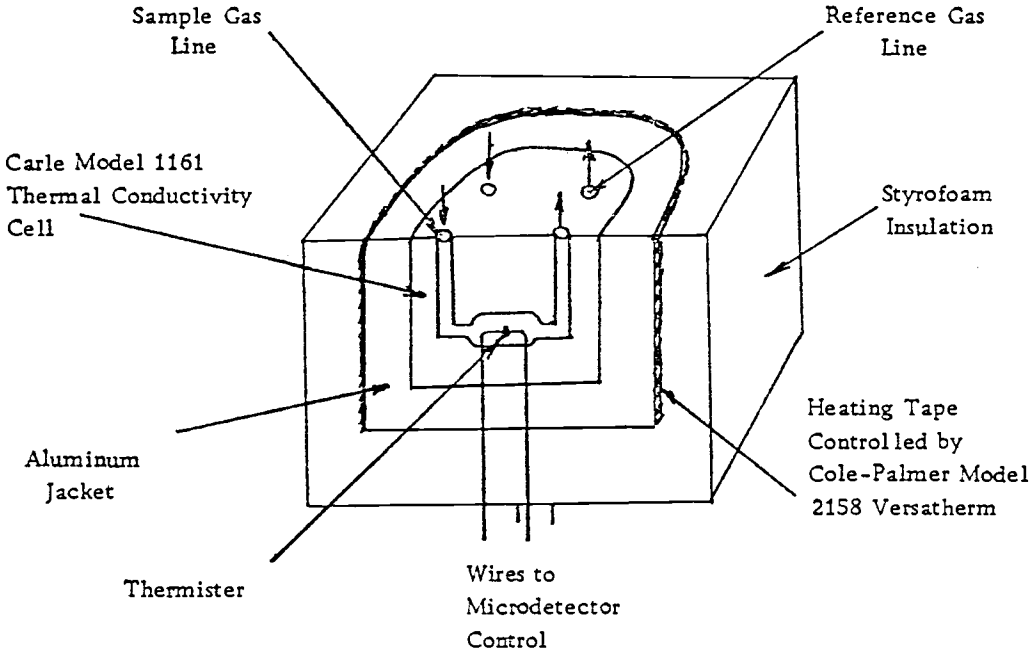

OPERATING CONDITIONS

Temperature	35°C Controlled by the heating tape
Current	20 ma (set with nitrogen flowing through both sides of the cell)
Flowrate	1.0 cc/min. (measured with a bubble flowmeter)

SENSITIVITY TO PERTURBATIONS (with 25% He flowing through the sampling line)

Temperature	4.0°C increase in temperature of the aluminum block holding the cell results in a voltage drop of .1 mv or .01 in mole fraction
Current	Changing from 25 to 20 ma increased the voltage output by .6 mv or .06 in mole fraction
Flowrate	Controlled by the pressure drop between the diffusion tube and the atmosphere. Changing the tube pressure from 20 to 10 cm Hg gauge increased the voltage output by .02 mv or .002 in mole fraction.

Figure 5.7. Cross-Sectional View of Thermal Conductivity Cell*

*From Stock (1972)

As shown in Figure 5.7, the thermal conductivity cell is wrapped with a heating tape controlled by a Cole-Palmer model 2158 Versatherm, and insulated with styrofoam. In this way the operating temperature of the cell assembly can be closely controlled. For the work discussed in this thesis, the temperature was maintained at approximately 35° C $\pm$ 0.1° C. The temperature of the cell assembly is monitored using a thermocouple mounted on it.

5.2.4.2. Flow Circuits for Gas Samples

Shown schematically in Figure 5.8 is the system of tubing and valves used for switching between the various flow circuits through which gas samples can be routed to the concentration detector. Carle micro-volume chromatography valves are installed in the system. Due to the small internal volumes of the valves, the thermal conductivity cell, and the small diameter tubing, the response lag-time is small (approximately two or three minutes) even though the gas sample flow rate is only about one cc/min. The driving force for flow through the system results from the difference between the operating pressure (10 cm Hg gage) within the diffusion cell and the atmospheric pressure.

The flow resistance tubing installed in each sample line as illustrated in Figure 5.8 serves two pur-

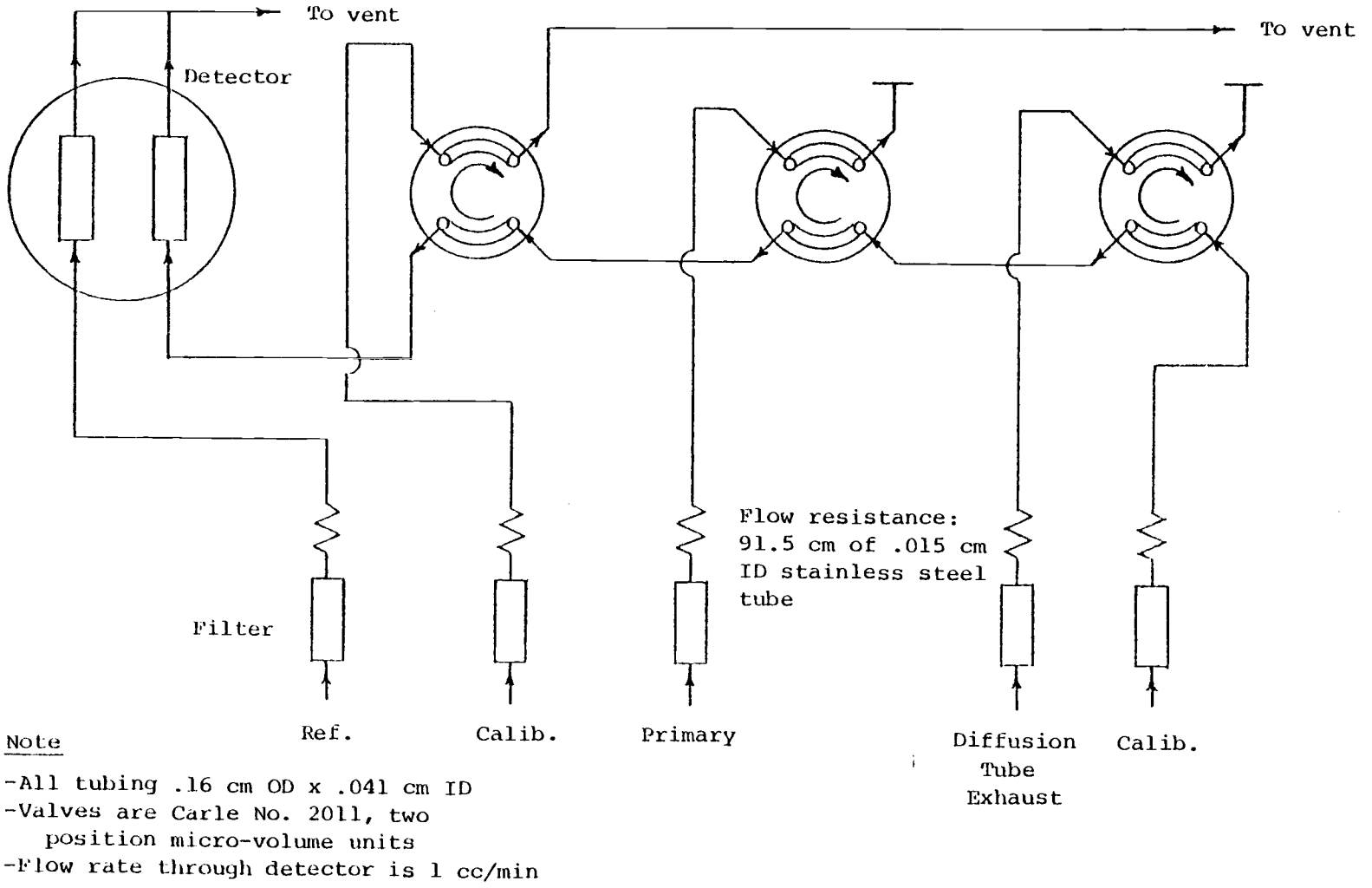

Note

-All tubing .16 cm OD x .041 cm ID
-Valves are Carle No. 2011, two position micro-volume units
-Flow rate through detector is 1 cc/min

Figure 5.8. Schematic Diagram of Flow Switching System for Thermal Conductivity Cell

poses: to restrict gas flow to the desired flow rate, and to essentially equalize the flow resistances of the sample lines. Variations in flow resistance due to variations in the configurations of the sample lines and valve assemblies are negligible compared to the restriction in each line associated with the flow resistance tubing.

Each sample line is equipped with a filter upstream of the flow resistance tubing to protect the tubing and valves from foreign material that might possibly enter the system.

Flow circuits connected to the switching system for the concentration detector include those for the primary gas (nitrogen) used to check the zero-point setting of the analyzer-recorder system, the vent gas from the diffusion tube, and two calibration gases (each a helium-nitrogen mixture of known composition) used to check the day-to-day performance of the analyzer and recorder. The reference gas (nitrogen) for the detector is on a flow circuit that is independent of the switching system.

5.2.4.3. Use of X-Y Recorder for Measuring Output Voltage of Concentration Detector

Although any type of voltmeter having suitable sensitivity can be used to measure the output voltage of the bridge circuit for the conductivity detector, an X-Y recorder is particularly advantageous for this purpose.

The output voltage of the conductivity detector slowly drifts toward a stable value in an asymptotic fashion as the gas sample to be analyzed displaces gas previously in the system. This process can be clearly observed on a recorder tracing of the output voltage as a function of time, but it is hard to detect if only voltage readings are available.

For the work discussed in this thesis, the output voltage of the bridge circuit was connected to the Y-axis of the recorder and the X-axis was operated in the sweep mode at a setting of 50 sec/cm. The output voltage was traced for at least five minutes after apparent equilibrium was reached, and rechecked at frequent intervals to verify that the desired operating conditions were maintained.

5.2.4.4. Calibration of Concentration Detector

The concentration detector-recorder system was calibrated by passing the following gases through the thermal conductivity cell and measuring the variation of output voltage with composition: helium, and mixtures containing nitrogen and 25%, 50%, and 75% helium. The three gas mixtures were left over from the earlier work done by Stock, and were obtained by him from a commercial supplier. Nitrogen was used as the reference gas.

Operating conditions for the calibration were the same as those established subsequently for collecting data in the diffusion apparatus.

The results of the calibration are included in Appendix E, together with the results of a similar calibration performed by Stock (1972). In addition to the stable operation exhibited in day-to-day testing, the concentration detector also exhibits excellent long-term repeatability and stability as shown by the close agreement between the two calibrations. The largest source of error in the calibrations is the uncertainty of the compositions of the gas mixtures, which were known to $\pm$ 0.5%.

Small variations in operating temperature, bridge current, and flow rate through the conductivity cell do not substantially affect the response of the concentration detector, as demonstrated by Stock (1972). The results of sensitivity tests performed by Stock are included in Figure 5.7.

5.3 Temperature Instrumentation for Diffusion Flow Field

5.3.1. Design of Thermocouple Assemblies Used in Diffusion Tube

Details of the design of the thermocouple assemblies used for measuring temperatures in the diffusion tube are shown in Figure 5.9. Each of the assemblies consists of a

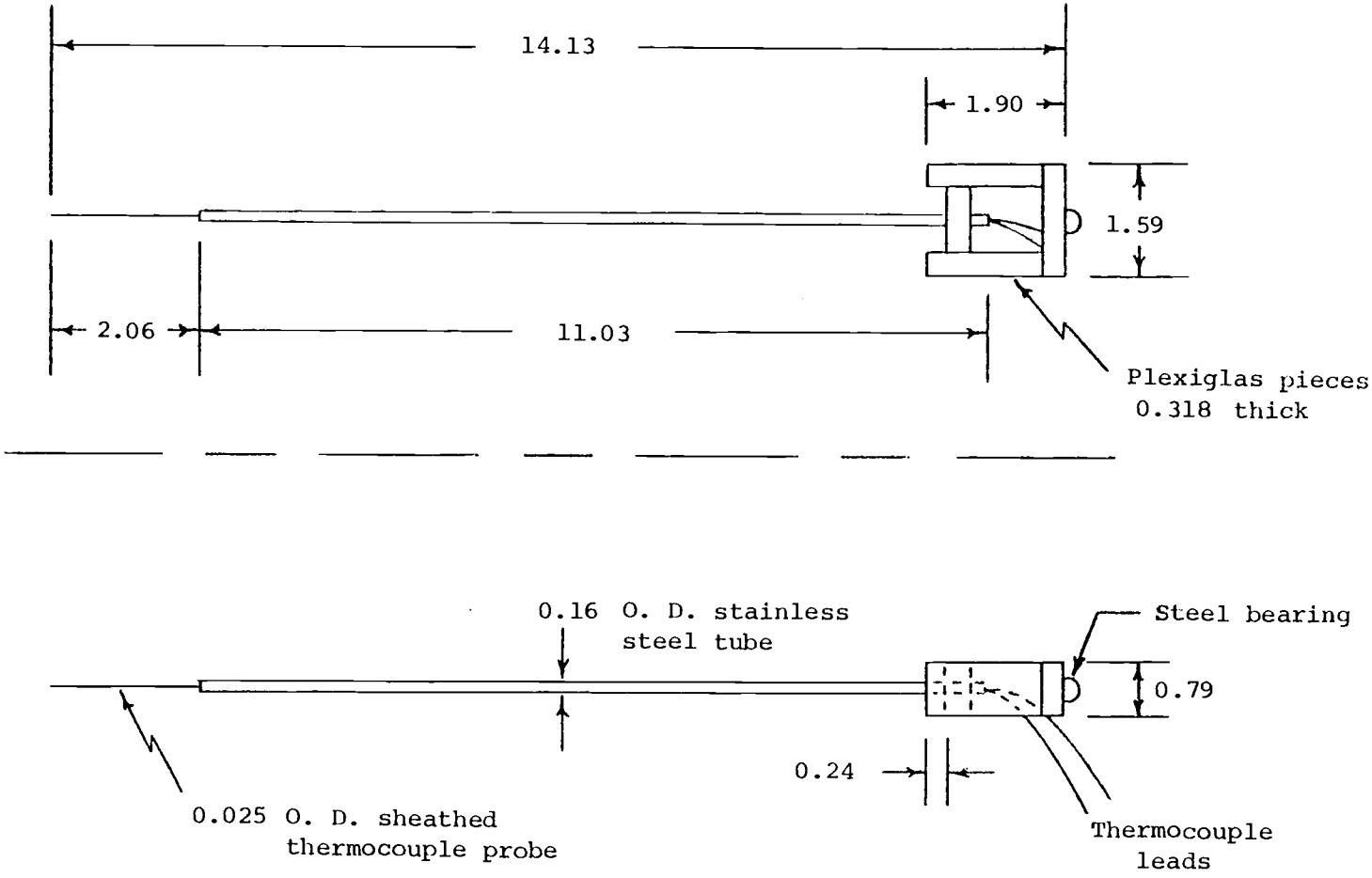

Note

-All dimensions in centimeters
-Drawn to full scale

Figure 5.9. Configuration of Diffusion Tube Thermocouple Assembly

sheathed thermocouple probe having an outside diameter of 0.025 cm (0.010 inch), housed along a portion of its length in a stainless steel tube having an outside diameter of 0.159 cm (1/16 inch). The housing is compatible in size with the Swagelok fitting and guide tubes in each diffusion tube port assembly. Mounted on one end of each thermocouple assembly is a collar that is used in conjunction with the radial probe positioning system.

In Figure 5.10 one of the thermocouple probes is shown inserted part way into the diffusion tube through the middle port assembly. The guide tubes for the thermocouple assemblies are visible in this figure within the plexiglass tubing used to connect them.

Shown in Figure 5.11 are the portions of the thermocouple assemblies that are cut off from view at the right boundary of Figure 5.10. Also shown in Figure 5.11 is the micrometer used to set the radial positions of the thermocouple probes. (The micrometer is a part of the radial probe positioning system which is discussed in section 5.4.2.)

The thermocouple probes used in the assemblies were manufactured by Omega Engineering, Inc. As illustrated in

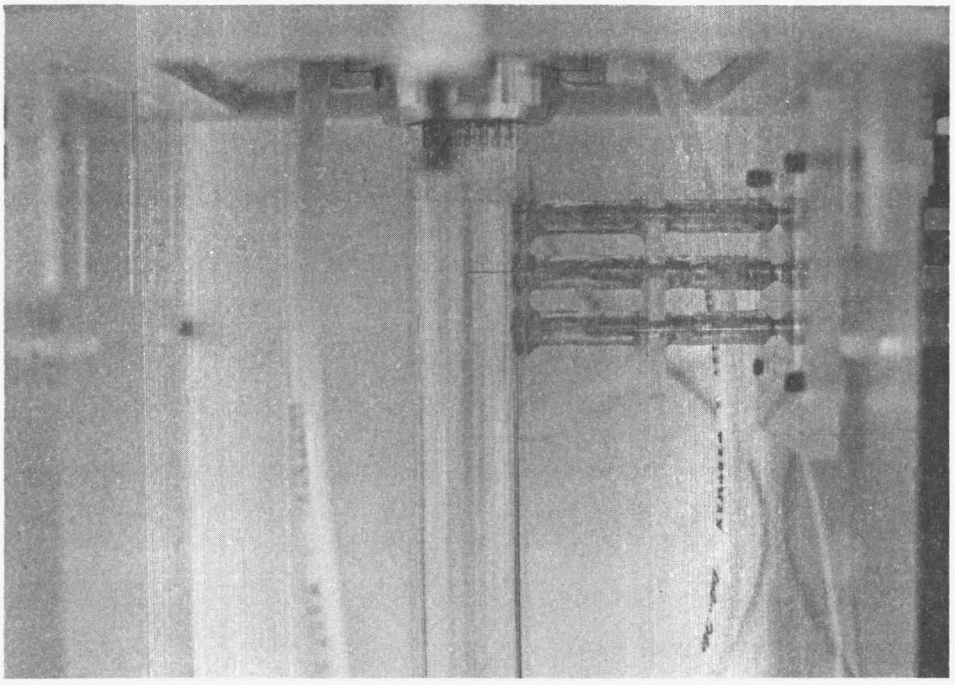

Figure 5.10. Thermocouple Probe Inserted into Diffusion Tube

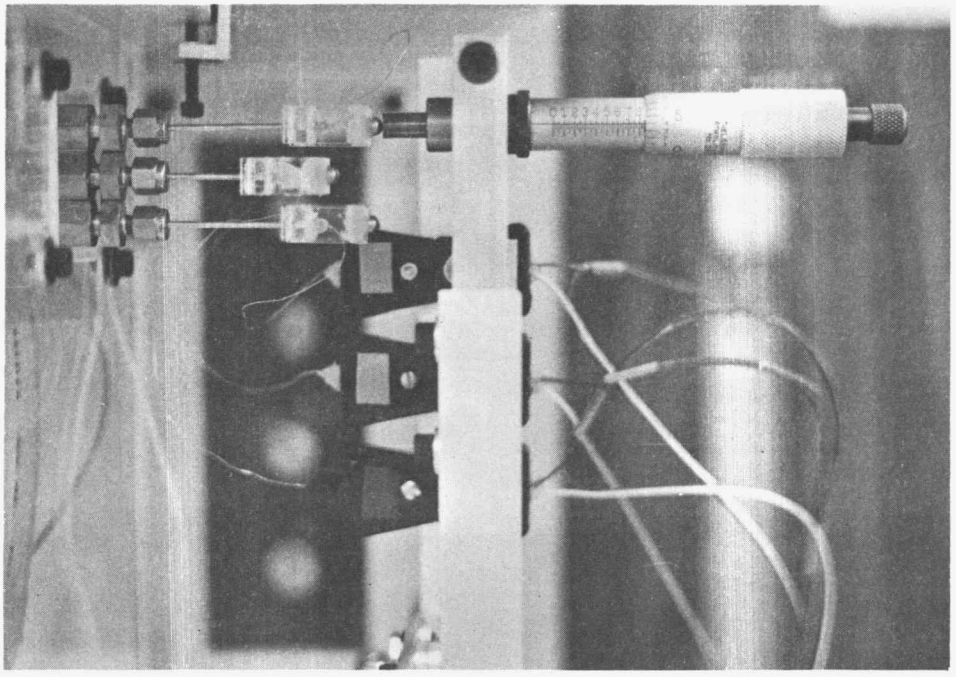

Figure 5.11. Thermocouple Assemblies and Micrometer for Setting Radial Positions of Probes

Figure 5.12, each probe is sheathed in stainless steel. Within the sheath are 0.0025 cm (0.001 inch) diameter iron-constantan thermocouple wires, tightly packed in magnesium oxide insulation. The thermocouple junction is formed at the probe tip. A connector to which the thermocouple wires are attached is provided with each thermocouple probe, which facilitates joining the probe to the extension wires for the corresponding thermocouple circuit. The connectors, which are mounted to the rear of and separately from the micrometer, are shown in Figure 5.11.

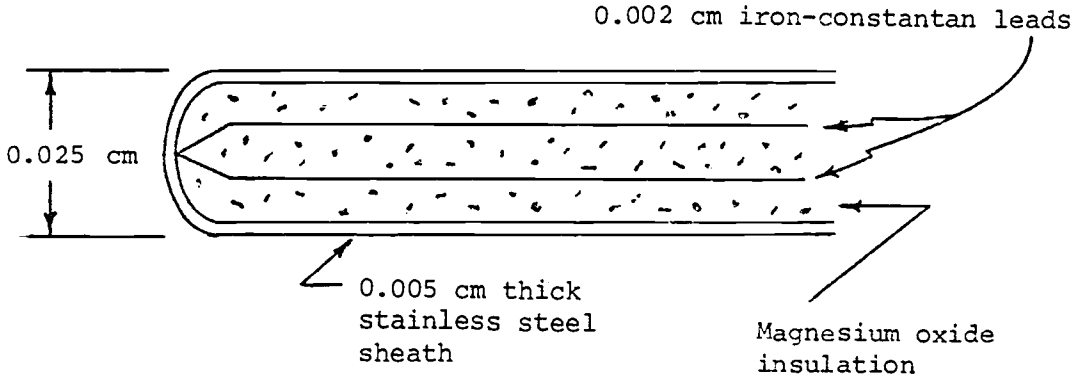

Figure 5.12. Cross-Sectional View of Diffusion Tube Thermocouple Probe

The portion of each probe assembly that can be inserted into the diffusion tube has the same outside diameter (0.025 cm) as the sampling probes used by Stock

(1972) for measuring concentration fields within the diffusion tube. Thus, disruptions in the diffusion flow field introduced by the presence of the instrumentation should be essentially the same for the thermocouple probes as for the concentration sampling probes. The combined experimental results from the two investigations were used to compute transport properties discussed later in this thesis.

5.3.2. Thermocouple Circuit

Illustrated in Figure 5.13 is the circuit design common to each of the three thermocouple assemblies used to measure temperatures in the diffusion tube. Included in each circuit is a diffusion tube thermocouple probe, a reference junction, and connecting wires.

In each circuit the reference junction is fabricated from ANSI type J, 24 B and S gage, iron-constantan thermocouple wire. The constantan lead from the reference junction is connected directly to the instrumentation discussed in section 5.3.3, and the iron lead is connected to the smaller diameter iron lead in the diffusion tube probe through the connector supplied with the probe. The connector also serves to join the constantan lead in the diffusion tube probe to a 24-gage constantan lead that is used to complete the circuit to the thermocouple instru-

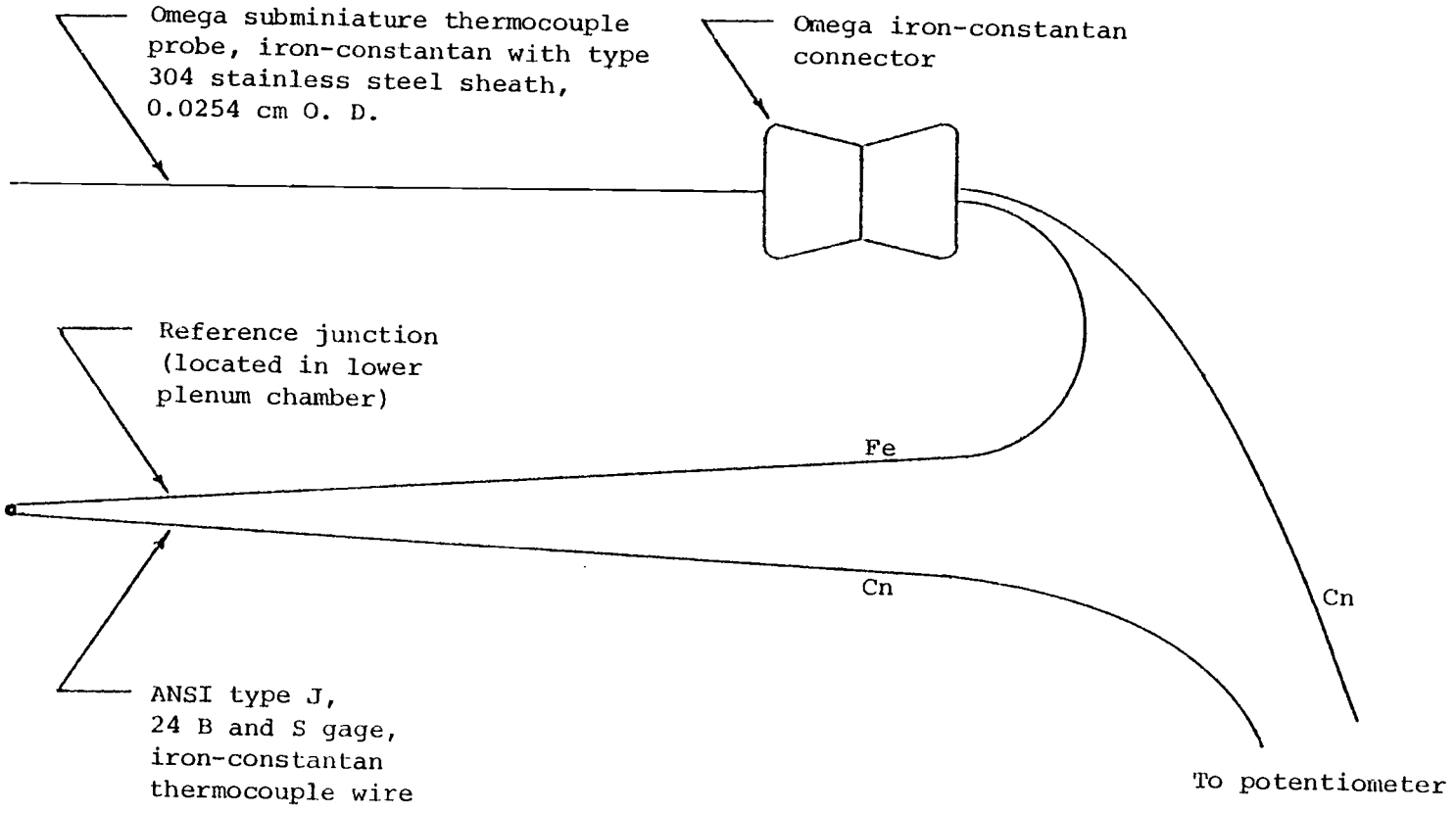

Figure 5.13. Schematic Diagram of Diffusion Tube Thermocouple Circuit

mentation. All of the 24-gage leads for the thermocouple assemblies are from the same spool of thermocouple wire.

Each of the three diffusion tube thermocouple circuits is separate from and independent of the others. Rather than using a selector switch between the thermocouple instrumentation and the individual thermocouple circuits, the leads from the circuit that is in use are connected directly to the instrumentation. In this way sources of error are avoided that could otherwise be introduced due to contact resistance and the presence of dissimilar materials in the switch.

The only connectors in the circuits are the ones supplied with the Omega thermocouple probes used in the diffusion tube. To avoid inaccuracies due to dissimilar metals, the connector prongs and inserts are made from matched thermocouple alloys which, according to the manufacturer, meet ANSI thermocouple calibration standards.

5.3.3. Location of Reference Junctions for Diffusion Tube Thermocouples

Of primary interest in the experimental work performed for this thesis are the changes in temperature in the diffusion flow field relative to the temperature of the incoming gases. Special provisions, including the aluminum sink/source cylinders discussed in section 5.2.1, the system thermocouples discussed in section 5.2.3, and the

thermal shielding discussed in section 5.5, are included in the diffusion test facility to ensure that the two gases enter the diffusion tube at the same temperature. Accordingly, temperature changes in the diffusion flow field could be measured relative to the temperature of either of the incoming gases.

It was found to be most convenient to measure the temperature changes relative to the temperature of the primary gas entering the diffusion tube through the lower plenum chamber. This chamber is therefore equipped with ports through which the reference junctions for the diffusion tube thermocouple probes are inserted into the primary gas stream. Swagelok fittings are used to provide leak-tight seals with the tubes in which the lead wires for the reference junctions are housed. Two of the reference junctions are shown in Figure 5.1 inserted through the thermal shielding into the lower plenum chamber, and the ports in the lower plenum chamber through which they are inserted are shown in Figure 5.3.

5.3.4. Instrumentation for Measuring Electrical Outputs of Diffusion Tube Thermocouples

Electrical outputs of the thermocouple assemblies in the diffusion tube are measured using a Leeds and Northrup model 7554, type K-4 potentiometer, in conjunction with a Leeds and Northrup model 9828 DC null detector. A front

view of the potentiometer and the null detector mounted on top of it is shown in Figure 5.1.

Other components used with the potentiometer include an Eppley standard cell, catalog number 100, and a Leeds and Northrup model 9879 DC constant voltage supply. The connections between the components and the provisions for electrical guarding and grounding are in strict accordance with the instructions provided by Leeds and Northrup in the manual for the potentiometer.

Scale divisions on the potentiometer allow for direct readings to the nearest 0.5 microvolt. In the low range used for the measurements discussed in this thesis, the limit of error is $\pm$ (0.007% of reading + 0.5 microvolt) according to specifications in the manual for the potentiometer.

5.3.5. Calibration of Thermocouples

Each of the thermocouple assemblies used for temperature measurements in the diffusion tube was calibrated together with its reference junction and lead wires utilizing a fixed temperature bath for the reference junction, a variable temperature bath for the diffusion tube probe, and a Hewlett-Packard model 2801A quartz thermometer. Two quartz sensors were used, one in the constant temperature bath and the other in the variable temperature bath, and

the temperature difference between the two was read out on the digital display of the instrument to which the sensors were connected.

The basis for operation of a quartz thermometer is that the frequency response of a quartz crystal varies with the temperature of the crystal. For the Hewlett-Packard quartz thermometer, the frequency response varies approximately 1000 hz/° C. A choice of resolution to 0.01, 0.001, and 0.0001° C is offered on the digital display of the instrument used to detect the variations in frequency response. According to the specifications in the manual for the instrument, the limit of error is $\pm$ 0.01° C over the range 0 - 100° C.

A reservoir on a Haake Rotovisco rotating viscometer was used as the variable temperature bath. The reservoir temperature is controlled by means of a circulating water system that contains both a thermostatically regulated heater and a cooling coil. Using a combination of cooling and intermittent heating, the reservoir temperature can be varied under carefully controlled conditions over a broad range that extends from below room temperature to well above room temperature. According to the manufacturer's specifications, the temperature can be controlled to within $\pm$ 0.02° C.

The constant temperature bath consisted of a thermos bottle of water maintained at the same temperature, 21.1° C $\pm$ 0.1° C, to which the reference junctions in the diffusion tube thermocouple circuits are exposed when the diffusion apparatus is in operation.

Each of the thermocouple assemblies was calibrated individually. With the diffusion tube probe and the reference junction of an assembly mounted, respectively, in the variable temperature bath and the constant temperature bath, the temperature difference between the two baths was varied over a range greater than that to which the thermocouple assembly would be exposed in the diffusion apparatus. The electrical outputs of each thermocouple assembly were recorded together with the temperature differences measured with the quartz sensors. The results of the calibration are included in Appendix E.

Electrical outputs from the thermocouple assemblies were measured with the instrumentation discussed in section 5.3.4. Prior to commencing the calibrations and subsequent measurements in the diffusion apparatus, the voltage of the standard cell used with the K-4 potentiometer was accurately measured to the nearest microvolt in the instrumentation shop of the Physics Department at Oregon State University.

In closing this section, it might be appropriate to comment on the reason why quartz thermometers were not used for measuring temperatures in the diffusion apparatus. The high sensitivity of quartz sensors to small temperature changes would be a valuable asset for measurements in a diffusion flow field, but the large size of the sensors (more than 0.7 cm in diameter for the Hewlett-Packard instrument) precluded their use for point temperature measurements.

5.4. Probe Positioning Systems

5.4.1. Axial Positioning System

The axial positions of the diffusion tube thermocouple probes relative to the secondary gas injection tubes are controlled by means of the vertical carriage of a machine that was salvaged for use on the diffusion apparatus. Shown in Figure 5.14 is an oblique view of the diffusion apparatus and the vertical carriage. Due to its heavy weight and rigid construction, the carriage is a very stable platform.

As discussed in section 5.1, the diffusion tube assembly and the lower plenum chamber are mounted on the vertical carriage. Provision for axial movement of these components relative to the rest of the apparatus is made in the upper mount for the diffusion tube.

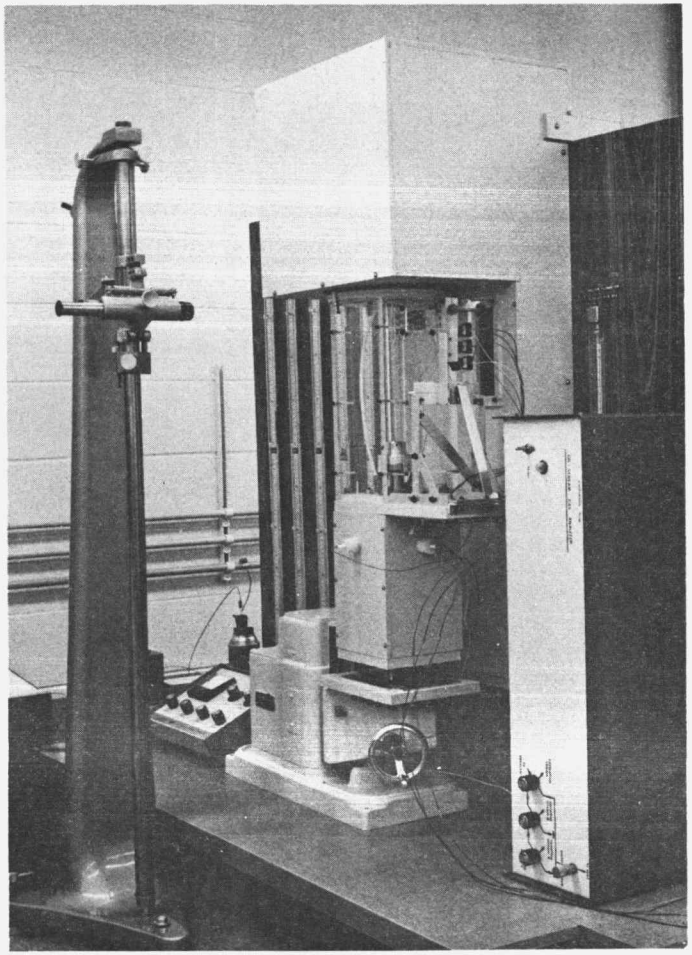

Figure 5.14. Oblique View of Diffusion Apparatus and Cathetometer

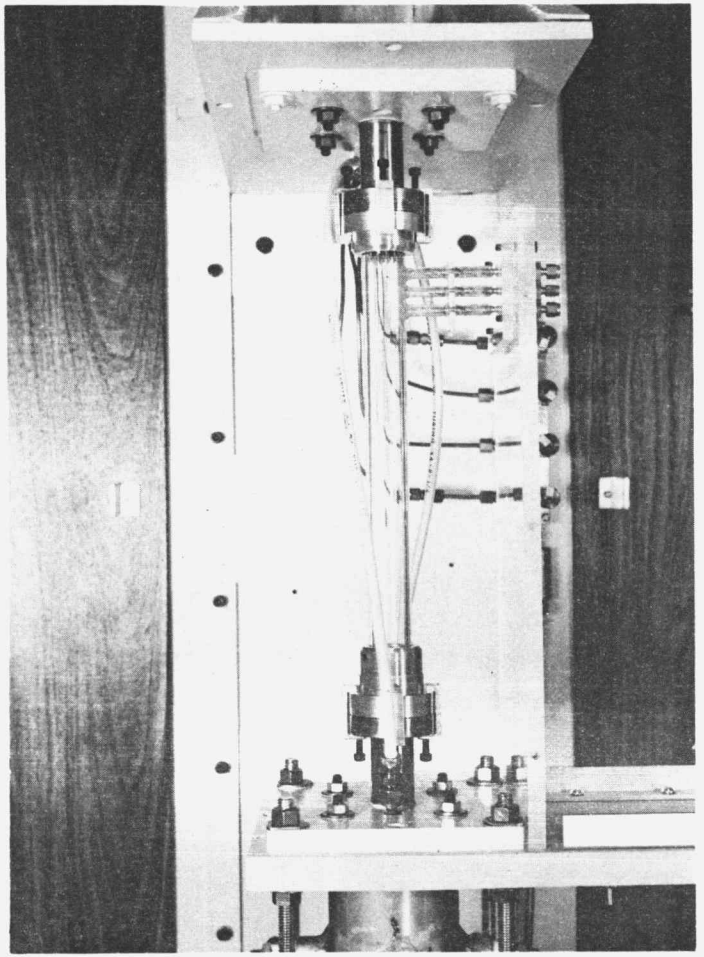

Figure 5.15. Diffusion Tube Mounted between Upper and Lower Plenum Chambers

As shown in Figure 5.15, the diffusion tube is installed between two aluminum end pieces that are in turn clamped with O-ring seals to extensions from the upper and lower plenum chambers. The lower end piece is rigidly attached to the diffusion tube with set screws and sealed with two O-rings. A slip fit is provided between the diffusion tube and the upper end piece, so that the diffusion tube can be moved axially within the end piece relative to the upper plenum chamber. To maintain a gas-tight seal between the diffusion tube and the upper end piece, an O-ring is provided near the inlet of the end piece. The diffusion tube can be moved approximately 1.6 cm axially without breaking the seal.

Since the secondary gas injection tubes are rigidly mounted in the upper plenum chamber, axial motion of the diffusion tube assembly results in varying the positions of the diffusion tube thermocouple probes relative to the injection tubes. The location of the diffusion flow field is not affected. To allow for measuring temperatures at any desired location in the diffusion flow field, the spacing between the three thermocouple ports is such that the upper limit on axial travel of each of the lower ports overlaps the lower limit on axial travel of the port above it.

In Figures 5.16 and 5.17 the diffusion tube assembly is shown in two different axial positions relative to the stationary portion of the apparatus. The difference in the two positions is most easily observed by noting the positions of the two circular plates located at the top of the plexiglass enclosure for the diffusion tube. In Figure 5.17 these plates are both visible, while in Figure 5.16 they are partially hidden from view.

The axial positions of the thermocouple probes are measured optically, using a Gaertner model M-912 cathetometer. As shown in Figure 5.14, the cathetometer is located in front of the diffusion apparatus. The cathetometer is equipped with a vernier scale, which is graduated to allow for readings to the nearest 0.001 cm. Other components of the cathetometer include a siting scope and a built-in magnifying glass for use when reading the vernier scale.

As part of the preparations each time that the diffusion apparatus is placed in operation, the cathetometer reading is taken for the injection plane formed by the outlets of the secondary gas injection tubes. This reading is then used as the basis for computing the cathetometer readings corresponding to the axial locations at which thermocouple readings are desired. When taking data, the cathetometer siting scope and, in turn, the diffusion tube probes are set to the desired axial locations.

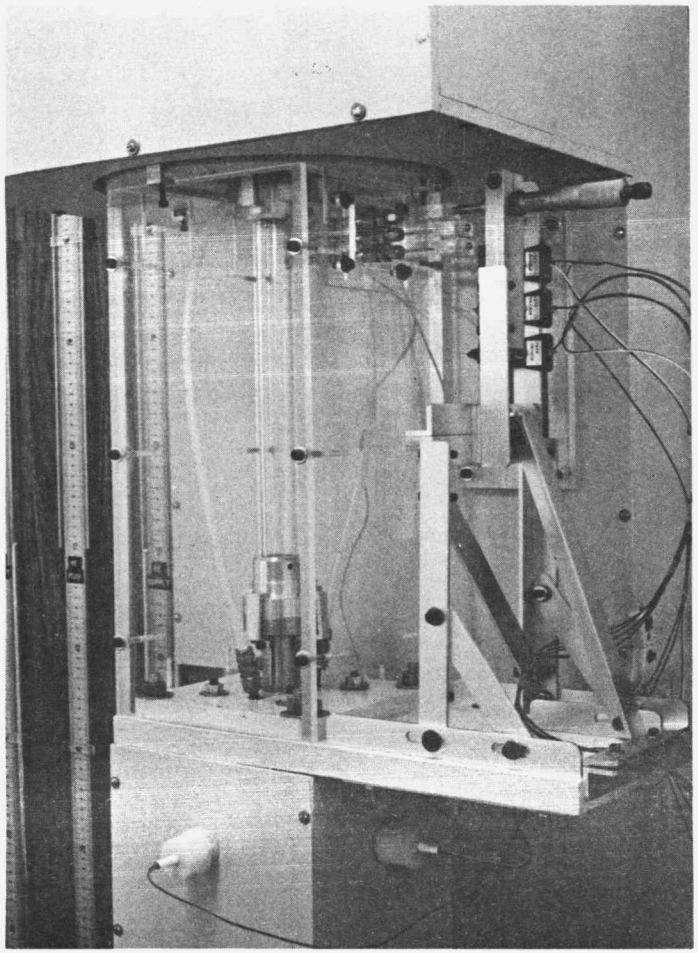

Figure 5.16. Diffusion Tube Assembly at Upper Limit of Travel

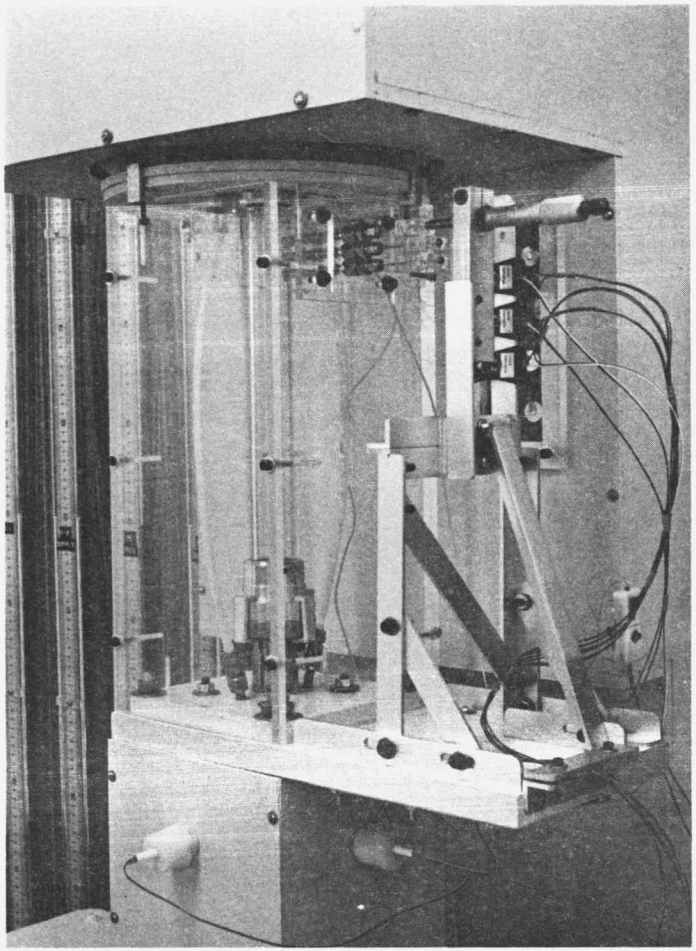

Figure 5.17. Diffusion Tube Assembly at Lower Limit of Travel

5.4.2. Radial Positioning System

A micrometer mounted on the framework shown in Figures 5.16 and 5.17 is used to set the radial positions of the thermocouple probes. To allow for aligning the micrometer with any of the three probes, the vertical position of the rectangular bar in which the micrometer is clamped can be varied relative to the rest of the framework. This is accomplished by loosening the mounting bolts for the rectangular bar, sliding it to the desired position along the vertically oriented slot through which the bolts pass, and then retightening the bolts. In Figures 5.16 and 5.17 the mounting bolts for the rectangular bar are visible, but the slot through which they pass is hidden from view.

The framework, which is light in weight but very rigid, is bolted to a plate that is attached to the diffusion tube assembly. Thus, when the axial position of the diffusion tube assembly is changed using the vertical carriage discussed in section 5.4.1, the radial probe positioning system moves with it.

Each time that the micrometer is realigned with a thermocouple probe, a reading is taken with the probe tip in contact with the opposite wall of the diffusion tube. Knowing this reading and the inside diameter of the tube

(1.923 cm), the micrometer readings corresponding to the radial positions at which temperatures are to be measured can be readily computed. These readings then form the basis for positioning the probe when making a radial traverse across the diffusion flow field.

The micrometer scale is in terms of inches rather than centimeters, with divisions down to 0.001 inch. Day-to-day measurements (such as, for example, the micrometer readings for the probes when in contact with the opposite wall of the diffusion tube) are repeatable within 0.002 in.

5.4.3. Circumferential Positioning System

As discussed in section 5.1, a ball-thrust bearing is used to connect the plate clamped on the vertical carriage to the frame for the lower plenum chamber and diffusion tube assembly. Thus, the positions of the diffusion tube thermocouple probes can be varied circumferentially as well as axially and radially relative to the secondary gas injection tubes mounted in the upper plenum chamber. In Figure 5.18 the diffusion tube assembly is shown rotated approximately 180° from the position shown in Figures 5.16 and 5.17.

The provision for varying the circumferential position of the probes was made in anticipation of possibly finding asymmetry in the radial profiles measured in the

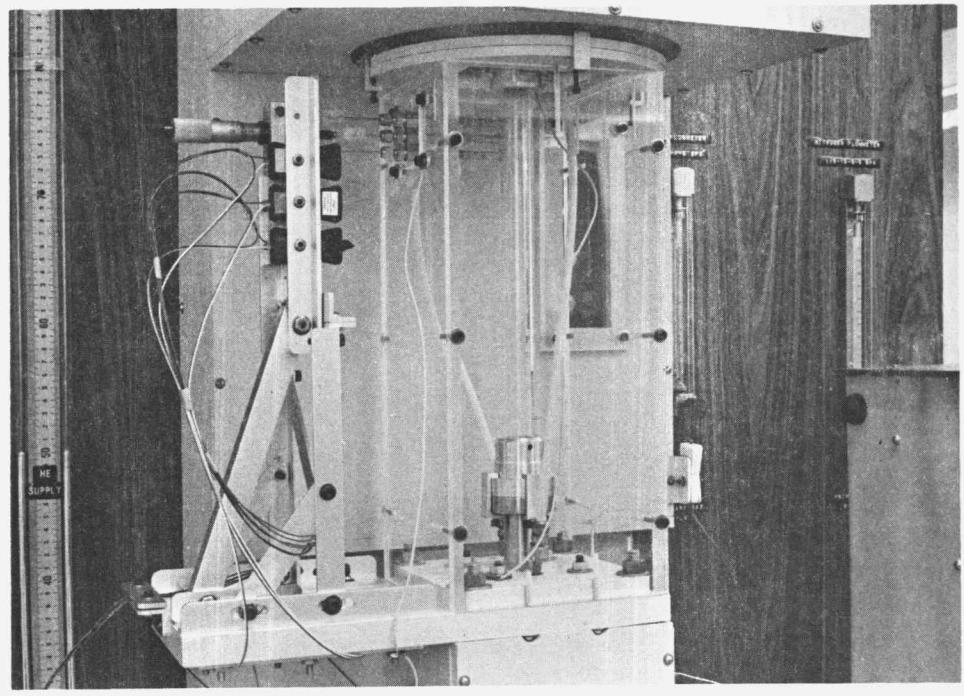

Figure 5.18. Diffusion Tube Assembly Rotated 180°

diffusion flow field. Measurements taken with the probes at different circumferential positions are useful in determining whether asymmetry is associated with the presence of probe assemblies in the flow field or is due to other causes.

Other investigators (e.g. Zeldin and Schmidt (1972)) have found that radial profiles measured in laminar flow fields tend to be asymmetric when the measurements are taken with probes inserted through the wall of the test facility. The probe assemblies used to take the data discussed in this thesis are very small in diameter but are, nevertheless, a source of disturbance when they are inserted into the diffusion flow field.

Obstructions in one or more of the secondary gas injection tubes could also cause asymmetry in radial profiles. Without the provision for varying the position of the probes circumferentially, it would be very difficult to distinguish between asymmetry caused by flow disturbances around the probes and that caused by malfunction of the secondary gas injection tubes.

To provide a means for securing the diffusion tube assembly at a given circumferential position, five jack screws are installed around the ball-thrust bearing in the space between the plate clamped to the vertical carriage

and the base plate for the framework of the diffusion tube assembly. The space in which the jack screws and bearing assembly are located can be seen in Figure 5.14.

When the jack screws are expanded between the two plates, the forces tending to separate the plates are counteracted by the restraining force of the bearing assembly to which the plates are attached. The tendency of the diffusion tube assembly to wobble due to the small amount of free play in the bearing is eliminated, and the assembly is held rigidly in position. By making small changes in the adjustments of the jack screws, the perpendicularity of the diffusion tube assembly can be adjusted within the limits allowed by the free play in the bearing.

5.5. Thermal Shielding

When taking data, the laboratory temperature is maintained at 21° C $\pm$ 0.5° C. Within these limits the temperature fluctuates in a periodic manner, in response to energy inputs to the laboratory (from the overhead lights and, during the late spring and summer months when data were taken, from the warmer outside surroundings) accompanied by intermittent cooling from a thermostatically controlled, auxiliary air conditioning unit.

A cover is installed over the diffusion cell to isolate the cell components and flow circuitry from the

small fluctuations in laboratory temperature. During preliminary tests without the cover, the temperatures of the primary and secondary gases entering the diffusion tube were found to fluctuate in response to fluctuations in laboratory temperature. The transient temperature characteristics of the gases were also found to differ, due in part to the differences in the primary and secondary gas flow circuits. As a result, small temperature differences generally existed between the two gases entering the diffusion tube. These temperature fluctuations and temperature differences were essentially eliminated within the diffusion cell following the installation of the cover and the aluminum sink-source cylinders discussed in section 5.2.1.

Only a relatively limited amount of insulating material is necessary for shielding the diffusion cell components and flow circuits from the small fluctuations in laboratory temperature. With the exception of the plexiglass enclosure for the diffusion tube, the material used for the diffusion cell cover is plywood that is 0.95 cm thick. The thickness of the plexiglass panels is also 0.95 cm, except for the front panel, which is 0.64 cm thick.

Special care was taken in the fabrication and assembly of the plexiglass enclosure to ensure that the

panels are parallel to the diffusion tube, and that the panels and the diffusion tube are plumb. These precautions are necessary to minimize optical distortion as a source of error when taking sitings through the plexiglass enclosure with the cathetometer discussed in section 5.4.1.

A foam rubber diaphragm, which is visible in Figure 5.17 above the plexiglass diffusion tube enclosure, is used to join the cover for the components mounted on the vertical carriage to the cover for the remaining diffusion cell components. The diaphragm has the flexibility necessary to accommodate changes in the axial position of the diffusion tube assembly relative to the upper plenum chamber.

Between the diaphragm and the plexiglass enclosure are two annular plates, both of which are made of plywood. One of the plates is attached to the diaphragm and the other is attached to the plexiglass enclosure, as shown in Figure 5.17. The plates are clamped together to form a joint than can be readily loosened when the diffusion tube assembly is to be rotated circumferentially relative to the upper plenum chamber, as shown in Figures 5.17 and 5.18.

VI. EQUATIONS FOR COMPUTING THERMAL DIFFUSION FACTORS AND MOLECULAR DIFFUSION COEFFICIENTS FROM EXPERIMENTAL DATA

For each of the four test conditions established in the diffusion apparatus, thermal diffusion factors and molecular diffusion coefficients were computed from the velocity and concentration distributions measured by Stock (1972) combined with the temperature distributions measured as part of the experimental investigation for this thesis. The models used for computing these transport properties are discussed in this chapter.

6.1. Model for Computing Thermal Diffusion Factors

Two approaches were followed in formulating a model for computing thermal diffusion factors from the experimental data. In the first approach, an energy balance was performed over a cylindrical control volume that could be varied arbitrarily in size in both the radial and axial directions, and that was assumed to be oriented so that its axis was coincident with the diffusion tube axis. The fluxes of the constituents of the gas mixture crossing the control volume surfaces were expressed in terms of the radial and axial components of the mass average velocity, and the radial and axial components of the velocities of the constituents. Since small errors in the experimental

data tend to be magnified in the mathematical operations necessary to compute velocity components from the data, the results obtained from this approach were erratic.

In the second approach, the need for computing velocity components from the experimental data was eliminated by setting the radius of the control volume equal to the radius of the diffusion tube and expressing the bulk motion of each gas in terms of its mass flow rate. Details of this approach are summarized in the following paragraphs.

6.1.1. Formulation of Equation for α_T

6.1.1.1. Energy Balance Over Control Volume

An equation for the thermal diffusion factor may be formulated on the basis of an energy balance over the control volume shown in Figure 6.1. The control volume is assumed to be bounded by the following three surfaces: plane AA located sufficiently far upstream of the gas B injection plane so that the mole fraction of gas B at plane AA is negligible, plane BB located at any arbitrary axial position downstream of plane AA within the diffusion flow field, and the inside surface of the diffusion tube between these two planes.

This analysis is based on the following assumptions: the bulk flow is steady, laminar, and axisymmetric; the gas

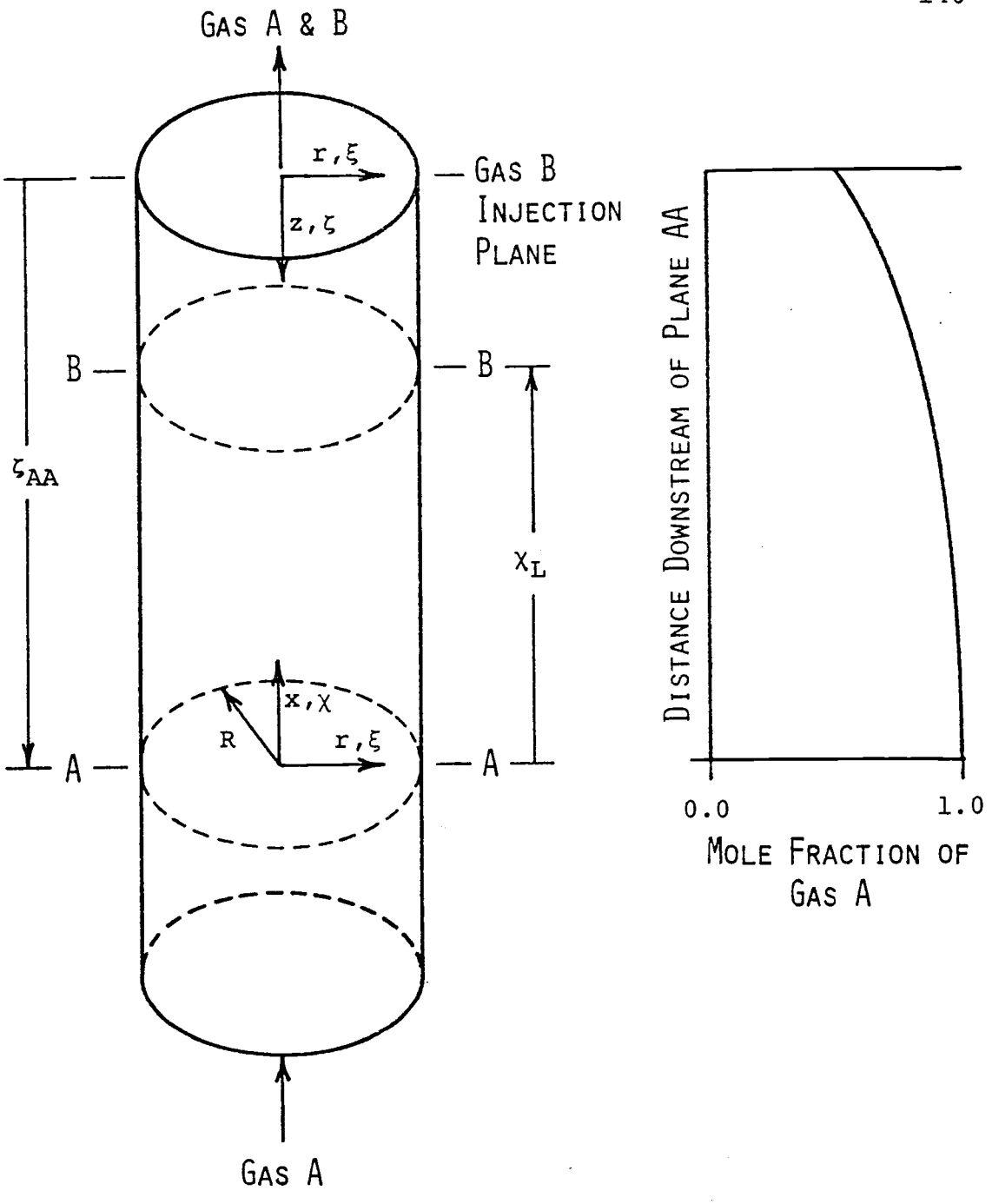

Figure 6.1. Control Volume for Formulating Equations Used to Compute Thermal Diffusion Factors and Molecular Diffusion Coefficients

mixture is dilute in the sense that only two-body collisions are likely to occur; the constituents of the gas mixture are ideal and nonreacting; and both gases enter the diffusion tube at the same temperature. In addition, the following contributions to the energy balance are assumed to be negligible and are therefore disregarded: radiant energy transfer within the gas mixture and between the gas mixture and its surroundings; changes in kinetic energy associated with the bulk flow; changes in potential energy as a function of position in the diffusion flow field; and frictional losses.

The first law of thermodynamics may be written as follows for a control volume (Welty, et al. (1969)):

$$\frac{\delta Q}{dt} - \frac{\delta W_s}{dt} = \iint_{c.s.} \left(\hat{e} + \frac{P}{\rho}\right)\rho(\vec{v}\cdot\vec{n})\,dA$$

$$+ \frac{\partial}{\partial t}\iiint_{c.v.} \hat{e}\rho\,dV + \frac{\delta W_\mu}{dt} \qquad (6.1)$$

where $\hat{e}$ is the energy per unit mass of the fluid. These terms represent, respectively, the rate of heat addition to the control volume, the rate of work done by the control volume on its surroundings that would cause a shaft to rotate or accomplish the raising of a weight; the net efflux of energy from the control volume; the rate of accumulation of energy within the control volume; and the

rate of work done to overcome viscous effects at the control surface. All symbols used in this equation and in the equations that follow are defined in Appendix A.

On the basis of the assumptions for this analysis, the second term on the left hand side and the second and third terms on the right hand side of equation 6.1 are zero. Contributions of the remaining terms to the energy balance over the control volume shown in Figure 6.1 may be expressed as follows:

Rate of energy transported out of the control volume across the cylindrical surface and surface BB	-	Rate of energy transported into the control volume across surface AA	=	0

or, in terms of the multicomponent energy flux $\vec{e}$, which includes all contributions to the transport of energy per unit area,

$$\int_{cyl} e_{cyl} dA + \int_{BB} e_{BB} dA - \int_{AA} e_{AA} dA = 0. \qquad (6.2)$$

6.1.1.2. Equation for Multicomponent Energy Flux $\vec{e}$

As shown in Appendix B (equation B.1), the multicomponent energy flux $\vec{e}$ within a dilute, nonreacting, binary gas mixture may be expressed as follows:

$$\vec{e} = -\lambda\vec{\nabla}T + (C_A H_A \vec{v}_A + C_B H_B \vec{v}_B)$$

$$+ knTX_A X_B \alpha_T (\vec{v}_A - \vec{v}_B). \qquad (6.3)$$

The terms grouped on the right hand side of this equation represent, respectively, energy transport by conduction due to inequalities of temperature in the gas mixture, energy transport associated with the molecules of gases A and B moving relative to stationary coordinates, and energy transport due to the diffusion-thermo effect.

As discussed in Appendix B, the Boltzmann constant k is related to the gas constant $\tilde{R}$ and the Avogadro number $\tilde{N}$ by $k = \tilde{R}/\tilde{N}$. In addition, $n = C\tilde{N}$, where n and C are, respectively, the number density and the molar density of the fluid. With these substitutions, equation 6.3 becomes

$$\vec{e} = -\lambda\vec{\nabla}T + (C_A H_A \vec{v}_A + C_B H_B \vec{v}_B)$$

$$+ C\tilde{R}TX_A X_B \alpha_T (\vec{v}_A - \vec{v}_B). \qquad (6.4)$$

6.1.1.3. Transport of Energy Across Individual Surfaces of the Control Volume

Equation 6.4 may be written as follows for the energy flux normal to surface BB of the control volume:

$$e_{BB} = \left[-\lambda\frac{\partial T}{\partial x} + (C_A H_A v_{A_x} + C_B H_B v_{B_x}) + C\mathring{R}TX_A X_B \alpha_T (v_{A_x} - v_{B_x})\right]_{BB}. \quad (6.5)$$

This equation may be integrated term-by-term over surface BB to obtain an expression for the rate at which energy is transported over the entire surface. Working first with the conduction term,

$$\int_{BB} -\lambda\frac{\partial T}{\partial x}\bigg|_{BB} dA = -2\pi\int_o^R \lambda\frac{\partial T}{\partial x}\bigg|_{BB} r dr. \quad (6.6)$$

The integral of the next two terms grouped together on the right hand side of equation 6.5 may be expressed as follows:

$$\int_{BB} (C_A H_A v_{A_x} + C_B H_B v_{B_x}) dA = \left[\bar{C}_A \bar{H}_A \bar{v}_{A_x} + \bar{C}_B \bar{H}_B \bar{v}_{B_x}\right]_{BB} A_{BB}.$$

In this equation and throughout the rest of this chapter, an overlined variable represents the average value of the variable over the flow cross section.

Noting that $\bar{\rho}_i \bar{v}_i A_{BB} = \dot{m}_i$, where $\dot{m}_i$ is the mass flow rate of constituent i over surface BB, the preceding equation may be written as follows:

$$\int_{BB} (C_A H_A v_{A_x} + C_B H_B v_{B_x}) dA = \left[\frac{\bar{C}_A}{\bar{\rho}_A} \bar{H}_A \dot{m}_A + \frac{\bar{C}_B}{\bar{\rho}_B} \bar{H}_B \dot{m}_B^{\,o}\right]_{BB}.$$

The last term is zero because the net mass flow rate of gas B is zero over any cross section through the diffusion flow field upstream of the gas B injection plane.

By definition, $C_i = \rho_i/M_i$, where C_i, ρ_i, and M_i are, respectively, the molar concentration, the mass density, and the molecular weight of constituent i. In addition, $\hat{H}_i = H_i/M_i$, where $\hat{H}_i$ is the enthalpy per unit mass and H_i is the partial molal enthalpy of constituent i. With these substitutions the preceding equation becomes

$$\int_{BB} (C_A H_A v_{A_X} + C_B H_B v_{B_X}) dA = \left[\hat{\bar{H}}_A \dot{m}_A\right]_{BB} . \qquad (6.7)$$

Proceeding in a similar manner with the last term of equation 6.5, the following equation is obtained:

$$\int_{BB} C\hat{R}T X_A X_B \alpha_T (v_{A_X} - v_{B_X}) dA = C\hat{R}\left[\frac{\bar{T}}{\bar{\rho}_A} \bar{X}_A \bar{X}_B \alpha_T \dot{m}_A\right]_{BB} .$$

As noted in section 4.2.1 of Chapter IV, $C_i = CX_i$, where C is the molar density of the mixture and X_i is the mole fraction of constituent i. With this relationship and the relationship $C_i = \rho_i/M_i$ discussed in the preceding paragraph, the last term of equation 6.5 may be written in the following form:

$$\int_{BB} C\hat{R}T X_A X_B \alpha_T (v_{A_X} - v_{B_X}) dA = \frac{\hat{R}}{M_A}\left[\bar{X}_B \bar{T} \alpha_T \dot{m}_A\right]_{BB} . \qquad (6.8)$$

Substituting equations 6.6 through 6.8 into equation 6.5, the rate at which energy is transported across surface BB of the control volume is as follows:

$$\int_{BB} e_{BB} dA = \left[-2\pi \int_{o}^{R} \lambda \frac{\partial T}{\partial x} \, r dr + \hat{\bar{H}}_A \dot{m}_A + \frac{\mathcal{R}}{M_A} \bar{X}_B \bar{T} \alpha_T \dot{m}_A \right]_{BB} . \tag{6.9}$$

In the formulation of equation 6.9, the only restriction placed on the axial position of surface BB of the control volume shown in Figure 6.1 is that it must be located upstream of the gas B injection plane. Equation 6.9 is therefore applicable to surface AA as well as to surface BB of the control volume.

Since surface AA is assumed to be located in a region of the flow field where only gas A is present, there are no concentration gradients and therefore no temperature gradients across it. Equation 6.9 may therefore be reduced to the following equation for the rate at which energy is transported across surface AA:

$$\int_{AA} e_{AA} dA = \left[\hat{\bar{H}}_A \dot{m}_A \right]_{AA} . \tag{6.10}$$

Across the cylindrical surface of the control volume, energy is assumed to be transported only by conduction. Accordingly,

$$\int_{cyl} e_{cyl} dA = -2\pi R \int_o^L \lambda \frac{\partial T}{\partial r}\Big|_R dx \qquad (6.11)$$

where L is the length and R is the radius of the cylinder.

6.1.1.4. Equation for α_T

After substituting equations 6.9 through 6.11 into equation 6.2, the equation for the energy balance over the control volume shown in Figure 6.1 becomes

$$-2\pi R \int_o^L \lambda \frac{\partial T}{\partial r}\Big|_R dx + \left[-2\pi \int_o^R \lambda \frac{\partial T}{\partial x} rdr + \hat{\bar{H}}_A \dot{m}_A + \frac{\hat{\bar{R}}}{M_A} \bar{X}_B \bar{T} \alpha_T \dot{m}_A \right]_{BB} - \left[\hat{\bar{H}}_A \dot{m}_A \right]_{AA} = 0.$$

This equation may be solved for the thermal diffusion factor α_T. Noting that the mass flow rate of nitrogen at any cross section through the flow field is constant, and using the perfect gas relationship $\Delta H = C_p \Delta T$, the equation for α_T may be expressed as follows:

$$\alpha_T\Big|_{BB} = \frac{1}{\dot{m}_A \frac{\hat{\bar{R}}}{M_A} \left[\bar{X}_B \bar{T} \right]_{BB}} \left[\dot{m}_A \hat{C}_{p_A} (\bar{T}_{AA} - \bar{T}_{BB}) + 2\pi \left(R \int_o^L \lambda \frac{\partial T}{\partial r}\Big|_R dx + \int_o^R \lambda \frac{\partial T}{\partial x}\Big|_{BB} rdr \right) \right] . \qquad (6.12)$$

For convenience in computing values of the thermal diffusion factor from the experimental data discussed in

Chapter VII, the integrals in equation 6.12 may be written in terms of the dimensionless coordinates $\xi = r/R$ and $\chi = x/R$. In terms of these coordinates, equation 6.12 becomes

$$\alpha_T\Big|_{BB} = \frac{1}{\dot{m}_A \frac{\mathring{R}}{M_A}[\bar{X}_B\bar{T}]_{BB}}\left[\dot{m}_A\hat{C}_{p_A}(\bar{T}_{AA} - \bar{T}_{BB}) + 2\pi R\left(\int_o^{\chi_L}\lambda\frac{\partial T}{\partial \xi}\Big|_{\xi=1}d\chi + \int_o^1 \lambda\frac{\partial T}{\partial \chi}\Big|_{BB}\xi d\xi\right)\right] . \quad (6.13)$$

A limitation of equations 6.12 and 6.13 is that neither can be used to compute the thermal diffusion factor corresponding to the flow conditions at any arbitrarily chosen point in the flow field. Rather, only the axial position of surface BB can be arbitrarily chosen. The thermal diffusion factor corresponding to a given position of surface BB is then computed on the basis of flow conditions averaged over the surface.

This limitation of equations 6.12 and 6.13 is not a serious one, however, for the diffusion flow conditions considered in the experimental investigation that is discussed in Chapter VII. As mentioned in section 3.5 of Chapter III, the thermal diffusion factor is a function of both the composition and the temperature of the gas mixture. Stock (1972) found that the radial variation in gas composition is relatively small (generally less than 2%) for all

of the flow conditions considered. On the basis of the data presented in Chapter VII, the largest variation in temperature measured for the flow fields is less than 1.5% on the Kelvin temperature scale. Accordingly, the thermal diffusion factor computed for flow conditions averaged over a given cross section through the diffusion flow field would not be expected to differ appreciably from values computed for individual points in the cross section.

6.1.2. Method of Solution

Program ALPHA, a copy of which is included in Appendix C, was written for use in computing values of the thermal diffusion factor from equation 6.13. Input required to run the program includes the mass flow rate of gas A, and the concentration, temperature, and mass average velocity distributions within the flow field. Although no terms for the mass average velocity appear explicitly in equation 6.13, the velocity distribution is necessary for evaluating the mixed mean temperatures and concentrations that are needed to compute values of the thermal diffusion factor.

6.1.2.1. Coordinate Systems and Grid for Numerical Computations

Two coordinate systems are shown in Figure 6.1. Experimental values of the velocity, concentration, and temperature distributions are organized on a grid relative to the (ζ,ξ) coordinate system, with an axial ($\Delta\zeta = \Delta z/R$) and radial ($\Delta\xi = \Delta r/R$) node spacing of 0.1. Values of the thermal diffusion factor are computed relative to the (χ,ξ) coordinate system.

As shown in Figure 6.2, the same grid is used for both coordinate systems. The grid nodes are numbered axially from k = 1 to k = NK relative to the (ζ,ξ) coordinates, with the origin (where k = 1) located at the gas B injection plane. Relative to the (χ,ξ) coordinates the nodes are numbered axially from m = 1 to m = MEND, with the origin located at surface AA of the control volume used in the formulation of equation 6.13. As noted in Figure 6.2, m = 1 corresponds to k = KSTRT, where KSTRT is the node number of surface AA relative to the gas B injection plane. The m and k numbering schemes are related in accordance with the equation k = KSTRT + 1 - m.

The grid is bounded radially by the diffusion tube centerline and the diffusion tube wall, and axially by the gas B injection plane and a cross section located sufficiently far upstream of the injection plane so that only

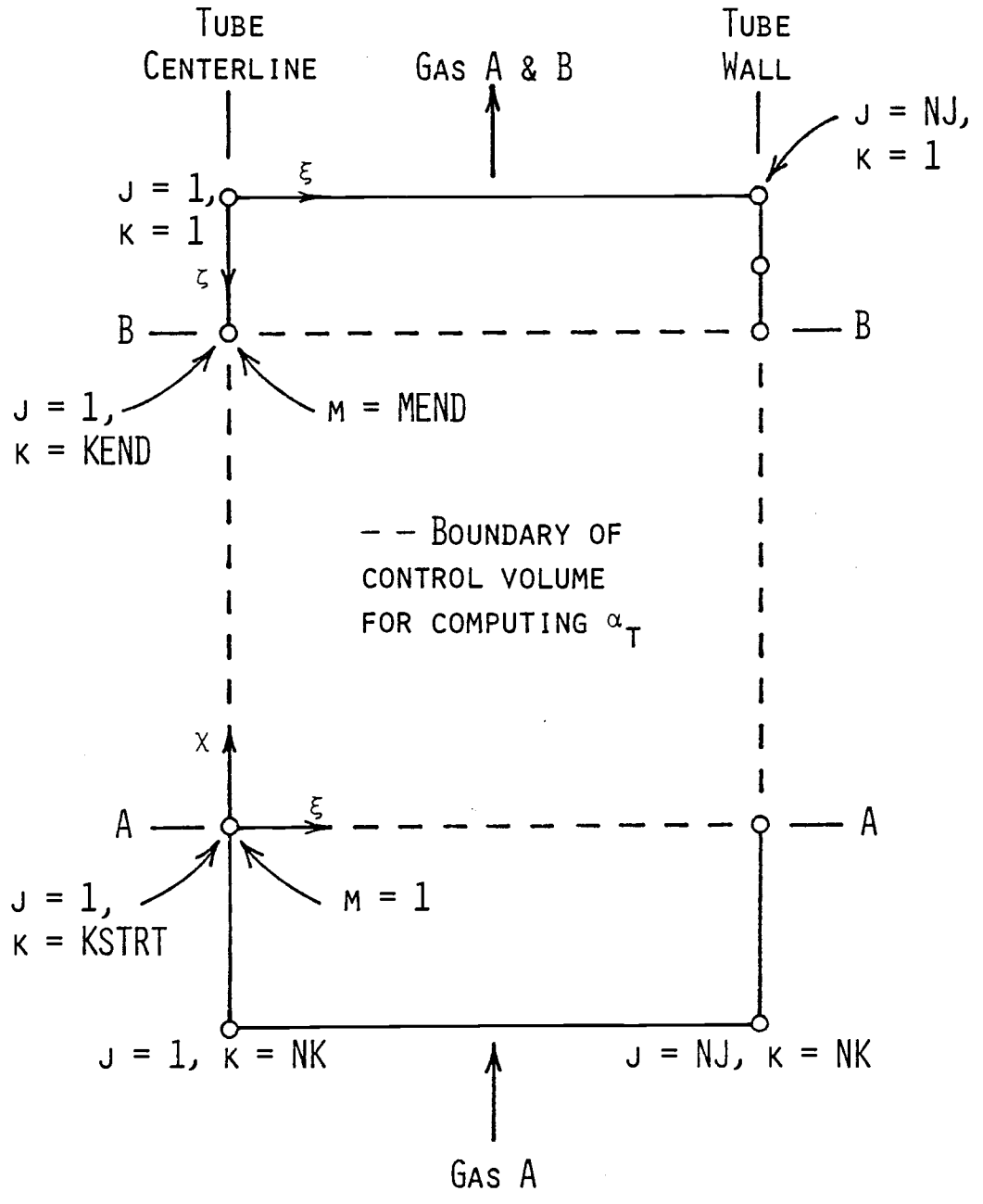

Figure 6.2. Grid System for Computing Thermal Diffusion Factors and Molecular Diffusion Coefficients

gas A flows over the cross section. To accommodate changes in the length of the diffusion flow field as a function of the flow conditions, the axial length of the grid may be varied relative to the gas B injection plane.

6.1.2.2. Computational Scheme for Evaluating α_T

Values of the thermal diffusion factor are computed in program ALPHA in the following manner. As part of the input data for the program, the axial position of surface AA of the control volume shown in Figure 6.1 is fixed at node k = KSTRT upstream of the gas B injection plane. The axial position of surface BB, and therefore the length of the control volume, is varied through the flow field starting two nodes downstream of surface AA and then proceeding in two-node increments toward the gas B injection plane. (The number of increments must be even to be compatible with the scheme used in program ALPHA for evaluating integrals over the surfaces of the control volume.) For each axial position of surface BB, the thermal diffusion factor is computed from equation 6.13. Program output includes values of the mixed mean composition of the gas mixture for all axial positions of surface BB, and the corresponding values of the thermal diffusion factor.

An abbreviated flow chart for program ALPHA is shown in Figure 6.3. The variables used in the flow chart

Program ALPHA

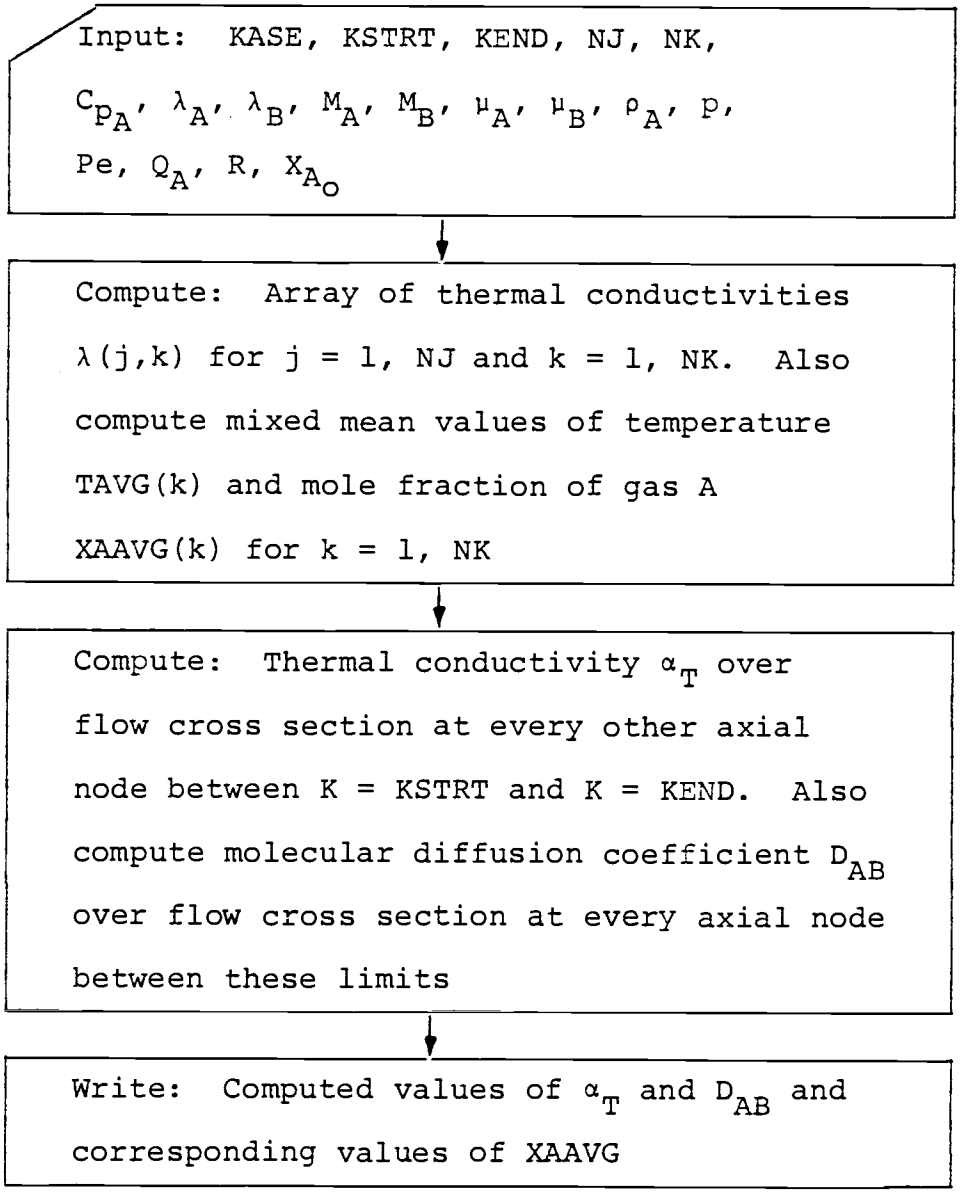

Figure 6.3. Flow Chart for Program ALPHA

are defined in the listing of program ALPHA included in Appendix C. As noted in Figure 6.3, program ALPHA is used to compute molecular diffusion coefficients as well as thermal diffusion factors. Procedures for computing molecular diffusion coefficients are discussed later in this chapter.

6.1.2.3. Numerical Formulas for Evaluating Derivatives and Integrals

Derivatives are evaluated in program ALPHA using the five-point differentiation formulas discussed in section 4.2.1 of Chapter IV. As noted in that section, the five-point formulas tend to reduce the effects of irregularities in the experimental data that would otherwise be magnified when taking derivatives of the data.

Simpson's rule is used in program ALPHA to evaluate integrals. In terms of the notation used in this thesis, Simpson's rule may be written as follows for performing integration in the radial direction:

$$\int_A^B F(\xi)\,d\xi = \frac{\Delta\xi}{3}\left[F(A) + 4F(A+1) + 2F(A+2) + \ldots + 4F(A+N-1) + F(B)\right] \qquad (6.14)$$

where N is the number of nodes. With a change in notation from ξ to χ, this formula is also applicable in the axial direction. A constraint that must be observed when preparing input data for program ALPHA is that Simpson's rule

as written above is applicable for use with only an even number of subintervals (and therefore an odd number of nodes).

6.1.2.4. Equations for Computing Average Values of Temperature, Gas Composition, and Velocity over the Flow Cross Section

As part of the data required to compute values of the thermal diffusion factor from equation 6.13, average values of the temperature and mole fraction of gas A are required over surface BB of the control volume shown in Figure 6.1. These values could be computed as arithmetic mean averages over the surface. A preferable approach, and the one used in program ALPHA, is to compute mixed mean values of these variables. The mixed mean values correspond to those that would be measured in a container if the fluid flowing through the cross section of interest were collected in the container and thoroughly mixed. Such values are therefore sometimes referred to in the literature as mixing-cup values.

An equation for the mixed mean temperature of the gas mixture flowing across surface BB may be formulated by considering the rate at which energy is transported by convection across the surface. This transport of energy may be expressed mathematically in several equivalent ways as follows:

$$\text{Energy convected across surface BB} = \left[\dot{m}\hat{C}_p\bar{T}\right]_{BB} = \left[(A\bar{v}\rho)\hat{C}_p\bar{T}\right]_{BB}$$

$$= 2\pi\int_o^R \left[v\rho\hat{C}_pT\right]_{BB} rdr.$$

Assuming that the variation in ρ and C_p over surface BB is negligible, this equation may be reduced to the following:

$$\bar{T}_{BB} = \frac{2\pi}{[A\bar{v}]_{BB}}\int_o^R [vT]_{BB} rdr.$$

After substituting πR^2 for A_{BB} and incorporating the dimensionless variables $\xi = r/R$ and $V = v/\left|\bar{V}_{A_o}\right|$, where $\bar{V}_{A_o}$ is the average velocity of gas A over any diffusion tube cross section located sufficiently far upstream of the gas B injection plane so that only gas A is present, the preceding equation becomes

$$\bar{T}_{BB} = \frac{2}{\bar{V}_{BB}}\int_o^1 [VT]_{BB}\xi d\xi. \qquad (6.15)$$

In a similar manner an equation may be formulated for the mixed mean mole fraction of gas A over surface BB. The result is as follows:

$$\bar{X}_{A_{BB}} = \frac{2}{\bar{V}_{BB}}\int_o^1 [VX_A]_{BB}\xi d\xi. \qquad (6.16)$$

Included in equations 6.15 and 6.16 is a term for the average velocity of the gas mixture across surface BB. An equation for the average velocity may be formulated by considering the mass flow rate across surface BB as follows:

$$\dot{m}_{BB} = [\rho \bar{v} A]_{BB} = \int_{BB} [v\rho]_{BB} dA.$$

If the radial variation of the gas density is assumed to be negligible,

$$\bar{v}_{BB} = \frac{1}{A_{BB}} \int_{BB} v_{BB} dA.$$

In terms of the dimensionless variables $\xi = r/R$ and $V = v/|\bar{V}_{A_o}|$, the preceding equation becomes

$$\bar{V}_{BB} = 2 \int_{o}^{1} V \xi d\xi. \qquad (6.17)$$

6.1.2.5. Procedure for Estimating Missing Data

At every node in the grid illustrated in Figure 6.2, values of the velocity, concentration, and temperature must be specified as part of the input data for program ALPHA. Over 700 nodes are used in the grid for the flow conditions considered in this thesis. Since the diffusion flow field can be well defined without taking data at that many nodes, it is necessary to have a means for estimating

values of missing data needed as input for program ALPHA. Program RADTEMP, a copy of which is included in Appendix C, was written for this purpose.

The discussion that follows is limited to comments on the use of program RADTEMP for estimating the radial temperature profile at any cross section through the flow field where only the centerline temperature is known. The program is also suitable, however, for use in estimating values of radial concentration and velocity profiles over cross sections where they were not measured.

At any cross section through the flow field where the temperature is known only at the centerline, the missing values of the radial temperature profile are estimated in program RADTEMP as follows. Let ζ_A denote the axial position of the cross section. In addition, let ζ_U and ζ_D denote, respectively, the positions of cross sections upstream and downstream of ζ_A for which radial temperature measurements are available. Then, assuming that the missing values of the radial profile are on a curve that passes through the measured centerline value, denoted as $T_{\zeta_A}\big|_{CL}$, and that the curve is similar in shape to the measured temperature profiles, the temperature $T_{\zeta_A}\big|_{\xi_R}$ at any radial location ξ_R may be estimated using the following equation:

$$\left.\frac{T_{\zeta_A} - T_{\zeta_U}}{T_{\zeta_D} - T_{\zeta_U}}\right|_{\xi_R} = \left.\frac{T_{\zeta_A} - T_{\zeta_U}}{T_{\zeta_D} - T_{\zeta_U}}\right|_{CL} \tag{6.18}$$

where all temperatures used to estimate $T_{\zeta_A}\big|_{\xi_R}$ are experimental values. This equation is used to estimate missing values of the radial temperature profile for all of the nodes over the cross section.

6.2. Model for Computing Molecular Diffusion Coefficients

In the following paragraphs, an equation is formulated for use in computing molecular diffusion coefficients from data taken in the experimental apparatus discussed in Chapter V. Attention is restricted in this formulation to flow-coupled diffusion occurring within the diffusion tube illustrated in Figure 6.1.

6.2.1. Formulation of Equation for D_{AB}

This analysis is based on the following assumptions: the bulk flow is steady, laminar, and axisymmetric; throughout the flow field, the pressure is constant; the gas mixture is dilute in the sense that only two-body collisions are likely to occur; the constituents of the gas mixture are ideal and nonreacting; gravity is the only force field acting on the constituents of the gas mixture; and both gases enter the diffusion tube at the same temperature.

It is convenient to commence this analysis by considering the general equation of diffusion, which may be

written as follows for a binary gas mixture (Chapman and Cowling (1970), equation 14.1,1):

$$\vec{V}_{D_A} - \vec{V}_{D_B} = -\frac{D_{AB}}{X_A X_B}\left[\vec{\nabla}X_A + \frac{n_A n_B (m_B - m_A)}{n\rho}\,\vec{\nabla}\ln(p) + k_T\vec{\nabla}\ln(T) - \frac{\rho_A \rho_B}{p\rho}\,(\vec{F}_A - \vec{F}_B)\right]. \qquad (6.19)$$

In this equation, $\vec{V}_{D_A}$ and $\vec{V}_{D_B}$ are the diffusion velocities of gases A and B relative to the mass average velocity of the gas mixture. The four groups of terms on the right hand side of the equation represent, respectively, components of diffusion due to nonuniformities of composition, pressure, and temperature of the gas mixture, and a component of diffusion that occurs if each constituent of the gas mixture is under the influence of a different external force. (This last term is significant when, for example, ionic constituents of a mixture diffuse under the influence of an electric field.)

On the basis of the assumptions for this analysis, the pressure diffusion and forced diffusion terms in equation 6.19 are zero. Furthermore, the thermal diffusion term is negligible compared to the term associated with nonuniformity of gas composition. This latter simplification may be made because, as discussed in Chapter II, temperature gradients are much less significant than con-

centration gradients as driving forces for the transport of mass. With these simplifications, equation 6.19 becomes

$$\vec{V}_{D_A} - \vec{V}_{D_B} = -\frac{D_{AB}}{X_A X_B}\vec{\nabla}X_A. \tag{6.20}$$

As shown in Appendix B,

$$\vec{V}_{D_A} - \vec{V}_{D_B} = \vec{v}_A - \vec{v}_B$$

where $\vec{v}_A$ and $\vec{v}_B$ are the mass average velocities of gases A and B, respectively, relative to stationary coordinates. In addition, as shown in the development of equation B.4 of Appendix B,

$$\vec{v}_A - \vec{v}_B = \frac{M(\vec{v}_A - \vec{v})}{X_B M_B}$$

where $\vec{v}$ is the mass average velocity of the gas mixture. With the use of these two equations, equation 6.20 may be written as follows:

$$\frac{M}{M_B}(\vec{v}_A - \vec{v}) = -\frac{D_{AB}}{X_A}\vec{\nabla}X_A . \tag{6.21}$$

The mass flux of gas A relative to the mass average velocity $\vec{v}$ of the gas mixture is defined as follows (Bird, et al. (1960)):

$$\vec{j}_A = \rho_A(\vec{v}_A - \vec{v}).$$

This equation may be combined with equation 6.21 to yield the following equation for $\vec{j}_A$:

$$\vec{j}_A = -D_{AB} \frac{\rho_A M_B}{X_A M} \vec{\nabla} X_A \ .$$

Noting that $\rho_A = C_A M_A$, $X_A = C_A/C$, and $C = \rho/M$ (Bird, et al. (1960)), the preceding equation may be written in the following form:

$$\vec{j}_A = -D_{AB} C \frac{M_A M_B}{M} \vec{\nabla} X_A \ . \qquad (6.22)$$

For later computational convenience, it is desirable to relate the molecular diffusion coefficient D_{AB} to $\dot{m}_A$, the mass flow rate of gas A, rather than to $\vec{j}_A$. Referring to Figure 6.1, the following equation may be written for the mass flow rate of gas A normal to cross section BB located at any arbitrary axial position in the diffusion flow field:

$$\dot{m}_A = \left[\vec{j}_{A_x} + \overline{\rho \omega_A} \bar{v}_x \right]_{BB} A_{CS}$$

where A_{CS} is the area of the cross section through the flow field and ω_A, the mass fraction of gas A, is defined as $\omega_A = \rho_A/\rho$. As in section 6.1 of this chapter, an overlined variable represents the average value of the variable over the flow cross section.

As noted previously in this section, $\rho_A = C_A M_A$ and $C_A = CX_A$. With these relationships and the relationship $\omega_A = \rho_A/\rho$, the preceding equation for $\dot{m}_A$ may be written as follows:

$$\dot{m}_A = \left[\bar{j}_{A_x}\right]_{BB} A_{CS} + M_A\left[\bar{C}\bar{X}_A\bar{v}_x\right]_{BB} A_{CS} . \tag{6.23}$$

Equations 6.22 and 6.23 may be combined to yield the following equation relating $\dot{m}_A$ and D_{AB}:

$$\dot{m}_A = -M_A M_B\left[\frac{D_{AB}\bar{C}}{\bar{M}}\frac{d\bar{X}_A}{dx}\right]_{BB} A_{CS} + M_A\left[\bar{C}\bar{X}_A\bar{v}_x\right]_{BB} A_{CS} . \tag{6.24}$$

A similar equation may be written for $\dot{m}_B$. Noting that the net mass flow rate of gas B is zero over any cross section through the diffusion flow field upstream of the gas B injection plane,

$$\dot{m}_B = -M_A M_B\left[\frac{D_{BA}\bar{C}}{\bar{M}}\frac{d\bar{X}_B}{dx}\right]_{BB} A_{CS} + M_B\left[\bar{C}\bar{X}_B\bar{v}_x\right]_{BB} A_{CS} = 0. \tag{6.25}$$

Equation 6.25 may be solved for $\bar{v}_x$, and the resulting expression may be substituted for $\bar{v}_x$ in equation 6.24. The equation for $\bar{v}_x$ is as follows:

$$\bar{v}_x\Big|_{BB} = \dot{M}_A\left[\frac{D_{BA}}{\bar{X}_B\bar{M}}\frac{d\bar{X}_B}{dx}\right]_{BB}$$

or, noting that $D_{BA} = D_{AB}$ and $\frac{d\bar{X}_B}{dx} = \frac{d}{dx}(1-\bar{X}_A) = -\frac{d\bar{X}_A}{dx}$,

$$\bar{v}_x\Big|_{BB} = -M_A\left[\frac{D_{AB}}{\bar{X}_B\bar{M}}\frac{d\bar{X}_A}{dx}\right]_{BB} . \tag{6.26}$$

With the use of equation 6.26 and the relationship $X_AM_A + X_BM_B = M$ (Bird, et al. (1960)), equation 6.24 takes the form

$$\dot{m}_A = -M_AA_{CS}\left[\frac{D_{AB}\bar{C}}{\bar{X}_B}\frac{d\bar{X}_A}{dx}\right]_{BB} . \tag{6.27}$$

As discussed in Appendix B, the molar density C of the mixture is related to the pressure and temperature of the mixture by the expression $C = p/(\mathring{R}T)$, where $\mathring{R}$ is the gas constant. With the use of this relationship, equation 6.27 may be rearranged to yield the following:

$$D_{AB}\Big|_{BB} = -\frac{\dot{m}_A\mathring{R}}{pA_{CS}M_A}\left[\frac{\bar{T}\bar{X}_B}{\frac{d\bar{X}_A}{dx}}\right]_{BB} . \tag{6.28}$$

For convenience in computing values of the molecular diffusion coefficient from the experimental data discussed in Chapter VII, the derivative in equation 6.28 may be written in terms of the dimensionless coordinate $\chi = x/R$. With this change and with the use of the relationship $X_A + X_B = 1$, equation 6.28 becomes

$$D_{AB}\Big|_{BB} = -\frac{\dot{m}_A \tilde{R} R}{p A_{CS} M_A}\left[\frac{\bar{T}(1 - \bar{X}_A)}{\frac{d\bar{X}_A}{dX}}\right]_{BB} . \qquad (6.29)$$

Equation 6.29 is in the form used in program ALPHA for computing molecular diffusion coefficients.

6.2.2. Method of Solution

The molecular diffusion coefficient corresponding to any arbitrary axial position of cross section BB through the diffusion flow field is computed from equation 6.29 on the basis of flow conditions averaged over the cross section. As discussed in section 6.1.1.4, radial variations of the gas temperature and the gas composition are relatively small (generally less than 2%) over any cross section through the flow field for the flow conditions considered in the experimental investigation. Accordingly, the molecular diffusion coefficient computed for flow conditions averaged over any given cross section would not be expected to differ appreciably from values computed for individual points in the cross section.

The computations are performed in program ALPHA using the grid system discussed in section 6.1.2.1. Referring to Figure 6.2, the axial position of cross section BB is varied through the flow field starting at the node corresponding to m = 1 and then proceeding axially node-by-node toward the

gas B injection plane. For each axial position of cross section BB, the molecular diffusion coefficient is computed from equation 6.29. Program output includes values of the mixed mean composition of the gas mixture for all axial positions of cross section BB, and the corresponding values of the molecular diffusion coefficient.

Values of the derivative term in equation 6.29 are evaluated in program ALPHA using the five-point differentiation formulas discussed in section 4.2.1 of Chapter IV. Mixed mean values of variables over cross section BB are evaluated using the equations discussed in section 6.1.2.4.

VII. RESULTS OF EXPERIMENTAL INVESTIGATION AND INTERPRETATION OF DATA

Experimental measurements of temperature effects associated with flow-coupled diffusion are presented in this chapter. The measurements were taken for a variety of flow conditions established in the experimental apparatus described in Chapter V.

Also presented in this chapter are thermal diffusion factors and molecular diffusion coefficients that were computed on the basis of the concentration and velocity fields measured by Stock (1972) combined with the temperature fields measured as part of the experimental investigation for this thesis. These transport coefficients were computed using the equations developed in Chapter VI. The results are compared with predictions from existing analytical models and with experimental results obtained by other investigators.

7.1. Temperature Measurements

Axial and radial temperature profiles were measured for four sets of flow conditions established in the vertically oriented, cylindrical diffusion tube illustrated in Figure 5.4 of Chapter V. The flow conditions under which measurements were taken are the same as those for which predicted temperature distributions were computed on the

basis of the theory discussed in Chapter IV. These flow conditions are as follows:

$$Pe = 1.9, \quad X_{A_o} = 0.5,$$

$$Pe = 3.8, \quad X_{A_o} = 0.5,$$

$$Pe = 3.8, \quad X_{A_o} = 0.7,$$

$$\text{and } Pe = 5.9, \quad X_{A_o} = 0.7.$$

For each set of flow conditions, the value of X_{A_o} is the mole fraction of gas A (nitrogen) at the secondary gas injection plane.

Whenever the apparatus was operated for taking data, the laboratory temperature was maintained at 21° C $\pm$ 0.5° C. The thermal shielding described in section 5.5 of chapter V was effective for isolating the diffusion tube and flow circuitry from fluctuations in the laboratory temperature. No temperature differences detectable with the instrumentation used in the apparatus existed between the two gases entering the diffusion tube.

The diffusion tube pressure was maintained at 10 $\pm$ 0.1 cm Hg gage for all tests. As discussed in section 5.2.4.2, the diffusion apparatus must be operated at a pressure higher than atmospheric pressure so that a pressure difference is available for inducing gas samples to flow from the apparatus to the concentration detector used to analyze gas composition.

7.1.1. Centerline Temperature Profiles

Centerline temperature profiles for the four flow conditions under which data were taken are shown in Figures 7.1 through 7.4. Also shown in these figures are centerline concentration profiles plotted from data taken by Stock (1972).

Each centerline temperature profile in Figures 7.1 through 7.4 is drawn through the mean values of corresponding measurements from two sets of data for the profile. A period of days or, in some cases, weeks elapsed between the initial run to obtain temperature data for a given set of flow conditions and a repeated run to confirm the data. Accordingly, the operating conditions in the diffusion apparatus were reset anew whenever a run was repeated. The data obtained during these runs are tabulated in Appendix F, and sources of error in the data are discussed in section 7.1.4.

The coordinate system used in Figures 7.1 through 7.4 is the same as that used in Figures 4.5 through 4.8 for plots of the centerline temperature profiles computed on the basis of theory. As discussed in section 4.4.3 of Chapter IV, the axial coordinate ($\zeta = z/R$) used in these figures is a reference for positions upstream of and relative to the helium injection plane. The origin of this coordinate coincides with the injection plane, and

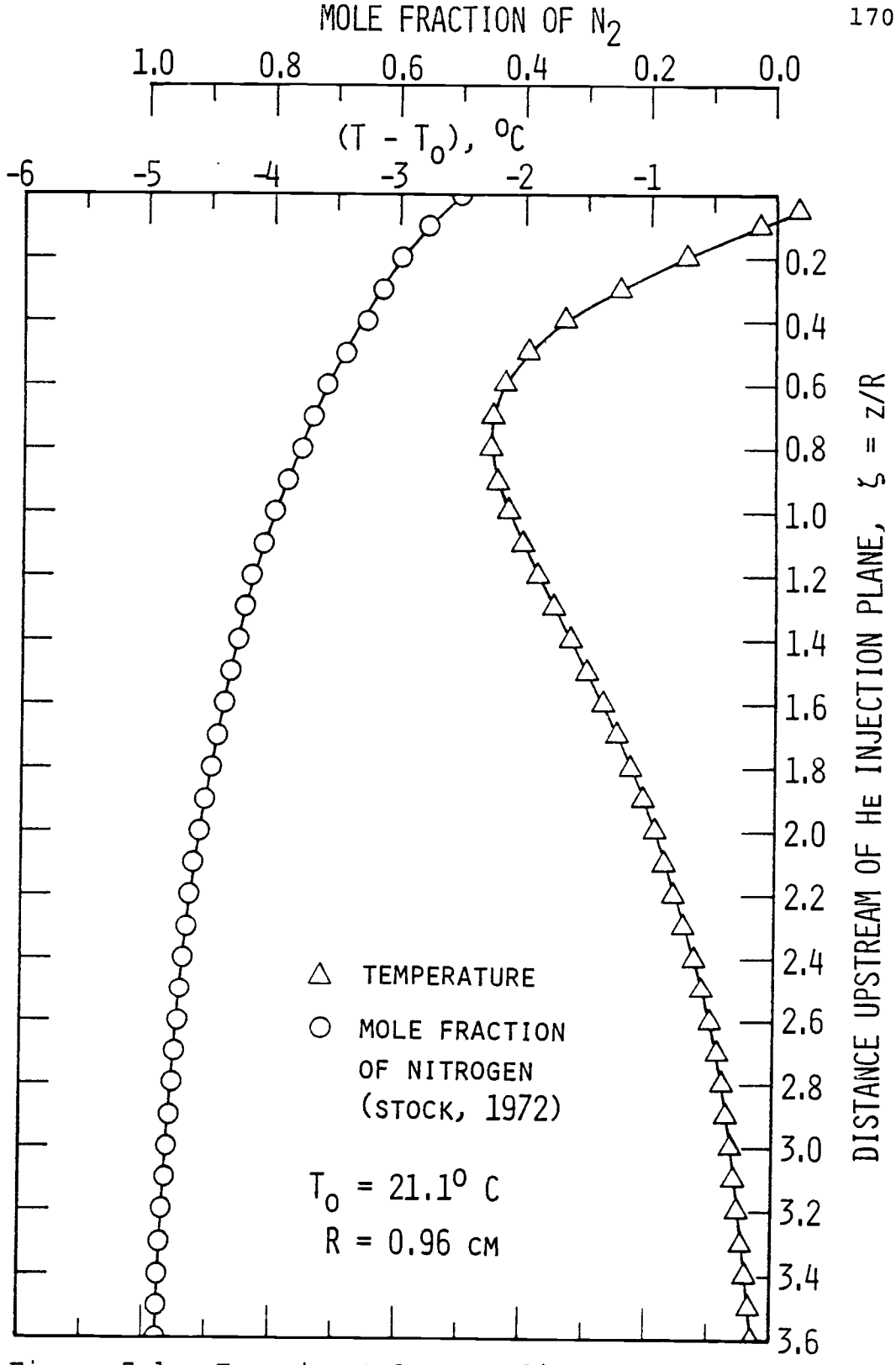

Figure 7.1. Experimental Centerline Temperature and Concentration Profiles for Pe = 1.9, X_{A_o} = 0.5

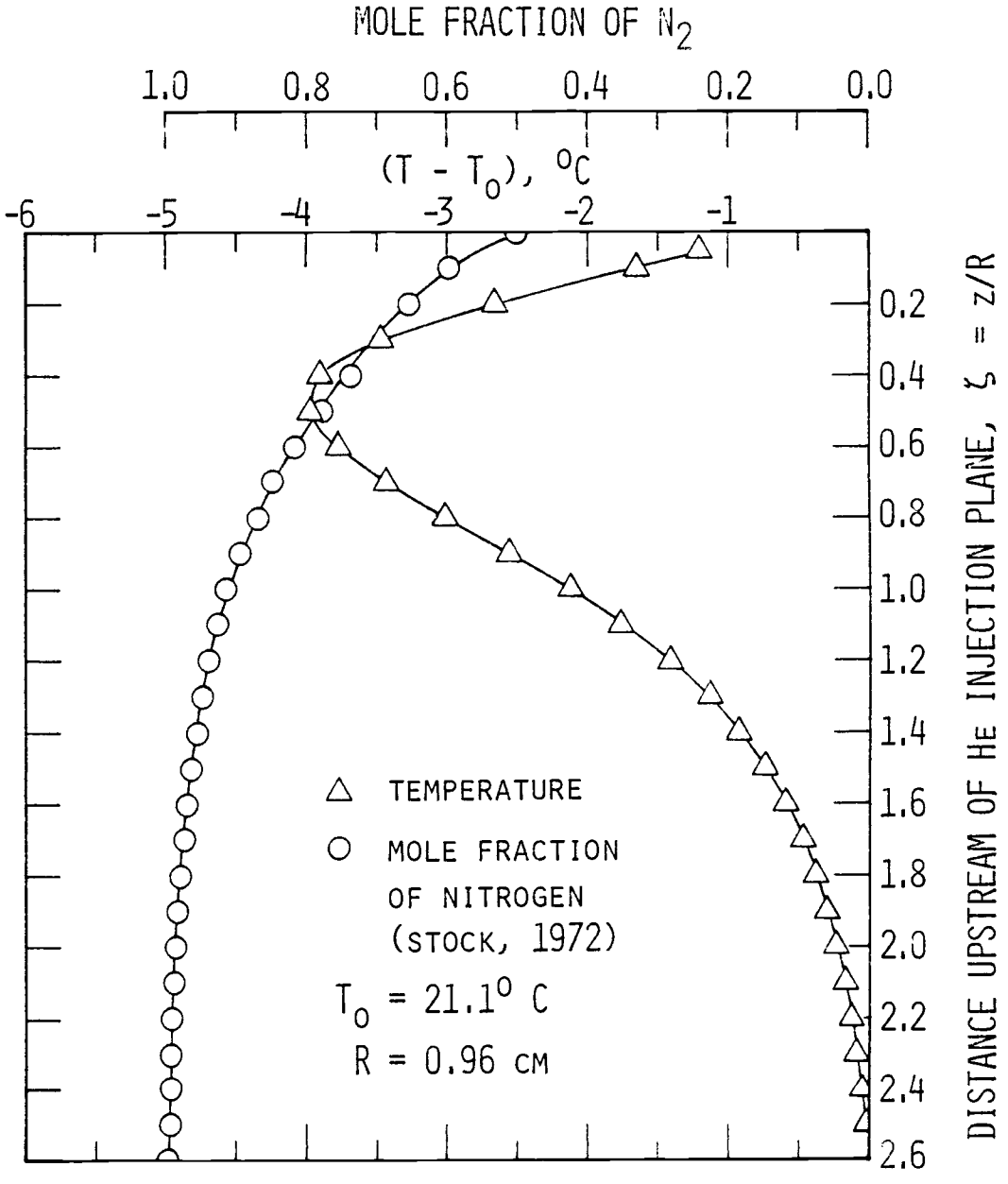

Figure 7.2. Experimental Centerline Temperature and Concentration Profiles for Pe = 3.8, $X_{A_o} = 0.5$

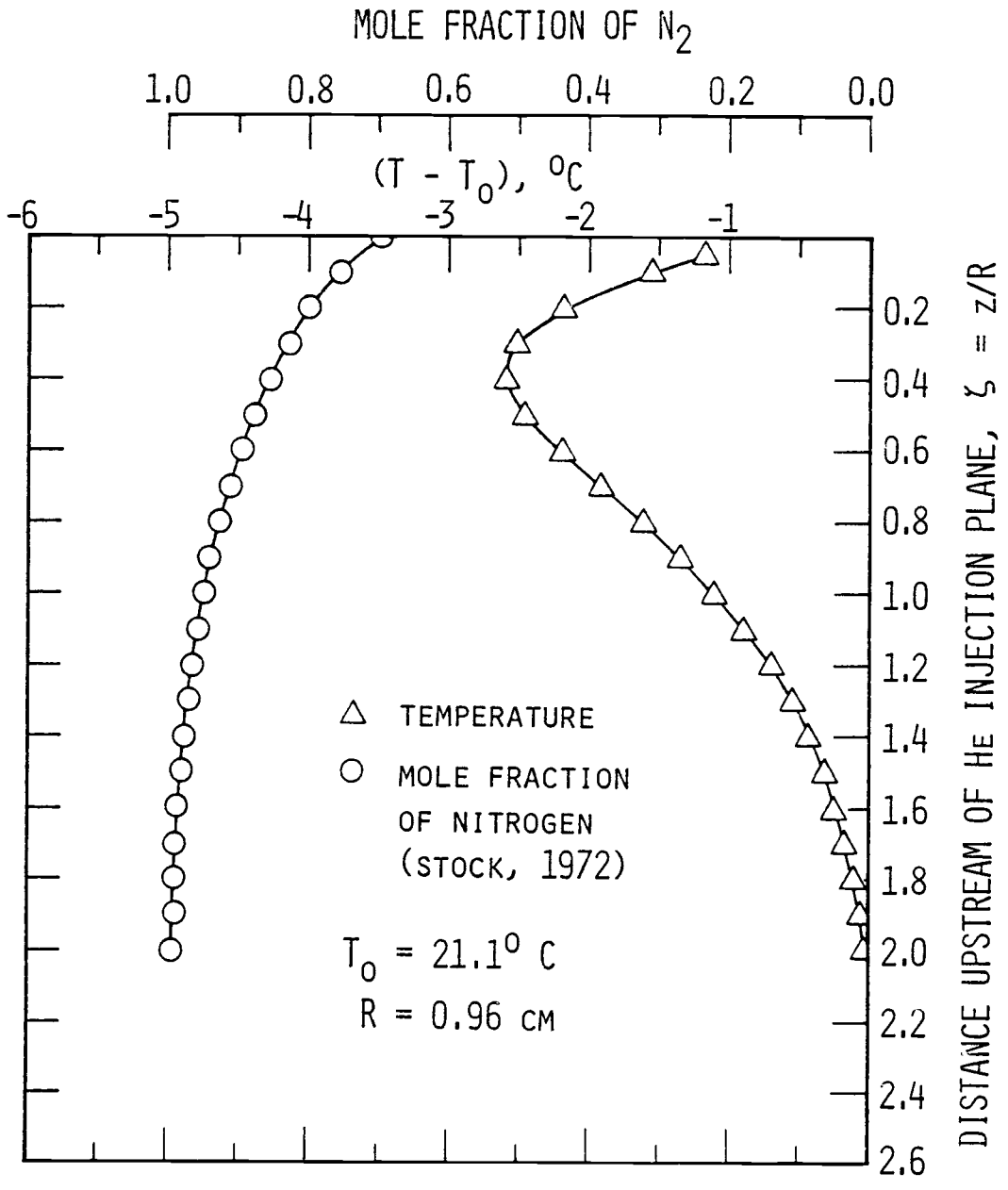

Figure 7.3. Experimental Centerline Temperature and Concentration Profiles for Pe = 3.8, $X_{A_o} = 0.7$

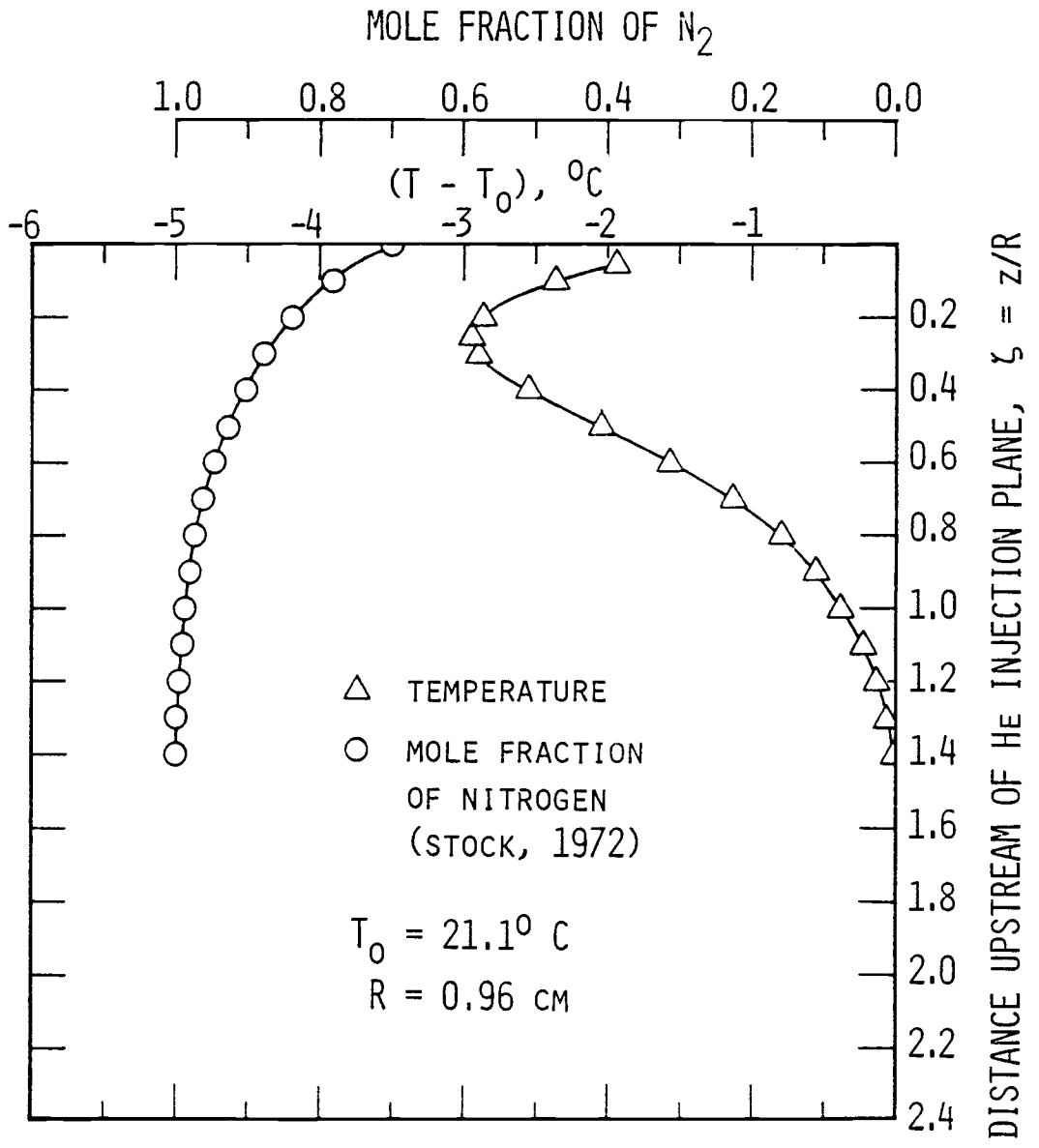

Figure 7.4. Experimental Centerline Temperature and Concentration Profiles for Pe = 5.9, X_{A_o} = 0.7

the coordinate is positive in the direction opposite to the direction of bulk flow through the diffusion tube.

It is useful for the discussion that follows to briefly review the flow paths followed by the gases supplied to the diffusion tube. Referring to Figure 5.4, nitrogen flows upward through the diffusion tube, and helium is injected through the plane formed by the outlets of the secondary gas injection tubes. Under each set of flow conditions considered in this investigation, the average velocity of the nitrogen is sufficiently low so that helium diffuses against the bulk flow. Thus, along the direction of bulk flow the proportion of helium contained in the gas mixture increases from zero at locations far upstream of the helium injection plane to a value that can be varied arbitrarily at the injection plane. The gas mixture flows past the injection tubes to the diffusion tube outlet.

Under these flow conditions, mass is transported by both convection and diffusion in the region immediately upstream of the helium injection plane. This combined transport may be referred to as flow-coupled diffusion. As discussed in Chapter I, the relative magnitudes of these two transport processes may be expressed in terms of the mass Peclet number for the flow. Upper and lower bounds on the Peclet number range for flows in which both transport processes are significant are discussed in

section 4.1 of Chapter IV.

Associated with the concentration gradients upstream of the helium injection plane are temperature gradients resulting from energy transport due to the diffusion-thermo effect. As shown in Figures 7.1 through 7.4, the temperature distributions vary with the diffusion flow conditions, but the centerline temperature profiles for the flow conditions considered in this investigation all have a common characteristic shape. Comments on the general shape of these profiles are included in section 4.4.3 of Chapter IV, where the centerline temperature profiles computed on the basis of theory are discussed.

As may be seen by comparing Figures 7.2 and 7.3, the temperature effects associated with flow-coupled diffusion in flow fields for which the Peclet number is the same are strongly influenced by the relative proportions of the two gases at the helium injection plane. The temperature profiles in both figures are for flows corresponding to a Peclet number of 3.8, but the mole fraction of nitrogen at the helium injection plane is 0.5 for the profile in Figure 7.2 and 0.7 for the profile in Figure 7.3. Relative to the reference temperature of the gases entering the diffusion tube, the minimum value of the temperature profile in the former figure is approximately 53% lower than that in the latter.

A strong Peclet number influence on the temperature

effects associated with flow-coupled diffusion is observed when comparing the temperature measurements taken in flow fields for which the Peclet numbers differ but in which flow conditions are otherwise the same. The Peclet number influence on the temperature fields is illustrated in Figures 7.1 and 7.2 (for Peclet numbers of 1.9 and 3.8, respectively, with the mole fraction of nitrogen at the helium injection plane, X_{A_o}, set at 0.5) and in Figures 7.3 and 7.4 (for Peclet numbers of 3.8 and 5.9, respectively, with X_{A_o} set at 0.7). As may be seen by comparing the centerline concentration profiles plotted in these figures, axial concentration gradients in the diffusion field are less steep, and the diffusion field extends further upstream from the helium injection plane for flows corresponding to lower Peclet numbers than for those corresponding to higher Peclet numbers. Accompanying the steeper concentration gradients in the latter flows are more pronounced temperature changes, as shown in these figures.

7.1.2. Radial Temperature Profiles

Shown in Figure 7.5 are two radial temperature profiles that were measured at the same axial position relative to the helium injection plane and under the same flow conditions. The radial traverse to measure the data identified by squares in that figure, however, was taken with a thermocouple probe inserted at a circumferential

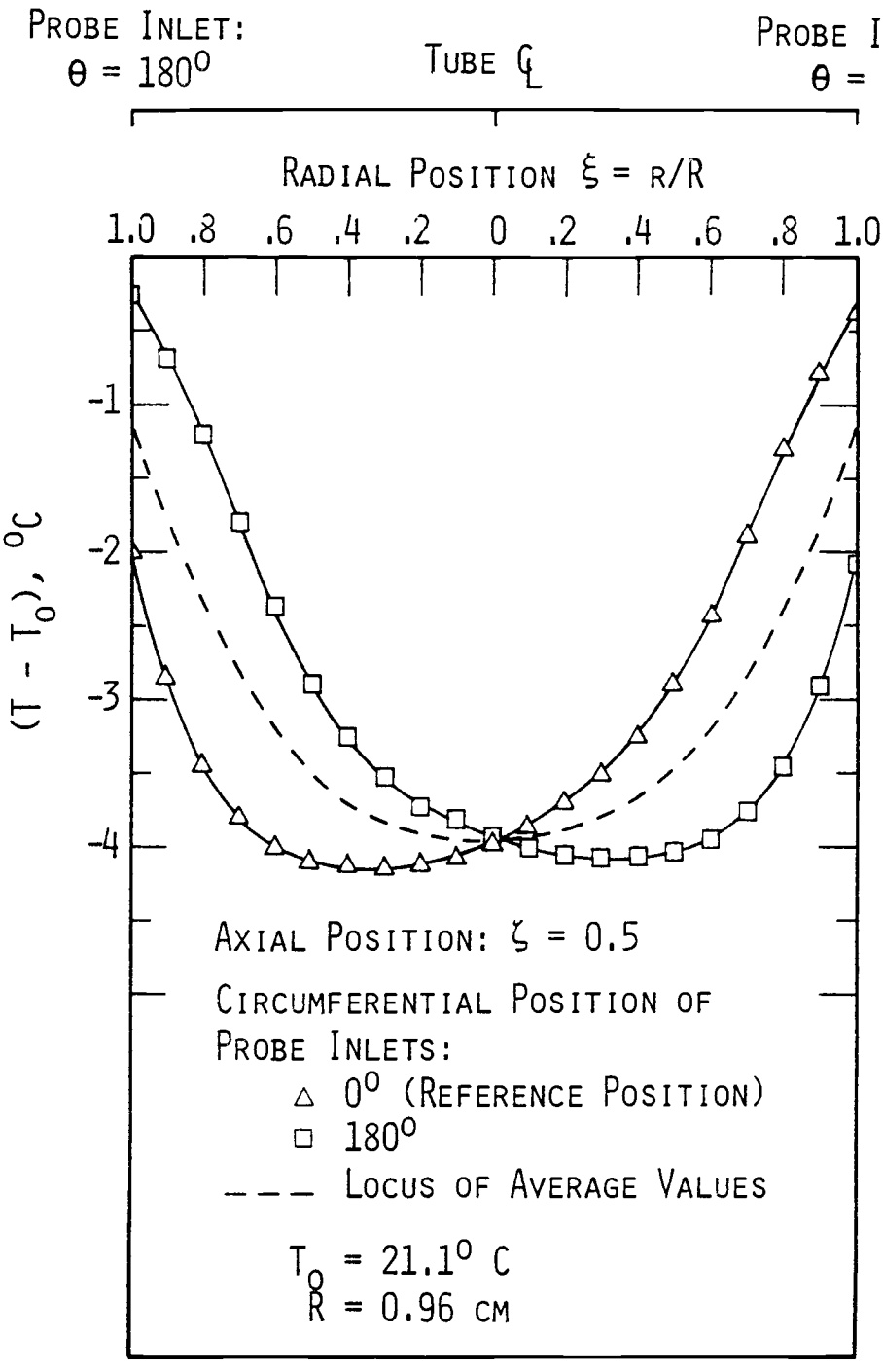

Figure 7.5. Radial Temperature Profiles for Pe = 3.8, X_{A_o} = 0.5, Measured with Probe Entering Flow Field from Opposite Circumferential Positions

position opposite the one for the traverse to measure the data identified by triangles. (Using the probe positioning systems discussed in section 5.4 of Chapter V, the positions of the diffusion tube thermocouple probes can be varied circumferentially as well as axially and radially relative to the helium injection plane.) These two profiles exhibit the asymmetry common to the radial profiles measured for all of the test conditions considered in this investigation. The data for these profiles are included in Appendix F.

The fact that the two radial temperature profiles in Figure 7.5 are essentially mirror images of each other provides a strong indication that the actual temperature distribution in the flow field is axisymmetric. Possible causes of the asymmetry in the as-measured profiles include (1) flow disturbances associated with the presence of a thermocouple probe in the flow field, and (2) the much greater thermal conductivity of the probe compared to that of the gas mixture.

Each thermocouple probe used in the diffusion apparatus is small in diameter (0.025 cm O.D.). The Reynolds number for flow over a probe of this diameter is less than unity under all four sets of flow conditions for which data were taken. Flow disturbances due to the presence of a probe in the diffusion tube are therefore minimal, and are not likely to be a significant cause of the asymmetry

found in the radial temperature profiles.

As discussed in section 5.3 of Chapter V, the leads in each diffusion tube thermocouple probe are tightly packed in magnesium oxide insulation and surrounded by a thin stainless steel sheath. The thermal conductivity of such an assembly is relatively small (approximately 0.10 watt/(cm^{o}K)). Nevertheless, this thermal conductivity is over 100 times greater than that typical of the gas mixtures in which temperatures were measured.

When the relatively large difference between the thermal conductivity of the thermocouple probes and the thermal conductivity characteristic of gases is taken into consideration, the asymmetry in the as-measured radial temperature profiles is not surprising. A thermocouple probe constitutes a path along which heat can be transferred by conduction. Heat transferred along that path to or from the sensing junction at the tip of the probe can significantly affect the values measured at the junction. The effect on the thermocouple reading is dependent, in part, on the temperature gradients to which the probe is exposed in the flow field.

As shown in Figure 7.5, temperature effects measured at radial locations between a given probe inlet passage and the diffusion tube centerline are not as large in magnitude as those measured at corresponding radial locations on the opposite side of the centerline. (Tempera-

tures in the diffusion tube are measured relative to the common temperature of the gases entering the diffusion tube, as discussed in section 5.3.3 of Chapter V.) When a probe is inserted to any position between its wall-mounted inlet and the diffusion tube centerline, the probe tip is exposed to a colder temperature than the temperatures at other points along the probe body. Accordingly, heat is transferred by conduction along the probe body to the sensing junction at the probe tip, with the result that the temperature sensed at the junction is not as low as the actual gas temperature at that location.

When a probe is inserted radially to a position on the opposite side of the diffusion tube centerline from its wall-mounted inlet, the probe tip is exposed to a warmer temperature than that to which the probe body is exposed at the centerline. Consequently, heat is transferred by conduction along the probe body from the sensing junction at the probe tip toward the tube centerline, with the result that the temperature sensed at the junction is lower than the actual gas temperature at that location.

For the reasons discussed above, the errors in temperature measurements taken in a traverse between a wall-mounted probe inlet passage and the diffusion tube centerline are different from those in measurements taken with the probe inserted to corresponding locations on the opposite side of the centerline. Thus, even if the tempera-

ture field being measured is axisymmetric, the as-measured radial temperature profiles exhibit asymmetry as shown in Figure 7.5.

7.1.2.1. Reduction of As-Measured Radial Temperature Profiles to a Form Suitable for Use in Computing Transport Coefficients

The experimental temperature data discussed in this chapter, together with the velocity and concentration data measured by Stock (1972), may be used as input for computing thermal diffusion factors and molecular diffusion coefficients from the equations developed in Chapter VI. Before using the temperature data for this purpose, however, it is necessary to reduce the radial temperature profiles to a form that is consistent with the axisymmetric flow conditions under which they were measured.

One way to correct the as-measured temperature data for a given set of flow conditions would be to compute estimates of the errors as a function of position in the flow field, and then use these estimates as correction factors for the data. Such estimates may be obtained by analyzing the temperature probe as a fin extending from the diffusion tube wall into the flow field.

Equations for this purpose that are available in the literature (e.g. Welty, et al. (1969)) are generally formulated by treating the fin as a surface in a fluid of constant temperature. In addition, the heat transfer

coefficient is generally assumed to be constant along the fin surface. These assumptions do not hold for the flow conditions under which data were taken in this investigation, however, because radial variations of fluid temperature and velocity were found to be substantial.

If variations in fluid temperature and velocity along probe surfaces were to be taken into account in an error analysis to generate correction factors for the temperature data measured in this investigation, the complexity of the analysis would be formidable. Accordingly, an alternate scheme was used to reduce the as-measured data for the radial temperature profiles to a form that is consistent with the axisymmetric flow conditions in the diffusion tube. This scheme is discussed in the following paragraphs. A discussion of uncertainties in the data is deferred until section 7.1.4.

As noted previously in this section, any two radial temperature profiles measured under the same flow conditions and at the same axial location, but with a probe inserted at opposite circumferential positions around the flow field, are essentially mirror images of each other. Accordingly, if the two as-measured values at each radial position over a cross section are averaged, the resulting values fall on a curve that is symmetrical about the diffusion tube centerline. An example of a typical curve of average values is shown as a dashed line in Figure 7.5.

Such a curve is, of course, only an approximation of the temperature distribution that exists over the cross section where the data were taken, but it is a better approximation than either of the two as-measured curves from which it was computed because it more accurately represents the axisymmetric distribution of the temperature field.

It is of interest to note that the centerline values of the two as-measured temperature profiles shown in Figure 7.5 are virtually identical. This follows from the fact that these two profiles are essentially mirror images of each other. Accordingly, when the as-measured values for these two profiles are averaged in the manner discussed in the preceding paragraph, the average value at the centerline is essentially unchanged from the two as-measured values at that location. Since this close agreement between as-measured and averaged values at the diffusion tube centerline is typical for data obtained at other axial positions and under all four sets of flow conditions, the centerline values of radial profiles generated by means of the aforementioned averaging process are in very close agreement with the as-measured values for the centerline temperature profiles plotted in Figures 7.1 through 7.4.

Referring to Figure 7.5, the aforementioned averaging process is equivalent to working with the data for

just one of the two as-measured profiles and averaging the values for corresponding points to either side of the centerline. The results obtained by the latter process are identical with those obtained by the former process if traverses made at a given cross section with a probe inserted from opposite circumferential positions yield profiles that are exact mirror images of each other. Having verified by measurements such as those plotted in Figure 7.5 that this condition is met within a negligibly small margin of error, most of the radial traverses were made with probes inserted into the diffusion flow field from only one circumferential position. Symmetrical radial profiles were then generated from the as-measured data over the various cross sections by using the averaging process just described for single traverses.

7.1.2.2. Results for the Test Conditions under Which Data Were Taken

Shown in Figures 7.6 through 7.9 are as-measured radial temperature profiles for the four sets of flow conditions under which data were taken. Also shown in these figures are profiles generated from the as-measured data in the manner described in the preceding paragraph. These latter profiles, which are symmetrical about the diffusion tube centerline, were used as part of the input data for computing transport coefficients discussed in

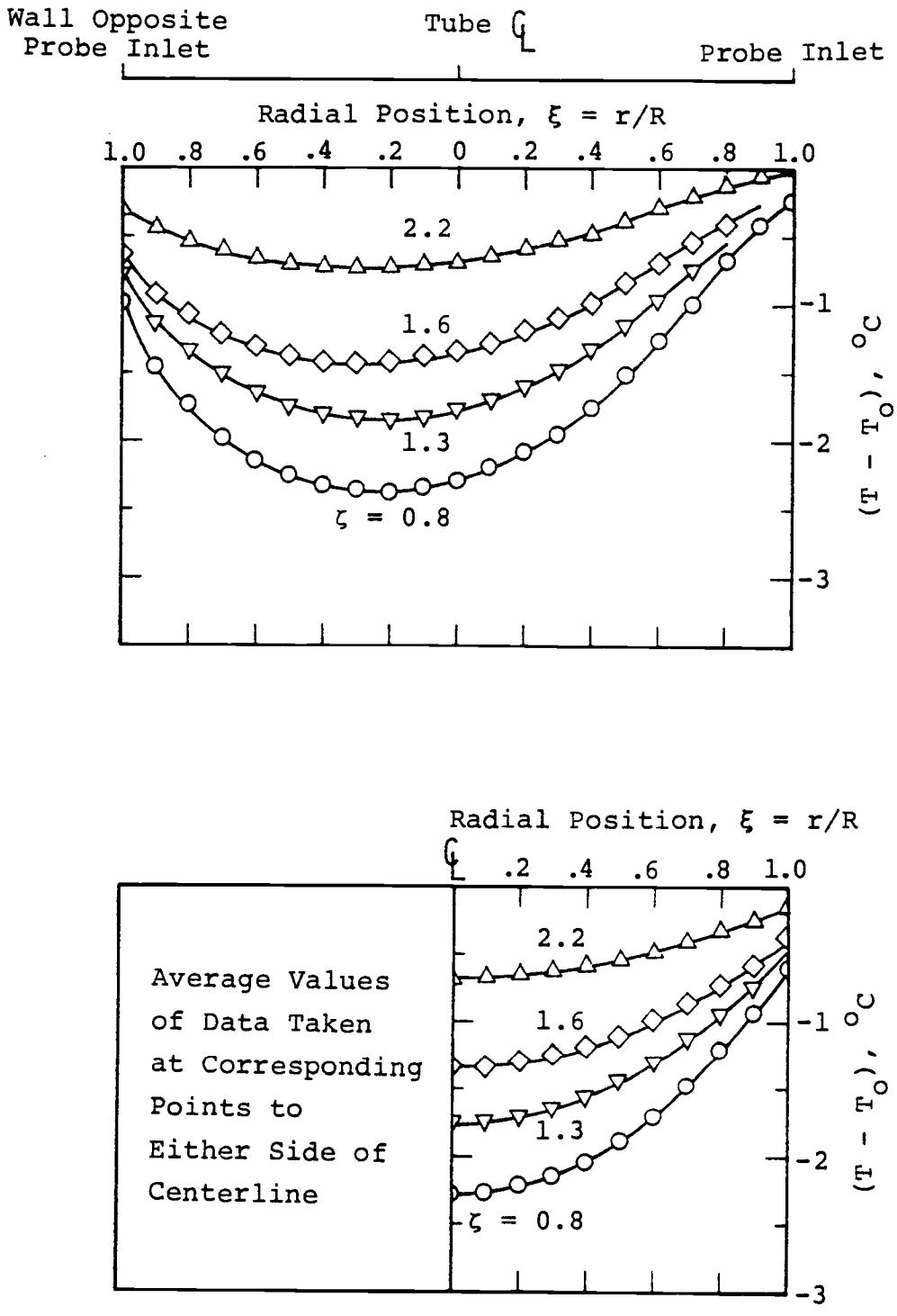

Figure 7.6. Experimental Radial Temperature Profiles for Pe = 1.9, X_{A_o} = 0.5

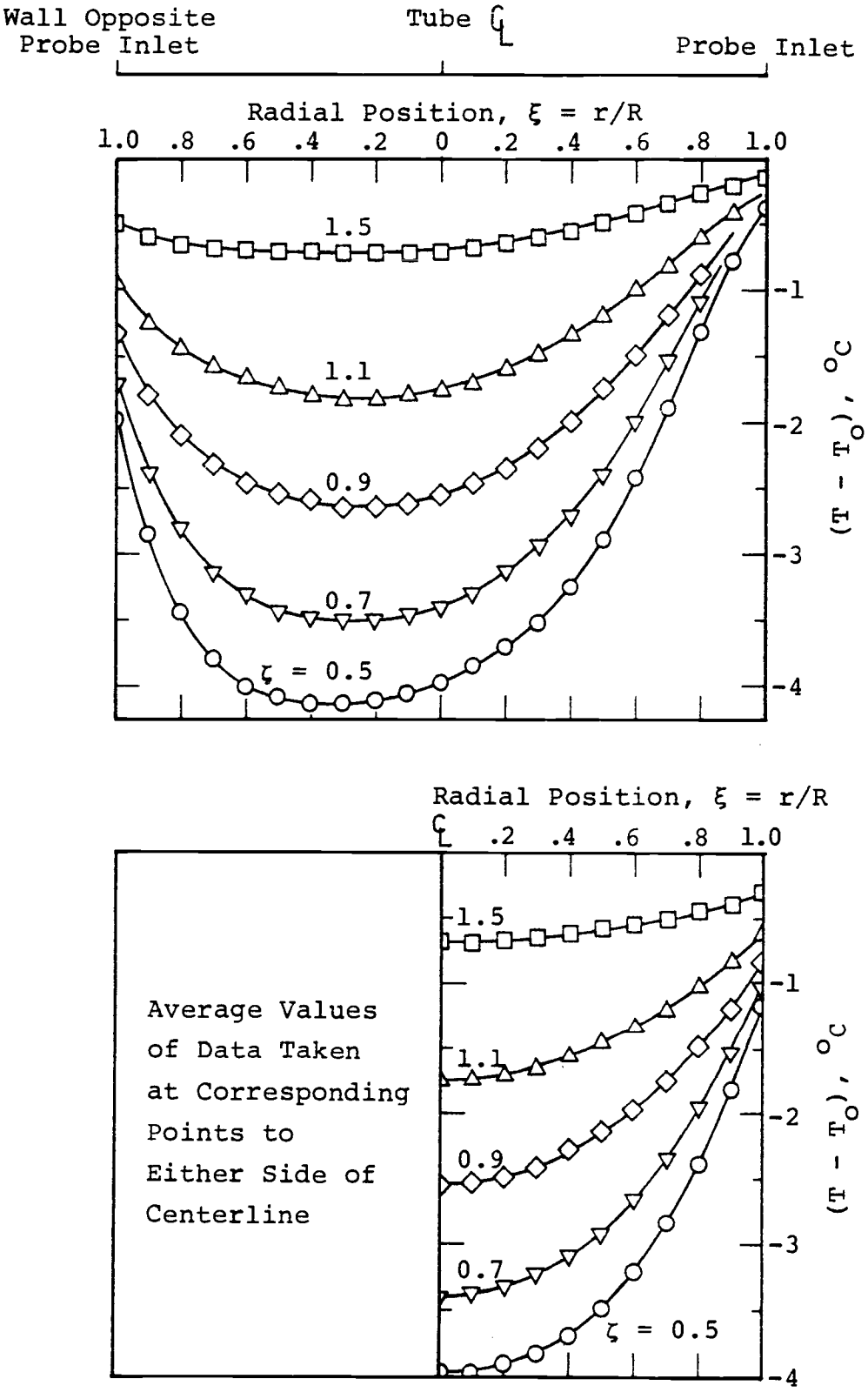

Figure 7.7. Experimental Radial Temperature Profiles for Pe = 3.8, X_{A_o} = 0.5

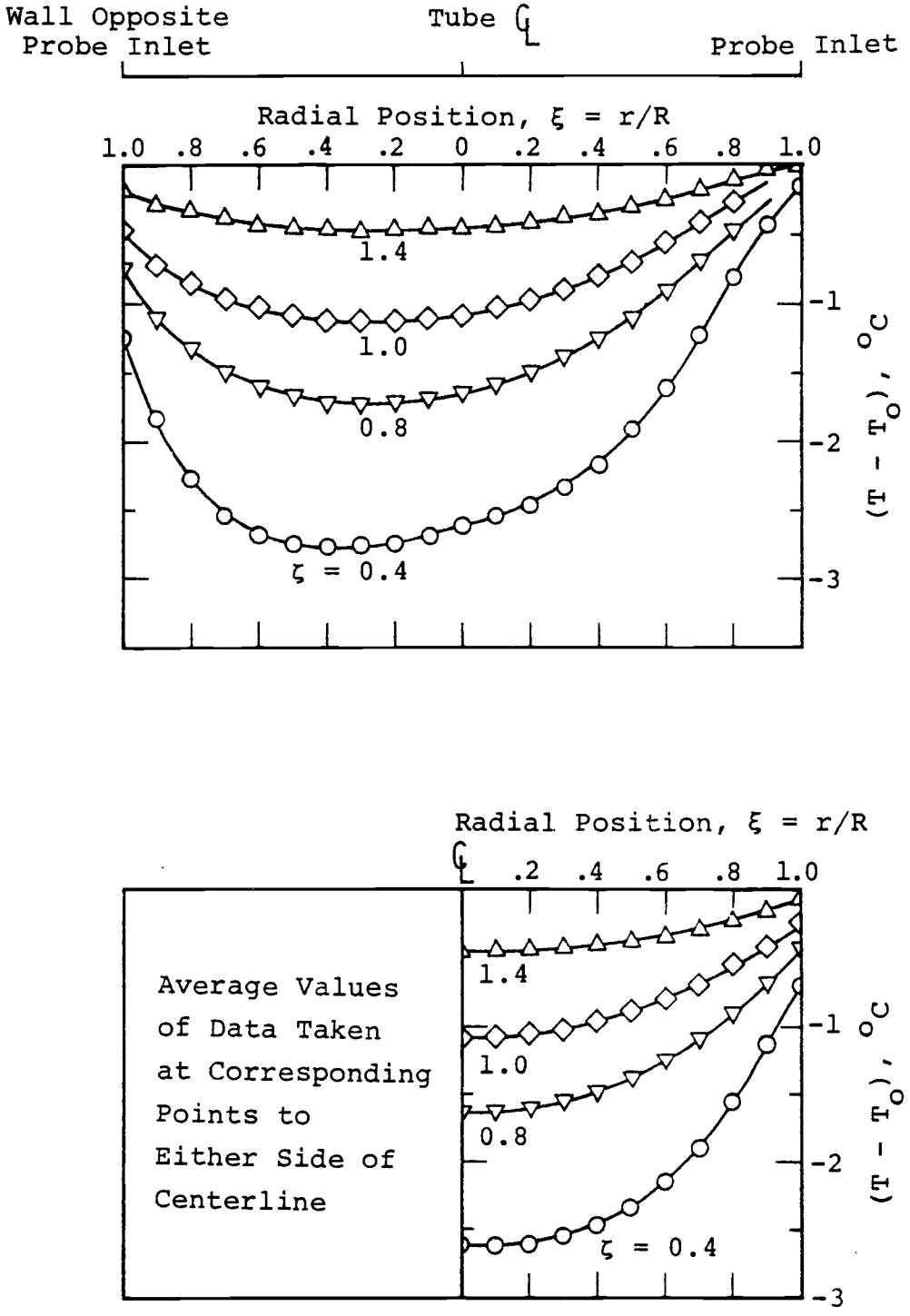

Figure 7.8. Experimental Radial Temperature Profiles for Pe = 3.8, X_{A_o} = 0.7

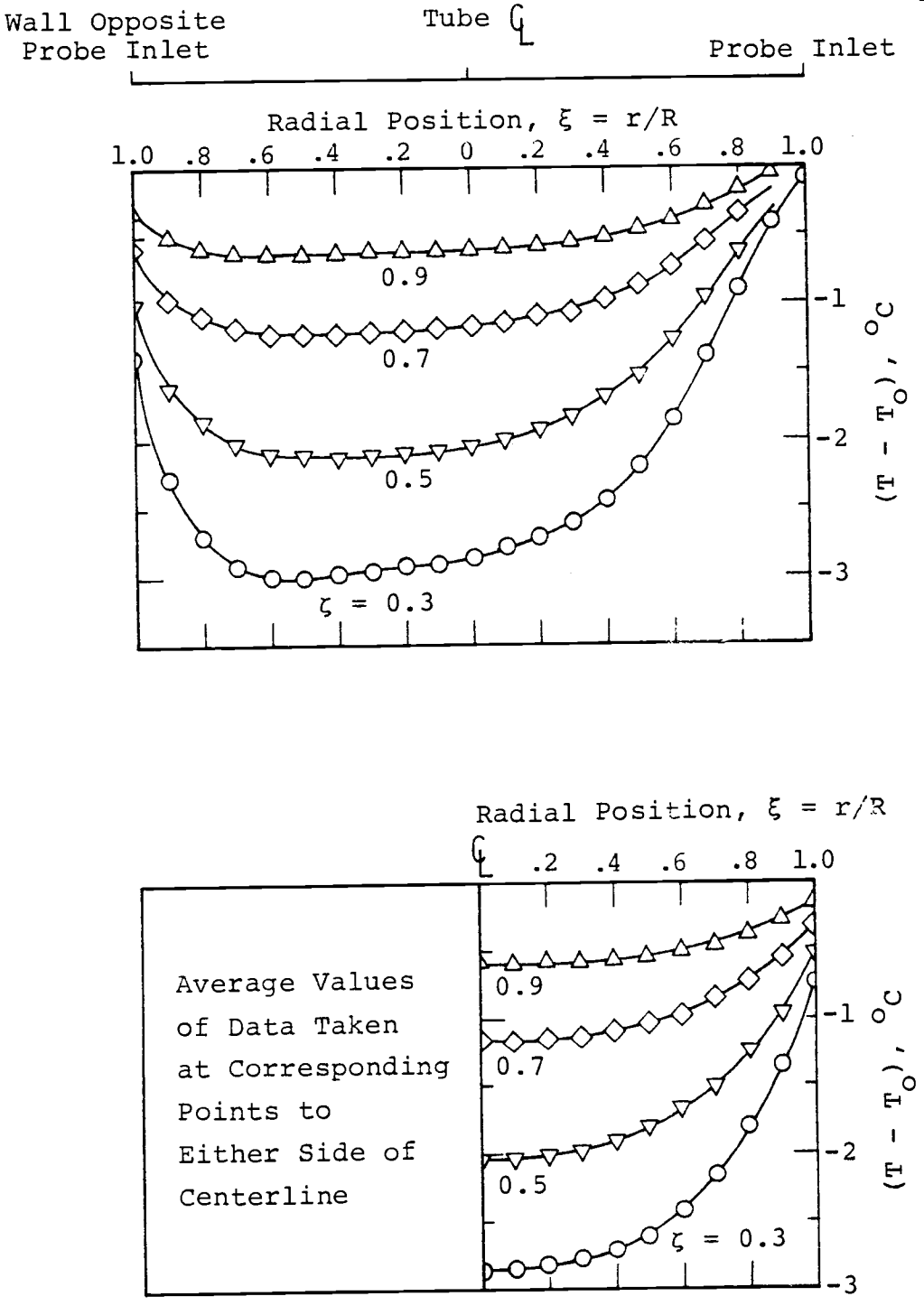

Figure 7.9. Experimental Radial Temperature Profiles for Pe = 5.9, X_{A_o} = 0.7

subsequent sections of this chapter. The data for these profiles are tabulated in Appendix F.

After making allowances for the asymmetry that occurs due to the factors discussed in the preceding section, the radial temperature profiles for all four sets of flow conditions are essentially parabolic in shape. The magnitude of the minimum in each profile is a function of both the axial position at which the profile was measured and the flow conditions under which the measurements were taken. Comments on these effects are included in the discussion of the centerline temperature profiles presented in section 7.1.1.

On the basis of the data plotted in Figures 7.8 and 7.9 (for Peclet numbers of 3.8 and 5.9, respectively, with the mole fraction of nitrogen at the helium injection plane, X_{A_o}, set at 0.7), the radial temperature profiles for the flow conditions corresponding to the highest Peclet number considered in this investigation are flatter in the central core of the flow field than those measured under similar flow conditions except for a lower Peclet number. This difference in the profiles may be attributed to the effects of a change in the Peclet number on the relative magnitudes of driving forces for radial and axial energy transport under the two sets of flow conditions.

As discussed in section 7.1.1, axial concentration gradients in a diffusion flow field become steeper with

increasing values of the Peclet number. Radial concentration gradients, however, vary to a much lesser extent with changes in the Peclet number (Stock (1972)). Accompanying steeper axial concentration gradients is increased energy transport in the axial direction due to the diffusion-thermo effect. Thus, for increasing values of the Peclet number radial energy transport becomes a smaller proportion of the total energy transported in a diffusion flow field, and therefore the radial temperature profiles for flows corresponding to higher Peclet numbers tend to be flatter than those for flows corresponding to lower Peclet numbers under conditions that are otherwise the same. (As noted in the preceding paragraph, this effect is strongly evident when the profiles in Figure 7.8 are compared to those in Figure 7.9. It may also be detected, but to a barely noticeable degree, in a comparison of the profiles plotted in Figures 7.6 and 7.7, which are for Peclet numbers of 1.9 and 3.8, respectively, with $X_{A_o} = 0.5$.)

7.1.3. Influence of Temperature Distributions on Velocity Distributions in Diffusion Flow Fields

Velocity profiles measured by Stock (1972) under the same conditions as those for which temperature profiles were measured in this investigation vary considerably in shape along the direction of bulk flow upward through the vertically oriented diffusion tube. Typical changes that

occur in the velocity profiles are illustrated in Figure 7.10, in which profiles are plotted for flow conditions corresponding to Pe = 1.9, X_{A_o} = 0.5. For reasons discussed in this section, changes in velocity profiles such as those illustrated in Figure 7.10 are likely to be influenced by temperature variations in the flowing fluid.

Under the flow conditions considered in this investigation, the velocity profiles are parabolic at axial positions sufficiently far upstream of the helium injection plane so that the flow field is essentially unaffected by diffusion phenomena and nitrogen is the only gas present. An example of such a profile is the one shown in Figure 7.10 for the velocity distribution at ζ = 5.0. (The coordinate ζ = z/R is a reference for axial positions upstream of and relative to the helium injection plane, as noted previously.)

As the proportion of nitrogen contained in the fluid decreases along the direction of bulk flow, however, the velocities in the central core of the flow field become smaller relative to those nearer to the diffusion tube wall, with the result that central concavity develops in the profiles at axial locations within approximately three diffusion tube radii upstream of the helium injection plane. This is illustrated in Figure 7.10 in the profiles for the velocity distributions at ζ = 2.5 and ζ = 0.8. The degree of central concavity observed in the velocity

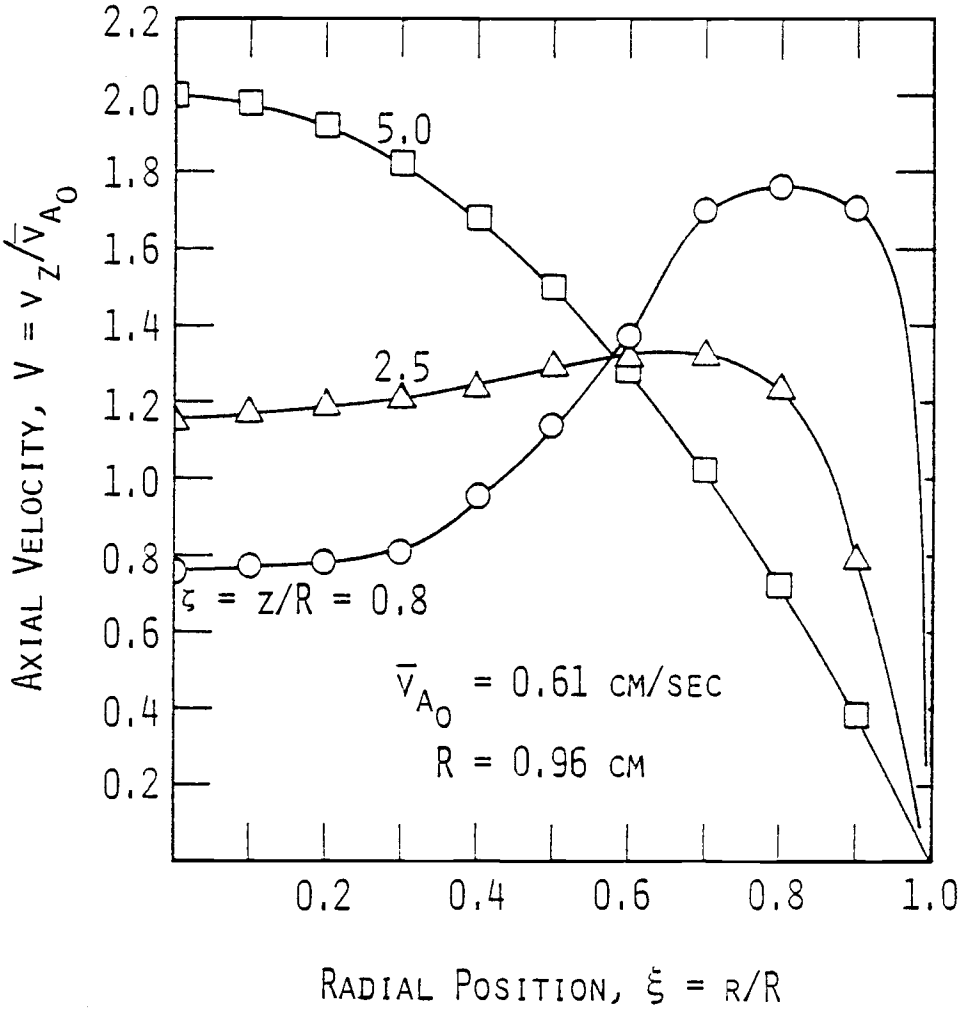

Figure 7.10. Dimensionless Velocity Profiles for Pe = 1.9, X_{A_o} = 0.5*

*Measured by Stock (1972)

profiles for a given flow field is inversely proportional to the Peclet number for the flow field, as may be seen by comparing Stock's velocity data (which are included in Appendix H) for the four flow conditions under which the data were taken.

Fluid motion may be strongly influenced by nonuniformities in the gravitational body force field acting on the fluid. Such nonuniformities are associated with fluid density gradients, because at any point in a fluid the gravitational body force is proportional to the local fluid density. For flow conditions such as those under which data were taken in this investigation, fluid density gradients are induced by concentration gradients and by temperature gradients, with the former causing more significant density changes than the latter.

For the flow conditions under which the velocity profiles plotted in Figure 7.10 were measured, the composition of the flowing fluid changes substantially along the direction of bulk flow but is essentially uniform over any given cross section through the flow field. This may be seen by referring to Stock's concentration data for $Pe = 1.9$, $X_{A_o} = 0.5$, which are included in Appendix H. Accordingly, while density changes associated with changes in fluid composition are significant along the direction of bulk flow, they are of little significance insofar as contributing to nonuniformities in the gravitational body

force field over any given cross section through the flow field. It is therefore unlikely that these composition related density changes would cause the velocity profiles to change in the manner illustrated in Figure 7.10.

Of the temperature data discussed in sections 7.1.1 and 7.1.2, the axial and radial profiles shown in Figures 7.1 and 7.6, respectively, were measured under the same flow conditions (Pe = 1.9, X_{A_o} = 0.5) as those established for measuring the velocity profiles shown in Figure 7.10. The manner in which the temperature changes recorded in the former figure may have contributed to the changes in the velocity profiles shown in the latter figure is discussed in the following paragraphs.

As shown in Figure 7.6, the fluid temperature changes along the centerline of the diffusion flow field are more pronounced than those adjacent to the wall boundary, with the result that radial temperature gradients become steeper along the direction of flow until the axial position is reached where the bulk fluid temperature passes through a minimum. In the flow field for which Pe = 1.9, X_{A_o} = 0.5, this minimum occurs at an axial position of ζ = 0.8 relative to the helium injection plane, as indicated in Figure 7.1. At this axial position the fluid temperature at the centerline is approximately 2.3^{o} C lower than the temperature of the gases entering the diffusion tube, and the fluid temperature adjacent to

the diffusion tube wall is approximately 0.6° C lower than that of the incoming gases. This temperature decrease at the centerline is over three times greater than that adjacent to the tube wall.

Radial density gradients associated with the radial temperature gradients result in radial gradients in the gravitational body force field acting on the fluid. On the basis of the temperature changes discussed in the preceding paragraph, these radial gradients act in such a way as to decrease the fluid velocities in the central core of the flow field relative to the velocities nearer to the diffusion tube wall. The pattern of changes in the velocity profiles plotted in Figure 7.10 is in agreement with what would be expected due to this effect.

7.1.4. Uncertainties in Temperature Measurements

Discussed in the following paragraphs are two types of errors that affect the accuracy of the temperature data taken under the flow conditions considered in this investigation. These are (1) random errors, which may be caused by such factors as inconsistencies in the method of taking data and fluctuations in the operating conditions, and (2) fixed errors, or systematic errors, which are essentially constant for repeated readings. An informative discussion of such errors is presented in Beckwith and Buck (1969).

Estimated uncertainties in the temperature data are summarized in Table 7.1. These uncertainties, which are based on information discussed in detail in Appendix G, are applicable to the temperature data taken under all four sets of flow conditions considered in this investigation.

7.1.4.1. Random Errors

Random errors associated with operation of the diffusion apparatus are small. As discussed in Appendix G, the largest differences observed between values of repeated centerline temperature measurements are those for the two sets of data plotted in Figure G.1 of that appendix. A time interval of over three weeks elapsed between the first and second runs to measure the two sets of data, which are for flow conditions corresponding to Pe = 1.9, $X_{A_o} = 0.5$. Nevertheless, corresponding values (which were measured relative to the common temperature of the two gases entering the diffusion tube) are in agreement within 0.1° C.

The close agreement between values of repeated temperature measurements for the flow conditions under which data were taken confirms that the diffusion apparatus and instrumentation used in this experimental investigation can be operated with a high degree of precision. Even the worst-case differences between repeated measurements are quite small considering all of the variables that can affect the measurements.

Table 7.1. Summary of Estimated Uncertainties in Values of Temperatures Measured in Diffusion Flow Fields Corresponding to Peclet Numbers between 1.9 and 5.9

NOTE: Values of temperatures in the diffusion flow fields were measured relative to the reference temperature of the two gases entering the diffusion tube.

Source of Uncertainty	Value
1. Scatter of data obtained in repeated measurements	$\pm$ 0.1° C
2. Estimated errors in calibrations of thermocouples and associated instrumentation	$\pm$ 0.03° C
3. Heat conduction along stem of thermocouple probe, and thermal radiation between probe and surroundings	
a. Conduction error (Estimate is applicable only to centerline temperature measurements. Increases up to 80% or more for temperatures measured at radial positions near the tube wall.)	5-7% of temperature measurement
b. Thermal radiation error	1-2% of temperature measurement

Overall uncertainty in centerline temperature measurements relative to the reference temperature of the gases entering the diffusion tube: 6-9% of measured value $\pm$ 0.1° C.

Uncertainty of reference temperature of gases entering the diffusion tube: $\pm$ 0.1° C. (This uncertainty is of importance only when temperatures measured in the diffusion tube are to be expressed directly in terms of their values on a temperature scale rather than as differences relative to the temperature of the gases entering the diffusion tube.)

7.1.4.2. Fixed Errors

Errors inherent in measuring temperatures with a probe inserted into a flow field include those resulting from (1) conduction of heat along the probe and (2) energy exchange by thermal radiation between the probe and its surroundings. Estimates of these errors for temperature measurements taken along the diffusion tube centerline are formulated in Appendix G. To obtain these estimates, the probe was modeled as a fin extending into a fluid of constant temperature.

Of the results presented in Appendix G, the magnitudes of the largest conduction and radiation errors that were computed for temperature measurements taken along the diffusion tube centerline are 0.2^{o} C and 0.05^{o} C, respectively. These errors apply to the largest temperature difference (-3.96^{o} C) recorded between the temperature at a point in a diffusion flow field and the reference temperature of the gases entering the diffusion tube. (This temperature difference was measured in the flow field for which Pe = 3.8, $X_{A_o} = 0.5$.)

The manner in which thermocouple conduction errors vary for temperatures measured along the diffusion tube centerline is illustrated in Figure G.2 of Appendix G. As would be expected, the magnitudes of the conduction errors are inversely proportional to the differences between the

centerline temperature in the diffusion tube and the reference temperature of the two gases entering the diffusion tube.

7.1.4.3. Effects of Temperature Errors on Values of Transport Coefficients Computed from the Experimental Data

Errors in the temperature measurements affect the accuracy of the transport coefficients that may be computed by combining the temperature data with corresponding velocity and concentration data and using the data as input for the equations formulated in Chapter VI. Referring to equation 6.29, the molecular diffusion coefficient at a given cross section through a diffusion flow field is proportional to the mean temperature of the gas mixture at the cross section. Temperature data used in that equation must be expressed in degrees Kelvin (or degrees Rankine if English units are used). When temperatures measured in the diffusion tube are expressed directly in degrees Kelvin rather than as differences relative to the reference temperature of the incoming gases, the errors in the temperature measurements, including the uncertainty of the reference temperature, are less than 0.5% of the values on the Kelvin scale. These errors have a correspondingly small effect on the accuracy of molecular diffusion coefficients computed from the experimental data.

The effects of temperature errors on the accuracy of

thermal diffusion factors that may be computed from equation 6.13 are difficult to predict, because computations performed in accordance with that equation involve both integration and differentiation of temperature data. As shown in Figure G.2 of Appendix G, errors in the temperature measurements vary in proportion to the magnitudes of the measurements relative to the reference temperature of the gases entering the diffusion tube. Accordingly, these errors affect not only the values of the temperatures measured at individual positions in a diffusion flow field but also the slopes of profiles drawn through the measured values. The effects of these errors on the accuracy of thermal diffusion factors computed from equation 6.13 cannot be readily estimated.

7.2. Thermal Diffusion Factors

Thermal diffusion factors that were computed on the basis of the experimental data for the four sets of flow conditions described in section 7.1 are discussed in the following paragraphs. The results are compared with predictions based on theoretical approximations and with results obtained by other investigators under considerably different experimental conditions.

7.2.1. Results Computed from Experimental Data for This Investigation

Values of the thermal diffusion factor (α_T) that were computed from data for the flow conditions described in section 7.1 are plotted in Figure 7.11 as a function of the mole fraction of nitrogen. Also plotted in this figure are experimental results obtained by other investigators, and theoretical predictions computed by Yang (1966) using approximations developed by Chapman and Cowling and by Kihara. The latter experimental and theoretical results are discussed in sections 7.2.2 and 7.2.3 of this chapter.

Program ALPHA was used to compute the values of α_T from the data for the flow conditions described in section 7.1. As discussed in section 6.1.2 of Chapter VI, program ALPHA is written to perform the calculations in accordance with equation 6.13. Experimental data used in the calculations included the temperature distributions discussed in section 7.1 and the velocity and concentration distributions measured by Stock (1972). The data files are tabulated in Appendix H.

As discussed in section 6.1.2 of Chapter VI, values of α_T are computed in program ALPHA over diffusion tube cross sections located at equally spaced axial positions in the region upstream of the helium injection plane. The grid system for the computations is shown in Figure 6.2. Results of the computations for a given set of flow condi-

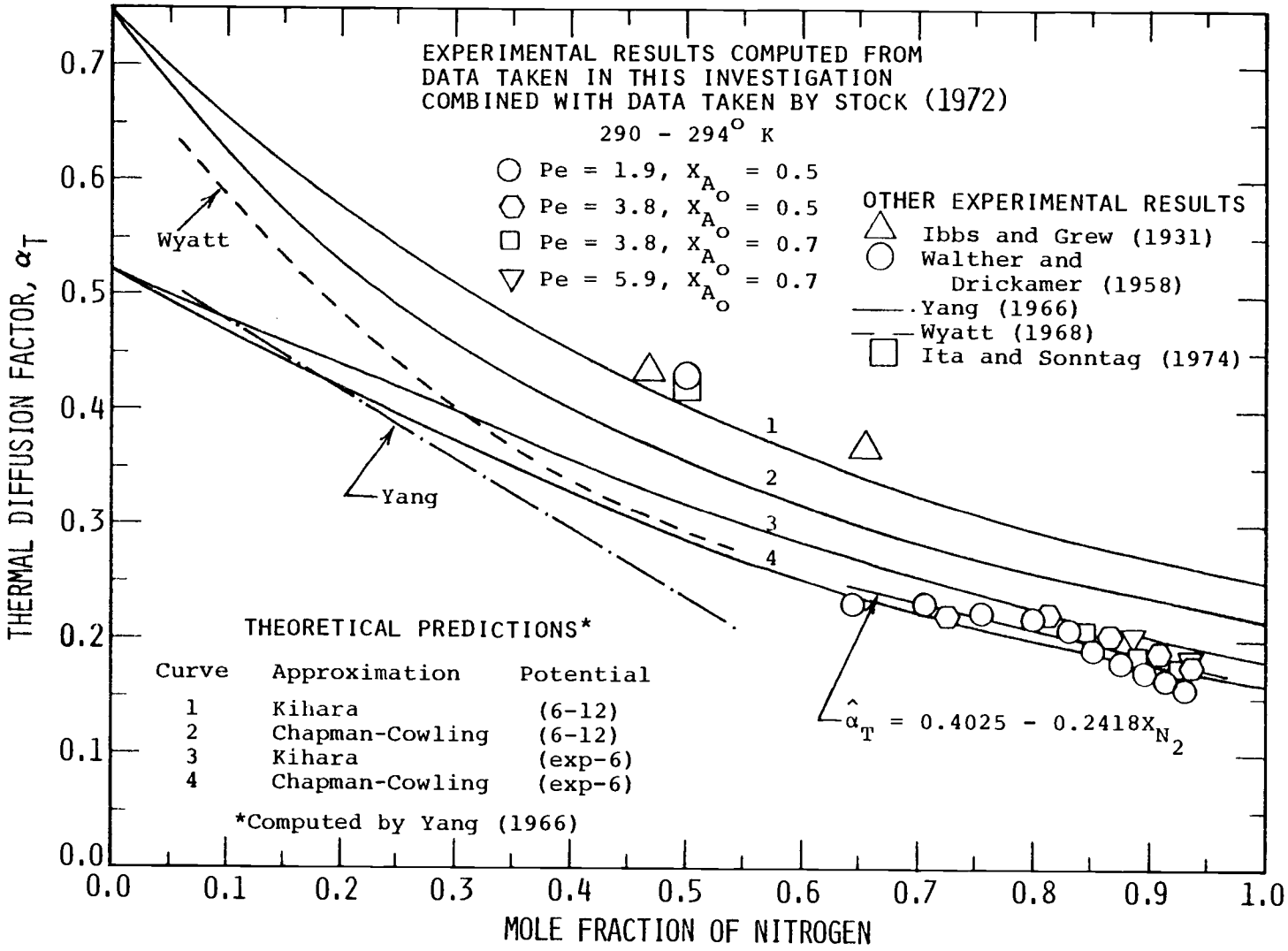

Figure 7.11. Thermal Diffusion Factors as a Function of Composition for Helium-Nitrogen Mixtures

tions include the mixed mean temperature and composition of the gas mixture and the corresponding value of α_T at each of the cross sections. The results computed for the test conditions described in section 7.1 are tabulated in Appendix J.

7.2.1.1. Fluid Properties Used in the Computations

Fluid properties of helium and nitrogen and related data used in the computations are summarized in Table 4.1 of Chapter IV. (These fluid properties were also used in computations of the predicted temperature distributions that are presented in Chapter IV.)

A fluid property not listed in Table 4.1 that must be known in order to use equation 6.13 for computing values of α_T is the thermal conductivity of the gas mixture as a function of the relative proportions of the constituents. Experimental values of this property for helium-nitrogen mixtures are not generally available in the literature. Accordingly, the required values were estimated from the values for the pure gases using equation 4.14 of Chapter IV.

7.2.1.2. Limitations on the Range of Gas Composition for Which Values of α_T Were Computed

As shown in Figures 7.1 through 7.4, the mole fraction of nitrogen in the diffusion tube increases as a

function of distance upstream of the helium injection plane. At axial locations sufficiently far upstream of the helium injection plane so that the mole fraction of nitrogen approaches unity, the temperature effects associated with flow-coupled diffusion are so small that they are on the order of the uncertainty with which they can be measured. Values of α_T computed on the basis of data for such conditions are subject to much larger errors than those computed on the basis of data taken at locations where the effects of flow-coupled diffusion are more pronounced. The values of α_T plotted in Figure 7.11 for the flow conditions described in section 7.1 are therefore limited to those computed for mole fractions of nitrogen no greater than 0.94.

At axial locations in close proximity to the plane formed by the outlets of the helium injection tubes (which are illustrated in Figure 5.4), the velocity, concentration, and temperature distributions for any given set of flow conditions are subject to substantial deviations from what they would be if helium were introduced uniformly over the plane. Accordingly, values of these distributions measured at axial locations between ζ (= z/R) = 0.0 and ζ = 0.3 relative to the helium injection plane are not considered suitable for use in computing values of α_T.

The effect of the latter restriction may be illus-

trated by considering the values of α_T computed on the basis of data for Pe = 1.9, X_{A_o} = 0.5. Referring to Figure 7.11, the lower limit of the range of mole fractions of nitrogen for which values of α_T are plotted for this set of flow conditions is approximately 0.64. The lower limit would be 0.5, the mole fraction of nitrogen set for these conditions at the helium injection plane, if data taken in close proximity to the injection plane were included in the calculations.

Similar restrictions on the range of gas compositions for which values of α_T were computed apply for the other sets of flow conditions described in section 7.1. The effect of excluding data taken in close proximity to the helium injection plane varies with the flow conditions, because the velocity, concentration, and temperature distributions are functions of both the Peclet number for the flow field and the mole fraction of nitrogen set at the helium injection plane.

7.2.1.3. Invariance of Values of α_T as a Function of Peclet Number

Large differences exist in the diffusion flow fields corresponding to the Peclet numbers for the four sets of flow conditions described in section 7.1, as may be seen by comparing the temperature profiles or the concentration profiles shown in Figures 7.1 through 7.4.

The values of α_T computed on the basis of the data for these flow conditions are, nevertheless, in close agreement as a function of gas composition. Referring to Figure 7.11, these values of α_T differ by no more than $\pm$ 10% from corresponding values on the regression line for the combined results. This close agreement provides strong evidence that there is essentially no Peclet number influence on the variation of α_T as a function of gas composition.

7.2.1.4. Estimate of Uncertainty in Values of α_T

Values of α_T computed from equation 6.13 of Chapter VI are strongly dependent on the following variables, which are listed together with their estimated uncertainties for the data taken under the four sets of flow conditions described in section 7.1:

- Mass flow rate of nitrogen: $\pm$ 3%.
- Mole fraction of nitrogen: $\pm$ 0.01.
- Temperature relative to the reference temperature of the gases entering the diffusion tube (estimate is from Table 7.1): 9% of measured value $\pm$ 0.1° C.

The uncertainties listed above are of interest as indicators of some of the sources of error associated with computing values of α_T from data taken under the flow conditions described in section 7.1. However, the

effects of these uncertainties on the uncertainty of the values of α_T computed from the experimental data are difficult to predict because of the complexity of the mathematical operations involved in performing the calculations. Referring to equation 6.13, these mathematical operations include differentiation and integration of the experimental temperature data.

An indication of the uncertainty in the values of α_T computed from data for the four sets of flow conditions described in section 7.1 may be obtained by examining the results plotted in Figure 7.11 for these flow conditions. As noted in section 7.2.1.3, individual values differ by no more than $\pm$ 10% from the regression line for the combined results. Furthermore, as discussed in section 7.2.4, the values are in excellent agreement with theoretical approximations that have been found to be satisfactory for estimating values of α_T for noble gas mixtures containing helium. It is therefore reasonable to estimate that the uncertainty of the values of α_T determined for the flow conditions considered in this investigation is $\pm$ 10%.

7.2.2. Experimental Results Obtained for Helium-Nitrogen Mixtures by Other Investigators

A thorough literature search was performed to identify original references in which values of α_T (or

the related coefficient k_T) have been reported for helium-nitrogen mixtures. Only five such references were found. Applicable data from these references are plotted in Figure 7.11, and the experimental approaches taken to obtain the data are briefly described in the following paragraphs.

Ibbs and Grew (1931) obtained thermal diffusion data for helium-nitrogen mixtures (and other binary mixtures) using a two-bulb apparatus of the type that is described in section 3.4.1 of Chapter III. With their apparatus they studied the changes in composition that occur when a gas mixture initially of uniform composition is exposed to a temperature gradient. Except for the two values of α_T plotted in Figure 7.11 on the basis of their data, their results are for temperatures far lower than those used in the other experimental investigations discussed in this section.

Walther and Drickamer (1958) performed experiments with an apparatus of the two-bulb type to obtain data on the variation of α_T as a function of pressure for a variety of binary gas mixtures. In the only helium-nitrogen mixture that they tested, the mole fraction of each constituent was 0.5. Their data indicate that the variation of α_T for this mixture is not large (less than 30%) as a function of pressure up to the maximum pressure, 500 atm, at which the data were taken. The value of α_T plotted in Figure 7.11 from their work is for data taken at a pressure

of approximately 50 atm.

Yang (1966) and Wyatt (1968) investigated diffusion flow fields in which they established concentration gradients so as to induce temperature gradients due to the diffusion-thermo effect. Their investigations were conducted for flow fields corresponding to Peclet numbers less than 2.5. Both investigators used the same type of apparatus, which is described in section 3.6 of Chapter III, but Wyatt used a larger diameter diffusion tube than the one used by Yang. Values of α_T obtained in their investigations are represented by curves drawn in Figure 7.11. The scatter of the data for each of these curves is approximately 10%.

Ita and Sonntag (1974) used an apparatus of the two-bulb type to investigate the influence of pressure on thermal diffusion in binary and ternary mixtures of helium, nitrogen, and neon. They obtained, over a pressure range of 3 to 40 atm, values of α_T for a helium-nitrogen mixture in which the mole fraction of each constituent was 0.5. The value of α_T plotted in Figure 7.11 from their work is for data taken at a pressure of 3 atm.

7.2.3. Comments on Results Obtained in This Investigation Compared to Experimental Results Obtained by Other Investigators

There is no set of data from the experimental investigations discussed in the preceding section that con-

stitutes a definitive standard against which the values of α_T obtained in this investigation may be compared. As may be seen by referring to Figure 7.11, the range of mole fractions for which data were obtained in the former investigations differs from that for which data were obtained in this investigation. Furthermore, substantial discrepancies exist between the sets of data from the former investigations.

Accordingly, the comments in the following paragraphs are limited to some general observations pertaining to the experimental data. Inferences that may be made on the basis of comparisons of the experimental data with theoretical approximations are discussed in section 7.2.4.

Referring to Figure 7.11, the values of α_T from the experimental investigations discussed in section 7.2.2 and from data for the flow conditions described in section 7.1 fall into three distinct groups:

1. The data point from Walther and Drickamer (1958) is in close agreement with the one from Ita and Sonntag (1974) for the same proportions of helium and nitrogen, and both are consistent with the two values from Ibbs and Grew (1931). These data are, however, over 40% higher than any of the other experimental data plotted in Figure 7.11 for similar gas compositions.

2. Although there is a gap between the highest mole

fraction of nitrogen for which Wyatt (1968) obtained values of α_T and the lowest mole fraction of nitrogen for which values of α_T were obtained under the test conditions described in section 7.1, the results of these two investigations appear to be consistent to the extent that they essentially coincide when extrapolated over the gap. This observation, however, does not provide a sufficient basis for drawing a conclusion as to whether the the data from these two investigations are consistent in terms of their respective trends as a function of gas composition. This latter aspect is checked in section 7.2.4, where the experimental data are compared with theoretical approximations.

3. The experimental results obtained by Yang (1966) are 10 to 25 percent lower than those obtained by Wyatt (1968) using the same type of apparatus. Wyatt (1968) concluded that the lack of agreement in these results is due in part to the fact that the method of data reduction used in the former investigation does not account for a component of energy transport that is taken into consideration in the latter investigation.

Lack of agreement in the values of α_T determined experimentally for helium-nitrogen mixtures is most pronounced between groups 1 and 2 of the data described above.

All values in group 1 are from investigations of thermal diffusion, while those in group 2 are from investigations of the diffusion-thermo effect. Agreement between values of α_T is satisfactory for most gas mixtures for which results have been obtained in investigations of these two phenomena (Grew and Ibbs (1952)). Accordingly, while the lack of agreement between groups 1 and 2 of the data discussed above might be due in part to the different methods used to obtain the data, the large discrepancies between the two groups are likely due to other causes.

As may be seen from some of the experimental results evaluated by Saxena and Mathur (1965) in their critical review of thermal diffusion data, large inconsistencies are not uncommon between values of α_T obtained in different experimental investigations for gas mixtures of the same constituents and composition. The inconsistencies are perhaps due in part to the fact that experimental investigations to determine values of α_T involve measurements of variables that are inherently small due to the nature of the coupled phenomena associated with thermal diffusion and the diffusion-thermo effect. As discussed in section 2.2 of Chapter II, the thermal diffusion factor relates fluxes of energy and mass to gradients of concentration and temperature, respectively. Concentration gradients are much less significant than temperature gradients as driving forces for the transport of energy, and, similarly,

temperature gradients are much less significant than concentration gradients as driving forces for the transport of mass. Consequently, even small errors in measurements of thermal diffusion and diffusion-thermo phenomena are likely to be significant in proportion to the values of the variables measured.

7.2.4. Comparisons with Theoretical Predictions

7.2.4.1. Theoretical Curves Used in Comparisons

Included in Figure 7.11 are theoretical curves for the variation of α_T as a function of composition in helium-nitrogen mixtures. These curves were computed by Yang (1966) on the basis of the theoretical approximations and intermolecular potential energy functions discussed in section 4.3.2 of Chapter IV. As may be seen in Figure 7.11, the theoretical curves are strongly influenced by the type of potential energy function chosen to model the molecular interactions, and they are influenced to a lesser extent by the type of approximation used to perform the computations.

7.2.4.2. Inferences from Comparisons of Theoretical and Experimental Results

The following comments, which are discussed in more detail in section 4.3.2 of Chapter IV, are pertinent as background information for use in making comparisons of

the experimental and theoretical data shown in Figure 7.11:

- The Chapman-Cowling first approximation and the Kihara first approximation used by Yang (1966) to compute the theoretical curves shown in Figure 7.11 are alternate methods to obtain approximate solutions for α_T from the general (and very complex) set of equations formulated for this transport coefficient as part of the rigorous kinetic theory of gases. Mason, et al. (1964) found neither approximation to be generally superior to the other when the two were compared with experimental data for a variety of binary mixtures containing monatomic and polyatomic gases.
- Saxena and Mathur (1965) concluded from a review of thermal diffusion data for noble gases that for binary mixtures containing helium as a constituent, use of the Lennard-Jones (12-6) potential in theoretical predictions of α_T yields results that are systematically larger than those determined on the basis of experimental data. They also concluded that the modified Buckingham (exp-6) potential is a satisfactory model for representing molecular interactions in such mixtures.

Since Saxena and Mathur (1965) based their foregoing

conclusions on data from investigations of noble gas mixtures, their conclusions do not necessarily apply to mixtures containing nitrogen as a constituent. If, however, their conclusions are hypothesized to apply to helium-nitrogen mixtures, the following inferences may be made regarding the experimental data plotted in Figure 7.11:

- The values of α_T from the experimental investigations performed by Ibbs and Grew (1931), Walther and Drickamer (1958), and Ita and Sonntag (1974) appear to be systematically too high. These values are in agreement with the theoretical curve for which molecular interactions were modeled with the Lennard-Jones (12-6) potential. The other experimental values within the same range of gas compositions all fall close to or below the theoretical curves for which molecular interactions were modeled with the modified Buckingham (exp-6) potential. On the basis of the above mentioned conclusions of Saxena and Mathur (1965), the former values are likely to be in greater error than the latter.
- The values of α_T from data for the four test conditions described in section 7.1 are credible on the basis of their agreement with theoretical curves for which molecular interactions were modeled with the modified Buckingham (exp-6)

potential. In the middle of the range of gas compositions for which these experimental data were obtained, the results tend to fall between the two theoretical curves computed from the Chapman-Cowling and Kihara approximations in conjunction with the (exp-6) potential. The experimental results corresponding to gas compositions near the limits of the range for which these data were obtained tend to fall slightly below, but still in close agreement with, the lower of the aforementioned theoretical curves.

For reasons discussed in section 7.2.1.2, the uncertainty of the values of α_T from data for each of the four test conditions described in section 7.1 is not constant over the range of gas compositions for which the data were obtained. The values of α_T corresponding to gas compositions near the limits of the range are subject to greater uncertainty than those corresponding to gas compositions in the middle of the range investigated under each of the aforementioned test conditions. Accordingly, the former values are less suitable than the latter for use in comparisons with theoretical predictions.

Since, as noted previously, the latter values of α_T tend to fall between the two theoretical curves for which molecular interactions were modeled with the (exp-6) potential, nothing definitive may be concluded as to whether

they are in closer agreement with one curve or the other. It is of interest to note in this regard that on the basis of the investigation by Mason, et al. (1964) referred to earlier in this section, neither of the first approximations (Chapman-Cowling or Kihara) used in computing the theoretical curves is necessarily superior to the other as a model for use in predicting values of α_T. Rather, the two curves plotted in Figure 7.11 on the basis of those approximations and the (exp-6) potential are useful as alternate theoretical estimates of α_T that should be reasonable for helium-nitrogen mixtures, assuming that the conclusions of Saxena and Mathur (1965) referred to previously are applicable to such mixtures.

Neither the experimental results of Yang (1966) nor those of Wyatt (1968) are consistent as a function of gas composition with any of the theoretical curves plotted in Figure 7.11. Toward the upper limit of the range of mole fractions of nitrogen for which the latter investigator obtained experimental data, his results approach, in an asymptotic manner, the theoretical curve computed from the Chapman-Cowling approximation in conjunction with the modified Buckingham (exp-6) potential. For low mole fractions of nitrogen, the results obtained by the former investigator are in agreement with the theoretical curves for which molecular interactions were modeled with the (exp-6) potential, but the agreement fails to hold for

larger mole fractions of nitrogen.

7.3. Molecular Diffusion Coefficients

Shown in Figure 7.12 are values of the molecular diffusion coefficient (D_{AB}) computed from data taken under the four sets of flow conditions described in section 7.1. Also shown in this figure are experimental results obtained by two other investigators, and a theoretical curve computed by Yang (1966) on the basis of the modified Buckingham (exp-6) intermolecular potential energy function used in conjunction with an approximation developed by Chapman and Cowling. The (exp-6) potential function is discussed in section 4.3.2 of Chapter IV.

Program ALPHA was used to compute values of D_{AB} from data for the flow conditions described in section 7.1. As discussed in Chapter VI, program ALPHA is written to compute values of D_{AB} in accordance with equation 6.29. Results of the computations are included in Appendix J. The input data files used in the computations were also used for computing values of α_T, and are tabulated in Appendix H.

Unlike values of α_T, which are strongly dependent on temperature changes associated with diffusion, values of D_{AB} are dependent only to a very limited extent on such temperature changes. For example, the largest variation in temperature (approximately 4° C) measured exper-

imentally under the flow conditions described in section 7.1 results in a variation of less than 1.5% in values of D_{AB} computed from equation 6.29 of Chapter VI. Due to the relative insensitivity of this transport coefficient to the temperature effects upon which the research discussed in this thesis is focused, the comments that follow regarding values of D_{AB} are much more limited than those in section 7.2 regarding values of α_T.

As shown in Figure 7.12, experimental values of D_{AB} reported by Walker and Westenberg (1958) and by Yang (1966) are in excellent agreement with the theoretical curve plotted in that figure. These results are for a range of mole fractions that overlaps the range for which values of D_{AB} were computed from data taken under the flow conditions described in section 7.1.

Values of D_{AB} computed from data taken under the latter flow conditions exhibit considerable scatter as a function of gas composition, as may be seen by referring to the statistical data summarized in Table 7.2 for these values. The scatter is most likely associated with taking derivatives of the experimental concentration data as part of the process of computing values of D_{AB} in accordance with equation 6.29. Although the five-point differentiation formulas discussed in section 4.2.1 of Chapter IV were used to reduce the consequences of irregularities in the data, the process of differentiation still tends to

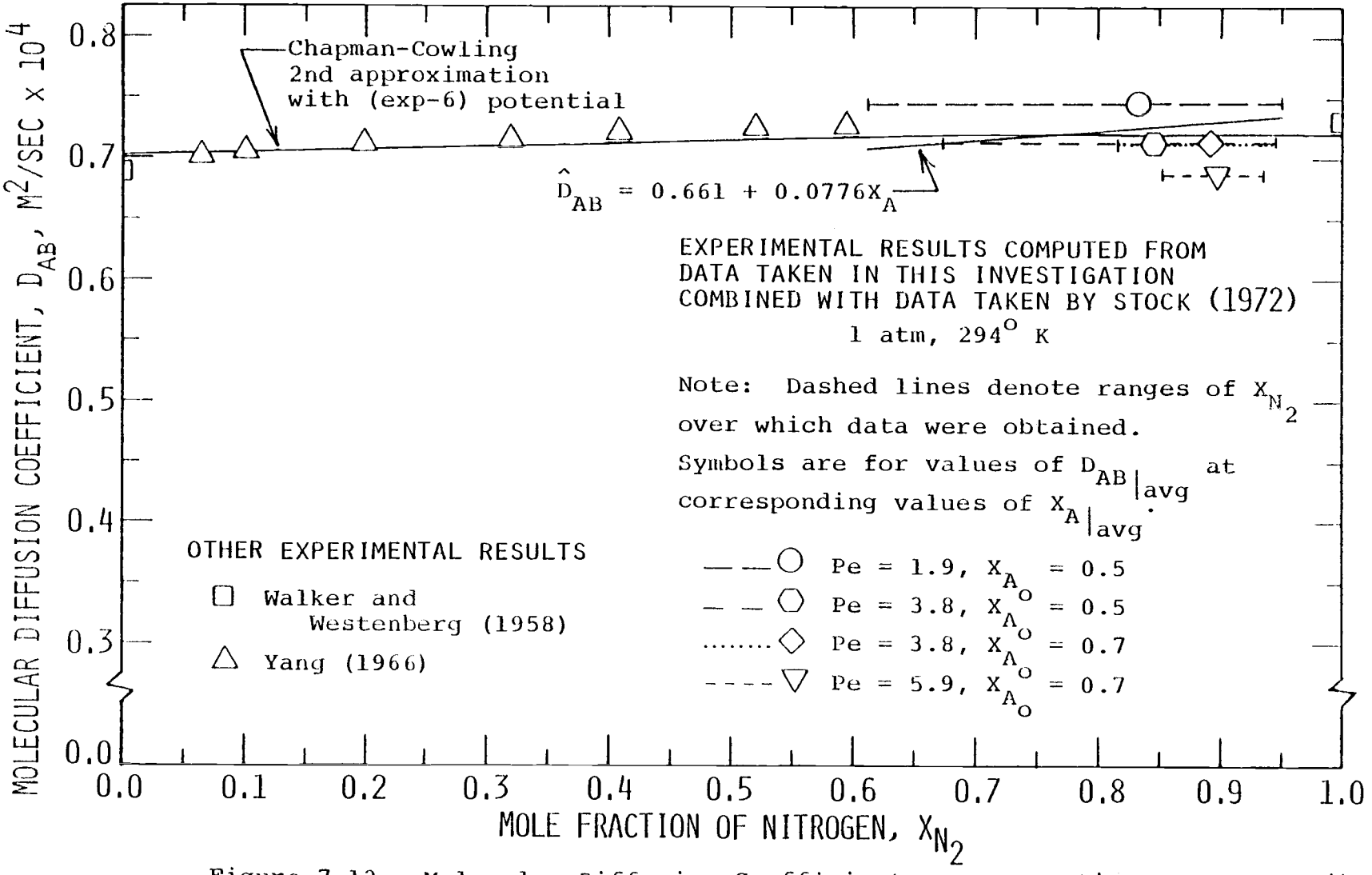

Figure 7.12. Molecular Diffusion Coefficients as a Function of Composition for Helium-Nitrogen Mixtures

Table 7.2. Statistical Information for Molecular Diffusion Coefficients Computed from Experimental Data Taken Under the Flow Conditions Described in Section 7.1

NOTES:

1. "Sample Size" refers to the number of values of D_{AB} computed for a given set of flow conditions.

2. Numbers listed under "X_A" are the maximum, minimum, and average values of the mole fraction of nitrogen for which corresponding values of D_{AB} were computed from the experimental data.

	Flow Conditions			
	Pe = 1.9, X_{A_o} = 0.5	Pe = 3.8, X_{A_o} = 0.5	Pe = 3.8, X_{A_o} = 0.7	Pe = 5.9, X_{A_o} = 0.7
sample size	24	11	8	4
D_{AB}				
average	0.746	0.713	0.712	0.688
maximum	0.893	0.831	0.730	0.706
minimum	0.674	0.676	0.681	0.677
std. deviation	0.064	0.047	0.018	0.013
X_A				
average	0.834	0.845	0.892	0.897
maximum	0.950	0.945	0.947	0.935
minimum	0.612	0.674	0.816	0.852

magnify the effects of such irregularities.

The average value of D_{AB} for each of the four flow conditions referred to above is plotted in Figure 7.12. Also shown in that figure is the range of mole fractions of nitrogen over which values of D_{AB} were computed for each of the flow conditions. Although the individual values of D_{AB} on which the averages are based are not plotted, an indication of the trend of the individual values as a function of gas composition is given by the regression line plotted for these values in Figure 7.12. The regression line represents a best linear fit for the combined values of D_{AB} obtained for all four of the flow conditions.

As illustrated in Figure 7.12, the theoretically predicted variation of D_{AB} as a function of composition in helium-nitrogen mixtures is small (less than 3% over the full range of mole fractions of either gas). This variation is considerably smaller than the scatter in the values of D_{AB} computed from data taken under the four sets of flow conditions described in section 7.1. It is of interest to note, however, that the average values of D_{AB} for the four flow conditions are in relatively close agreement (within $\pm$ 5%) with the theoretical curve. This agreement demonstrates that, despite the scatter in the computed values of D_{AB}, the central tendency of the results for each of the four flow conditions is consistent with values

predicted on the basis of theory. Furthermore, the regression line plotted in Figure 7.12 for the combined values of D_{AB} computed for the four flow conditions is somewhat steeper than, but nevertheless in close agreement with, the theoretical curve.

The scatter in the average values of D_{AB} plotted in Figure 7.12 for the flow conditions referred to above is most likely due to the uncertainty in the measurement of the mass flow rate of nitrogen for each of the flow conditions. As may be seen by referring to equation 6.29, values of D_{AB} computed for a given set of flow conditions are directly proportional to the mass flow rate of the heavier gas. Due to limitations of the flow meter used in the apparatus in which the above mentioned flow conditions were established, the uncertainty in measurements of mass flow rates is estimated to be $\pm$ 3%. This uncertainty is second only to the uncertainty associated with taking derivatives of experimental concentration data insofar as its influence on the values of D_{AB} computed from equation 6.29.

VIII. SUMMARY OF ACCOMPLISHMENTS AND SUGGESTIONS FOR FUTURE WORK

The following are the principal tasks that have been accomplished during the course of the research performed for this thesis:

- An apparatus developed at Oregon State University by D. E. Stock and R. J. Zaworski and described previously by Stock (1972) has been modified to allow for measurements of temperature fields associated with flow-coupled diffusion. These modifications involved incorporating temperature instrumentation, mechanical devices for precise radial and axial positioning of diffusion tube instrument probes, thermal shielding, and other changes that facilitate taking measurements of temperature profiles in diffusion flow fields.
- Radial and axial temperature profiles have been measured for four sets of flow conditions in the Peclet number range between 1.9 and 5.9. The data confirm that the apparatus referred to above can be operated with a high degree of precision, since corresponding temperature measurements taken in repeated runs are in agreement within $\pm$ 0.1^{o} C. Through the use of very small diameter, stainless-steel sheathed thermocouple probes, errors resulting from conduction and radiation

heat transfer between the sensing junctions, their support materials, and their surroundings are minimized. The uncertainty associated with these errors for any given centerline temperature measurement is estimated to be less than 10% of the measured value.

- Models have been formulated for computing thermal diffusion factors and molecular diffusion coefficients from experimental values of velocity, concentration, and temperature distributions measured in the apparatus referred to above, and the models have been programmed for machine calculations of these transport coefficients. Values of these coefficients computed from data for the four sets of flow conditions considered in this investigation are consistent with theoretical predictions and with experimental data reported by other investigators.
- A model has also been developed for predicting the temperature field corresponding to a given set of diffusion flow conditions if the velocity and concentration fields are known. The model, which is applicable to flow-coupled diffusion in a vertically oriented, cylindrical tube, is in the form of a second order, elliptic, partial differential equation, in two dimensions. It

allows for both radial and axial gradients in the velocity and concentration fields. A computer program has been written to solve the model numerically. Temperature distributions predicted with this model for the flow conditions considered in this investigation are similar in shape to those measured experimentally, but quantitative comparisons of the predicted and experimental results are precluded because of the approximate nature of the experimental velocity and concentration distributions used as input for predicting the temperature distributions.

Suggestions for future work are as follows:

- The differential equation developed in Chapter IV for predicting temperature distributions associated with flow-coupled diffusion could be incorporated into a system of equations that would serve as a model for predicting the interrelated velocity, concentration, and temperature distributions in diffusion flow fields. Such a model would be useful for analyzing the effects of varying the diffusion tube diameter, operating under different flow conditions, and utilizing different gas pairs. Solutions generated from the model could also be compared with

experimental results, thus providing a means for gaining additional insight into the fundamental processes associated with diffusion phenomena.

- An alternate method for measuring velocity distributions in the diffusion tube would be desirable. Stock (1972) measured velocity profiles by injecting pulses of smoke perpendicular to the direction of bulk flow and then taking multiple-exposure photographs of the pulses, which were illuminated with a strobe light. According to Stock, the method is well suited for measuring velocity profiles in the central core of diffusion flow fields, but it is subject to substantial uncertainty for measurements of velocities near the diffusion tube wall. Stock also states that many steps are required to infer velocities at individual points from information recorded on the photographs, and that each step increases the uncertainty of the final results. It would be preferable to have a scheme for measuring velocities at individual points directly. Perhaps a laser-doppler anemometer could be used for this purpose.
- The apparatus could be used to obtain experimental data for gas pairs other than helium and nitrogen. With the computer programs included

in Appendix C, thermal diffusion factors and molecular diffusion coefficients could be computed from the experimental data and compared with results obtained by other investigators.

BIBLIOGRAPHY

Atkins, B. E., R. E. Bastick and T. L. Ibbs. 1939. "Thermal Diffusion in Mixtures of Inert Gases." Proceedings of the Royal Society of London, Series A, Vol. 172, No. 948, pp. 142-157.

Beckwith, T. G. and N. L. Buck. 1969. Mechanical Measurements. Reading, Massachusetts: Addison-Wesley Publishing Company.

Bird, R. B., W. E. Stewart and E. N. Lightfoot. 1960. Transport Phenomena. New York: John Wiley and Sons, Inc.

Chapman, S. 1916. "The Kinetic Theory of Simple and Composite Monatomic Gases: Viscosity, Thermal Conduction, and Diffusion." Proceedings of the Royal Society of London, Series A, Vol. 93, pp. 1-20.

Chapman, S. 1958. "Thermal Diffusion in Gases." In Transport Properties in Gases (A. B. Cambel and J. B. Fenn, eds.), pp. 143-150. Evanston, Illinois: Northwestern University Press.

Chapman, S. 1962. "Some Recent Advances in Gas Transport Theory." In Progress in International Research on Thermodynamics and Transport Properties (J. F. Masi and D. H. Tsai, eds.), pp. 257-265. New York: Academic Press.

Chapman, S. and T. G. Cowling. 1970. The Mathematical Theory of Non-Uniform Gases, 3rd. ed. London: Cambridge University Press.

Chapman, S. and F. W. Dootson. 1917. "A Note on Thermal Diffusion." Philosophical Magazine and Journal of Science, Vol. 33, pp. 248-253.

Draper, N. R. and H. Smith. 1966. Applied Regression Analysis. New York: John Wiley and Sons, Inc.

Ferziger, J. H. and H. G. Kaper. 1972. Mathematical Theory of Transport Processes in Gases. Amsterdam: North-Holland Publishing Company.

Grew, K. E. 1946. "Thermal Diffusion in Mixtures of the Inert Gases." Proceedings of the Royal Society of London, Series A, Vol. 189, No. A1018, pp. 402-414.

Grew, K. E. and B. E. Atkins. 1936. "Thermal Diffusion in Deuterium Mixtures." Proceedings of the Physical Society of London, Vol. 48, pp. 415-420.

Grew, K. E. and T. L. Ibbs. 1952. Thermal Diffusion in Gases. London: Cambridge University Press.

Grew, K. E., F. A. Johnson and W. E. J. Neal. 1954. "The Thermal Diffusion Factor and Temperature." Proceedings of the Royal Society of London, Series A, Vol. 224, No. 1159, pp. 513-526.

Heymann, D. and J. Kistemaker. 1959. "Thermal Diffusion of Xenon at Tracer Concentrations." Physica, Vol. 25, No. 7, pp. 556-567.

Hirschfelder, J. O., C. F. Curtiss and R. B. Bird. 1960. Molecular Theory of Gases and Liquids. New York: John Wiley and Sons, Inc.

Ibbs, T. L. and K. E. Grew. 1931. "The Influence of Low Temperatures on the Thermal Diffusion Effect." Proceedings of the Physical Society of London, Vol. 43, Part 2, pp. 142-156.

Ita, L. E. and R. E. Sonntag. 1974. "Influence of Pressure on Thermal Diffusion in Binary and Ternary Mixtures of Helium, Nitrogen, and Neon." Journal of Chemical and Engineering Data, Vol. 19, No. 1, pp. 33-35.

Kestin, J., E. Paykoc and J. V. Sengers. 1971. "On the Density Expansion for Viscosity in Gases." Physica, Vol. 54, No. 1, pp. 1-10.

Kihara, T. 1953. "Virial Coefficients and Models of Molecules in Gases." Reviews of Modern Physics, Vol. 25, No. 4, pp. 831-843.

Laranjeira, M. F. 1960. "An Elementary Theory of Thermal and Pressure Diffusion in Gaseous Binary and Complex Mixtures. II. Binary Mixtures with Experimental Comparison." Physica, Vol. 26, pp. 417-430.

Lonsdale, H. K. and E. A. Mason. 1957. "Thermal Diffusion and the Approach to the Steady State in H_2-CO_2 and He-CO_2." The Journal of Physical Chemistry, Vol. 61, No. 11, pp. 1544-1551.

Mason, E. A. 1939. "Higher Approximations for the Transport Properties of Binary Gas Mixtures. I. General Formulas." The Journal of Chemical Physics, Vol. 27, No. 1, pp. 75-84.

Mason, E. A., R. J. Munn and F. J. Smith. 1966. "Thermal Diffusion in Gases." Advances in Atomic and Molecular Physics, Vol. 2, pp. 33-91.

Mason, E. A. and S. C. Saxena. 1958. "Approximate Formula for the Thermal Conductivity of Gas Mixtures." The Physics of Fluids, Vol. 1, No. 5, pp. 361-369.

Mason, E. A., S. Weissman and R. P. Wendt. 1964. "Composition Dependence of Gaseous Thermal Diffusion Factors and Mutual Diffusion Coefficients." The Physics of Fluids, Vol. 7, No. 2, pp. 174-179.

McAdams, W. H. 1954. Heat Transmission, 3rd. ed. New York: McGraw-Hill Book Company, Inc.

Monchick, L. and E. A. Mason. 1967. "Free-Flight Theory of Gas Mixtures." The Physics of Fluids, Vol. 10, No. 7, pp. 1377-1390.

Onsager, L. 1931. "Reciprocal Relations in Irreversible Processes."
I. Physical Review, Vol. 37, No. 4, pp. 405-426.
II. Physical Review, Vol. 38, No. 12, pp. 2265-2279.

Rostigi, R. P. and G. L. Madan. 1965. "Dufour Effect in Liquids." The Journal of Chemical Physics, Vol. 43, No. 11, pp. 4179-4180.

Saxena, S. C. and E. A. Mason. 1959. "Thermal Diffusion and the Approach to the Steady State in Gases: II." Molecular Physics, Vol. 2, No. 4, pp. 379-395.

Saxena, S. C. and B. P. Mathur. 1965. "Thermal Diffusion in Binary Gas Mixtures and Intermolecular Forces." Reviews of Modern Physics, Vol. 37, No. 2, pp. 316-325.

Scheid, F. 1968. Schaum's Outline of Theory and Problems of Numerical Analysis. New York: McGraw-Hill Book Company, Inc.

Sparrow, E. M., W. J. Minkowycz, E. R. G. Eckert and W. E. Ibele. 1964. "The Effect of Diffusion Thermo and Thermal Diffusion for Helium Injection into Plane and Axisymmetric Stagnation Flow of Air." Journal of Heat Transfer, Transactions ASME, Series C, Vol. 86, pp. 311-319.

Stock, D. E. 1972. Concentration and Velocity Profiles for Flow-Coupled Diffusion. Doctoral dissertation, Oregon State University, Corvallis.

Stock, D. E. and R. J. Zaworski. 1973. "Velocity and Concentration Profiles for Binary Diffusion in a Two-Dimensional Laminar Flow Field." In Proceedings of the Sixth Symposium on Thermophysical Properties (P. E. Liley, ed.), pp. 134-142. New York: ASME, United Engineering Center.

Strobridge, T. R. 1962. "The Thermodynamic Properties of Nitrogen from 64 to 300° K between 0.1 and 200 Atmospheres." National Bureau of Standards Technical Note 129. Washington, D. C.: U. S. Department of Commerce.

Tewfik, O. E. and Ji-Wu Yang. 1962. "The Thermodynamic Coupling between Heat and Mass Transfer in Free Convection with Helium Injection." International Journal of Heat and Mass Transfer, Vol. 6, pp. 915-923.

Touloukian, Y. S., P. E. Liley and S. C. Saxena. 1970. "Thermal Conductivity: Nonmetallic Liquids and Gases." Thermophysical Properties of Matter. Vol. 3. New York: IFI/Plenum.

Touloukian, Y. S. and T. Makita. 1970. "Specific Heat: Nonmetallic Liquids and Gases." Thermophysical Properties of Matter. Vol. 6. New York: IFI/Plenum.

Wagman, D. D., W. H. Evans, V. B. Parker, I. Halow, S. M. Bailey and R. H. Schumm. 1968. "Selected Values of Chemical Thermodynamic Properties." National Bureau of Standards Technical Note 270-3. Washington, D. C.: U. S. Department of Commerce.

Waldmann, L. 1947. "Die Temperaturerscheinungen bei der Diffusion in ruhenden Gasen und ihre meßtechnische Anwendung." Z. Physik, Vol. 124, No. 2, pp. 2-29.

Waldmann, L. 1949. "Über die Druck- und Temperaturabhängigkeit der Wärmeerscheinungen bei der Diffusion." Z. Naturforschung, Vol. 4A, pp. 105-117.

Walker, R. E. and A. A. Westenberg. 1958. "Molecular Diffusion Studies in Gases at High Temperature. I. The 'Point Source' Technique." The Journal of Chemical Physics, Vol. 29, No. 5, pp. 1139-1146.

Walther, J. E. and H. G. Drickamer. 1958. "Thermal Diffusion in Dense Gases." Journal of Physical Chemistry, Vol. 62, pp. 421-425.

Welty, J. R., C. E. Wicks and R. E. Wilson. 1969. Fundamentals of Momentum, Heat and Mass Transfer. New York: John Wiley and Sons, Inc.

Wyatt, W. G. 1968. Determination of Thermal Diffusion Factors in Binary Gas Systems. Doctoral dissertation, University of Minnesota, Minneapolis.

Wylie, C. R., Jr. 1960. Advanced Engineering Mathematics, 2nd. ed. New York: McGraw-Hill Book Company, Inc.

Yang, Ji-Wu. 1966. A New Method of Measuring the Mass Diffusion Coefficient and Thermal Diffusion Factor in a Binary Gas System. Doctoral dissertation, University of Minnesota, Minneapolis.

Zaworski, R. J. 1966. Calorimetric Measurements of Heat of Transport in the Diffusion of Hydrogen through Nitrogen. Doctoral dissertation, Massachusetts Institute of Technology, Cambridge.

Zeldin, B. and F. W. Schmidt. 1972. "Developing Flow with Combined Forced-Free Convection in an Isothermal Vertical Tube." Journal of Heat Transfer, Transactions ASME, Series C, Vol. 94, No. 2, pp. 211-223.

APPENDICES

Appendix A. NOMENCLATURE

Symbols that are used only infrequently in the manuscript are not listed below. Such symbols are defined at the appropriate locations within the manuscript.

C molar density of mixture = $C_A + C_B$

C_i molar concentration of constituent i, = $\frac{\rho_i}{M_i}$

C_p specific heat at constant pressure

D_{AB} molecular diffusion coefficient for system A-B

D_T coefficient of thermal diffusion

$\vec{e}$ multicomponent energy flux relative to stationary coordinates

E internal fluid energy

h_i enthalpy per molecule of constituent i

H enthalpy of gas mixture

H_i partial enthalpy of constituent i

$\vec{J}_i$ mass flux of constituent i relative to the mass average velocity = $\rho_i(\vec{v}_i - \vec{v})$

k Boltzmann's constant

k_T thermal diffusion ratio = $\frac{D_T}{D_{AB}}$

$\dot{m}$ mass flow rate

M number mean molecular weight of gas mixture = $\frac{\rho}{C} = X_A M_A + X_B M_B$

M_i molecular weight of constituent i

n molecules of gas mixture per unit volume

n_i molecules of constituent i per unit volume

$\mathcal{N}$ Avogadro's number

p pressure

$\vec{q}$ multicomponent energy flux relative to mass average velocity $\vec{v}$

Q_i volume flow rate of constituent i

r radial distance from centerline of diffusion tube

R radius of diffusion tube

$\mathcal{R}$ gas constant

T gas temperature

U dimensionless radial velocity $= \dfrac{v_r}{|\bar{V}_{A_o}|}$

$\vec{v}$ mass average velocity $= (1/\rho)(\rho_A \vec{v}_A + \rho_B \vec{v}_B)$

$\vec{v}_i$ velocity of constituent i relative to stationary coordinates

$\vec{V}$ dimensionless axial velocity $= \dfrac{v_z}{|\bar{V}_{A_o}|}$

$\vec{V}_{D_i}$ diffusion velocity of constituent i relative to the mass average velocity $= \vec{v}_i - \vec{v}$

x axial distance relative to a reference plane located where only gas A is present in the diffusion tube (used in Chapter VI)

X_i mole fraction of constituent i, $= C_i/C$

z axial distance upstream of and relative to the gas B injection plane

Greek symbols

α_T thermal diffusion factor = $k_T/X_A X_B$

β dimensionless density = ρ/ρ_{A_o}

ζ dimensionless axial coordinate = z/R

θ dimensionless temperature = $\dfrac{T - T_o}{T_o}$

λ thermal conductivity

μ viscosity

ξ dimensionless radial coordinate = r/R

ρ_i mass concentration of constituent i, = $C_i M_i$

ρ mass density of mixture = $\rho_A + \rho_B$

χ dimensionless axial coordinate (= x/R) relative to a reference plane where only gas A is present in the diffusion tube (used in Chapter VI)

ω mass fraction of constituent i, = ρ_i/ρ

Overlines

$\hat{}$ per unit mass

$\bar{}$ average over flow cross section

Subscripts

A refers to the heavier gas

B	refers to the lighter gas
j,k	computational grid indices in the radial and axial directions
o	refers to axial positions sufficiently far upstream of the gas B injection plane so that only gas A is present in the flow field
r	radial direction
x	axial direction relative to (x,χ) coordinates
z	axial direction relative to (z,ζ) coordinates

Appendix B. DIFFERENTIAL EQUATION FOR THE TEMPERATURE DISTRIBUTION IN THE DIFFUSION FLOW FIELD

As discussed in section 4.1.3 of Chapter IV, a differential equation for the temperature distribution in the diffusion flow field may be developed from the following three equations:

$$\vec{\nabla} \cdot \vec{e} = 0 \tag{4.5}$$

where

$$\vec{e} = \vec{q} + (C_A H_A + C_B H_B)\vec{v} \tag{4.6}$$

and

$$\vec{q} = -\lambda \vec{\nabla} T + (n_A h_A \vec{V}_{D_A} + n_B H_B \vec{V}_{D_B}) + knTX_A X_B \alpha_T (\vec{V}_{D_A} - \vec{V}_{D_B}). \tag{4.7}$$

After substituting for $\vec{q}$ in equation 4.6 using the terms given in equation 4.7, the divergence of equation 4.6 is taken in accordance with equation 4.5. The resulting equation may be expressed in terms of the temperature T and its derivatives. Details of the formulation are outlined in the following paragraphs.

When the terms given for $\vec{q}$ in equation 4.7 are substituted into equation 4.6, the $n_i h_i \vec{V}_i$ in the former

equation may be combined with the $C_i H_i \vec{v}$ in the latter. Noting that $n_i h_i = C_i H_i$ and that $\vec{V}_{D_i} = \vec{v}_i - \vec{v}$, where the nomenclature is the same as that defined in Chapter IV and Appendix A,

$$n_A h_A \vec{V}_{D_A} + n_B h_B \vec{V}_{D_B} + (C_A H_A + C_B H_B)\vec{v} = C_A H_A (\vec{v}_A - \vec{v})$$

$$+ C_B H_B (\vec{v}_B - \vec{v}) + (C_A H_A + C_B H_B)\vec{v}$$

$$= C_A H_A \vec{v}_A + C_B H_B \vec{v}_B .$$

Noting also that

$$\vec{V}_{D_A} - \vec{V}_{D_B} = (\vec{v}_A - \vec{v}) - (\vec{v}_B - \vec{v}) = \vec{v}_A - \vec{v}_B ,$$

equation 4.6 may be expressed as follows after substituting for $\vec{q}$ using the terms given in equation 4.7:

$$\vec{e} = -\lambda \vec{\nabla} T + (C_A H_A \vec{v}_A + C_B H_B \vec{v}_B)$$

$$+ knTX_A X_B \alpha_T (\vec{v}_A - \vec{v}_B) \qquad \text{(B.1)}$$

where $\vec{v}_A$ and $\vec{v}_B$ are the velocities of gases A and B relative to stationary coordinates.

It will be found convenient for computational purposes to have $\vec{v}_B$ in equation B.1 expressed in terms of $\vec{v}$ and $\vec{v}_A$. The mass average velocity $\vec{v}$ is related to velocities $\vec{v}_A$ and $\vec{v}_B$ as follows (Bird, et al. (1960)):

$$\rho\vec{v} = \rho_A\vec{v}_A + \rho_B\vec{v}_B.$$

Thus,

$$\vec{v}_B = \frac{\rho}{\rho_B}\vec{v} - \frac{\rho_A}{\rho_B}\vec{v}_A .$$

Noting that $C_i = \rho_i/M_i$, where C_i is the molar concentration of constituent i,

$$\vec{v}_B = \frac{CM}{C_B M_B}\vec{v} - \frac{C_A M_A}{C_B M_B}\vec{v}_A .$$

Noting also that $X_i = C_i/C$, where X_i is the mole fraction of constituent i and C is the molar density of the mixture,

$$\vec{v}_B = \frac{M}{X_B M_B}\vec{v} - \frac{X_A M_A}{X_B M_B}\vec{v}_A . \qquad (B.2)$$

The first set of terms in brackets on the right hand side of equation B.1 may be rewritten as follows, using equation B.2 and the relationship $X_i = C_i/C$:

$$C_A H_A\vec{v}_A + C_B H_B\vec{v}_B = C\left[X_A\left(H_A - H_B\frac{M_A}{M_B}\right)\vec{v}_A + H_B\frac{M}{M_B}\vec{v}\right] . \qquad (B.3)$$

Again, using equation B.2, the difference in velocities in the last term of equation B.1 may be written as:

$$\vec{v}_A - \vec{v}_B = \frac{M(\vec{v}_A - \vec{v})}{X_B M_B} . \qquad (B.4)$$

The divergence of equation B.1 will now be taken term-by-term. Starting with the first term,

$$\vec{\nabla}\cdot(-\lambda\vec{\nabla}T) = -\frac{\partial}{\partial r}\left(\lambda\frac{\partial T}{\partial r}\right) - \frac{\lambda}{r}\frac{\partial T}{\partial r} - \frac{\partial}{\partial z}\left(\lambda\frac{\partial T}{\partial z}\right) . \qquad (B.5)$$

The divergence of the next two terms grouped together in brackets in equation B.1 is equivalent to the divergence of equation B.3. Working with the first term on the right hand side of the latter equation,

$$\vec{\nabla}\cdot(CX_A H_A \vec{v}_A) = \vec{\nabla}\cdot(C_A H_A \vec{v}_A) = \vec{\nabla}\cdot\left(\frac{\rho_A}{M_A} H_A \vec{v}_A\right)$$

$$= \frac{1}{M_A}\vec{\nabla}\cdot(\rho_A H_A \vec{v}_A) .$$

When the right hand side of the preceding equation is expanded, the terms include the product of H_A and $\vec{\nabla}\cdot(\rho_A\vec{v}_A)$. In accordance with the continuity equation for constituent A, $\vec{\nabla}\cdot(\rho_A\vec{v}_A) = 0$. Thus,

$$\vec{\nabla}\cdot(CX_A H_A \vec{v}_A) = \frac{\rho_A}{M_A}\left(v_{A_r}\frac{\partial H_A}{\partial r} + v_{A_z}\frac{\partial H_A}{\partial z}\right) .$$

After taking the divergence of the remaining terms on the right hand side of equation B.3 in the manner illustrated above, the result is as follows:

$$\vec{\nabla}\cdot(C_A H_A \vec{v}_A + C_B H_B \vec{v}_B) = \frac{\rho_A}{M_A}\left(v_{A_r}\frac{\partial H_A}{\partial r} + v_{A_z}\frac{\partial H_A}{\partial z}\right)$$

$$- \frac{\rho_A}{M_B}\left(v_{A_r}\frac{\partial H_B}{\partial r} + v_{A_z}\frac{\partial H_B}{\partial z}\right) + \frac{\rho}{M_B}\left(v_r\frac{\partial H_B}{\partial r} + v_z\frac{\partial H_B}{\partial z}\right) . \qquad (B.6)$$

Before taking the divergence of the last term in equation B.1, several substitutions will be made that will be convenient for later computations. First, Boltzmann's constant k is related to the gas constant $\tilde{R}$ and Avogadro's number $\tilde{N}$ by the equation $k = \tilde{R}/\tilde{N}$ (Bird, et al. (1960)). In addition, the number density n of the fluid is related to the molar density C and Avogadro's number by $n = C\tilde{N}$. Finally, $CX_A = C_A = \rho_A/M_A$, where the nomenclature is as defined previously. With these substitutions and with the use of equation B.4, the last term of equation B.1 becomes:

$$knTX_AX_B\alpha_T(\vec{v}_A - \vec{v}_B) = \frac{\rho_A}{M_A}\frac{M}{M_B}\tilde{R}\alpha_T T(\vec{v}_A - \vec{v}) .$$

The divergence of the preceding equation may be taken as follows:

$$\vec{\nabla}\cdot\left[knTX_AX_B\alpha_T(\vec{v}_A - \vec{v}_B)\right] = \frac{\tilde{R}}{M_AM_B}\left[\vec{\nabla}\cdot(\rho_A\alpha_T TM\vec{v}_A) - \vec{\nabla}\cdot(\rho_A\alpha_T TM\vec{v})\right] . \qquad (B.7)$$

In accordance with the continuity equation for constituent A, $\vec{\nabla}\cdot(\rho_A\vec{v}_A) = 0$. Therefore, the divergence of the first term within the square brackets on the right hand side of equation B.7 is

$$\vec{\nabla}\cdot(\rho_A\alpha_T TM\vec{v}_A) = \rho_A v_{A_r}\left[\frac{\partial(\alpha_T TM)}{\partial r}\right] + \rho_A v_{A_z}\left[\frac{\partial(\alpha_T TM)}{\partial z}\right] . \qquad (B.8)$$

Noting that $M = \rho/C$ and that, in accordance with the continuity equation for the mixture, $\vec{\nabla}\cdot(\rho\vec{v}) = 0$, the divergence of the second term on the right hand side of equation B.7 is

$$\vec{\nabla}\cdot(\rho_A\alpha_T{}^T M\vec{v}) = \rho v_r \frac{\partial}{\partial r}\left(\frac{\rho_A\alpha_T{}^T}{C}\right) + \rho v_z \frac{\partial}{\partial z}\left(\frac{\rho_A\alpha_T{}^T}{C}\right). \qquad (B.9)$$

The molar density C in equation B.9 may be expressed in terms of an equivalent function of temperature. A relationship between C and T may be developed from the following equation for the hydrostatic pressure p:

$$p = knT. \qquad (B.10)$$

Although the applicability of equation B.10 is limited to ideal gases in equilibrium or to ideal, nonuniform gases in which the molecules have only translatory energy, it is correct to a close approximation for a gas with internal energy (Chapman and Cowling (1970)).

As discussed previously (following equation B.6), $k = \tilde{R}/\tilde{N}$ and $n = C\tilde{N}$. With these substitutions, equation B.10 may be written as $p = C\tilde{R}T$, or $C = p/(\tilde{R}T)$. Making use of the latter relationship and the relationship $M = \rho/C$, equation B.9 becomes:

$$\vec{\nabla}\cdot(\rho_A\alpha_T{}^T M\vec{v}) = Mv_r\left[\rho_A{}^T\frac{\partial\alpha_T}{\partial r} + \alpha_T{}^T\frac{\partial\rho_A}{\partial r} + 2\rho_A\alpha_T\frac{\partial T}{\partial r}\right] + Mv_z\left[\rho_A{}^T\frac{\partial\alpha_T}{\partial z} + \alpha_T{}^T\frac{\partial\rho_A}{\partial z} + 2\rho_A\alpha_T\frac{\partial T}{\partial z}\right]. \quad (B.11)$$

With the aid of equations B.1, B.5 through B.9, B.11, and the ideal gas relationship $\frac{\partial H_i}{\partial x_j} = C_{p_i}\frac{\partial T}{\partial x_j}$, equation 4.5 may be written as follows:

$$-\frac{\partial}{\partial r}\left(\lambda\frac{\partial T}{\partial r}\right) - \frac{\lambda}{r}\frac{\partial T}{\partial r} - \frac{\partial}{\partial z}\left(\lambda\frac{\partial T}{\partial z}\right) + \rho_A\left(\frac{C_{p_A}}{M_A} - \frac{C_{p_B}}{M_B}\right)\left(v_{A_r}\frac{\partial T}{\partial r} + v_{A_z}\frac{\partial T}{\partial z}\right) + \frac{\rho C_{p_B}}{M_B}\left(v_r\frac{\partial T}{\partial r} + v_z\frac{\partial T}{\partial z}\right) + \frac{\rho_A\bar{R}}{M_A M_B}\left(v_{A_r}\frac{\partial(\alpha_T{}^T M)}{\partial r} + v_{A_z}\frac{\partial(\alpha_T{}^T M)}{\partial z}\right) - \frac{M\tilde{R}}{M_A M_B}\left[v_r\left(\alpha_T{}^T\frac{\partial\rho_A}{\partial r} + 2\rho_A\alpha_T\frac{\partial T}{\partial r} + \rho_A{}^T\frac{\partial\alpha_T}{\partial r}\right) + v_z\left(\alpha_T{}^T\frac{\partial\rho_A}{\partial z} + 2\rho_A\alpha_T\frac{\partial T}{\partial z} + \rho_A{}^T\frac{\partial\alpha_T}{\partial z}\right)\right] = 0.$$

After some additional rearranging, the differential equation for the temperature distribution in the diffusion flow field becomes

$$\lambda\frac{\partial^2 T}{\partial r^2} + \lambda\frac{\partial^2 T}{\partial z^2} + \left[\frac{\partial\lambda}{\partial r} + \frac{\lambda}{r} - \rho_A\left(\frac{C_{p_A}}{M_A} - \frac{C_{p_B}}{M_B} + \frac{M\tilde{R}\alpha_T}{M_A M_B}\right)v_{A_r} - \left(\frac{\rho C_{p_B}}{M_B} - \frac{2M\tilde{R}\rho_A\alpha_T}{M_A M_B}\right)v_r\right]\frac{\partial T}{\partial r}$$

$$+ \left[\frac{\partial \lambda}{\partial z} - \rho_A\left(\frac{C_{p_A}}{M_A} - \frac{C_{p_B}}{M_B} + \frac{M\mathring{R}\alpha_T}{M_A M_B}\right)v_{A_z} - \left(\rho\frac{C_{p_B}}{M_B}\right.\right.$$

$$\left.\left. - 2\frac{M\mathring{R}\rho_A\alpha_T}{M_A M_B}\right)v_z\right]\frac{\partial T}{\partial z} - \frac{\mathring{R}}{M_A M_B}\left[\rho_A\left(v_{A_r}\ \frac{\partial(\alpha_T M)}{\partial r}\right.\right.$$

$$\left.\left. + v_{A_z}\ \frac{\partial(\alpha_T M)}{\partial z}\right) - M\left(v_r\ \frac{\partial(\alpha_T\rho_A)}{\partial r} + v_z\ \frac{\partial(\alpha_T\rho_A)}{\partial z}\right)\right]T = 0. \quad (4.8)$$

Appendix C

COMPUTER PROGRAMS

For Chapter 4:

Program TFIELD

Program VELOCITY

For Chapter 6:

Program ALPHA

Program RADTEMP

```
      PROGRAM TFIELD
C
C     THIS PROGRAM IS USED TO SOLVE A SECOND ORDER, PARTIAL DIFFERENTIAL
C     EQUATION FOR THE DIMENSIONLESS TEMPERATURE FIELD, THETA(J,K),
C     CORRESPONDING TO GIVEN FLOW CONDITIONS IN A DIFFUSION FIELD
C     OF A BINARY GASEOUS MIXTURE.
C
C        ********  DEFINITIONS OF PROGRAM VARIABLES  ********
C
C     TWO-DIMENSIONAL ARRAYS USED IN THE COMPUTATIONS --
C
C     ALPHA(J,K)   THERMAL DIFFUSION FACTOR, DIMENSIONLESS.
C         C(J,K)   COEFFICIENTS IN EQUATION FOR THETA, DIMENSIONLESS.
C        C1(J,K)      "    "    "   "    "    "    "       "     "
C        C2(J,K)      "    "    "   "    "    "    "       "     "
C        C3(J,K)      "    "    "   "    "    "    "       "     "
C       LAM(J,K)   THERMAL CONDUCTIVITY OF GAS MIXTURE, CAL/(CM SEC K).
C     THETA(J,K)   TEMPERATURE OF GAS MIXTURE, DIMENSIONLESS.
C         U(J,K)   MASS AVERAGE VELOCITY OF GAS MIXTURE IN RADIAL
C                  DIRECTION, DIMENSIONLESS.
C         V(J,K)   MASS AVERAGE VELOCITY OF GAS MIXTURE IN AXIAL
C                  DIRECTION, DIMENSIONLESS.
C        UA(J,K)   VELOCITY OF GAS A IN RADIAL DIRECTION RELATIVE
C                  TO STATIONARY COORDINATES, DIMENSIONLESS.
C        VA(J,K)   VELOCITY OF GAS A IN AXIAL DIRECTION RELATIVE
C                  TO STATIONARY COORDINATES, DIMENSIONLESS.
C        XA(J,K)   MOLE FRACTION OF GAS A, DIMENSIONLESS.
C
C     OTHER VARIABLES --
C
C     BCW          SIGNAL FOR BOUNDARY CONDITION TO BE IMPOSED AT
C                  TUBE WALL.
C                     BCW = 0 -- ADIABATIC WALL
C                     BCW = 1 -- ISOTHERMAL WALL
C     CPA          SPECIFIC HEAT OF GAS A, CAL/(G K).
C     CPB          SPECIFIC HEAT OF GAS B, CAL/(G K).
C     DAB          MOLECULAR DIFFUSION COEFFICIENT, CM**2/SEC.
C     DPMAX        MAXIMUM RELATIVE ERROR IN THETA FOLLOWING EACH
C                  ITERATION.
C     DR           RADIAL NODE SPACING, DIMENSIONLESS.
C     DZ           AXIAL NODE SPACING, DIMENSIONLESS.
C     EXT          LIEBMANN EXTRAPOLATION FACTOR, USED IN ITERATIVE
C                  CALCULATIONS OF THETA(J,K).
C     ITMAX        MAXIMUM NUMBER OF ITERATIONS ALLOWED FOR CALCULATING
C                  THETA(J,K).
C     ITNO         NUMBER OF ITERATIONS COMPLETED FOR CALCULATING
C                  THETA(J,K).
C     KASE         IDENTIFICATION NUMBER FOR CASE UNDER CONSIDERATION.
C     LAMA         THERMAL CONDUCTIVITY OF GAS A, CAL/(CM SEC K).
C     LAMB         THERMAL CONDUCTIVITY OF GAS B, CAL/(CM SEC K).
C     MA           MOLECULAR WEIGHT OF GAS A, G/G-MOLE.
C     MB           MOLECULAR WEIGHT OF GAS B, G/G-MOLE.
C     MUA          VISCOSITY OF GAS A, G/(CM SEC).
C     MUB          VISCOSITY OF GAS B, G/(CM SEC).
C     NJ           NUMBER OF GRID POINTS, R-DIRECTION.
C     NK           NUMBER OF GRID POINTS, Z-DIRECTION.
```

```
C     NOR(J)        NUMBERING FOR OUTPUT HEADINGS ON LINE PRINTER.
C     NTTY          SIGNAL FOR TELETYPE OR BATCH PROGRAM CONTROL.
C                      NTTY = 0 -- BATCH OPERATION
C                      NTTY = 1 -- TELETYPE CONTROL
C     NURUN         SIGNAL FOR CONTINUED ITERATION FROM EXISTING FILE.
C     PE            MASS PECLET NUMBER (2*R*VINF/DAB).
C     PHIAB         CONSTANT USED IN CALCULATION OF LAM(J,K).
C     PHIBA         CONSTANT USED IN CALCULATION OF LAM(J,K).
C     RAD           INSIDE RADIUS OF DIFFUSION TUBE, CM.
C     RBAR          UNIVERSAL GAS CONSTANT, CAL/(G-MOLE K).
C     RHOA          DENSITY OF GAS A AT ENTRANCE TO DIFFUSION TUBE, G/CC.
C     VINF          AVERAGE VELOCITY, CM/SEC, OF GAS A FAR UPSTREAM OF
C                   THE GAS B INJECTION PLANE.
C     XAO           MOLE FRACTION OF GAS A AT THE GAS B INJECTION PLANE.
C     XI            RADIAL COORDINATE, DIMENSIONLESS.
C
      COMMON        C(14,63),C1(14,63),C2(14,63),C3(14,63)
      COMMON        THETA(14,63),U(14,63),V(14,63)
      COMMON        UA(14,63),VA(14,63),XA(14,63)
      COMMON        IN,ITNO,J1,J2,K1,K2,KASE,NJ,NK,NODE1,NODE2,NTTY
      COMMON        BCW,DPMAX,DR,DZ,EXT,OUT,PE,VINF,XAO
      COMMON        LAM(14,63),ALPHA(14,63)
    1 FORMAT(10I5)
    2 FORMAT(7F10.5)
    3 FORMAT(*0 FOR ITERATION*,I4,* MAX. RELATIVE ERROR IN*/
     1* THETA IS*,E14.7,* AT NODE*,2(I4))
    4 FORMAT(*0 RELATIVE ERROR IN THETA LESS THAN .00001 AT*/
     1* ITERATION NUMBER*,I4)
      INTEGER BCW, OUT
      REAL LAM
      IN            = 40
      OUT           = 41
      READ(IN,1) KASE,NURUN,NJ,NK,BCW,ITMAX,NTTY
      WRITE(61,1) KASE,NURUN,NJ,NK,BCW,ITMAX,NTTY
      READ(IN,2) EXT,DR,DZ,PE,XAO
      WRITE(61,2) EXT,DR,DZ,PE,XAO
      READ(5) U,V,UA,VA,XA
      J1            = NJ-1
      J2            = NJ-2
      K1            = NK-1
      K2            = NK-2
      DR2           = DR*DR
      DZ2           = DZ*DZ
      CALL READY
      CALL OUTPUT(1)
      IF(NURUN.EQ.0) GO TO 20
      READ(6) ITNO,THETA
      GO TO 40
C     SET TEMPERATURE FIELD WITHIN BOUNDARIES TO ZERO
   20 DO 25     J = 3,J2
      DO 25     K = 3,K2
      THETA(J,K) = 0.
   25 CONTINUE
C     SET BOUNDARIES HAVING CONSTANT TEMPERATURES TO SPECIFIED VALUES
      DO 30     J = 2,J1
      THETA(J,2) = 0.
```

```
      THETA(J,K1)= 0.
   30 CONTINUE
      IF(BCW.EQ.0) GO TO 35
      DO 35     K = 3,K2
      THETA(J1,K)= 0.
   35 CONTINUE
C     PERFORM THE ITERATIVE CALCULATIONS FOR THE TEMPERATURE FIELD
      ITNO       = 0
      KOUNT      = 0
      NUM        = 0
   40 ITNO       = ITNO+1
      DPMAX      = 0.
C     SET TEMPERATURE FIELD AT WALL BOUNDARY FOR THIS ITERATION IF
C     ADIABATIC BOUNDARY CONDITION IS SPECIFIED
      IF(BCW.EQ.1) GO TO 45
      DO 45     K = 3,K2
      THETA(NJ,K)= THETA(J2,K)
   45 CONTINUE
C     SET TEMPERATURE FIELD AT CENTERLINE BOUNDARY FOR THIS ITERATION
      DO 50     K = 3,K2
      THETA(1,K) = THETA(3,K)
   50 CONTINUE
C     COMPUTE THE TEMPERATURE FIELD FOR THIS ITERATION
      IF(BCW.EQ.0) LIMJ = J1
      IF(BCW.EQ.1) LIMJ = J2
      DO 60     J = 2,LIMJ
      DO 60     K = 3,K2
      THETAO       = THETA(J,K)
      TEMP1        = (THETA(J+1,K)+THETA(J-1,K))/DR2
      TEMP2        = (THETA(J,K+1)+THETA(J,K-1))/DZ2
      TEMP3        = C2(J,K)*(THETA(J+1,K)-THETA(J-1,K))/DR
      TEMP4        = C3(J,K)*(THETA(J,K+1)-THETA(J,K-1))/DZ
      THETA(J,K)   = C1(J,K)*(TEMP1+TEMP2+TEMP3+TEMP4+C(J,K))
      THETA(J,K)   = THETAO+EXT*(THETA(J,K)-THETAO)
      DEL          = ABS((THETA(J,K)-THETAO)/THETA(J,K))
      IF(DEL.LT.DPMAX) GO TO 60
      DPMAX        = DEL
      NODE1        = J
      NODE2        = K
   60 CONTINUE
      WRITE(6) ITNO,THETA
      REWIND 6
      IF(MOD(ITNO,10).NE.0) GO TO 65
      IF(NTTY.EQ.0) GO TO 65
      WRITE(61,3) ITNO,DPMAX,NODE1,NODE2
   65 IF(ITNO.GE.ITMAX) GO TO 80
      IF(DPMAX.GT.0.00001) GO TO 40
      IF(KOUNT.GT.0) GO TO 70
      IF(NTTY.EQ.1) WRITE(61,4) ITNO
      WRITE(OUT,4) ITNO
      KOUNT        = ITNO
   70 NUM          = NUM+1
      IF(NUM.LT.4) GO TO 40
      ITEST        = KOUNT+3
      IF(ITNO.EQ.ITEST) GO TO 90
      KOUNT        = 0
```

```
      NUM         = 0
      GO TO 40
   80 IF(NTTY.EQ.0) GO TO 90
      MORIT       = TTYIN(4HADDI,4HTION,4HAL I,4HTERA,4HTION,4HS = )
      IF(MORIT.EQ.0) GO TO 90
      ITMAX       = ITMAX+MORIT
      EXT         = TTYIN(4HTYPE,4H VAL,4HUE O,4HF EX,4HTRAP,4H. FA,
     14HCTOR,4H FOR,4H ADD,4H. IT,4HER. )
      GO TO 40
   90 CALL OUTPUT(2)
      STOP
      END
C
      SUBROUTINE READY
C     SETS UP CONSTANTS NECESSARY FOR PERFORMING THE ITERATIVE
C     CALCULATIONS, USING AS INPUT KNOWN VALUES OF UA(J,K), VA(J,K),
C     AND XA(J,K).
      COMMON        C(14,63),C1(14,63),C2(14,63),C3(14,63)
      COMMON        THETA(14,63),U(14,63),V(14,63)
      COMMON        UA(14,63),VA(14,63),XA(14,63)
      COMMON        IN,ITNO,J1,J2,K1,K2,KASE,NJ,NK,NODE1,NODE2,NTTY
      COMMON        BCW,DPMAX,DR,DZ,EXT,OUT,PE,VINF,XAO
      COMMON        LAM(14,63),ALPHA(14,63)
    1 FORMAT(6F12.8)
      INTEGER BCW,OUT
      REAL LAM,LAMA,LAMB,MA,MB,MUA,MUB
      READ(IN,1) LAMA,LAMB,MA,MB,MUA,MUB
      WRITE(61,1) LAMA,LAMB,MA,MB,MUA,MUB
      READ(IN,1) CPA,CPB,RAO,RHOA,VINF
      WRITE(61,1) CPA,CPB,RAO,RHOA,VINF
      RBAR        = 1.98717
C     CALCULATE THERMAL DIFFUSION FACTORS ALPHA(J,K).  EQUATION FITS
C     POINTS CALCULATED FROM CHAPMAN-COWLING EXP-SIX MODEL.
      DO 10     J = 1,J1
      DO 10     K = 1,NK
      TEMP        = XA(J,K)
C     ALPHA(J,K) = 0.52030-0.57230*TEMP+0.21043*TEMP**2
      ALPHA(J,K) = 0.70644-1.3717*TEMP+1.3425*TEMP**2-0.52108*TEMP**3
   10 CONTINUE
C     CALCULATE THERMAL CONDUCTIVITIES LAM(J,K)
      PHIAB       = 1.065*(1.+SQRT(MUA/MUB)*SQRT(SQRT(MB/MA)))**2
     1              /(SQRT(8.)*SQRT(1.+MA/MB))
      PHIBA       = 1.065*(1.+SQRT(MUB/MUA)*SQRT(SQRT(MA/MB)))**2
     1              /(SQRT(8.)*SQRT(1.+MB/MA))
      DO 20     J = 1,J1
      DO 20     K = 1,NK
      TEMP        = XA(J,K)
      LAM(J,K)    = (TEMP*LAMA)/(TEMP+(1.-TEMP)*PHIAB)+((1.-TEMP)*LAMB)
     1              /((1.-TEMP)+TEMP*PHIBA)
   20 CONTINUE
C     SET UP CONSTANTS TO BE USED IN CALCULATING COEFFICIENTS FOR THE
C     DIFFERENTIAL EQUATION FOR THETA(J,K)
      CONST1      = RBAR/(MA*MB)
      CONST2      = RHOA*VINF*RAO
      DMASX       = MA-MB
C     CALCULATE COEFFICIENTS C(J,K).  DERIVATIVES OF XA(J,K) ARE
```

```
C     COMPUTED USING FIVE-POINT FORMULAS.
      DO 25     K = 3,K2
      C(2,K)      = 0.
   25 CONTINUE
      DO 35     J = 3,J1
      DO 35     K = 3,K2
C     DALPHX      = -0.57230+0.42086*XA(J,K)
      DALPHX      = -1.3717+2.6850*TEMP-1.56324*TEMP**2
      IF(J2-J) 26,27,28
   26 DXAR        = (54.*XA(J,K)-13.*XA(J-1,K)-40.*XA(J-2,K)
     1              -27.*XA(J-3,K)+26.*XA(J-4,K))/(70.*DR)
      GO TO 30
   27 DXAR        = (6.*XA(J-3,K)-17.*XA(J-2,K)-20.*XA(J-1,K)
     1              -3.*XA(J,K)+34.*XA(J+1,K))/(70.*DR)
      GO TO 30
   28 DXAR        = (-2.*XA(J-2,K)-XA(J-1,K)+XA(J+1,K)
     1              +2.*XA(J+2,K))/(10.*DR)
   30 IF(K.GT.3) GO TO 32
      DXAZ        = (-34.*XA(J,K-1)+3.*XA(J,K)+20.*XA(J,K+1)
     1              +17.*XA(J,K+2)-6.*XA(J,K+3))/(70.*DZ)
      GO TO 33
   32 DXAZ        = (-2.*XA(J,K-2)-XA(J,K-1)+XA(J,K+1)
     1              +2.*XA(J,K+2))/(10.*DZ)
   33 TEMP1       = XA(J,K)/LAM(J,K)
      TEMP2       = ALPHA(J,K)*DMASX*DXAR
      TEMP3       = (XA(J,K)*(MA-MB)+MB)*DALPHX*DXAR
      TEMP4       = ALPHA(J,K)*DMASX*DXAZ
      TEMP5       = (XA(J,K)*(MA-MB)+MB)*DALPHX*DXAZ
      TEMP6       = (XA(J,K)*(MA-MB)+MB)/LAM(J,K)
      TEMP7       = ALPHA(J,K)*DXAR
      TEMP8       = XA(J,K)*DALPHX*DXAR
      TEMP9       = ALPHA(J,K)*DXAZ
      TEMP10      = XA(J,K)*DALPHX*DXAZ
      C(J,K)      = -CONST1*CONST2*(TEMP1*(UA(J,K)*(TEMP2+TEMP3)
     1              +VA(J,K)*(TEMP4+TEMP5))-TEMP6*(U(J,K)*(TEMP7
     2              +TEMP8)+V(J,K)*(TEMP9+TEMP10)))
   35 CONTINUE
C     CALCULATE COEFFICIENTS C1(J,K)
      DO 40     J = 2,J1
      DO 40     K = 3,K2
      C1(J,K)     = 1./(2./DR**2+2./DZ**2-C(J,K))
   40 CONTINUE
C     CALCULATE COEFFICIENTS C2(J,K) AND C3(J,K)
      DO 60     J = 2,J1
      DO 60     K = 3,K2
      TEMP1       = XA(J,K)*(MA-MB)+MB
      TEMP2       = XA(J,K)*((CPA-CPB)+CONST1*TEMP1*ALPHA(J,K))/LAM(J,K)
      TEMP3       = XA(J,K)+(1.-XA(J,K))*MB/MA
      TEMP4       = (TEMP3*CPB-2.*CONST1*XA(J,K)*TEMP1*ALPHA(J,K))
     1              /LAM(J,K)
      RJ          = J
      XI          = (RJ-2.)*DR
      IF(J2-J) 45,48,50
   45 TEMP5       = (1./LAM(J,K))*((54.*LAM(J,K)-13.*LAM(J-1,K)
     1              -40.*LAM(J-2,K)-27.*LAM(J-3,K)+26.*LAM(J-4,K))
     2              /(70.*DR))+1./XI-CONST2*(TEMP2*UA(J,K)+TEMP4*U(J,K))
```

```
      GO TO 52
   48 TEMP5      = (1./LAM(J,K))*((34.*LAM(J+1,K)-3.*LAM(J,K)
     1             -20.*LAM(J-1,K)-17.*LAM(J-2,K)+6.*LAM(J-3,K))
     2             /(70.*DR))+1./XI-CONST2*(TEMP2*UA(J,K)+TEMP4*U(J,K))
      GO TO 52
   50 TEMP5      = (1./LAM(J,K))*((-2.*LAM(J-2,K)-LAM(J-1,K)
     1             +LAM(J+1,K)+2.*LAM(J+2,K))/(10.*DR))+1./XI
     2             -CONST2*(TEMP2*UA(J,K)+TEMP4*U(J,K))
   52 IF(K.GT.3) GO TO 55
      TEMP6      = (1./LAM(J,K))*((-34.*LAM(J,K-1)+3.*LAM(J,K)
     1             +20.*LAM(J,K+1)+17.*LAM(J,K+2)-6.*LAM(J,K+3))
     2             /(70.*DZ))-CONST2*(TEMP2*VA(J,K)+TEMP4*V(J,K))
      GO TO 57
   55 TEMP6      = (1./LAM(J,K))*((-2.*LAM(J,K-2)-LAM(J,K-1)
     1             +LAM(J,K+1)+2.*LAM(J,K+2))/(10.*DZ))
     2             -CONST2*(TEMP2*VA(J,K)+TEMP4*V(J,K))
   57 C2(J,K)    = TEMP5/2.
      C3(J,K)    = TEMP6/2.
   60 CONTINUE
      RETURN
      END
C
      SUBROUTINE OUTPUT(MODE)
C     OUTS SELECTED RESULTS TO TELETYPE AND LINE PRINTER
      COMMON       C(14,63),C1(14,63),C2(14,63),C3(14,63)
      COMMON       THETA(14,63),U(14,63),V(14,63)
      COMMON       UA(14,63),VA(14,63),XA(14,63)
      COMMON       IN,ITNO,J1,J2,K1,K2,KASE,NJ,NK,NODE1,NODE2,NTTY
      COMMON       BCW,DPMAX,DR,DZ,EXT,OUT,PE,VINF,XAO
      COMMON       LAM(14,63),ALPHA(14,63)
      DIMENSION    NUR(20)
    1 FORMAT(1S1,
     1/1X1     INPUT FOR CASE NUMBER ,I3)
    2 FORMAT(1H-,
     1/1X      MASS PECLET NUMBER- - - - - - - - - - - - - - -1X,F10.4
     2/1X      MOLE FRACTION OF GAS A AT INJECTION PLANE - - -1X,F10.4
     3/1X      REFERENCE VELOCITY OF GAS A, CM/SEC - - - - - -1X,F10.4
     4/1X      NUMBER OF GRID POINTS (R-DIRECTION) - - - - - -1X,I5
     5/1X      NUMBER OF GRID POINTS (Z-DIRECTION) - - - - - -1X,I5
     6/1X      NODE THICKNESS IN R-DIRECTION, DR - - - - - - -1X,F10.4
     7/1X      NODE THICKNESS IN Z-DIRECTION, DZ - - - - - - -1X,F10.4
     8/1X      LIEBMANN EXTRAPOLATION FACTOR - - - - - - - - -1X,F10.4
     9/1X      BOUNDARY CONDITION AT TUBE WALL1X,
     A/1X      (0 = ADIABATIC, 1 = ISOTHERMAL) - - - - - - - -1X,I5
     B///)
    3 FORMAT(1H-      RESULTS FOR ITERATION NUMBER1X,I5/
     1/1X      MAXIMUM RELATIVE ERROR IN THETA IS1X,E12.3,
     2/1X      AT NODE 1X,I2,1X,I2)
    4 FORMAT(1X1       DIMENSIONLESS TEMPERATURE FOR ITERATION NUMBER1X,I5)
    5 FORMAT(1X1       RADIAL MASS AVG. VELOCITY U(J,K), DIMENSIONLESS1X)
    6 FORMAT(1X1       AXIAL MASS AVG. VELOCITY V(J,K), DIMENSIONLESS1X)
    7 FORMAT(1X1       DIMENSIONLESS HORIZONTAL VELOCITY, UA(J,K)1X)
    8 FORMAT(1X1       DIMENSIONLESS VERTICAL VELOCITY, VA(J,K)1X)
    9 FORMAT(1X1       MOLE FRACTION OF GAS A, XA(J,K)1X)
   10 FORMAT(1X1       THERMAL DIFFUSION FACTOR, ALPHA(J,K)1X)
   11 FORMAT(1X1       THERMAL CONDUCTIVITY, LAM(J,K), CAL/(CM SEC K)1X)
```

```
12  FORMAT(≠0       J = ≠,10(I8,4X))
13  FORMAT(≠ K = ≠,I2,2X,10(E12.3))
14  FORMAT(≠ ≠,E12.4)
    INTEGER BCW, OUT
    REAL LAM
    IF(MODE.GT.1) GO TO 20
    IF(NTTY.EQ.0) GO TO 15
    WRITE(61,1) KASE
    WRITE(61,2) RE,XAO,VINF,NJ,NK,DR,DZ,EXT,BCW
15  WRITE(OUT,1) KASE
    WRITE(OUT,2) RE,XAO,VINF,NJ,NK,DR,DZ,EXT,BCW
    GO TO 125
20  WRITE(61,14) (THETA(2,K),K = 5,15)
    DO 25     M = 1,NJ
    NOR(M)      = M
25  CONTINUE
    WRITE(OUT,3) ITNO,DPMAX,NODE1,NODE2
    KOUNT       = 0
30  KOUNT       = KOUNT+1
    N2          = 0
35  N1          = N2+1
    N2          = N1+9
    IF(N2.GT.NJ) N2 = NJ
    IF(KOUNT.EQ.8) GO TO 110
    IF(KOUNT-2)40,50,58
40  WRITE(OUT,4) ITNO
    WRITE(OUT,12) (NOR(J),J = N1,N2)
    DO 45     K = 1,NK
    WRITE(OUT,13) K,(THETA(J,K),J = N1,N2)
45  CONTINUE
    GO TO 120
50  WRITE(OUT,5)
    WRITE(OUT,12) (NOR(J),J = N1,N2)
    DO 55     K = 1,NK
    WRITE(OUT,13) K,(U(J,K),J = N1,N2)
55  CONTINUE
    GO TO 120
58  IF(KOUNT-4)60,70,78
60  WRITE(OUT,6)
    WRITE(OUT,12) (NOR(J),J = N1,N2)
    DO 65     K = 1,NK
    WRITE(OUT,13) K,(V(J,K),J = N1,N2)
65  CONTINUE
    GO TO 120
70  WRITE(OUT,7)
    WRITE(OUT,12) (NOR(J),J = N1,N2)
    DO 75     K = 1,NK
    WRITE(OUT,13) K,(UA(J,K),J = N1,N2)
75  CONTINUE
    GO TO 120
78  IF(KOUNT-6)80,90,100
80  WRITE(OUT,8)
    WRITE(OUT,12) (NOR(J),J = N1,N2)
    DO 85     K = 1,NK
    WRITE(OUT,13) K,(VA(J,K),J = N1,N2)
85  CONTINUE
```

```
      GO TO 120
   90 WRITE(OUT,9)
      WRITE(OUT,12) (NOR(J),J = N1,N2)
      DO 95    K = 1,NK
      WRITE(OUT,13) K,(XA(J,K),J = N1,N2)
   95 CONTINUE
      GO TO 120
  100 WRITE(OUT,10)
      WRITE(OUT,12) (NOR(J),J = N1,N2)
      DO 105   K = 1,NK
      WRITE(OUT,13) K,(ALPHA(J,K),J = N1,N2)
  105 CONTINUE
      GO TO 120
  110 WRITE(OUT,11)
      WRITE(OUT,12) (NOR(J),J = N1,N2)
      DO 115   K = 1,NK
      WRITE(OUT,13) K,(LAM(J,K),J = N1,N2)
  115 CONTINUE
  120 IF(N2.NE.NJ) GO TO 35
      IF(KOUNT.LT.8) GO TO 30
  125 RETURN
      END
C
      FUNCTION MOD(N,M)
C     RETURNS ZERO WHENEVER N IS EVENLY DIVISIBLE BY M
      MOD        = N-(N/M)*M
      RETURN
      END
```

```
      PROGRAM VELOCITY
C     USING AS INPUT KNOWN VALUES OF THE AXIAL COMPONENTS OF THE MASS
C     AVERAGE VELOCITY FIELD, THIS PROGRAM COMPUTES RADIAL COMPONENTS
C     OF THE VELOCITY FIELD, AND RADIAL AND AXIAL COMPONENTS OF THE
C     VELOCITY FIELD OF GAS A.
C
C     ARRAYS USED IN COMPUTATIONS --
C
C       DMV(J,K)    DERIVATIVE W/R TO DIMENSIONLESS AXIAL COORDINATE
C                   OF M(J,K)*V(J,K).
C      DXVA(J,K)    DERIVATIVE W/R TO DIMENSIONLESS AXIAL COORDINATE
C                   OF XA(J,K)*VA(J,K).
C         M(J,K)    MOLECULAR WEIGHT OF GAS MIXTURE, G/G-MOLE.
C         U(J,K)    MASS AVERAGE VELOCITY OF GAS MIXTURE IN RADIAL
C                   DIRECTION, DIMENSIONLESS.
C         V(J,K)    MASS AVERAGE VELOCITY OF GAS MIXTURE IN AXIAL
C                   DIRECTION, DIMENSIONLESS.
C        UA(J,K)    VELOCITY OF GAS A IN RADIAL DIRECTION RELATIVE
C                   TO STATIONARY COORDINATES, DIMENSIONLESS.
C        VA(J,K)    VELOCITY OF GAS A IN AXIAL DIRECTION RELATIVE
C                   TO STATIONARY COORDINATES, DIMENSIONLESS.
C
C     OTHER VARIABLES --
C
C     DR            RADIAL NODE SPACING, DIMENSIONLESS.
C     DZ            AXIAL NODE SPACING, DIMENSIONLESS.
C     MA            MOLECULAR WEIGHT OF GAS A, G/G-MOLE.
C     MB            MOLECULAR WEIGHT OF GAS B, G/G-MOLE.
C     NJ            NUMBER OF GRID POINTS, R-DIRECTION.
C     NK            NUMBER OF GRID POINTS, Z-DIRECTION.
C     PE            MASS PECLET NUMBER (2*R*VINF/DAB).
C     RAD           INSIDE RADIUS OF DIFFUSION TUBE, DIMENSIONLESS.
C     VINF          AVERAGE VELOCITY, CM/SEC, OF GAS A FAR UPSTREAM OF
C                   THE GAS B INJECTION PLANE.
C
      DIMENSION     U(14,63),V(14,63),UA(14,63),VA(14,63),XA(14,63)
      DIMENSION     DMV(14,63),DXVA(14,63),M(14,63)
    1 FORMAT(5I5)
    2 FORMAT(7F10.4)
    3 FORMAT(11F6.0)
      REAL M,MA,MB
      READ(10,1) NJ,NK
      WRITE(61,1)NJ,NK
      READ(10,2) DR,DZ,MA,MB,PE,RAD,VINF
      WRITE(61,2)DR,DZ,MA,MB,PE,RAD,VINF
      J1          = NJ-1
      J2          = NJ-2
      K1          = NK-1
      K2          = NK-2
      K3          = NK-3
      READ(10,3)((XA(J,K),J=2,J1),K=2,K1)
      WRITE(61,3)XA(J1,K1)
C     SET XA(J,K) FOR GRID POINTS OUTSIDE PHYSICAL BOUNDARIES
      DO 5      J = 2,J1
      XA(J,1)     = XA(J,3)
      XA(J,NK)    = XA(J,K2)
```

```
    5  CONTINUE
       DO 8      K = 1,NK
       XA(1,K)     = XA(3,K)
       XA(NJ,K)    = XA(J2,K)
    8  CONTINUE
       READ(10,3) ((V(J,K),J=2,J1),K=2,K1)
       WRITE(61,3)V(J1,K1)
C      INCORPORATE MINUS SIGN TO REFLECT DIRECTION OF FLOW
C      W/R TO AXIAL COORDINATE.
       DO 10     J = 2,J1
       DO 10     K = 2,K1
       V(J,K)      = -V(J,K)
   10  CONTINUE
C      COMPUTE MOLECULAR WEIGHT OF GAS MIXTURE.
       DO 20     J = 2,J1
       DO 20     K = 2,K1
       M(J,K)      = XA(J,K)*(MA-MB)+MB
   20  CONTINUE
C      COMPUTE DMV(J,K), USING FIVE-POINT FORMULAS
       DO 30     J = 2,J1
       DMV(J,2)    = (-54.*M(J,2)*V(J,2)+13.*M(J,3)*V(J,3)+40.*M(J,4)
      1              *V(J,4)+27.*M(J,5)*V(J,5)-26.*M(J,6)*V(J,6))/(70.*DZ)
       DMV(J,3)    = (-34.*M(J,2)*V(J,2)+3.*M(J,3)*V(J,3)+20.*M(J,4)
      1              *V(J,4)+17.*M(J,5)*V(J,5)-6.*M(J,6)*V(J,6))/(70.*DZ)
       DMV(J,K2)   = (34.*M(J,K1)*V(J,K1)-3.*M(J,K2)*V(J,K2)
      1              -20.*M(J,K3)*V(J,K3)-17.*M(J,NK-4)*V(J,NK-4)
      2              +6.*M(J,NK-5)*V(J,NK-5))/(70.*DZ)
       DMV(J,K1)   = 0.
       DO 30     K = 4,K3
       DMV(J,K)    = (-2.*M(J,K-2)*V(J,K-2)-M(J,K-1)*V(J,K-1)+M(J,K+1)
      1              *V(J,K+1)+2.*M(J,K+2)*V(J,K+2))/(10.*DZ)
   30  CONTINUE
C      COMPUTE RADIAL COMPONENTS OF MASS AVERAGE VELOCITY FIELD, USING
C      TRAPEZOID RULE.
       DO 40     K = 2,K1
       U(2,K)      = 0.
       U(3,K)      = -(DR/2.)*DR*DMV(3,K)/(DR*M(3,K))
   40  CONTINUE
       DO 50     J = 4,J1
       RJ            = J
       SUM           = 0.
       N             = J-1
       DO 45     L = 3,N
       RL            = L
       SUM           = SUM+(RL-2.)*DR*DMV(L,K)
   45  CONTINUE
       DO 50     K = 2,K1
       U(J,K)      = -(DR/2.)*(2.*SUM+(RJ-2.)*DR*DMV(J,K))/((RJ-2.)
      1              *DR*M(J,K))
   50  CONTINUE
C      COMPUTE AXIAL COMPONENTS OF VELOCITY FIELD FOR GAS A.
       DO 60     J = 2,J1
       VA(J,2)     = V(J,2)-(2.*ME/(XA(J,2)*M(J,2)*PE))
      1              *(-54.*XA(J,2)+13.*XA(J,3)+40.*XA(J,4)
      2              +27.*XA(J,5)-26.*XA(J,6))/(70.*DZ)
       VA(J,3)     = V(J,3)-(2.*ME/(XA(J,3)*M(J,3)*PE))
```

```
     1              *(-34.*XA(J,2)+3.*XA(J,3)+20.*XA(J,4)
     2              +17.*XA(J,5)-6.*XA(J,6))/(70.*DZ)
      VA(J,K2)    = V(J,K2)-(2.*MB/(XA(J,K2)*M(J,K2)*PE))
     1              *(34.*XA(J,K1)-3.*XA(J,K2)-20.*XA(J,K3)
     2              -17.*XA(J,NK-4)+6.*XA(J,NK-5))/(70.*DZ)
      VA(J,K1)    = V(J,K1)
      DO 60     K = 4,K3
      VA(J,K)     = V(J,K)-(2.*MB/(XA(J,K)*M(J,K)*PE))
     1              *(-2.*XA(J,K-2)-XA(J,K-1)+XA(J,K+1)+2.*XA(J,K+2))
     2              /(10.*DZ)
   60 CONTINUE
C     COMPUTE DXVA(J,K), USING FIVE-POINT FORMULAS
      DO 65     J = 2,J1
      DXVA(J,2)   = (-54.*XA(J,2)*VA(J,2)+13.*XA(J,3)*VA(J,3)
     1              +40.*XA(J,4)*VA(J,4)+27.*XA(J,5)*VA(J,5)
     2              -26.*XA(J,6)*VA(J,6))/(70.*DZ)
      DXVA(J,3)   = (-34.*XA(J,2)*VA(J,2)+3.*XA(J,3)*VA(J,3)
     1              +20.*XA(J,4)*VA(J,4)+17.*XA(J,5)*VA(J,5)
     2              -6.*XA(J,6)*VA(J,6))/(70.*DZ)
      DXVA(J,K2)  = (34.*XA(J,K1)*VA(J,K1)-3.*XA(J,K2)*VA(J,K2)
     1              -20.*XA(J,K3)*VA(J,K3)-17.*XA(J,NK-4)*VA(J,NK-4)
     2              +6.*XA(J,NK-5)*VA(J,NK-5))/(70.*DZ)
      DXVA(J,K1)  = 0.
      DO 65     K = 4,K3
      DXVA(J,K)   = (-2.*XA(J,K-2)*VA(J,K-2)-XA(J,K-1)*VA(J,K-1)
     1              +XA(J,K+1)*VA(J,K+1)+2.*XA(J,K+2)*VA(J,K+2))/(10.*DZ)
   65 CONTINUE
C     COMPUTE RADIAL COMPONENTS OF VELOCITY FIELD FOR GAS A, USING
C     TRAPEZOID RULE.
      DO 70     K = 2,K1
      UA(2,K)     = 0.
      UA(3,K)     = -(DR/2.)*DR*DXVA(3,K)/(DR*XA(3,K))
   70 CONTINUE
      DO 80     J = 4,J1
      RJ          = J
      SUM         = 0.
      N           = J-1
      DO 75     L = 3,N
      RL          = L
      SUM         = SUM+(RL-2.)*DR*DXVA(L,K)
   75 CONTINUE
      DO 80     K = 2,K1
      UA(J,K)     = -(DR/2.)*(2.*SUM+(RJ-2.)*DR*DXVA(J,K))/((RJ-2.)
     1              *DR*XA(J,K))
   80 CONTINUE
      WRITE(5) U,V,UA,VA,XA
      STOP
      END
```

```
      PROGRAM ALPHA
C
C     THIS PROGRAM COMPUTES THERMAL DIFFUSION FACTORS BASED ON AN ENERGY
C     BALANCE FOR A CONTROL VOLUME IN A DIFFUSION FIELD OF A BINARY
C     GASEOUS MIXTURE.  ALSO COMPUTED IN THIS PROGRAM ARE MOLECULAR
C     DIFFUSION COEFFICIENTS BASED ON A MASS BALANCE FOR THE CONTROL
C     VOLUME.  THE DIFFUSION FIELD IS SUCH THAT THERE IS NO NET AXIAL
C     FLOW OF GAS B.
C
C     ARRAYS USED IN COMPUTATIONS --
C
C         F(J)      ARRAY OF VALUES OF FUNCTION TO BE INTEGRATED WHEN
C                   CALLING SUBROUTINE SIMP.
C        FR(M)      ARRAY OF VALUES OF FUNCTION TO BE INTEGRATED WHEN
C                   COMPUTING ENERGY TRANSFER BY CONDUCTION ACROSS
C                   CYLINDRICAL SURFACE OF CONTROL VOLUME.
C     LAM(J,K)      THERMAL CONDUCTIVITY OF GAS MIXTURE AT NODE (J,K),
C                   CAL/(CM SEC K).
C       T(J,K)      TEMPERATURE OF GAS MIXTURE AT NODE (J,K), MEASURED
C                   IN MICROVOLTS.
C      TAVG(K)      BULK (MIXING-CUP) TEMPERATURE OF GAS MIXTURE AT
C                   AXIAL NODE K, DEGREES KELVIN.
C       V(J,K)      MASS AVERAGE VELOCITY OF GAS MIXTURE IN AXIAL
C                   DIRECTION AT NODE (J,K), DIMENSIONLESS.
C     XAAVG(K)      BULK (MIXING-CUP) CONCENTRATION OF GAS MIXTURE AT
C                   AXIAL NODE K, DIMENSIONLESS.
C
C     OTHER VARIABLES --
C
C     ACS           CROSS SECTIONAL AREA OF DIFFUSION TUBE, CM**2.
C     ALPH          THERMAL DIFFUSION FACTOR, DIMENSIONLESS.
C     CPA           SPECIFIC HEAT OF GAS A, CAL/(G K).
C     DAB           MOLECULAR DIFFUSION COEFFICIENT, CM**2/SEC.
C     DXI           RADIAL NODE SPACING, DIMENSIONLESS.
C     DZETA         AXIAL NODE SPACING, DIMENSIONLESS.
C     JMAX          NUMBER OF NODES IN RADIAL DIRECTION.
C     KASE          IDENTIFICATION NUMBER FOR DATA INPUT TO PROGRAM.
C     KEND          AXIAL NODE UPSTREAM OF INJECTORS WHERE SOLUTION
C                   FOR ALPHA ENDS.
C     KOUNT         VARIABLE USED TO DETERMINE INCREMENT IN AXIAL
C                   DIRECTION OVER WHICH INTEGRATION IS TO BE PERFORMED.
C     KSTRT         AXIAL NODE UPSTREAM OF INJECTORS WHERE SOLUTION
C                   FOR ALPHA BEGINS.
C     LAMA          THERMAL CONDUCTIVITY OF GAS A, CAL/(CM SEC K).
C     LAMB          THERMAL CONDUCTIVITY OF GAS B, CAL/(CM SEC K).
C     MA            MOLECULAR WEIGHT OF GAS A, G/G-MOLE.
C     MB            MOLECULAR WEIGHT OF GAS B, G/G-MOLE.
C     MDOTA         MASS FLOW RATE OF GAS A, G/SEC.
C     MUA           VISCOSITY OF GAS A, G/(CM SEC).
C     MUB           VISCOSITY OF GAS B, G/(CM SEC).
C     NJ            NUMBER OF GRID POINTS, RADIAL DIRECTION.
C     NK            NUMBER OF GRID POINTS, AXIAL DIRECTION.
C     NRUN          SIGNAL TO INDICATE WHETHER OR NOT DATA FOR
C                   ADDITIONAL CASES FOLLOWS THE DATA TO BE ENTERED.
C     NSUB          SIGNAL TO INDICATE WHETHER OR NOT DATA TO BE
C                   ENTERED IS FOR A SUBCASE OF THE CASE JUST RUN.
```

```
C     NTTY          SIGNAL TO INDICATE IF SELECTED INFORMATION IS TO BE
C                   PRINTED ON TELETYPE (0 - NO, 1 - YES).
C     P             PRESSURE IN DIFFUSION TUBE, ATM.
C     PE            MASS PECLET NUMBER, (2*RAD*VINF/DAB).
C     QA            VOLUME FLOW RATE OF GAS A AT ENTRANCE TO
C                   DIFFUSION TUBE, CC/SEC.
C     RAD           INSIDE RADIUS OF DIFFUSION TUBE, CM.
C     RBAR          UNIVERSAL GAS CONSTANT.  UNITS ARE AS FOLLOWS:
C                      FOR COMPUTING ALPH - CAL/(G-MOLE K).
C                      FOR COMPUTING DAB - (ATM CC)/(G-MOLE K).
C     RHOA          DENSITY OF GAS A AT ENTRANCE TO DIFFUSION TUBE, G/CC.
C     TKREF         REFERENCE TEMPERATURE OF GASES ENTERING
C                   DIFFUSION TUBE, DEGREES K.
C     VAVG          AVERAGE VALUE OF V(I,K) OVER CROSS SECTION OF
C                   DIFFUSION TUBE AT AXIAL LOCATION K, DIMENSIONLESS.
C     XAO           MOLE FRACTION OF GAS A AT GAS B INJECTION PLANE.
C
      COMMON        DXI,DZETA,F(14),JMAX
      DIMENSION     FR(83),LAM(14,83),T(14,83),TAVG(83),V(14,83)
      DIMENSION     XA(14,83),XAAVG(83)
      REAL          LAM,LAMA,LAME,MA,MB,MDOTA,MUA,MUB
    1 FORMAT(10I5)
    2 FORMAT(6E12.5)
    3 FORMAT(11F6.3)
    4 FORMAT(11F7.0)
    5 FORMAT(*S*,
     1/*1*,13X,*OUTPUT FOR CASE NUMBER  - - - - - - - - - - -*,I5,
     2/* *,13X,*MASS PECLET NUMBER  - - - - - - - - - - - - -*,F7.1,
     3/* *,13X,*MOLE FRACTION OF N2 AT HE INJECTION PLANE - -*,F7.1)
    6 FORMAT(*-*,25X,*UPSTREAM*,3X,*CYLINDRICAL*,40X,*TEMP. AT AXIAL*,
     1/26X,*SURFACE*,6X,*SURFACE*,7X,*- - - - DOWNSTREAM SURFACE - - -*,
     26X,*POSITION K,*,3X*MOLE FRAC.*,5X,*THERMAL*,/26X,*CAL/SEC*,6X,
     3*CAL/SEC*,19X,*CAL/SEC*,17X,*DEGREES K*,6X,*NITROGEN*,5X,
     4*DIFF. FAC.*,/*0*,10X,*AXIAL NODE*,6X,*CONVA*,8X,*CONDR*,8X,
     5*CONDB*,8X,*CONVB*,8X,*DIFFS*,8X,*TAVG*,9X,*XA-AVG*,7X,*ALPHA-T*,
     6//)
    7 FORMAT(* *,12X,*K = *,I2,3X,6(E13.4),E13.3,E13.2)
    8 FORMAT(*0 K = *,I2,3X,*XA-AVG = *,E13.4,4X,*ALPHA-T = *,E13.4)
    9 FORMAT(*1*,13X,*MOLECULAR DIFFUSION COEFFICIENTS*,
     1/*-*,13X,*AXIAL NODE*,7X,*TAVG*,11X,*CXZ*,10X,*XA-AVG*,9X,
     2*DAB,DT*,6X,*DAB, 1 ATM*,/* *,28),*DEGREES K*,35X,*M**2/SEC*,
     36X,*M**2/SEC*//)
   10 FORMAT(* *,15X,*K = *,I2,3X,2(E14.4),E14.3,2(E14.2))
   11 FORMAT(*1*,17X,*CONSTANTS ENTERED FROM HEADER FILE*,
     1/*-*,17X,*KEND*,5X,*KSTRT*,7X,*NK*,7X,*NTTY*,
     2/*0*,10X,4(I10),
     3/*0*,16X,*CPA*,10X,*LAMA*,10X,*LAME*,11X,*MA*,12X,*MB*,11X,*RHOA*,
     4/*0*,10X,6(E14.5),
     5/*0*,16X,*MUA*,11X,*MUB*,11X,*P*,13X,*PE*,12X,*QA*,12X,*XAO*,
     6/*0*,10X,6(E14.5))
   12 FORMAT(*1*,13X,*MOLE FRACTIONS OF GAS A IN FLOW FIELD*//)
   13 FORMAT(* *,9X,11(F8.3))
   14 FORMAT(*1*,13X,*MASS AVERAGE AXIAL VELOCITIES*//)
   15 FORMAT(*1*,13X,*TEMPERATURE ARRAY USED IN PROGRAM,*,
     1* IN MICROVOLTS*//)
   16 FORMAT(* *,9X,11(F9.1))
```

```
   17  FORMAT(≠1≠,13X,≠ARRAY OF THERMAL CONDUCTIVITIES COMPUTED IN ≠,
      1≠PROGRAM, CAL/(CM-SEC-K)≠///)
   18  FORMAT(≠ ≠,6X,11(E11.3))
       READ(40,1)    NRUN
   19  READ(40,1)    KASE,KENC,KSTRT,NK,NTTY
       READ(40,2)    CPA,LAMA,LAME,MA,MB,RHOA
       READ(40,2)    MUA,MUB,F,FE,QA,XAO
       NJ          = 11
       JMAX        = 11
       READ(40,3)    ((XA(J,K),J=1,NJ),K=1,NK)
       READ(40,3)    ((V(J,K),J=1,NJ),K=1,NK)
   20  READ(40,4)    ((T(J,K),J=1,JMAX),K=1,KSTRT)
       WRITE(61,1)   KASE,KENC,KSTRT,NK,NTTY
       WRITE(61,2)   CPA,LAMA,LAME,MA,MB,RHOA
       WRITE(61,2)   MUA,MUB,F,FE,QA,XAO
C      CHANGE SIGN OF TEMPERATURE READINGS TO AGREE WITH REFERENCE
C      SYSTEM FOR THIS PROGRAM
       DO 21     J = 1,JMAX
       DO 21     K = 1,KSTRT
       T(J,K)      = -T(J,K)
       IF(T(J,K).EQ.-0.) T(J,K) = 0.
   21  CONTINUE
C      INCORPORATE CONSTANTS, AND SET INITIAL VALUES FOR VARIABLES USED
C      LATER IN PROGRAM
       PI          = 3.1415927
       RAD         = 0.96
       ACS         = PI*RAD*RAD
       DXI         = 0.1
       DZETA       = 0.1
       KOUNT       = 0
       MDOTA       = QA*RHOA
       RBAR        = 1.98717
       TKREF       = 294.26
C      PRINT HEADINGS FOR OUTPUT
       WRITE(41,5)   KASE,FE,XAO
       WRITE(41,6)
C      CALCULATE THERMAL CONDUCTIVITIES LAM(J,K)
       PHIAB       = 1.065*(1.+SQRT(MUA/MUB)*SQRT(SQRT(MB/MA)))**2
      1              /(SQRT(8.)*SQRT(1.+MA/MB))
       PHIBA       = 1.065*(1.+SQRT(MUB/MUA)*SQRT(SQRT(MA/MB)))**2
      1              /(SQRT(8.)*SQRT(1.+MB/MA))
       DO 22     J = 1,NJ
       DO 22     K = 1,NK
       TEMP        = XA(J,K)
       LAM(J,K)    = (TEMP*LAMA)/(TEMP+(1.-TEMP)*PHIAB)+((1.-TEMP)*LAMB)
      1              /((1.-TEMP)+TEMP*PHIBA)
   22  CONTINUE
C      COMPUTE AVERAGE VALUES OF XA AND T OVER CROSS SECTION AT EACH
C      AXIAL LOCATION K, WEIGHTED ACCORDING TO VELOCITY PROFILE
       DO 35     K = 1,NK
C      COMPUTE AVERAGE VELOCITY OVER CROSS SECTION
       DO 23     J = 1,JMAX
       RINT        = J-1
       XI          = RINT*DXI
       F(J)        = V(J,K)*XI
   23  CONTINUE
```

```
      CALL SIMP(ZINTG)
      VAVG      = 2.*ZINTG
C     COMPUTE AVERAGE VALUE OF XA
      DO 28     J = 1,JMAX
      RINT        = J-1
      XI          = RINT*DXI
      F(J)        = V(J,K)*XA(J,K)*XI
   28 CONTINUE
      CALL SIMP(ZINTG)
      XAAVG(K)    = 2.*ZINTG/VAVG
C     COMPUTE TAVG IN TERMS OF MICROVOLTS
      IF(K-KSTRT) 32,32,30
   30 TAVG(K)     = TKREF
      GO TO 35
   32 DO 33     J = 1,JMAX
      RINT        = J-1
      XI          = RINT*DXI
      F(J)        = V(J,K)*T(J,K)*XI
   33 CONTINUE
      CALL SIMP(ZINTG)
      TVOLT       = 2.*ZINTG/VAVG
C     CONVERT TO TAVG IN TERMS OF DEGREES KELVIN.  NOTE - REGRESSION OF
C     CALIBRATION DATA FOR THERMOCOUPLE PROBES YIELDED THE FOLLOWING
C     EQUATION -- (T-TREF),C = 0.019672+0.019330*(V,MICROVOLTS)
      TAVG(K)     = 0.019672+0.019330*TVOLT+TKREF
      IF(TAVG(K).GT.TKREF.AND.K.GT.5) TAVG(K) = TKREF
   35 CONTINUE
C     COMPUTE ENERGY TRANSFER ACROSS UPSTREAM SURFACE OF CONTROL VOLUME
      CONVA       = RHOTA*CPA*TKREF
C     COMPUTE ENERGY TRANSFER BY CONDUCTION ACROSS CYLINDRICAL SURFACE
C     OF CONTROL VOLUME
      CONDR       = 0.
      KSTOP       = KEND+2
   38 KOUNT       = KOUNT+1
      ML          = 2*KOUNT-1
      MM          = ML+1
      MU          = ML+2
      J           = JMAX
      DO 40     M = ML,MU
      K           = KSTRT+1-M
      DTR         = (0.019330/(70.*DXI))*(54.*T(J,K)-13.*T(J-1,K)
     1              -40.*T(J-2,K)-27.*T(J-3,K)+26.*T(J-4,K))
      FR(M)       = -LAM(J,K)*DTR
   40 CONTINUE
C     PERFORM INTEGRATION OVER CYLINDRICAL SURFACE OF CONTROL VOLUME
C     USING SIMPSONS RULE
C     INTEGRAL FR(X)DX = (H/3.)*(FR(ML)+4.*FR(MM)+FR(MU))
      RINTG       = (DZETA/3.)*(FR(ML)+4.*FR(MM)+FR(MU))
C     USE RESULT OF INTEGRATION TO COMPUTE ENERGY TRANSFER BY CONDUCTION
      COND        = 2.*PI*RAD*RINTG
      CONDR       = COND+CONDR
C     COMPUTE ENERGY TRANSFER ACROSS DOWNSTREAM SURFACE OF CONTROL VOLUME
      K           = KSTRT+1-MU
C     ENERGY TRANSFER BY CONDUCTION ACROSS DOWNSTREAM SURFACE OF
C     CONTROL VOLUME
      DO 50     J = 1,JMAX
```

```
      RINT        = J-1
      XI          = RINT*DXI
C     COMPUTE TEMPERATURE GRADIENT USING A FIVE-POINT FORMULA
      IF(K.LT.3) GO TO 45
      DTZ         = (0.019330/(10.*DZETA))*(-2.*T(J,K+2)-T(J,K+1)
     1              +T(J,K-1)+2.*T(J,K-2))
      GO TO 48
   45 IF(K.LT.2) GO TO 46
      DTZ         = (0.019330/(70.*DZETA))*(6.*T(J,K+3)-17.*T(J,K+2)
     1              -20.*T(J,K+1)-3.*T(J,K)+34.*T(J,K-1))
      GO TO 48
   46 DTZ         = (0.019330/(70.*DZETA))*(54.*T(J,K)-13.*T(J,K+1)
     1              -40.*T(J,K+2)-27.*T(J,K+3)+26.*T(J,K+4))
   48 F(J)        = -LAM(J,K)*DTZ*XI
   50 CONTINUE
      CALL SIMP(ZINTG)
C     USE RESULT OF INTEGRATION TO COMPUTE ENERGY TRANSFER BY CONDUCTION
      CONDB       = 2.*PI*RAD*ZINTG
C     ENERGY TRANSFER BY CONVECTION ACROSS DOWNSTREAM SURFACE
      CONVB       = MDOTA*CPA*TAVG(K)
C     ENERGY TRANSFER BY DIFFUSION-THERMC ACROSS DOWNSTREAM SURFACE
      COEFB       = (MDOTA*REAR*TAVG(K)*(1.-XAAVG(K)))/MA
C     COMPUTE THERMAL DIFFUSION FACTOR BASED ON ENERGY BALANCE FOR
C     CONTROL VOLUME
      ALPH        = (CONVA-CONDR-(CONDB+CONVB))/COEFB
      IF(ALPH.EQ.2.OR.ALPH.LT.0.) ALPH = 0.
      DIFFB       = ALPH*COEFB
C     PRINT RESULTS
      WRITE(41,7)  K,CONVA,CONDR,CONDB,CONVB,DIFFB,TAVG(K),
     1             XAAVG(K),ALPH
      IF(NTTY.EQ.0) GO TO 60
      IF(MOD(KOUNT,2).NE.0) GO TO 60
      WRITE(61,8)  K,XAAVG(K),ALPH
   60 IF(K-KSTOP) 65,38,38
C
C     COMPUTE MOLECULAR DIFFUSION COEFFICIENT AT EACH AXIAL NODE IN THE
C     DIFFUSION FIELD
   65 MEND        = KSTRT
      WRITE(41,9)
      RBAR        = 82.0559
C     COMPUTE DAB
      DO 100   M = 1,MEND
      K           = KSTRT+1-M
C     COMPUTE AXIAL CONCENTRATION GRADIENT FOR GAS A USING A
C     FIVE-POINT FORMULA
      IF(K.LT.3)    GO TO 85
      DXZ         = (1./(10.*DZETA))*(-2.*XAAVG(K+2)-XAAVG(K+1)
     1              +XAAVG(K-1)+2.*XAAVG(K-2))
      GO TO 90
   85 IF(K.LT.2)    GO TO 87
      DXZ         = (1./(70.*DZETA))*(6.*XAAVG(K+3)-17.*XAAVG(K+2)
     1              -20.*XAAVG(K+1)-3.*XAAVG(K)+34.*XAAVG(K-1))
      GO TO 90
   87 DXZ         = (1./(70.*DZETA))*(54.*XAAVG(K)-13.*XAAVG(K+1)
     1              -40.*XAAVG(K+2)-27.*XAAVG(K+3)+26.*XAAVG(K+4))
C     COMPUTE DAB FOR CONDITIONS ESTABLISHED IN DIFFUSION TUBE,
```

```
C     IN METERS SQUARED PER SECCND
  90  DAB         = -((MOOTA*REAR*RAD*TAVG(K)*(1.-XAAVG(K)))
     1              /(P*ACS*PA*CXZ))*.0001
      IF(DXZ.EQ.0.OR.DAB.LT.0.) DAB = 0.
C     CORRECT DAB TO ATMOSPHERIC PRESSURE, USING FACTOR
C     (86 CM HG)/(76 CM HG)
      DABC        = 86.*DAB/76.
C     PRINT RESULTS
      WRITE(41,10) K,TAVG(K),CXZ,XAAVG(K),DAB,DABC
 100  CONTINUE
      WRITE(41,11) KEND,KSTRT,NK,NTTY,CPA,LAMA,LAMB,MA,MB,RHOA,
     1             MUA,MUB,P,PE,GA,XAG
      WRITE(41,12)
      WRITE(41,13) ((XA(J,K),J=1,NJ),K=1,NK)
      WRITE(41,14)
      WRITE(41,13) ((V(J,K),J=1,NJ),K=1,NK)
      WRITE(41,15)
      WRITE(41,16) ((T(J,K),J=1,JMAX),K=1,KSTRT)
      WRITE(41,17)
      WRITE(41,18) ((LAM(J,K),J=1,NJ),K=1,NK)
      IF(NRUN.EQ.0) GO TO 110
      READ(40,1)   NRUN,NSUB
      IF(NSUB) 19,19,102
 102  READ(40,1) KASE
      GO TO 20
 110  STOP
      END
C
      SUBROUTINE SIMP(ZINTG)
C     PERFORMS INTEGRATIONS USING SIMPSONS RULE FOR GIVEN SETS OF
C     INPUT DATA
C     INTEGRAL F(X)DX = (H/3.)*(F(A)+4F(A+1)+2F(A+2)+...+4F(A+N-1)+F(B))
      COMMON        DXI,DZETA,F(14),JMAX
      SUM1        = F(1)+F(JMAX)
C     COMPUTE 4.*(F(A+1)+F(A+3)+...+F(A+N-1))
      J1          = JMAX-1
      SUM4        = 0.
      DO 20     J = 2,J1,2
      SUM4        = SUM4+F(J)
  20  CONTINUE
      SUM4        = 4.*SUM4
C     COMPUTE 2.*(F(A+2)+F(A+4)+...+F(A+N-2))
      J2          = JMAX-2
      SUM2        = 0
      DO 25     J = 3,J2,2
      SUM2        = SUM2+F(J)
  25  CONTINUE
      SUM2        = 2.*SUM2
C     COMBINE ABOVE RESULTS TO OBTAIN VALUE OF INTEGRAL
      ZINTG       = (DXI/3.)*(SUM1+SUM2+SUM4)
      RETURN
      END
C
      FUNCTION MOD(N,M)
C     RETURNS ZERO WHENEVER N IS EVENLY DIVISIBLE BY M
      MOD         = N-(N/M)*M
```

```
      RETURN
      END
```

```
      PROGRAM RADTEMP
C     USING AS INPUT EXPERIMENTAL DATA FOR THE AXIAL TEMPERATURE PROFILE
C     ON THE DIFFUSION TUBE CENTERLINE TOGETHER WITH DATA FOR RADIAL
C     TEMPERATURE PROFILES, THIS PROGRAM PREDICTS TEMPERATURES BY
C     INTERPOLATION AT GRID POINTS WHERE EXPERIMENTAL MEASUREMENTS
C     WERE NOT TAKEN.
C
C     ARRAYS USED IN COMPUTATIONS --
C
C      T(J,K)       ARRAY OF TEMPERATURES IN FLOW FIELD.  T(1,K) VALUES
C                   ARE THOSE MEASURED ON DIFFUSION TUBE CENTERLINE.
C     TR(J,L)       RADIAL TEMPERATURES BASED ON EXPERIMENTAL DATA.
C
C     OTHER VARIABLES --
C
C     JMAX          NUMBER OF NODES IN RADIAL DIRECTION.
C     KASE          IDENTIFICATION NUMBER FOR INPUT DATA.
C     KFILE         SIGNAL TO INDICATE WHETHER OR NOT RESULTS ARE TO BE
C                   STORED IN A FILE.
C                       KFILE = 0 -- NO FILE.
C                       KFILE = 1 -- STORE ON FILE EQUIPPED TO LUN 43.
C     KMAX          VALUE OF K UPSTREAM OF THE HELIUM INJECTION PLANE
C                   AT WHICH MEASURED TEMPERATURE FIELD ENDS.
C     KPUN          SIGNAL TO INDICATE WHETHER OR NOT RESULTS ARE TO BE
C                   PUNCHED ON CARDS.
C                       KPUN = 0 -- NO CARDS.
C                       KPUN = 1 -- PUNCH CARDS (EQUIP LUN 42 TO PUNCH).
C     LMAX          INDICATES NUMBER OF EXPERIMENTALLY DETERMINED RADIAL
C                   TEMPERATURE PROFILES AVAILABLE FOR INTERPOLATION.
C     PE            MASS PECLET NUMBER FOR FLOW IN DIFFUSION TUBE.
C     TREF          TEMPERATURE OF GASES ENTERING DIFFUSION TUBE.
C     XAO           MOLE FRACTION OF NITROGEN AT HELIUM INJECTION PLANE.
C
      DIMENSION     NOR(14),T(14,83),TEMP(14,83),TR(14,83)
    1 FORMAT(5I5)
    2 FORMAT(11F7.1)
    3 FORMAT(*1*,13X,*OUTPUT FOR CASE NUMBER  - - - - - - - - - - -*,I5,
     1/* *,13X,*MASS PECLET NUMBER  - - - - - - - - - - - - -*,F7.1,
     2/* *,13X,*MOLE FRACTION OF N2 AT HE INJECTION PLANE - -*,F7.1)
    4 FORMAT(*1*,10X,*TEMPERATURE (T-TREF) IN MICROVOLTS*//)
    5 FORMAT(*1*,10X,*TEMPERATURE (T-TREF) IN DEGREES KELVIN*//)
    6 FORMAT(*1*,10X,*DIMENSIONLESS TEMPERATURE, (T-TREF)/TREF*//)
    7 FORMAT(* *,8X,*J = *,11(I6,5X))
    8 FORMAT(* *,4X,*K = *,I2,2X,11(F8.1,3X))
    9 FORMAT(* *,4X,*K = *,I2,2X,11(F9.5,2X))
   10 FORMAT(* *,4X,*K = *,I2,2X,11(E11.3))
      JMAX        = 11
      READ(40,1)    KASE,KFILE,KMAX,KPUN,LMAX
      READ(40,2)    PE,XAO
      READ(40,2)    ((TR(J,L),J=1,JMAX),L=1,LMAX)
      READ(40,2)    (T(1,K),K=1,KMAX)
      DO 40     K = 1,KMAX
      KNEG        = 0
      IF(T(1,K))    11,35,12
   11 KNEG        = K
      T(1,K)      = -T(1,K)
```

```
C     FIND VALUES OF TR(1,L) TO BE USED WHEN INTERPOLATING TO FIND
C     RADIAL TEMPERATURE PROFILE CORRESPONDING TO T(1,K)
  12  DO 18     L = 1,LMAX
      IF(T(1,K)-TR(1,L)) 14,16,18
  14  KOUNT       = L
      GO TO 20
  16  KOUNT       = L
      GO TO 30
  18  CONTINUE
      KOUNT       = LMAX
C     CALCULATIONS FOR RADIAL TEMPERATURE PROFILE WHEN T(1,K) IS NOT
C     EQUAL TO A GIVEN VALUE OF TR(1,L)
  20  LL          = KOUNT-1
      LU          = KOUNT
      RATIO       = (T(1,K)-TR(1,LL))/(TR(1,LU)-TR(1,LL))
      DO 25     J = 2,JMAX
      T(J,K)      = TR(J,LL)+RATIO*(TR(J,LU)-TR(J,LL))
  25  CONTINUE
      GO TO 37
C     RADIAL TEMPERATURE PROFILE WHEN T(1,K) HAS THE SAME VALUE
C     AS TR(1,L)
  30  DO 33     J = 2,JMAX
      L           = KOUNT
      T(J,K)      = TR(J,L)
  33  CONTINUE
      GO TO 37
  35  DO 36     J = 2,JMAX
      T(J,K)    = 0.
  36  CONTINUE
      GO TO 40
  37  IF(KNEG.EQ.0) GO TO 40
      DO 38     J = 1,JMAX
      T(J,KNEG)   = -T(J,KNEG)
  38  CONTINUE
  40  CONTINUE
C     PRINT OUT RESULTS
      WRITE(41,3)   KASE,PE,XAO
      DO 50     J = 1,JMAX
      NOR(J)      = J
  50  CONTINUE
C     PRINT OUT TEMPERATURES IN TERMS OF MICROVOLTS
      WRITE(41,4)
      WRITE(41,7)   (NOR(J),J=1,JMAX)
      DO 70     K = 1,KMAX
      DO 65     J = 1,JMAX
      TEMP(J)     = -T(J,K)
      IF(T(J,K).EQ.0.) TEMP(J) = T(J,K)
  65  CONTINUE
      WRITE(41,8)   K,(TEMP(J),J=1,JMAX)
  70  CONTINUE
C     PRINT OUT TEMPERATURES IN TERMS OF (T-TREF)
      WRITE(41,5)
      WRITE(41,7)   (NOR(J),J=1,JMAX)
      DO 80     K = 1,KMAX
      DO 75     J = 1,JMAX
      TEMP(J)     = 0.019652-0.019330*T(J,K)
```

```
      IF(TEMP(J).GT.0.AND.K.GT.5) TEMP(J) = 0.
   75 CONTINUE
      WRITE(41,9)  K,(TEMP(J),J=1,JMAX)
   80 CONTINUE
C     PRINT OUT TEMPERATURES IN TERMS OF (T-TREF)/TREF
      WRITE(41,6)
      WRITE(41,7)  (NCR(J),J=1,JMAX)
      DO 90    K = 1,KMAX
      DO 85    J = 1,JMAX
      TEMP(J)    = (0.019652-0.019330*T(J,K))/294.26
      IF(TEMP(J).GT.0.AND.K.GT.5) TEMP(J) = 0.
   85 CONTINUE
      WRITE(41,10) K,(TEMP(J),J=1,JMAX)
   90 CONTINUE
C     PRINT OUT TEMPERATURES ON CARDS IN TERMS OF MICROVOLTS,
C     IF KPUN = 1
      IF(KPUN.EQ.0) GO TO 100
      WRITE(42,2)((T(J,K),J=1,JMAX),K=1,KMAX)
C     STORE RESULTS ON A FILE, IF KFILE = 1
  100 IF(KFILE.EQ.0) GO TO 110
      WRITE(43,2)((T(J,K),J=1,JMAX),K=1,KMAX)
  110 STOP
      END
```

Appendix D. COMPUTED VALUES FOR TEMPERATURE DISTRIBUTIONS IN DIFFUSION FLOW FIELDS

NOTES:

1. The data in this appendix are grouped according to the flow conditions for which they were computed. These flow conditions are:

   $Pe = 1.9, X_{A_o} = 0.5$

   $Pe = 3.8, X_{A_o} = 0.5$

   $Pe = 3.8, X_{A_o} = 0.7$

   $Pe = 5.9, X_{A_o} = 0.7$

2. Axial positions are those upstream of and relative to the helium injection plane. Radial positions are those relative to the diffusion tube centerline.

3. The diffusion tube radius, R, is 0.96 cm.

4. The reference temperature, T_o, is the temperature common to the two gases entering the diffusion tube. For the results that follow, $T_o = 294.26^o$ K (21.11^o C).

5. For values computed on the basis of an isothermal wall boundary condition,

$$T_{wall} = T_o.$$

Computed centerline temperature profiles

Flow conditions: Pe = 1.9, X_{A_o} = 0.5

NOTES:

1. $\theta = \frac{T - T_o}{T_o}$; $T - T_o = (T_o)(\theta) = (294.26)(\theta)$.

2. All temperature values listed below are negative in sign.

3. The data listed below are plotted in Figure 4.5.

Axial Position, ζ = z/R	Isothermal Wall		Adiabatic Wall	
	θ	$T - T_o$ °C	θ	$T - T_o$ °C
0	0	0	0	0
0.1	3.608E-03	1.062	6.401E-03	1.884
0.2	7.082	2.084	1.274E-02	3.749
0.3	9.898	2.913	1.804	5.308
0.4	1.189E-02	3.499	2.190	6.444
0.5	1.305	3.840	2.422	7.127
0.6	1.360	4.002	2.514	7.398
0.7	1.332	3.920	2.493	7.336
0.8	1.277	3.758	2.390	7.033
0.9	1.196	3.519	2.234	6.574
1.0	1.109	3.263	2.049	6.029
1.1	1.004	2.954	1.856	5.461
1.2	9.127E-03	2.686	1.670	4.914
1.3	8.316	2.447	1.502	4.420
1.4	7.659	2.241	1.353	3.981
1.5	6.997	2.059	1.220	3.590
1.6	6.424	1.890	1.100	3.237
1.7	5.872	1.728	9.877E-03	2.906
1.8	5.398	1.588	8.866	2.609
1.9	4.838	1.424	7.937	2.336
2.0	4.375	1.287	7.102	2.090
2.1	3.950	1.162	6.355	1.870
2.2	3.573	1.051	5.696	1.676
2.3	3.244	0.955	5.124	1.508
2.4	2.961	0.871	4.627	1.362
2.5	2.711	0.798	4.189	1.233
2.6	2.480	0.730	3.791	1.116
2.7	2.265	0.666	3.428	1.009

Flow Conditions: Pe = 1.9, X_{A_o} = 0.5

Axial Position, $\zeta = z/R$	Isothermal Wall		Adiabatic Wall	
	θ	$T - T_o$ °C	θ	$T - T_o$ °C
2.8	2.067E-03	0.608	3.100E-03	0.912
2.9	1.885	0.555	2.802	0.825
3.0	1.718	0.506	2.531	0.745
3.1	1.566	0.461	2.287	0.673
3.2	1.429	0.420	2.068	0.609
3.3	1.307	0.385	1.873	0.551
3.4	1.197	0.352	1.698	0.500
3.5	1.096	0.323	1.538	0.453
3.6	1.002	0.295	1.392	0.410
3.7	9.150E-04	0.269	1.259	0.370
3.8	8.348	0.246	1.137	0.335
3.9	7.628	0.224	1.027	0.302
4.0	6.971	0.205	9.273E-04	0.273
4.1	6.326	0.186	8.322	0.245
4.2	5.701	0.168	7.424	0.218
4.3	5.108	0.150	6.588	0.194
4.4	4.601	0.135	5.867	0.173
4.5	4.191	0.123	5.267	0.155
4.6	3.821	0.112	4.732	0.139
4.7	3.454	0.102	4.219	0.124
4.8	3.096	0.091	3.735	0.110
4.9	2.765	0.081	3.293	0.097
5.0	2.484	0.073	2.917	0.086
5.1			2.570	0.076
5.2			2.235	0.066
5.3			1.915	0.056
5.4			1.617	0.048
5.5			1.373	0.040
5.6			1.136	0.033
5.7			9.295E-05	0.027

Computed centerline temperature profiles

Flow conditions: Pe = 3.8, X_{A_o} = 0.5

NOTES:

1. $\theta = \frac{T - T_o}{T_o}$; $T - T_o = (T_o)(\theta) = (294.26)(\theta)$.

2. All temperature values listed below are negative in sign.

3. The data listed below are plotted in Figure 4.6.

Axial Position, ζ = z/R	Isothermal Wall		Adiabatic Wall	
	θ	$T - T_o$ °C	θ	$T - T_o$ °C
0	0	0	0	0
0.1	7.369E-03	2.168	8.489E-03	2.498
0.2	1.381E-02	4.064	1.594E-02	4.690
0.3	1.778	5.232	2.050	6.032
0.4	1.902	5.597	2.186	6.433
0.5	1.813	5.335	2.071	6.094
0.6	1.596	4.696	1.808	5.320
0.7	1.331	3.917	1.494	4.396
0.8	1.076	3.166	1.197	3.522
0.9	8.581E-03	2.525	9.462E-03	2.784
1.0	6.811	2.004	7.455	2.194
1.1	5.411	1.592	5.889	1.733
1.2	4.347	1.279	4.709	1.386
1.3	3.564	1.049	3.843	1.131
1.4	2.968	0.873	3.185	0.937
1.5	2.474	0.728	2.646	0.779
1.6	2.041	0.601	2.177	0.641
1.7	1.663	0.489	1.772	0.521
1.8	1.356	0.399	1.442	0.424
1.9	1.114	0.328	1.184	0.348
2.0	9.240E-04	0.272	9.803E-04	0.288
2.1	7.688	0.226	8.144	0.240
2.2	6.431	0.189	6.801	0.200
2.3	5.352	0.157	5.652	0.166
2.4	4.445	0.131	4.688	0.138
2.5	3.675	0.108	3.872	0.114
2.6	3.024	0.089	3.184	0.094
2.7	2.508	0.074	2.637	0.078
2.8	2.102	0.062	2.206	0.065

Flow conditions: Pe = 3.8, X_{A_o} = 0.5

Axial Position, ζ = z/R	Isothermal Wall		Adiabatic Wall	
	θ	$T - T_o$ °C	θ	$T - T_o$ °C
2.9	1.762E-04	0.052	1.845E-04	0.064
3.0	1.492	0.044	1.558	0.046
3.1	1.279	0.038	1.331	0.039
3.2	1.072	0.032	1.112	0.033
3.3	8.951E-05	0.026	9.259E-05	0.027
3.4	7.510	0.022		

Computed centerline temperature profiles

Flow conditions: Pe = 3.8, X_{A_o} = 0.7

NOTES:

1. $\theta = \frac{T - T_o}{T_o}$; $T - T_o = (T_o)(\theta) = (294.26)(\theta)$.

2. All temperature values listed below are negative in sign.

3. The data listed below are plotted in Figure 4.7.

Axial Position, ζ = z/R	Isothermal Wall		Adiabatic Wall	
	θ	$T - T_o$ °C	θ	$T - T_o$ °C
0	0	0	0	0
0.1	5.116E-03	1.505	5.733E-03	1.687
0.2	8.718	2.565	9.797	2.883
0.3	1.030E-02	3.031	1.158E-02	3.408
0.4	1.027	3.022	1.152	3.390
0.5	9.294E-03	2.735	1.037	3.051
0.6	7.942	2.337	8.800E-03	2.589
0.7	6.572	1.934	7.229	2.148
0.8	5.347	1.573	5.842	1.719
0.9	4.316	1.270	4.689	1.380
1.0	3.493	1.028	3.778	1.112
1.1	2.845	0.837	3.064	0.902
1.2	2.340	0.689	2.511	0.739
1.3	1.938	0.570	2.074	0.610
1.4	1.605	0.472	1.712	0.504
1.5	1.321	0.389	1.407	0.414
1.6	1.084	0.319	1.153	0.339
1.7	8.998E-04	0.265	9.545E-04	0.281
1.8	7.622	0.224	8.063	0.237
1.9	6.516	0.192	6.871	0.202
2.0	5.483	0.161	5.769	0.170
2.1	4.501	0.132	4.731	0.139
2.2	3.720	0.109	3.906	0.115
2.3	3.087	0.091	3.237	0.095
2.4	2.569	0.076	2.690	0.079
2.5	2.143	0.063	2.240	0.066
2.6	1.788	0.053	1.865	0.055
2.7	1.501	0.044	1.562	0.046
2.8	1.270	0.037	1.318	0.039

Flow conditions: Pe = 3.8, X_{A_o} = 0.7

Axial Position, ζ = z/R	Isothermal Wall		Adiabatic Wall	
	θ	$T - T_o$ °C	θ	$T - T_o$ °C
2.9	1.041E-04	0.031	1.078E-04	0.032
3.0	8.619E-05	0.025	8.899E-05	0.026

Computed centerline temperature profiles

Flow conditions: Pe = 5.9, X_{A_o} = 0.7

NOTES:

1. $\theta = \frac{T - T_o}{T_o}$; $T - T_o = (T_o)(\theta) = (294.26)(\theta)$.

2. All temperature values listed below are negative in sign.

3. The data listed below are plotted in Figure 4.8.

Axial Position, ζ = z/R	Isothermal Wall		Adiabatic Wall	
	θ	$T - T_o$ °C	θ	$T - T_o$ °C
0	0	0	0	0
0.1	7.120E-03	2.095	7.250E-03	2.133
0.2	1.045E-02	3.075	1.063E-02	3.128
0.3	9.745E-03	2.868	9.892E-03	2.910
0.4	7.266	2.138	7.354	2.164
0.5	4.984	1.467	5.029	1.480
0.6	3.405	1.002	3.427	1.008
0.7	2.377	0.699	2.390	0.703
0.8	1.675	0.493	1.682	0.495
0.9	1.177	0.346	1.181	0.348
1.0	8.107E-04	0.239	8.132E-04	0.239
1.1	5.290	0.156	5.305	0.156
1.2	3.186	0.094	3.196	0.094
1.3	1.700	0.050	1.706	0.050
1.4	9.051E-05	0.027	9.088E-05	0.027
1.5	5.816	0.015		

Computed radial temperature profiles

Flow conditions: Pe = 1.9, X_{A_o} = 0.5

NOTES:

1. $\theta = \frac{T - T_o}{T_o}$; $T - T_o = (T_o)(\theta) = (294.26)(\theta)$.

2. All temperature values listed below are negative in sign.

3. These results are for an isothermal wall boundary condition.

4. The data listed below are plotted in Figure 4.9.

Radial Position $\xi = r/R$	$\zeta = 0.6$		$\zeta = 1.0$	
	θ	$T - T_o$ °C	θ	$T - T_o$ °C
0.0	1.360E-02	4.002	1.109E-02	3.263
0.1	1.375	4.046	1.115	3.281
0.2	1.379	4.058	1.100	3.237
0.3	1.370	4.031	1.067	3.140
0.4	1.344	3.955	1.014	2.984
0.5	1.293	3.805	9.391E-03	2.763
0.6	1.197	3.522	8.366	2.462
0.7	1.040	3.060	6.997	2.059
0.8	7.981E-03	2.348	5.193	1.528
0.9	4.543	1.337	2.851	0.839
1.0	0	0	0	0

Radial Position $\xi = r/R$	$\zeta = 1.4$		$\zeta = 1.8$	
	θ	$T - T_o$ °C	θ	$T - T_o$ °C
0.0	7.659E-03	2.254	5.398E-03	1.588
0.1	7.696	2.265	5.442	1.601
0.2	7.563	2.234	5.365	1.579
0.3	7.292	2.146	5.183	1.525
0.4	6.882	2.025	4.898	1.441
0.5	6.318	1.859	4.503	1.325
0.6	5.576	1.641	3.982	1.172
0.7	4.602	1.354	3.295	0.970
0.8	3.348	0.985	2.407	0.708
0.9	1.786	0.526	1.287	0.379
1.0	0	0	0	0

Appendix E. RESULTS OF CALIBRATIONS OF INSTRUMENTATION

The results summarized in this appendix are for the following instrumentation used in the diffusion apparatus discussed in Chapter V:

1. Nitrogen flowmeter.
2. Concentration detector.
3. Diffusion tube thermocouple circuits.
4. Thermocouples used to monitor temperatures at locations other than in the diffusion tube.

Calibration of Nitrogen Flowmeter

Flowmeter type:

Manufacturer	Schuttle and Koerling
Tube	1/8 - 15 - G - 5
Float	BP 4 black glass

Calibration instrument: bubble flowmeter used in conjunction with a stopwatch

Calibration conditions:

Laboratory temperature: 21° C $\pm$ 0.5° C
Barometric pressure: 75.58 - 75.77 cm Hg
Flowmeter pressure: 10.0 cm Hg gage

The nitrogen flowmeter was calibrated in place at operating pressure and temperature by measuring a total of 127 data points relating flowmeter readings to volume flow rates of nitrogen passing through the meter. A regression equation for the calibration data is as follows:

$$\text{Nitrogen flow rate at } 21^{\circ}\text{ C, 86 cm Hg} = 20.156 - 21.310X + 16.943X^2 - 0.797X^3 \text{ cubic centimeters/minute}$$

where X is the nitrogen flowmeter reading. This equation, which fits the calibration data with a coefficient of determination, R^2, of 0.9997, is applicable over a range of flowmeter readings between 0.9 and 9.3.

Calibration of concentration detector

Principal components: Carle model 1161 Micro-Detector wrapped with a heating tape controlled by a Cole-Palmer model 2158 Versatherm. Detector output is measured with a Hewlett-Packard model 7001AM X-Y recorder.

Calibration conditions:

Laboratory temperature	21° C $\pm$ 0.5° C
Diffusion tube pressure	10 cm Hg gage
Operating temperature of thermal conductivity cell	35° C
Current to cell	20 ma
Gas flow rate	1.0 cc/min

Calibration data

Calibration Gas %N_2	%He	Plotter reading cm	Attenuation	Voltage mv att 100	Corresponding results from Stock (1972)*
100	0	0.0	5	0.00	0.00
75	25	24.3	10	2.43	2.43
50	50	11.1	50	5.55	5.55
25	75	20.3	50	10.15	10.20
0	100	17.3	100	17.30	17.40

*The close agreement between Stock's results and those obtained in the recalibration for this investigation show that the concentration detector has excellent long term repeatability and stability.

Regression equation for data obtained in this recalibration:

$$X_A = 0.98855 - 0.099379V + 0.0024561V^2$$

where

X_A = mole fraction of nitrogen

and V = voltage output at attenuation 100.

This equation fits the calibration data with a coefficient of correlation, R^2, of 0.9988.

Calibration of diffusion tube thermocouple circuits

Thermocouple instrumentation (three sets)

Sensing junction: Subminiature (0.0254 cm O.D.) thermocouple probe, iron-constantan with type 304 stainless steel sheath, manufactured by Omega Engineering, Inc.

Reference junction: ANSI type J, 24 B and S gage, iron-constantan leads

Potentiometer: Leeds and Northrup model 7554, type K-4

Calibration instrument: Hewlett-Packard model 2801A quartz thermometer

Each of the three diffusion tube thermocouple circuits was calibrated using a fixed temperature (21^{o} C) bath for the reference junction and a variable temperature bath for the diffusion tube probe. Two quartz sensors were used, one in the constant temperature bath and the other in the variable temperature bath, and the temperature differences between them were compared with voltage outputs of the thermocouple probes.

The voltage outputs of the three thermocouple circuits exhibited essentially the same variation as a function of temperature. Accordingly, a single regression equation was written for the 133 data points taken for the three circuits. This equation is as follows:

$$(T - T_o), {}^{o}C = 0.019672 + 0.019330V$$

where T is the temperature of the diffusion tube sensing

junction, T_o is the temperature of the reference junction (21° C), and V is the output, in microvolts, of the thermocouple circuit.

The preceding equation, which fits the data with a coefficient of determination, R^2, of 0.9998, is applicable to values of V in the range between +25 and -255 microvolts. (Corresponding values of $T - T_o$ are in the range between approximately $+0.5^\circ$ and -5.0° C.)

Calibration of thermocouple instrumentation used to monitor temperatures in diffusion apparatus

Thermocouple instrumentation: copper-constantan thermocouples; ice-bath reference

Potentiometer: Leeds and Northrup millivolt potentiometer

Calibration instrument: Hewlett-Packard model 2801A quartz thermometer

The thermocouples used for monitoring temperatures in the diffusion apparatus are independent of those used for measuring temperature fields in the diffusion tube. They were calibrated using a variable temperature bath for the "hot" junctions, an ice bath for the reference junctions, and a quartz thermometer. A regression equation for the 122 calibration data points that were measured over the range between 17.5° C and 24.5° C is as follows:

$$T, {}^{\circ}C = 0.4401 + 0.02459V$$

where T is the temperature of the "hot" junction and V is the voltage output, in millivolts, of the thermocouple circuit. The coefficient of determination, R^2, for this equation is 0.9996.

Appendix F. DATA FOR AXIAL AND RADIAL TEMPERATURE PROFILES MEASURED IN DIFFUSION FLOW FIELDS

NOTES:

1. The data in this appendix are grouped according to the flow conditions under which they were measured. These flow conditions are:

   Pe = 1.9, X_{A_o} = 0.5,

   Pe = 3.8, X_{A_o} = 0.5,

   Pe = 3.8, X_{A_o} = 0.7,

   and Pe = 5.9, X_{A_o} = 0.7.

2. Temperatures in flow fields were measured relative to the temperature of nitrogen entering the diffusion tube. Although this temperature, designated as T_o, varied within the range of 21° C $\pm$ 0.5° C from run-to-run, during any given run it was held essentially constant at some value within this range.

3. Temperatures relative to the reference temperature, T_o, are related to output voltages of the diffusion tube thermocouple circuits as follows (regression equation is from Appendix E):

$$(T - T_o)\ °C = 0.019672 + 0.019330(V)$$

where V is in microvolts.

4. Axial positions are those upstream of and relative to the helium injection plane. Radial positions are those relative to the diffusion tube centerline.

5. θ = circumferential position of wall-mounted probe inlet passages.

6. For all measurements, the diffusion tube pressure was 10 cm Hg gage.

7. Diffusion tube radius, R, is 0.96 cm.

8. References to figure numbers indicate where results are plotted in text of this thesis.

Centerline temperature profiles

Flow conditions: Pe = 1.9, X_{A_o} = 0.5

NOTE: All temperature data listed below are negative except those designated by a plus sign.

Axial Position, ζ = z/R	June 11 θ = 0° Voltage, μv	June 11 θ = 0° $T - T_o$, °C	July 6 θ = 0° Voltage, μv	July 6 θ = 0° $T - T_o$, °C	Average $T - T_o$ Fig. 7.1
0.05	+11.6	+0.24	+4.7	+0.11	+0.18
0.1	3.3	0.04	12.4	0.22	0.13
0.2	34.0	0.64	41.7	0.79	0.72
0.3	62.0	1.18	68.6	1.31	1.25
0.4	84.5	1.61	90.0	1.72	1.67
0.5	100.0	1.91	105.6	2.02	1.97
0.6	110.3	2.11	115.0	2.20	2.16
0.7	114.8	2.20	119.9	2.30	2.25
0.8	115.4	2.21	120.1	2.30	2.26
0.9	112.7	2.16	118.1	2.26	2.21
1.0	108.0	2.07	114.0	2.18	2.13
1.1	102.1	1.95	108.1	2.07	2.01
1.2	95.5	1.83	101.6	1.94	1.89
1.3	88.6	1.69	95.1	1.82	1.76
1.4	81.7	1.56	88.5	1.69	1.63
1.5	75.0	1.43	80.2	1.53	1.48
1.6	68.5	1.30	73.3	1.40	1.35
1.7	62.7	1.19	68.0	1.30	1.25
1.8	57.2	1.09	62.1	1.18	1.14
1.9	52.2	0.99	56.6	1.07	1.03
2.0	47.9	0.91	51.8	0.98	0.95
2.1	43.6	0.82	47.9	0.91	0.87
2.2	39.8	0.75	42.8	0.81	0.78
2.3	35.6	0.67	39.2	0.74	0.71
2.4	31.1	0.58	34.6	0.65	0.62
2.5	27.6	0.51	31.7	0.59	0.55
2.6	23.4	0.43	29.1	0.54	0.49
2.7	20.4	0.38	25.5	0.47	0.43
2.8	18.7	0.34	23.5	0.44	0.39
2.9	17.1	0.31	21.4	0.39	0.35
3.0	15.5	0.28	19.7	0.36	0.32
3.1	13.9	0.25	18.8	0.34	0.30
3.2	12.4	0.22	16.8	0.30	0.26
3.3	10.9	0.19	15.0	0.27	0.23

Flow conditions: Pe = 1.9, X_{A_o} = 0.5

Axial Position, ζ = z/R	June 11 θ = 0° Voltage, μv	June 11 θ = 0° $T - T_o$, °C	July 6 θ = 0° Voltage, μv	July 6 θ = 0° $T - T_o$, °C	Average $T - T_o$ Fig. 7.1
3.4	9.4	0.16	13.2	0.24	0.20
3.5	7.4	0.12	11.6	0.20	0.16
3.6	6.2	0.10	10.3	0.18	0.14
3.7	5.5	0.09	9.3	0.16	0.13
3.8	4.9	0.08	8.2	0.14	0.11

The following temperature data are plotted in Figure G.1.

Axial Position, ζ = z/R	July 2 θ = 180° Voltage, μv	July 2 θ = 180° $T - T_o$, °C	Axial Position, ζ = z/R	July 2 cont. Voltage, μv	July 2 cont. $T - T_o$ °C
0.05	+6.0	+0.14	2.1	46.3	0.88
0.1	9.8	0.17	2.2	41.7	0.79
0.2	40.6	0.76	2.3	38.5	0.72
0.3	67.9	1.29	2.4	33.8	0.63
0.4	89.7	1.71	2.5	30.9	0.58
0.5	105.1	2.01	2.6	28.0	0.52
0.6	114.5	2.19	2.7	25.2	0.47
0.7	119.3	2.29	2.8	22.7	0.42
0.8	119.5	2.29	2.9	20.7	0.38
0.9	117.0	2.24	3.0	18.6	0.34
1.0	112.7	2.16	3.1	16.8	0.30
1.1	106.6	2.04	3.2	15.2	0.27
1.2	99.5	1.90	3.3	13.8	0.25
1.3	92.8	1.78	3.4	12.7	0.23
1.4	86.2	1.65	3.5	11.5	0.20
1.5	78.6	1.50	3.6	10.5	0.18
1.6	71.7	1.37	3.7	9.5	0.16
1.7	66.0	1.26	3.8	8.4	0.14
1.8	60.1	1.14			
1.9	55.9	1.06			
2.0	50.9	0.96			

Centerline temperature profiles

Flow conditions: Pe = 3.8, X_{A_o} = 0.5

NOTE: All temperature data listed below are negative.

Axial Position, ζ = z/R	June 7 θ = 0° Voltage, μv	June 7 θ = 0° $T - T_o$, °C	July 6 θ = 0° Voltage, μv	July 6 θ = 0° $T - T_o$ °C	Average $T - T_o$ Fig. 7.2
0.05	67.8	1.29	57.5	1.09	1.19
0.1	88.4	1.69	83.2	1.59	1.64
0.2	141.2	2.71	134.2	2.57	2.64
0.3	182.3	3.50	178.2	3.42	3.46
0.4	203.6	3.92	200.4	3.85	3.89
0.5	207.2	3.99	205.0	3.94	3.96
0.6	196.8	3.78	195.1	3.75	3.76
0.7	178.3	3.43	177.3	3.41	3.42
0.8	156.0	3.00	155.6	2.99	3.00
0.9	133.6	2.56	132.2	2.54	2.55
1.0	111.6	2.14	109.9	2.10	2.12
1.1	92.3	1.76	90.8	1.74	1.75
1.2	74.7	1.42	72.9	1.39	1.41
1.3	60.2	1.14	59.0	1.12	1.13
1.4	49.3	0.93	47.7	0.90	0.92
1.5	40.2	0.76	37.4	0.70	0.73
1.6	32.9	0.62	29.3	0.55	0.59
1.7	26.6	0.49	23.3	0.43	0.46
1.8	21.6	0.40	18.4	0.34	0.37
1.9	17.1	0.31	14.3	0.26	0.29
2.0	13.6	0.24	10.8	0.19	0.22
2.1	10.9	0.19	8.1	0.14	0.16
2.2	8.3	0.14	5.8	0.09	0.12
2.3	5.8	0.09	4.2	0.06	0.08
2.4	3.8	0.05	2.7	0.03	0.04
2.5	1.5	0.01	1.7	0.01	0.01
2.6	0.8	0	0	0	0

Centerline temperature profiles

Flow conditions: Pe = 3.8, X_{A_o} = 0.7

NOTE: All temperature data listed below are negative.

Axial Position, ζ = z/R	June 8 θ = 0° Voltage, μv	June 8 θ = 0° $T - T_o$ °C	June 28 θ = 0° Voltage, μv	June 28 θ = 0° $T - T_o$ °C	Average $T - T_o$ Fig. 7.3
0.05	59.8	1.14	63.1	1.20	1.17
0.1	79.9	1.52	81.7	1.56	1.54
0.2	112.4	2.15	114.1	2.19	2.17
0.3	130.1	2.50	130.9	2.51	2.50
0.4	134.2	2.57	134.4	2.58	2.58
0.5	127.4	2.44	127.8	2.45	2.44
0.6	113.8	2.18	115.1	2.21	2.20
0.7	98.7	1.89	100.1	1.92	1.90
0.8	83.4	1.59	84.4	1.61	1.60
0.9	69.7	1.33	71.1	1.35	1.34
1.0	56.8	1.08	58.6	1.11	1.10
1.1	46.1	0.87	47.0	0.89	0.88
1.2	36.8	0.69	35.9	0.67	0.68
1.3	28.9	0.54	28.6	0.53	0.54
1.4	22.4	0.41	22.6	0.42	0.43
1.5	17.4	0.32	16.4	0.30	0.31
1.6	12.9	0.23	12.3	0.22	0.22
1.7	9.7	0.17	8.5	0.14	0.16
1.8	6.8	0.11	5.4	0.08	0.10
1.9	4.3	0.06	3.4	0.05	0.06
2.0	2.4	0.03	1.4	0.01	0.02
2.1	1.2	0	0	0	0

Centerline temperature profiles

Flow conditions: Pe = 5.9, X_{A_o} = 0.7

NOTE: All temperature data listed below are negative.

Axial Position, ζ = z/R	June 9 θ = 0° Voltage, μv	June 9 θ = 0° $T - T_o$ °C	June 28 θ = 0° Voltage, μv	June 28 θ = 0° $T - T_o$ °C	Average $T - T_o$ Fig. 7.4
0.05	99.1	1.90	102.7	1.97	1.93
0.1	121.3	2.33	124.8	2.39	2.36
0.2	148.4	2.85	149.6	2.87	2.86
0.3	152.6	2.93	152.8	2.93	2.93
0.4	150.8	2.90	149.9	2.88	2.89
0.5	133.4	2.56	131.3	2.52	2.54
0.6	108.2	2.07	105.8	2.03	2.05
0.7	83.5	1.59	80.6	1.54	1.57
0.8	59.9	1.14	58.6	1.11	1.13
0.9	42.5	0.80	41.8	0.79	0.80
1.0	29.4	0.55	28.9	0.54	0.54
1.1	20.0	0.37	19.9	0.36	0.36
1.2	12.7	0.23	12.6	0.22	0.22
1.3	6.8	0.11	7.6	0.13	0.12
1.4	3.2	0.04	4.1	0.06	0.05
1.5	0.4	0.01	1.8	0.02	0.02
	0	0	0	0	0

Radial temperature profiles

Flow conditions: Pe = 1.9, X_{A_o} = 0.5

NOTES:

1. All temperature data listed below are negative.
2. Date data were taken: June 11
3. Circumferential position of probe inlet passages: 0°.
4. Data are plotted in Figure 7.6.

Radial Location in Tube	Radial Position $\xi = r/R$	ζ = 0.4		ζ = 0.8	
		Voltage μv	$T - T_o$ °C	Voltage μv	$T - T_o$ °C
Probe Inlet	1.0	3.0	0.04	12.5	0.22
	0.9	13.1	0.23	22.6	0.42
	0.8	27.2	0.51	35.1	0.66
	0.7	42.0	0.79	51.2	0.97
	0.6	55.7	1.06	65.6	1.25
	0.5	66.3	1.26	79.3	1.51
	0.4	75.1	1.43	91.5	1.75
	0.3	80.3	1.53	101.1	1.94
	0.2	86.0	1.64	108.4	2.07
	0.1	89.2	1.71	114.3	2.19
Centerline	0.0	91.5	1.75	118.8	2.28
	0.1	93.4	1.79	121.6	2.33
	0.2	94.7	1.81	122.9	2.36
	0.3	95.8	1.83	122.8	2.35
	0.4	96.6	1.85	121.2	2.32
	0.5	96.5	1.85	117.7	2.26
	0.6	94.7	1.81	111.9	2.14
	0.7	89.6	1.71	103.3	1.98
	0.8	80.1	1.53	90.7	1.73
	0.9	65.8	1.25	75.8	1.45
Opposite Wall	1.0	42.1	0.79	51.5	0.98

Flow conditions: Pe = 1.9, X_{A_o} = 0.5

Radial Location in Tube	Radial Position $\xi = r/R$	ζ = 1.0 Voltage μv	ζ = 1.0 $T - T_o$ °C	ζ = 1.3 Voltage μv	ζ = 1.3 $T - T_o$ °C
Probe Inlet	1.0	10.8	0.19	9.5	0.16
	0.9	20.2	0.37	18.7	0.34
	0.8	30.7	0.57	29.0	0.54
	0.7	44.0	0.83	40.0	0.75
	0.6	57.8	1.10	50.2	0.95
	0.5	70.4	1.34	60.7	1.15
	0.4	81.1	1.55	69.4	1.32
	0.3	90.3	1.73	77.1	1.47
	0.2	98.1	1.88	83.4	1.59
	0.1	104.1	1.99	88.4	1.69
Centerline	0.0	108.2	2.07	92.1	1.76
	0.1	111.3	2.13	94.8	1.81
	0.2	112.8	2.16	95.8	1.83
	0.3	112.8	2.16	95.6	1.83
	0.4	111.0	2.13	93.7	1.79
	0.5	108.0	2.07	90.5	1.73
	0.6	102.3	1.96	85.8	1.64
	0.7	94.7	1.81	78.7	1.50
	0.8	82.8	1.58	69.7	1.33
	0.9	69.6	1.33	59.6	1.13
Opposite Wall	1.0	48.5	0.92	41.8	0.79

Flow conditions: Pe = 1.9, X_{A_o} = 0.5

Radial Location in Tube	Radial Position $\xi = r/R$	ζ = 1.6 Voltage μv	ζ = 1.6 $T - T_o$ °C	ζ = 1.9 Voltage μv	ζ = 1.9 $T - T_o$ °C
Probe Inlet	1.0	8.3	0.14	5.0	0.08
	0.9	14.3	0.26	8.3	0.14
	0.8	21.5	0.40	13.4	0.24
	0.7	28.7	0.54	19.3	0.35
	0.6	36.6	0.69	25.3	0.47
	0.5	44.4	0.84	30.9	0.58
	0.4	51.5	0.98	36.3	0.68
	0.3	57.7	1.10	41.2	0.78
	0.2	62.8	1.19	45.4	0.86
	0.1	67.1	1.28	48.9	0.93
Centerline	0.0	70.4	1.34	51.6	0.98
	0.1	72.7	1.39	53.3	1.01
	0.2	74.1	1.41	54.3	1.03
	0.3	74.3	1.42	54.5	1.03
	0.4	73.5	1.40	53.7	1.02
	0.5	71.3	1.36	52.2	0.99
	0.6	68.3	1.30	49.7	0.94
	0.7	63.2	1.20	46.0	0.87
	0.8	56.4	1.07	40.8	0.77
	0.9	48.4	0.92	34.8	0.65
Opposite Wall	1.0	34.6	0.65	24.2	0.45

Flow conditions: Pe = 1.9, X_{A_o} = 0.5

Radial Location in Tube	Radial Position $\xi = r/R$	$\zeta = 2.2$ Voltage μv	$T - T_o$ °C
Probe Inlet	1.0	0.8	0.00
	0.9	3.5	0.05
	0.8	7.3	0.12
	0.7	11.5	0.20
	0.6	16.1	0.29
	0.5	20.6	0.38
	0.4	24.7	0.46
	0.3	28.5	0.53
	0.2	31.7	0.59
	0.1	34.3	0.64
Centerline	0.0	36.5	0.69
	0.1	37.7	0.71
	0.2	38.5	0.72
	0.3	38.7	0.73
	0.4	38.2	0.72
	0.5	37.1	0.70
	0.6	35.0	0.66
	0.7	32.1	0.60
	0.8	28.8	0.54
	0.9	24.0	0.44
Opposite Wall	1.0	16.6	0.30

Radial temperature profiles

Flow conditions: Pe = 3.8, X_{A_o} = 0.5

NOTES:

1. All temperature data listed below are negative.
2. Date data were taken: June 7.
3. Circumferential position of probe inlet passages: 0°.
4. Data are plotted in Figure 7.5 (for ζ = 0.5) and in Figure 7.7.

Radial Location in Tube	Radial Position $\xi = r/R$	ζ = 0.5		ζ = 0.7	
		Voltage μv	$T - T_o$ °C	Voltage μv	$T - T_o$ °C
Probe Inlet	1.0	20.0	0.37	19.2	0.35
	0.9	41.2	0.78	36.8	0.69
	0.8	68.4	1.30	57.5	1.09
	0.7	98.2	1.88	81.0	1.55
	0.6	126.6	2.43	104.7	2.00
	0.5	150.1	2.88	126.0	2.42
	0.4	168.7	3.24	140.8	2.70
	0.3	182.7	3.51	153.4	2.95
	0.2	192.2	3.70	163.8	3.15
	0.1	200.0	3.85	171.8	3.30
Centerline	0.0	206.5	3.97	177.2	3.41
	0.1	210.7	4.05	180.4	3.47
	0.2	213.2	4.10	182.3	3.50
	0.3	214.7	4.13	182.5	3.51
	0.4	214.3	4.12	181.7	3.49
	0.5	212.5	4.09	178.7	3.44
	0.6	208.0	4.00	172.3	3.31
	0.7	197.3	3.79	163.5	3.14
	0.8	179.2	3.44	146.5	2.81
	0.9	148.3	2.85	123.6	2.37
Opposite Wall	1.0	103.0	1.97	89.3	1.71

Flow conditions: Pe = 3.8, X_{A_o} = 0.5

Radial Location in Tube	Radial Position $\xi = r/R$	$\zeta = 0.9$		$\zeta = 1.1$	
		Voltage μv	$T - T_o$ °C	Voltage μv	$T - T_o$ °C
Probe Inlet	1.0	18.7	0.34	15.2	0.27
	0.9	31.2	0.58	22.2	0.41
	0.8	46.2	0.87	31.5	0.59
	0.7	62.2	1.18	42.5	0.80
	0.6	78.2	1.49	52.4	0.99
	0.5	91.1	1.74	62.1	1.18
	0.4	103.5	1.98	69.8	1.33
	0.3	113.7	2.18	77.5	1.48
	0.2	122.1	2.34	83.4	1.59
	0.1	128.0	2.46	88.1	1.68
Centerline	0.0	132.7	2.54	91.5	1.75
	0.1	135.9	2.61	93.8	1.79
	0.2	137.3	2.63	95.2	1.82
	0.3	137.6	2.64	95.4	1.82
	0.4	134.5	2.58	93.8	1.79
	0.5	132.1	2.53	90.3	1.73
	0.6	128.2	2.46	86.9	1.66
	0.7	120.5	2.31	82.6	1.58
	0.8	109.0	2.09	75.4	1.44
	0.9	93.8	1.79	65.0	1.24
Opposite Wall	1.0	69.0	1.31	50.0	0.95

Flow conditions: Pe = 3.8, X_{A_o} = 0.5

Radial Location in Tube	Radial Position $\xi = r/R$	ζ = 1.3		ζ = 1.5	
		Voltage μv	$T - T_o$ °C	Voltage μv	$T - T_o$ °C
Probe Inlet	1.0	11.3	0.20	8.1	0.14
	0.9	16.2	0.29	10.8	0.19
	0.8	22.4	0.41	14.4	0.26
	0.7	29.1	0.54	18.3	0.33
	0.6	35.8	0.67	22.2	0.41
	0.5	41.5	0.78	25.7	0.48
	0.4	46.4	0.88	29.0	0.54
	0.3	51.0	0.97	31.4	0.59
	0.2	54.5	1.03	33.5	0.63
	0.1	57.2	1.09	35.4	0.66
Centerline	0.0	59.2	1.12	37.0	0.70
	0.1	60.8	1.16	37.5	0.70
	0.2	61.2	1.16	37.7	0.71
	0.3	61.6	1.17	37.3	0.70
	0.4	61.4	1.17	37.2	0.70
	0.5	61.1	1.16	37.0	0.70
	0.6	59.5	1.13	36.5	0.69
	0.7	56.5	1.07	36.1	0.68
	0.8	51.8	0.98	34.2	0.64
	0.9	46.2	0.87	31.9	0.60
Opposite Wall	1.0	37.0	0.70	25.7	0.48

Radial temperature profiles

Flow conditions: Pe = 3.8, X_{A_o} = 0.5

NOTES:

1. All temperature data listed below are negative.
2. Date data were taken: June 30.
3. Circumferential position of probe inlet passages: 180°.
4. Data for ζ = 0.5 are plotted in Figure 7.5.

Radial Location in Tube	Radial Position $\xi = r/R$	ζ = 0.5		ζ = 0.7	
		Voltage μv	$T - T_o$ °C	Voltage μv	$T - T_o$ °C
Opposite Wall	1.0	108.1	2.07	84.7	1.62
	0.9	151.4	2.91	122.7	2.35
	0.8	180.1	3.46	148.2	2.85
	0.7	195.6	3.76	164.3	3.16
	0.6	205.5	3.95	174.0	3.34
	0.5	210.4	4.05	180.2	3.46
	0.4	211.7	4.07	183.6	3.53
	0.3	212.1	4.08	184.7	3.55
	0.2	211.0	4.06	183.4	3.52
	0.1	208.5	4.01	180.6	3.47
Centerline	0.0	204.8	3.94	177.4	3.41
	0.1	198.6	3.82	171.1	3.29
	0.2	194.0	3.73	162.2	3.12
	0.3	184.2	3.54	154.0	2.96
	0.4	170.2	3.27	138.0	2.65
	0.5	151.7	2.91	121.2	2.32
	0.6	123.9	2.38	102.6	1.96
	0.7	95.3	1.82	78.6	1.50
	0.8	63.7	1.21	53.2	1.01
	0.9	36.5	0.69	31.2	0.58
Probe Inlet	1.0	14.1	0.25	13.9	0.25

Flow conditions: Pe = 3.8, X_{A_o} = 0.5

Radial Location in Tube	Radial Position $\xi = r/R$	$\zeta = 0.9$ Voltage μv	$T - T_o$ °C
Opposite Wall	1.0	64.7	1.23
	0.9	91.7	1.75
	0.8	108.5	2.08
	0.7	121.5	2.33
	0.6	129.5	2.48
	0.5	134.7	2.58
	0.4	137.3	2.63
	0.3	138.2	2.65
	0.2	137.4	2.64
	0.1	135.5	2.60
Centerline	0.0	132.2	2.54
	0.1	126.8	2.43
	0.2	119.8	2.30
	0.3	111.6	2.14
	0.4	101.4	1.94
	0.5	88.7	1.70
	0.6	76.5	1.46
	0.7	57.1	1.08
	0.8	42.8	0.81
	0.9	24.9	0.46
Probe Inlet	1.0	12.7	0.23

Radial temperature profiles

Flow conditions: Pe = 3.8, X_{A_o} = 0.7

NOTES:

1. All temperature data listed below are negative.
2. Date data were taken: June 28.
3. Circumferential position of probe inlet passages: 0^o.
4. Data are plotted in Figure 7.8.

Radial Location in Tube	Radial Position $\xi = r/R$	$\zeta = 0.4$		$\zeta = 0.6$	
		Voltage μv	$T - T_o$ °C	Voltage μv	$T - T_o$ °C
Probe Inlet	1.0	8.6	0.15	6.5	0.11
	0.9	23.3	0.43	17.3	0.32
	0.8	43.0	0.81	31.9	0.60
	0.7	64.7	1.23	47.9	0.91
	0.6	84.3	1.61	63.2	1.20
	0.5	100.0	1.91	76.9	1.47
	0.4	112.7	2.16	87.5	1.67
	0.3	121.4	2.33	96.6	1.85
	0.2	128.3	2.46	103.4	1.98
	0.1	133.1	2.55	108.5	2.08
Centerline	0.0	136.7	2.62	112.8	2.16
	0.1	139.9	2.68	115.2	2.21
	0.2	143.5	2.75	117.4	2.25
	0.3	143.8	2.76	118.4	2.27
	0.4	143.9	2.76	118.0	2.26
	0.5	143.1	2.75	115.7	2.22
	0.6	139.6	2.68	111.8	2.14
	0.7	132.4	2.54	104.8	2.01
	0.8	119.1	2.28	94.4	1.80
	0.9	96.0	1.84	77.9	1.49
Opposite Wall	1.0	65.8	1.25	52.8	1.00

Flow conditions: Pe = 3.8, X_{A_o} = 0.7

Radial Location in Tube	Radial Position $\xi = r/R$	$\zeta = 0.8$ Voltage μv	$\zeta = 0.8$ $T - T_o$ °C	$\zeta = 1.0$ Voltage μv	$\zeta = 1.0$ $T - T_o$ °C
Probe Inlet	1.0	7.1	0.12	2.9	0.04
	0.9	15.0	0.27	7.5	0.12
	0.8	25.6	0.48	14.6	0.26
	0.7	36.8	0.69	22.5	0.42
	0.6	47.8	0.90	30.1	0.56
	0.5	58.1	1.10	36.9	0.69
	0.4	65.8	1.25	42.6	0.80
	0.3	72.9	1.39	47.8	0.90
	0.2	78.4	1.50	51.7	0.98
	0.1	82.6	1.58	54.7	1.04
Centerline	0.0	85.9	1.64	57.2	1.09
	0.1	88.0	1.68	58.6	1.11
	0.2	89.3	1.71	59.2	1.12
	0.3	89.8	1.72	59.6	1.13
	0.4	89.2	1.70	58.9	1.12
	0.5	87.2	1.67	57.5	1.09
	0.6	83.7	1.60	54.9	1.04
	0.7	78.3	1.49	51.1	0.97
	0.8	69.9	1.33	45.4	0.86
	0.9	58.3	1.11	37.8	0.71
Opposite Wall	1.0	39.7	0.75	25.4	0.47

Flow conditions: Pe = 3.8, X_{A_o} = 0.7

Radial Location in Tube	Radial Position $\xi = r/R$	ζ = 1.2		ζ = 1.4	
		Voltage μv	$T - T_o$ °C	Voltage μv	$T - T_o$ °C
Probe Inlet	1.0	0.6	0.00	0.4	0.00
	0.9	3.4	0.05	3.3	0.04
	0.8	8.1	0.14	6.6	0.11
	0.7	13.7	0.24	10.3	0.18
	0.6	18.5	0.34	13.8	0.25
	0.5	23.5	0.44	16.7	0.30
	0.4	26.8	0.50	19.0	0.35
	0.3	30.0	0.56	20.9	0.38
	0.2	32.7	0.61	22.5	0.42
	0.1	34.8	0.65	23.6	0.44
Centerline	0.0	36.5	0.69	24.3	0.45
	0.1	37.5	0.70	24.8	0.46
	0.2	38.1	0.72	25.1	0.47
	0.3	38.8	0.73	25.2	0.47
	0.4	38.6	0.73	24.7	0.46
	0.5	37.8	0.71	24.2	0.45
	0.6	36.3	0.68	23.3	0.43
	0.7	33.8	0.63	21.4	0.39
	0.8	30.3	0.57	18.8	0.34
	0.9	25.4	0.47	15.6	0.28
Opposite Wall	1.0	16.8	0.30	9.7	0.17

Radial temperature profiles

Flow conditions: Pe = 5.9, X_{A_o} = 0.7

NOTES:

1. All temperature data listed below are negative.
2. Date data were taken: June 9.
3. Circumferential position of probe inlet passages: 0^o.
4. Data are plotted in Figure 7.9.

Radial Location in Tube	Radial Position $\xi = r/R$	$\zeta = 0.3$		$\zeta = 0.4$	
		Voltage μv	$T - T_o$ °C	Voltage μv	$T - T_o$ °C
Probe Inlet	1.0	5.3	0.08	4.8	0.07
	0.9	22.5	0.42	21.7	0.40
	0.8	47.6	0.90	44.4	0.84
	0.7	73.0	1.39	67.5	1.28
	0.6	96.7	1.85	88.0	1.68
	0.5	114.4	2.19	104.0	1.99
	0.4	127.5	2.44	114.0	2.18
	0.3	136.2	2.61	122.6	2.35
	0.2	141.3	2.71	127.4	2.44
	0.1	145.5	2.79	131.1	2.51
Centerline	0.0	149.0	2.86	134.3	2.58
	0.1	151.3	2.90	135.9	2.61
	0.2	152.2	2.92	137.5	2.64
	0.3	153.7	2.95	138.6	2.66
	0.4	154.6	2.97	139.5	2.68
	0.5	156.4	3.00	140.3	2.69
	0.6	156.2	3.00	139.7	2.68
	0.7	152.0	2.92	136.0	2.61
	0.8	140.9	2.70	126.0	2.42
	0.9	119.0	2.28	108.1	2.07
Opposite Wall	1.0	73.6	1.40	67.1	1.28

Flow conditions: Pe = 5.9, X_{A_o} = 0.7

Radial Location in Tube	Radial Position $\xi = r/R$	ζ = 0.5		ζ = 0.7	
		Voltage μv	$T - T_o$ °C	Voltage μv	$T - T_o$ °C
Probe Inlet	1.0	3.7	0.05	1.4	0.01
	0.9	16.5	0.30	9.0	0.15
	0.8	32.4	0.61	18.8	0.34
	0.7	50.7	0.96	28.9	0.54
	0.6	66.1	1.26	38.8	0.73
	0.5	79.0	1.51	45.9	0.87
	0.4	87.9	1.68	50.8	0.96
	0.3	95.6	1.83	54.8	1.04
	0.2	100.5	1.92	57.6	1.09
	0.1	104.1	1.99	59.5	1.13
Centerline	0.0	107.1	2.05	61.0	1.16
	0.1	108.1	2.07	62.2	1.18
	0.2	109.2	2.09	62.7	1.19
	0.3	109.8	2.10	63.0	1.20
	0.4	110.6	2.12	63.8	1.21
	0.5	110.3	2.11	63.7	1.21
	0.6	109.6	2.10	63.4	1.21
	0.7	106.1	2.03	61.5	1.17
	0.8	97.4	1.86	57.6	1.09
	0.9	84.9	1.62	50.1	0.95
Opposite Wall	1.0	53.0	1.00	32.4	0.61

Flow conditions: Pe = 5.9, X_{A_o} = 0.7

Radial Location in Tube	Radial Position $\xi = r/R$	$\zeta = 0.9$ Voltage μv	$T - T_o$ °C
Probe Inlet	1.0	0.1	0.00
	0.9	4.0	0.06
	0.8	9.3	0.16
	0.7	15.2	0.27
	0.6	20.5	0.38
	0.5	24.5	0.45
	0.4	27.2	0.51
	0.3	29.2	0.54
	0.2	30.5	0.57
	0.1	31.3	0.58
Centerline	0.0	31.9	0.60
	0.1	32.2	0.60
	0.2	32.4	0.61
	0.3	32.9	0.62
	0.4	33.7	0.63
	0.5	33.6	0.63
	0.6	33.4	0.63
	0.7	33.1	0.62
	0.8	31.0	0.58
	0.9	27.0	0.50
Opposite Wall	1.0	17.3	0.32

Appendix G. UNCERTAINTIES IN TEMPERATURE MEASUREMENTS

As discussed in section 7.1.4 of Chapter VII, there are two types of errors that affect the accuracy of the temperature data taken under the flow conditions considered in this investigation. These are (1) random errors, which may be caused by such factors as inconsistencies in the method of taking data and fluctuations in the operating conditions, and (2) fixed errors, or systematic errors, which are essentially constant for repeated readings.

Summarized in Table 7.1 of Chapter VII are estimates of uncertainties arising as a result of such errors in the temperature data taken in this investigation. The manner in which these uncertainties were estimated is discussed in detail in the following paragraphs.

G.1. Random Errors

Random errors associated with operation of the diffusion apparatus and the instrumentation with which it is equipped are small, as indicated by the close agreement that exists between values of temperature measurements repeated for each of the four sets of flow conditions under which data were taken. A worst-case example of the differences that were found between repeated measurements of centerline temperature profiles is shown in Figure G.1.

The two sets of data plotted in that figure are for flow conditions corresponding to Pe = 1.9, X_{A_o} = 0.5. To clearly illustrate the differences between corresponding measurements, the scale to which the temperature coordinate is drawn in Figure G.1 is 2.5 times larger than that used in Figures 7.1 through 7.9 of Chapter VII.

After data were taken in the first of the two runs for which results are plotted in Figure G.1, a time period of over three weeks elapsed before the second run was performed. In addition, for the second run the diffusion tube thermocouple probes were inserted into the flow field from a circumferential position that differed by 180° from that used for the first run. Nevertheless, corresponding values of the two sets of data (which were measured relative to the common temperature of the two gases entering the diffusion tube) are in agreement within 0.1°C.

Centerline temperature measurements from runs repeated for all four flow conditions considered in this investigation are included in Appendix F. With the exception of the two sets of data plotted in Figure G.1 for Pe = 1.9, X_{A_o} = 0.5, repeated measurements are in agreement within approximately 0.05°C. This agreement holds even for results (such as those tabulated in Appendix F for Pe = 3.8, X_{A_o} = 0.5) of runs repeated after time intervals as long or longer than the interval between the two runs for which data are plotted in Figure G.1.

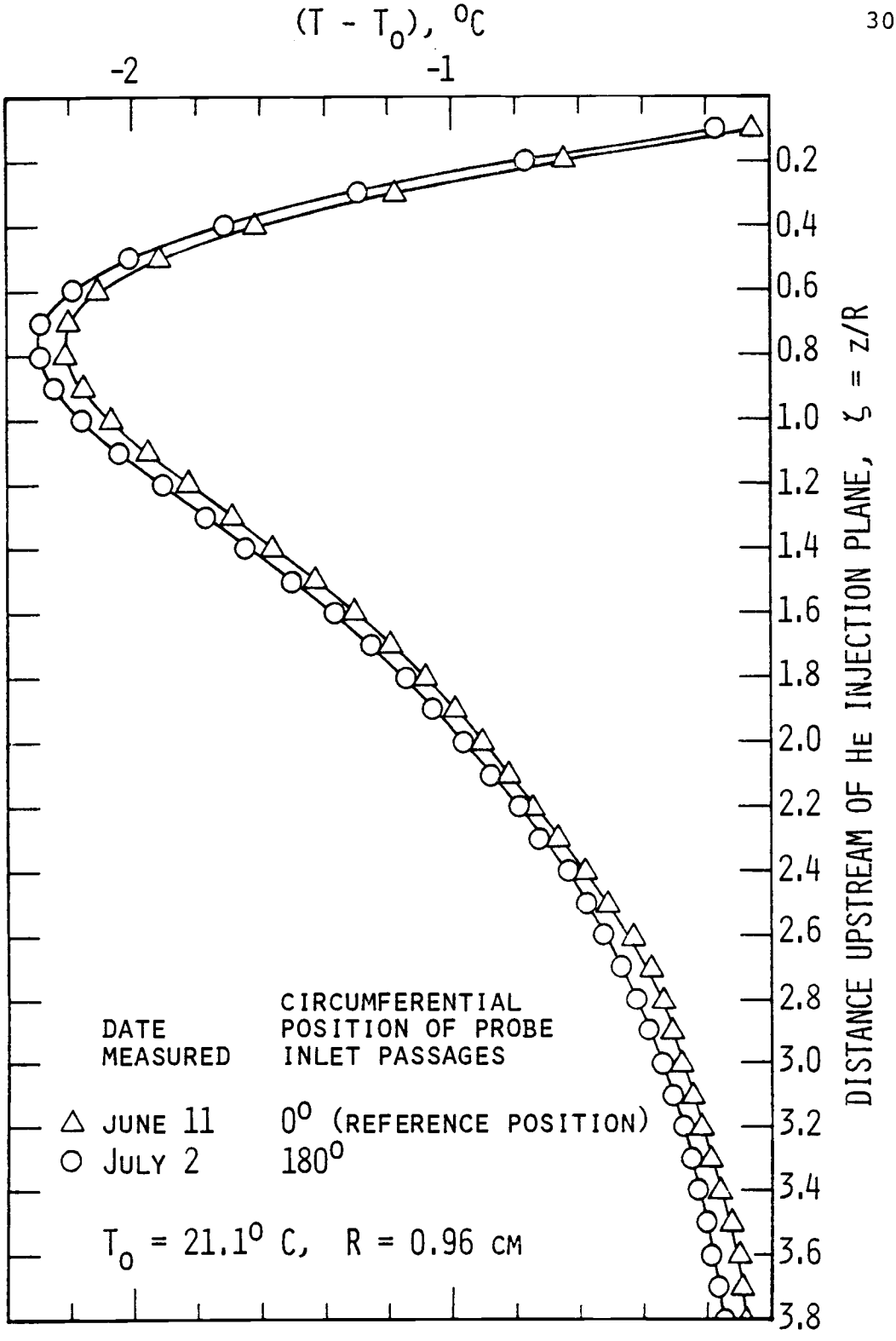

Figure G.1. Repeated Measurements of Centerline Temperature Profiles for Pe = 1.9, X_{A_o} = 0.5

On the basis of the very close agreement between values of repeated temperature measurements for the other flow conditions, the differences between the two profiles plotted in Figure G.1 for Pe = 1.9, X_{A_o} = 0.5 are larger than those that would be expected from random errors. A mistake in setting the test conditions or taking the data for one profile or the other might have been a factor contributing to the differences between the profiles plotted in that figure. For example, the diffusion tube probes might have been incorrectly positioned in one or both runs so that the temperatures measured were not those along the centerline of the flow field.

Included in Appendix F is a third set of measurements taken for Pe = 1.9, X_{A_o} = 0.5 as a recheck on the two profiles plotted in Figure G.1. The results of this third run agree within 0.05°C with the data points identified by circles plotted in Figure G.1. This confirms that there is nothing peculiar about the operating characteristics of the apparatus that precludes obtaining temperature data with very close repeatability for flow conditions corresponding to Peclet numbers as low as 1.9.

The close agreement between values of repeated temperature measurements for all four flow conditions under which data were taken confirms that the diffusion apparatus and instrumentation used in this experimental investigation can be operated with a high degree of precision. Even the

worst-case differences between repeated measurements (those between the profiles plotted in Figure G.1) are quite small considering all of the variables that can affect the measurements.

G.2. Fixed Errors

Errors inherent in measuring temperatures with a probe inserted into a flow field include those resulting from (1) conduction of heat along the probe stem and (2) energy exchange by thermal radiation between the probe and its surroundings. Since temperatures measured in the diffusion flow fields considered in this investigation differ by no more than 4°C from the temperature of the surrounding solid surfaces, the former source of error is more significant than the latter as shown later in this section.

The difference between the true fluid temperature at a point in a flow field and the temperature measured at that point with a probe inserted transversely into the flow field may be estimated by modeling the probe as a fin attached to the wall of the flow channel. This approach is taken in the following paragraphs. First, the errors are estimated on the assumption that those due to radiation heat transfer are negligible, and then the maximum additional error resulting from radiation heat transfer is considered.

G.2.1. Conduction Errors

Equations applicable for use in estimating errors resulting from heat conduction along a temperature probe modeled as a fin are readily available in the literature (e.g. Welty, et al. (1969)). In the formulation of such equations the fluid temperature and the convective heat transfer coefficient are generally assumed to be invariant along the length of the fin, and the thermal conductivity of the fin is generally assumed to be constant. For a fin that is thin relative to its length, the temperature at any cross section is assumed to be uniform.

To arrive at a specific equation for a given fin configuration, two boundary conditions must be specified. One boundary condition follows from the assumption that the temperature at the base of the fin is the same as the wall temperature. Any of several boundary conditions may be applicable at the probe tip, depending on the specific fin configuration; for a probe that is thin relative to its length, it is reasonable to assume that heat transfer through the probe tip is negligible and that therefore the temperature gradient at the probe tip is zero.

For each of the four flow conditions under which data were taken, an equation formulated on the basis of the preceding assumptions was used to estimate the thermocouple conduction error at the axial position within the diffusion

tube where the centerline temperature passes through a minimum. Both the minimum temperature in a diffusion flow field and the axial position where it occurs vary as a function of the flow conditions, as discussed in section 7.1.1 of Chapter VII. The equation used to estimate conduction errors, and the results computed for the four flow conditions, are included in Table G.1 together with a sketch of the probe configuration modeled.

The above mentioned approach for estimating errors yields results that are only rough approximations of the actual errors for the flow conditions considered in this investigation, because the assumptions of constant fluid temperature and constant heat transfer coefficient along the probe surface do not hold for these flow conditions. Accounting for variations in these latter variables as a function of radial position in the diffusion tube would result in substantially increasing the complexity of the error analysis. Although radial variations in these latter variables were neglected in computing the error estimates listed in Table G.1, the results nevertheless provide a useful indication of the magnitudes of the errors.

Heat transfer coefficients used in estimating the conduction errors listed in Table G.1 were computed with the following correlation from McAdams (1954):

$$Nu_D = \frac{\bar{h}_c D}{\lambda_f} = 0.32 + 0.43(Re_D)^{0.52}$$

Table G.1. Estimated Thermocouple Probe Conduction Errors for Minimum Centerline Temperature Measurements for Four Flow Conditions

Configuration Modeled

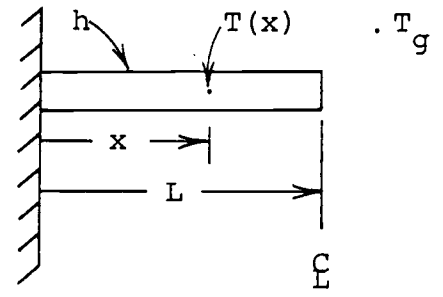

Boundary Conditions:

1. $T = T_w$ at $x = 0$

2. $\frac{dT}{dx} = 0$ at $x = L$

Applicable equation (Welty, et al. (1969)):

$$\frac{T - T_g}{T_w - T_g} = \frac{\cosh[m(L-x)]}{\cosh mL} \quad \text{where } m = \sqrt{\frac{hP}{kA}}$$

Flow Condition	Axial Position ($\zeta = z/R$) of $\lvert T_{CL}-T_o \rvert_{max}$	(1) $(T_{CL_{min}}-T_o)$ measured, °C	(2) $(T_{CL_{min}}-T_o)$ corrected, °C	$\frac{(2)-(1)}{(1)}$, %
Pe = 1.9, X_{A_o} = 0.5	0.8	-2.26	-2.39	5.8
Pe = 3.8, X_{A_o} = 0.5	0.5	-3.96	-4.15	4.8
Pe = 3.8, X_{A_o} = 0.7	0.4	-2.58	-2.73	5.8
Pe = 5.9, X_{A_o} = 0.7	0.25	-2.93	-3.09	5.5

NOTE: T_o, the reference temperature of the gases entering the diffusion tube, is 21.1°C.

where Nu_D is the Nusselt number and Re_D is the Reynolds number for flow over the probe, λ_f is the thermal conductivity of the fluid, D is the probe diameter, and $\bar{h}_c$ is the average convective heat transfer coefficient. According to McAdams, this correlation is applicable for cylinders in cross flow under flow conditions for which Re_D is as low as 0.1. (Values of Re_D for flow over the probes used in this investigation varied in the range from 0.2 to 0.5.) Since the preceding correlation is for experimental data taken in air as the flowing fluid, its applicability is restricted to fluids for which the Prandtl numbers are close to the Prandtl number of air.

Values of λ_f computed from equation 4.14 of Chapter IV were used in the computations of $\bar{h}_c$. With equation 4.14 the variation of λ_f as a function of gas composition can be taken into consideration.

Another variable that affects the magnitude of the thermocouple conduction error is the thermal conductivity of the probe assembly. The value of this latter variable was computed on the basis of the probe structure shown in cross section in Figure 5.12 of Chapter V. For the composite structure, the thermal conductivity is approximately 0.10 watts/(cm °C).

Referring to Table G.1, the thermocouple conduction error is estimated to be less than 0.2° C for the minimum temperature measured in the diffusion tube under each set

of flow conditions for which data were taken. In no case considered in this table is the estimated conduction error greater than 5.8% of the difference between the minimum temperature measured for a given set of flow conditions and the reference temperature of the two gases entering the diffusion tube.

Shown in Figure G.2 is a centerline temperature profile plotted through as-measured data points for flow conditions corresponding to Pe = 3.8, X_{A_o} = 0.5. This profile is a duplicate of the temperature profile plotted in Figure 7.2 of Chapter VII. Also shown in Figure G.2 is a temperature profile obtained by adding correction factors for thermocouple conduction errors to the values of the as-measured data plotted in that figure. The errors were computed in the same manner used to compute those listed in Table G.1. To facilitate comparisons of the as-measured and corrected data, the values plotted in Figure G.2 are listed in Table G.2. The differences between the as-measured and corrected temperature profiles plotted in Figure G.2 are typical of those for the other three sets of flow conditions under which data were taken.

As shown in Figure G.2, the thermocouple conduction errors vary with the measured values of the centerline temperatures for which they were computed. The error that is largest in magnitude occurs for the minimum temperature measured along the diffusion tube centerline. As the

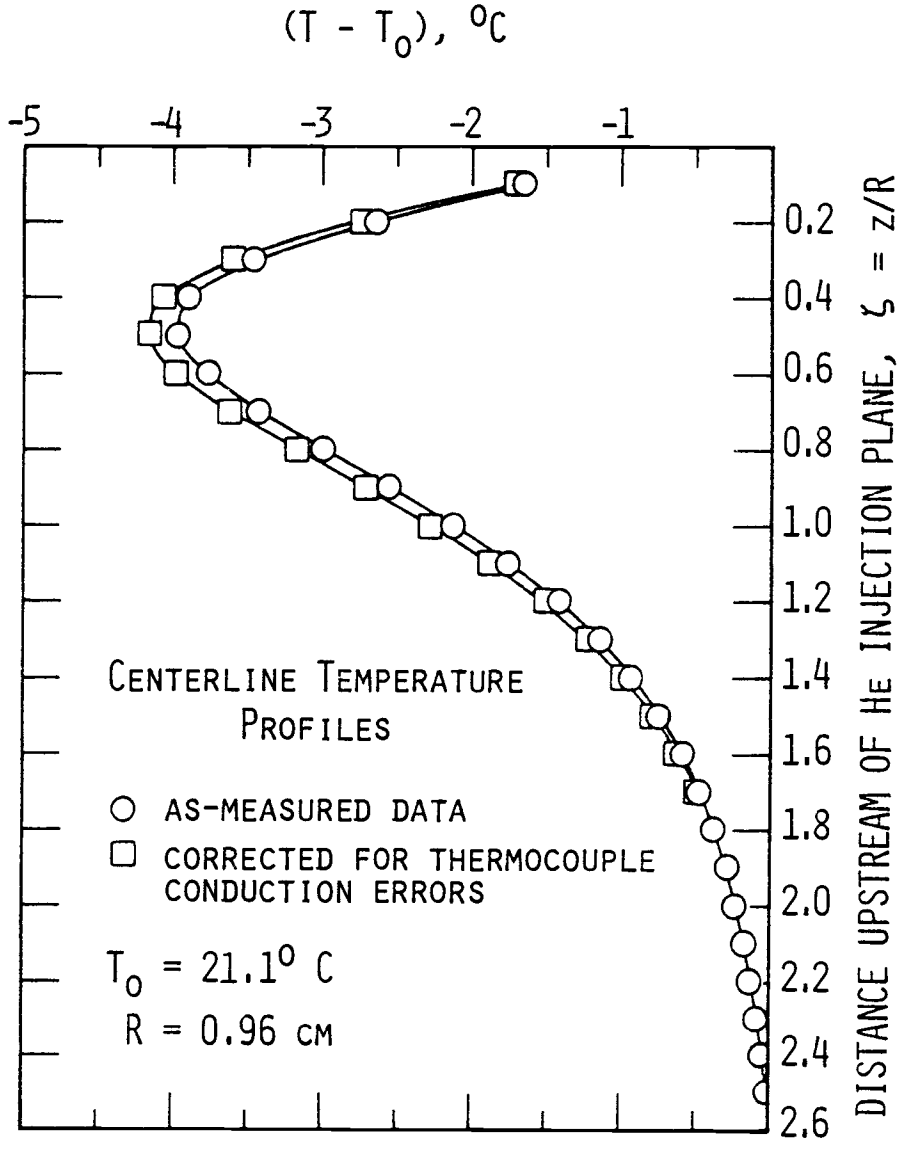

Figure G.2. As-Measured and Corrected Centerline Temperature Profiles for Pe = 3.8, X_{A_o} = 0.5

Table G.2. Estimated Thermocouple Probe Conduction Errors for Centerline Temperatures Measured for Pe = 3.8, X_{A_o} = 0.5

Axial Position $\zeta = z/R$	(1) $(T_{CL}-T_o)$ measured, °C	(2) $(T_{CL}-T_o)$ corrected for conduction error, °C	Conduction Error = (1)-(2), °C	$\left\|\frac{(1)-(2)}{(1)}\right\|$ %
0.1	-1.64	-1.68	0.04	2.4
0.2	-2.64	-2.72	0.08	3.0
0.3	-3.46	-3.60	0.14	4.0
0.4	-3.89	-4.05	0.16	4.1
0.5	-3.96	-4.14	0.19	4.8
0.6	-3.77	-3.96	0.19	5.0
0.7	-3.42	-3.61	0.19	5.6
0.8	-2.99	-3.17	0.18	6.0
0.9	-2.55	-2.71	0.16	6.3
1.0	-2.12	-2.26	0.14	6.6
1.1	-1.75	-1.87	0.12	6.9
1.2	-1.41	-1.50	0.09	6.4
1.3	-1.13	-1.21	0.08	7.1
1.4	-0.92	-0.98	0.06	6.5
1.5	-0.73	-0.78	0.05	6.8
1.6	-0.58	-0.62	0.04	6.9
1.7	-0.46	-0.49	0.03	6.5
1.8	-0.37	-0.39	0.02	5.4
1.9	-0.28	-0.30	0.02	7.1
2.0	-0.22	-0.23	0.01	4.5

NOTE: T_o, the reference temperature of the gases entering the diffusion tube, is 21.1°C.

centerline temperature approaches the reference temperature of the two gases entering the diffusion tube, the thermocouple conduction error goes to zero.

Due to the thermocouple conduction errors discussed above, the accuracy of the data for the larger temperature effects measured in this investigation is lower than the precision with which the data were measured. For example, the thermocouple conduction errors are nearly 0.2° C for the minimum values of the temperatures measured under the four flow conditions, as shown in Table G.1, but repeated values of these measurements differ by less than 0.1°C.

G.2.2. Thermal Radiation Errors

Energy exchange by thermal radiation between a thermocouple probe and its surroundings is an additional source of error in measurements taken with the probe. The effect of this source of error on a given temperature measurement may be estimated by accounting for thermal radiation in an energy balance on the probe used to take the measurement.

An energy balance was performed to obtain an estimate of the thermal radiation error for the largest difference (-3.96°C) recorded between the temperature at a point in a diffusion flow field and the reference temperature of the gases entering the diffusion tube. For this temperature

difference, which occurs along the diffusion tube centerline at an axial location of $\zeta = 0.5$ in the flow field corresponding to Pe = 3.8, $X_{A_o} = 0.5$, the estimated thermal radiation error is approximately 0.05^{o} C. This estimate is conservative in the sense that the probe emissivity was assumed to be 0.2, while the actual emissivity is likely to be less than 0.1 because the stainless steel surfaces of the diffusion tube thermocouple probes were polished to minimize their emissivity.

As noted in Table G.1, the estimated conduction error in the temperature measurement referred to above is 0.19^{o} C. The magnitude of this error is nearly four times as large as that of the estimated radiation error for the same temperature measurement.

Errors due to thermal radiation have also been estimated for other temperatures measured under the flow conditions considered in this investigation. All such errors are smaller in magnitude than the thermal radiation error discussed above for Pe = 3.8, $X_{A_o} = 0.5$. In addition, the magnitude of the radiation error for a given temperature measurement is in no case larger than 27% of the magnitude of the conduction error for the same temperature measurement.

G.2.3. Calibration Errors

Another source of error that affects the uncertainty of temperature measurements taken in this investigation is that associated with the calibration of the instrumentation used to measure outputs from the diffusion tube thermocouple assemblies. With the calibrations discussed in section 5.2.5 of Chapter V, the contribution of this source of error to the uncertainty of the temperature measurements is considered to be no more than $\pm$ 0.03°C.

Appendix H. CONCENTRATION, VELOCITY, AND TEMPERATURE DATA USED IN COMPUTATIONS OF THERMAL DIFFUSION FACTORS AND MOLECULAR DIFFUSION COEFFICIENTS

NOTES:

1. The data in this appendix are grouped according to the flow conditions under which they were measured. These flow conditions are:

   Pe = 1.9, X_{A_o} = 0.5,

   Pe = 3.8, X_{A_o} = 0.5,

   Pe = 3.8, X_{A_o} = 0.7,

   and Pe = 5.9, X_{A_o} = 0.7.

2. Values tabulated for velocity and concentration distributions are based on data taken by Stock (1972), and were supplied by him for use in this investigation.

3. Axial positions are those upstream of and relative to the helium injection plane. Radial positions are those relative to the diffusion tube centerline.

Flow conditions: Pe = 1.9, X_{A_o} = 0.5

Temperatures in diffusion flow field, $(T - T_o)$, °C

where T_o is the reference temperature of the gases entering the diffusion tube.

T_o = 21.11°C R = 0.96 cm

NOTE: All values listed below are negative except those designated by a plus sign.

Axial Position, ζ = z/R	Radial Position, ξ = r/R										
	0.0	0.1	0.2	0.3	0.4	0.5	0.6	0.7	0.8	0.9	1.0
0.0	+.40	+.40	+.39	+.37	+.35	+.32	+.29	+.25	+.21	+.17	+.11
0.1	.13	.13	.13	.12	.11	.10	.09	.07	.06	.04	.02
0.2	.71	.70	.68	.65	.61	.56	.50	.42	.35	.26	.16
0.3	1.24	1.23	1.20	1.16	1.10	1.01	.92	.80	.67	.54	.36
0.4	1.67	1.66	1.62	1.56	1.47	1.36	1.23	1.07	.89	.70	.46
0.5	1.97	1.96	1.92	1.85	1.74	1.62	1.45	1.26	1.03	.81	.53
0.6	2.16	2.14	2.10	2.03	1.92	1.78	1.60	1.38	1.13	.88	.57
0.7	2.25	2.23	2.19	2.12	2.01	1.86	1.67	1.45	1.18	.92	.59
0.8	2.26	2.24	2.20	2.13	2.02	1.87	1.68	1.46	1.19	.92	.59
0.9	2.21	2.20	2.15	2.08	1.97	1.83	1.64	1.42	1.16	.90	.58
1.0	2.13	2.11	2.07	2.00	1.89	1.75	1.57	1.36	1.11	.87	.56
1.1	2.01	2.00	1.96	1.89	1.78	1.65	1.48	1.28	1.05	.82	.54
1.2	1.89	1.88	1.84	1.77	1.67	1.55	1.39	1.21	.99	.78	.51
1.3	1.75	1.75	1.71	1.65	1.55	1.44	1.29	1.12	.93	.72	.48
1.4	1.63	1.62	1.58	1.52	1.44	1.33	1.20	1.04	.87	.68	.45
1.5	1.48	1.47	1.44	1.39	1.31	1.21	1.09	.96	.80	.63	.42
1.6	1.35	1.34	1.31	1.27	1.20	1.11	1.00	.88	.74	.59	.40
1.7	1.24	1.23	1.21	1.16	1.10	1.01	.92	.80	.67	.54	.36
1.8	1.13	1.12	1.10	1.05	.99	.92	.83	.72	.60	.48	.32
1.9	1.03	1.02	1.00	.96	.90	.83	.75	.65	.54	.43	.28
2.0	.94	.93	.91	.87	.82	.75	.68	.59	.48	.38	.25
2.1	.87	.86	.83	.80	.75	.69	.62	.53	.44	.34	.22
2.2	.78	.77	.75	.72	.67	.62	.55	.47	.39	.30	.18
2.3	.70	.69	.68	.65	.60	.55	.49	.41	.34	.26	.15
2.4	.61	.61	.59	.56	.53	.48	.43	.36	.30	.22	.13
2.5	.55	.54	.53	.51	.47	.43	.38	.32	.27	.20	.12
2.6	.49	.48	.47	.45	.42	.38	.34	.28	.23	.17	.10
2.7	.42	.42	.41	.39	.36	.33	.29	.25	.20	.15	.09
2.8	.39	.38	.37	.36	.33	.30	.27	.22	.18	.14	.08
2.9	.35	.35	.34	.32	.30	.27	.24	.20	.17	.12	.07

Flow conditions: Pe = 1.9, X_{A_o} = 0.5

Axial Position, ζ = z/R	Radial Position, ξ = r/R										
	0.0	0.1	0.2	0.3	0.4	0.5	0.6	0.7	0.8	0.9	1.0
3.0	.32	.32	.31	.29	.27	.25	.22	.18	.15	.11	.06
3.1	.30	.29	.29	.27	.25	.23	.20	.17	.14	.10	.06
3.2	.26	.26	.25	.24	.22	.20	.18	.15	.12	.09	.05
3.3	.23	.23	.22	.21	.20	.18	.16	.13	.11	.08	.04
3.4	.20	.20	.19	.18	.17	.15	.13	.11	.09	.06	.03
3.5	.16	.16	.16	.15	.14	.13	.11	.09	.07	.05	.02
3.6	.14	.14	.13	.13	.12	.11	.09	.08	.06	.04	.02
3.7	.11	.11	.11	.10	.10	.09	.07	.06	.05	.03	.01
3.8	.08	.08	.08	.07	.07	.06	.05	.04	.03	.02	.00
3.9	.05	.05	.05	.05	.04	.04	.03	.02	.02	.01	.00
4.0	.03	.03	.03	.02	.02	.02	.01	.01	.00	.00	.00
4.1	.01	.01	.01	.01	.00	.00	.00	.00	.00	.00	.00

Flow conditions: Pe = 1.9, X_{A_o} = 0.5

Mole fractions of nitrogen in diffusion flow field (based on data from Stock (1972))

R = 0.96 cm

Axial Position, ζ = z/R	Radial Position, ξ = r/R										
	0.0	0.1	0.2	0.3	0.4	0.5	0.6	0.7	0.8	0.9	1.0
0.0	.500	.500	.500	.500	.500	.500	.500	.500	.500	.500	.500
0.1	.554	.551	.547	.545	.541	.545	.545	.545	.545	.545	.545
0.2	.597	.592	.587	.585	.583	.583	.581	.580	.580	.580	.580
0.3	.623	.615	.613	.619	.620	.620	.610	.610	.610	.610	.615
0.4	.651	.650	.650	.651	.650	.645	.645	.645	.644	.645	.648
0.5	.685	.680	.680	.680	.680	.680	.680	.680	.678	.680	.680
0.6	.714	.711	.708	.707	.707	.707	.707	.708	.708	.707	.705
0.7	.735	.734	.733	.733	.733	.733	.733	.733	.732	.732	.731
0.8	.756	.756	.757	.757	.757	.757	.757	.757	.756	.756	.755
0.9	.779	.779	.780	.780	.780	.780	.780	.780	.779	.779	.778
1.0	.799	.799	.800	.800	.800	.800	.800	.800	.800	.799	.799
1.1	.816	.816	.817	.817	.817	.817	.817	.817	.817	.816	.816
1.2	.831	.831	.832	.832	.832	.832	.832	.832	.832	.831	.831
1.3	.843	.843	.844	.844	.844	.844	.844	.843	.843	.843	.842
1.4	.853	.853	.853	.853	.853	.853	.853	.852	.852	.852	.851
1.5	.865	.865	.865	.865	.865	.865	.865	.864	.864	.864	.863
1.6	.876	.876	.876	.876	.876	.876	.876	.875	.875	.875	.874
1.7	.887	.888	.888	.888	.888	.888	.888	.887	.887	.886	.885
1.8	.897	.898	.898	.898	.898	.898	.898	.897	.897	.896	.895
1.9	.906	.907	.907	.907	.907	.907	.907	.905	.906	.905	.904
2.0	.915	.915	.915	.915	.915	.915	.915	.914	.914	.914	.913
2.1	.923	.923	.923	.923	.923	.923	.923	.922	.922	.922	.921
2.2	.930	.930	.931	.931	.931	.931	.931	.931	.930	.930	.929
2.3	.934	.935	.935	.935	.935	.934	.934	.934	.934	.934	.933
2.4	.940	.940	.940	.940	.940	.940	.940	.939	.939	.939	.939
2.5	.945	.945	.945	.945	.945	.945	.945	.944	.945	.944	.944
2.6	.949	.950	.950	.950	.950	.950	.950	.949	.949	.949	.948
2.7	.953	.954	.954	.954	.954	.954	.954	.953	.953	.953	.953
2.8	.957	.958	.958	.958	.958	.958	.958	.957	.957	.957	.957
2.9	.961	.961	.962	.962	.961	.961	.961	.961	.961	.961	.960
3.0	.964	.965	.965	.965	.965	.964	.964	.964	.964	.964	.964
3.1	.967	.968	.968	.968	.968	.967	.967	.967	.967	.967	.967
3.2	.970	.970	.971	.970	.970	.970	.970	.970	.970	.970	.969
3.3	.972	.973	.973	.973	.973	.973	.973	.972	.972	.972	.972
3.4	.975	.975	.975	.975	.975	.975	.975	.974	.975	.975	.974
3.5	.977	.977	.977	.977	.977	.977	.977	.977	.977	.977	.976

Flow conditions: Pe = 1.9, X_{A_o} = 0.5

Axial Position, ζ = z/R	Radial Position, ξ = r/R										
	0.0	0.1	0.2	0.3	0.4	0.5	0.6	0.7	0.8	0.9	1.0
3.6	.979	.979	.979	.979	.979	.979	.979	.978	.979	.979	.978
3.7	.980	.981	.981	.981	.981	.981	.981	.980	.981	.981	.980
3.8	.982	.982	.983	.983	.982	.982	.982	.982	.982	.982	.982
3.9	.984	.984	.984	.984	.984	.984	.984	.983	.984	.984	.983
4.0	.985	.985	.985	.985	.985	.985	.985	.985	.985	.985	.985
4.1	.986	.986	.987	.987	.986	.986	.986	.986	.986	.986	.986
4.2	.987	.988	.988	.988	.988	.987	.987	.987	.987	.987	.987
4.3	.988	.989	.989	.989	.989	.988	.988	.988	.988	.988	.988
4.4	.989	.990	.990	.990	.990	.989	.989	.989	.989	.989	.989
4.5	.990	.990	.991	.991	.990	.990	.990	.990	.990	.990	.990
4.6	.991	.991	.991	.991	.991	.991	.991	.991	.991	.991	.991
4.7	.992	.992	.992	.992	.992	.992	.992	.992	.992	.992	.992
4.8	.992	.993	.993	.993	.993	.993	.993	.992	.993	.993	.992
4.9	.993	.993	.993	.993	.993	.993	.993	.993	.993	.993	.993
5.0	.994	.994	.994	.994	.994	.994	.994	.994	.994	.994	.994
5.1	.994	.994	.994	.994	.994	.994	.994	.994	.994	.994	.994
5.2	.995	.995	.995	.995	.995	.995	.995	.995	.995	.995	.995
5.3	.995	.995	.995	.995	.995	.995	.995	.995	.995	.995	.995
5.4	.996	.996	.996	.996	.996	.996	.996	.995	.996	.996	.995
5.5	.996	.996	.996	.996	.996	.996	.996	.996	.996	.996	.996
5.6	.996	.996	.996	.996	.996	.996	.996	.996	.996	.996	.996
5.7	.997	.997	.997	.997	.997	.997	.997	.996	.997	.997	.997
5.8	.997	.997	.997	.997	.997	.997	.997	.997	.997	.997	.997
5.9	.997	.997	.997	.997	.997	.997	.997	.997	.997	.997	.997
6.0	.997	.997	.997	.997	.997	.997	.997	.997	.997	.997	.997
6.1	.998	.998	.998	.998	.998	.998	.998	.998	.998	.998	.998
6.2	.998	.998	.998	.998	.998	.998	.998	.998	.998	.998	.998
6.3	.998	.998	.998	.998	.998	.998	.998	.998	.998	.998	.998
6.4	.998	.998	.998	.998	.998	.998	.998	.998	.998	.998	.998
6.5	.998	.998	.998	.998	.998	.998	.998	.998	.998	.998	.998
6.6	.998	.998	.999	.999	.998	.998	.998	.998	.998	.998	.998
6.7	.999	.999	.999	.999	.999	.999	.999	.999	.999	.999	.999
6.8	.999	.999	.999	.999	.999	.999	.999	.999	.999	.999	.999
6.9	.999	.999	.999	.999	.999	.999	.999	.999	.999	.999	.999
7.0	.999	.999	.999	.999	.999	.999	.999	.999	.999	.999	.999
7.1	.999	.999	.999	.999	.999	.999	.999	.999	.999	.999	.999
7.2	.999	.999	.999	.999	.999	.999	.999	.999	.999	.999	.999
7.3	.999	.999	.999	.999	.999	.999	.999	.999	.999	.999	.999
7.4	.999	.999	.999	.999	.999	.999	.999	.999	.999	.999	.999
7.5	.999	.999	.999	.999	.999	.999	.999	.999	.999	.999	.999

Flow conditions: Pe = 1.9, X_{A_o} = 0.5

Axial Position, ζ = z/R	Radial Position, ξ = r/R										
	0.0	0.1	0.2	0.3	0.4	0.5	0.6	0.7	0.8	0.9	1.0
7.6	.999	.999	.999	.999	.999	.999	.999	.999	.999	.999	.999
7.7	.999	.999	.999	.999	.999	.999	.999	.999	.999	.999	.999
7.8	.999	.999	.999	.999	.999	.999	.999	.999	.999	.999	.999
7.9	1.000	1.000	1.000	1.000	1.000	1.000	1.000	1.000	1.000	1.000	1.000

Flow conditions: Pe = 1.9, X_{A_o} = 0.5

Dimensionless mass average axial velocities in diffusion flow field (based on data from Stock (1972))

Values tabulated: $V(\xi,\zeta) = \frac{v(\xi,\zeta)}{\bar{V}_{A_o}}$

where $\bar{V}_{A_o}$ is the mass average velocity of nitrogen over flow cross sections far upstream of the helium injection plane.

$|\bar{V}_{A_o}|$ = 0.606 cm/sec for flow conditions under which the data listed below were taken.

R = 0.96 cm

Axial Position, ζ = z/R	Radial Position, ξ = r/R										
	0.0	0.1	0.2	0.3	0.4	0.5	0.6	0.7	0.8	0.9	1.0
0.0	.215	.380	.479	.628	.826	1.124	1.405	2.298	3.355	3.554	0
0.1	.298	.463	.512	.678	.843	1.140	1.405	2.149	3.058	3.223	0
0.2	.397	.512	.562	.661	.860	1.140	1.405	1.983	2.645	2.810	0
0.3	.463	.545	.628	.694	.876	1.140	1.388	1.950	2.562	2.612	0
0.4	.545	.612	.661	.744	.893	1.140	1.388	1.818	2.314	2.446	0
0.5	.628	.645	.694	.793	.909	1.140	1.388	1.785	2.149	2.231	0
0.6	.678	.678	.744	.810	.926	1.140	1.388	1.736	1.983	2.066	0
0.7	.744	.711	.760	.810	.942	1.140	1.372	1.719	1.868	1.901	0
0.8	.777	.760	.793	.810	.959	1.140	1.372	1.702	1.785	1.702	0
0.9	.810	.793	.810	.826	.975	1.157	1.355	1.653	1.736	1.620	0
1.0	.843	.843	.826	.860	.992	1.157	1.355	1.603	1.686	1.488	0
1.1	.866	.869	.856	.886	1.005	1.157	1.355	1.587	1.646	1.405	0
1.2	.889	.896	.886	.912	1.018	1.157	1.355	1.570	1.607	1.322	0
1.3	.912	.922	.916	.939	1.031	1.157	1.355	1.554	1.567	1.240	0
1.4	.936	.949	.945	.965	1.045	1.157	1.355	1.537	1.527	1.157	0
1.5	.959	.975	.975	.992	1.058	1.157	1.355	1.521	1.488	1.074	0
1.6	.975	1.002	.995	1.021	1.074	1.157	1.349	1.488	1.455	1.041	0
1.7	.992	1.028	1.015	1.051	1.091	1.157	1.342	1.455	1.421	1.008	0
1.8	1.008	1.055	1.035	1.081	1.107	1.157	1.336	1.421	1.388	.975	0
1.9	1.025	1.081	1.055	1.111	1.124	1.157	1.329	1.388	1.355	.942	0
2.0	1.041	1.107	1.074	1.140	1.140	1.157	1.322	1.355	1.322	.909	0
2.1	1.064	1.124	1.094	1.154	1.160	1.183	1.322	1.349	1.306	.886	0
2.2	1.088	1.140	1.114	1.167	1.180	1.210	1.322	1.342	1.289	.863	0
2.3	1.111	1.157	1.134	1.180	1.200	1.236	1.322	1.336	1.273	.840	0

Flow conditions: Pe = 1.9, X_{A_o} = 0.5

Axial Position, ζ = z/R	Radial Position, ξ = r/R										
	0.0	0.1	0.2	0.3	0.4	0.5	0.6	0.7	0.8	0.9	1.0
2.4	1.134	1.174	1.154	1.193	1.220	1.263	1.322	1.329	1.256	.817	0
2.5	1.157	1.190	1.174	1.207	1.240	1.289	1.322	.1322	1.240	.793	0
2.6	1.200	1.223	1.203	1.230	1.256	1.296	1.322	1.316	1.223	.767	0
2.7	1.243	1.256	1.233	1.253	1.273	1.302	1.322	1.309	1.207	.740	0
2.8	1.286	1.289	1.263	1.276	1.289	1.309	1.322	1.302	1.190	.714	0
2.9	1.329	1.322	1.293	1.299	1.306	1.316	1.322	1.296	1.174	.688	0
3.0	1.372	1.355	1.322	1.322	1.322	1.322	1.322	1.289	1.157	.661	0
3.1	1.421	1.382	1.355	1.345	1.339	1.332	1.322	1.269	1.124	.635	0
3.2	1.471	1.408	1.388	1.369	1.355	1.342	1.322	1.250	1.091	.608	0
3.3	1.521	1.435	1.421	1.392	1.372	1.352	1.322	1.230	1.058	.582	0
3.4	1.570	1.461	1.455	1.415	1.388	1.362	1.322	1.210	1.025	.555	0
3.5	1.620	1.488	1.488	1.438	1.405	1.372	1.322	1.190	.992	.529	0
3.6	1.633	1.521	1.511	1.464	1.421	1.379	1.316	1.174	.975	.522	0
3.7	1.646	1.554	1.534	1.491	1.438	1.385	1.309	1.157	.959	.516	0
3.8	1.660	1.587	1.557	1.517	1.455	1.392	1.302	1.140	.942	.509	0
3.9	1.673	1.620	1.580	1.544	1.471	1.398	1.296	1.124	.926	.502	0
4.0	1.686	1.653	1.603	1.570	1.488	1.405	1.289	1.107	.909	.496	0
4.1	1.729	1.693	1.646	1.587	1.504	1.425	1.288	1.089	.893	.473	0
4.2	1.772	1.732	1.689	1.603	1.521	1.443	1.286	1.073	.876	.450	0
4.3	1.815	1.772	1.732	1.620	1.537	1.463	1.283	1.055	.860	.426	0
4.4	1.858	1.812	1.775	1.636	1.554	1.481	1.281	1.038	.843	.403	0
4.5	1.901	1.851	1.818	1.653	1.570	1.501	1.279	1.020	.826	.380	0
4.6	1.921	1.878	1.838	1.686	1.592	1.501	1.279	1.020	.805	.380	0
4.7	1.940	1.902	1.860	1.719	1.613	1.501	1.279	1.020	.783	.380	0
4.8	1.960	1.929	1.879	1.754	1.636	1.501	1.279	1.020	.764	.380	0
4.9	1.980	1.954	1.901	1.787	1.658	1.501	1.279	1.020	.742	.380	0
5.0	2.000	1.980	1.921	1.820	1.679	1.501	1.279	1.020	.721	.380	0
5.1	2.000	1.980	1.921	1.820	1.679	1.501	1.279	1.020	.721	.380	0

Flow conditions: Pe = 3.8, X_{A_o} = 0.5

Temperatures in diffusion flow field, $(T - T_o)$, °C

where T_o is the reference temperature of the gases entering the diffusion tube.

T_o = 21.11°C R = 0.96 cm

NOTE: All values listed below are negative.

Axial Position, ζ = z/R	Radial Position, ξ = r/R										
	0.0	0.1	0.2	0.3	0.4	0.5	0.6	0.7	0.8	0.9	1.0
0.0	.59	.58	.56	.54	.52	.50	.46	.43	.38	.33	.26
0.1	1.64	1.63	1.60	1.55	1.47	1.37	1.25	1.12	.97	.79	.58
0.2	2.64	2.63	2.58	2.50	2.37	2.23	2.05	1.81	1.55	1.25	.85
0.3	3.46	3.44	3.38	3.29	3.16	2.98	2.71	2.39	2.02	1.59	1.04
0.4	3.89	3.86	3.81	3.73	3.59	3.40	3.13	2.76	2.32	1.78	1.12
0.5	3.96	3.94	3.89	3.81	3.67	3.48	3.21	2.83	2.38	1.81	1.14
0.6	3.77	3.75	3.69	3.61	3.47	3.28	3.01	2.66	2.24	1.72	1.10
0.7	3.42	3.40	3.34	3.24	3.11	2.94	2.67	2.35	1.99	1.57	1.03
0.8	2.99	2.97	2.92	2.83	2.70	2.55	2.33	2.06	1.75	1.39	.93
0.9	2.55	2.54	2.49	2.41	2.28	2.14	1.98	1.75	1.50	1.21	.83
1.0	2.12	2.11	2.07	2.00	1.90	1.77	1.63	1.45	1.25	1.01	.71
1.1	1.75	1.74	1.71	1.65	1.56	1.45	1.33	1.19	1.03	.84	.61
1.2	1.41	1.40	1.37	1.33	1.27	1.19	1.09	.98	.85	.70	.52
1.3	1.14	1.13	1.11	1.08	1.03	.98	.91	.81	.71	.60	.45
1.4	.92	.91	.89	.87	.83	.79	.73	.66	.58	.50	.38
1.5	.73	.72	.70	.68	.65	.62	.58	.53	.47	.41	.32
1.6	.58	.57	.56	.54	.52	.49	.46	.42	.38	.33	.25
1.7	.46	.46	.45	.43	.41	.39	.36	.34	.30	.26	.20
1.8	.37	.36	.35	.34	.33	.31	.29	.26	.23	.20	.16
1.9	.28	.28	.27	.26	.25	.24	.22	.20	.18	.16	.12
2.0	.22	.21	.21	.20	.19	.18	.17	.15	.14	.12	.09
2.1	.16	.16	.16	.15	.14	.14	.13	.12	.10	.09	.06
2.2	.12	.11	.11	.11	.10	.10	.09	.08	.07	.06	.04
2.3	.08	.08	.07	.07	.07	.06	.06	.05	.04	.04	.02
2.4	.04	.04	.04	.04	.04	.03	.03	.03	.02	.02	.01
2.5	.01	.01	.01	.01	.01	.01	.00	.00	.00	.00	.00

Flow conditions: Pe = 3.8, X_{A_o} = 0.5

Mole fractions of nitrogen in diffusion flow field (based on data from Stock (1972))

R = 0.96 cm

Axial Position, ζ = z/R	Radial Position, ξ = r/R										
	0.0	0.1	0.2	0.3	0.4	0.5	0.6	0.7	0.8	0.9	1.0
0.0	.500	.500	.500	.500	.500	.500	.500	.500	.500	.500	.500
0.1	.595	.585	.554	.554	.558	.549	.542	.526	.509	.531	.546
0.2	.652	.643	.628	.628	.628	.621	.615	.606	.597	.607	.614
0.3	.699	.693	.688	.688	.687	.683	.678	.673	.668	.670	.671
0.4	.736	.735	.734	.734	.735	.735	.731	.727	.722	.720	.717
0.5	.775	.776	.776	.776	.778	.779	.777	.774	.769	.766	.762
0.6	.815	.815	.815	.815	.816	.816	.816	.814	.810	.808	.806
0.7	.845	.845	.845	.845	.846	.846	.846	.845	.842	.840	.839
0.8	.869	.869	.869	.869	.869	.869	.868	.867	.866	.865	.864
0.9	.891	.891	.891	.891	.891	.891	.890	.889	.888	.887	.887
1.0	.911	.911	.911	.911	.910	.910	.909	.908	.907	.906	.905
1.1	.927	.927	.927	.927	.925	.925	.924	.923	.922	.921	.920
1.2	.939	.939	.939	.939	.938	.938	.937	.936	.935	.934	.933
1.3	.948	.948	.948	.948	.946	.946	.945	.944	.943	.942	.941
1.4	.954	.954	.953	.953	.952	.952	.951	.950	.949	.948	.947
1.5	.962	.962	.961	.961	.960	.960	.960	.959	.958	.957	.956
1.6	.969	.969	.968	.968	.967	.967	.967	.966	.965	.964	.963
1.7	.975	.975	.974	.974	.973	.973	.973	.972	.971	.970	.969
1.8	.979	.979	.978	.978	.977	.977	.977	.976	.975	.974	.974
1.9	.983	.983	.982	.982	.981	.981	.981	.980	.979	.978	.978
2.0	.985	.985	.985	.985	.984	.984	.984	.983	.982	.982	.981
2.1	.988	.988	.987	.987	.986	.986	.986	.986	.985	.984	.984
2.2	.990	.990	.989	.989	.989	.989	.988	.988	.987	.987	.987
2.3	.991	.991	.991	.991	.990	.990	.990	.990	.989	.989	.989
2.4	.993	.993	.992	.992	.992	.992	.992	.991	.991	.991	.990
2.5	.994	.994	.994	.994	.993	.993	.993	.993	.992	.992	.992
2.6	.995	.995	.995	.995	.994	.994	.994	.994	.994	.993	.993
2.7	.996	.996	.996	.996	.995	.995	.995	.995	.995	.994	.994
2.8	.997	.997	.996	.996	.996	.996	.996	.996	.995	.995	.995
2.9	.997	.997	.997	.997	.997	.997	.997	.996	.996	.996	.996
3.0	.998	.998	.997	.997	.997	.997	.997	.997	.997	.997	.996
3.1	.998	.998	.998	.998	.998	.998	.998	.997	.997	.997	.997
3.2	.998	.998	.998	.998	.998	.998	.998	.998	.998	.998	.997
3.3	.999	.999	.998	.998	.998	.998	.998	.998	.998	.998	.998
3.4	.999	.999	.999	.999	.999	.999	.999	.998	.998	.998	.998
3.5	.999	.999	.999	.999	.999	.999	.999	.999	.999	.998	.998

Flow conditions: Pe = 3.8, X_{A_o} = 0.5

Axial Position, ζ = z/R	Radial Position, ξ = r/R										
	0.0	0.1	0.2	0.3	0.4	0.5	0.6	0.7	0.8	0.9	1.0
3.6	.999	.999	.999	.999	.999	.999	.999	.999	.999	.999	.999
3.7	.999	.999	.999	.999	.999	.999	.999	.999	.999	.999	.999
3.8	.999	.999	.999	.999	.999	.999	.999	.999	.999	.999	.999
3.9	1.000	1.000	.999	.999	.999	.999	.999	.999	.999	.999	.999
4.0	1.000	1.000	1.000	1.000	.999	.999	.999	.999	.999	.999	.999
4.1	1.000	1.000	1.000	1.000	1.000	1.000	1.000	1.000	.999	.999	.999
4.2	1.000	1.000	1.000	1.000	1.000	1.000	1.000	1.000	1.000	1.000	1.000

Flow conditions: Pe = 3.8, X_{A_o} = 0.5

Dimensionless mass average axial velocities in diffusion flow field (based on data from Stock (1972))

Values tabulated: $V(\xi,\zeta) = \frac{v(\xi,\zeta)}{\bar{V}_{A_o}}$

where $\bar{V}_{A_o}$ is the mass average velocity of nitrogen over flow cross sections far upstream of the helium injection plane.

$|\bar{V}_{A_o}|$ = 1.186 cm/sec for flow conditions under which the data listed below were taken.

R = 0.96 cm

Axial Position, ζ = z/R	Radial Position, ξ = r/R										
	0.0	0.1	0.2	0.3	0.4	0.5	0.6	0.7	0.8	0.9	1.0
0.0	.371	.440	.338	.531	.692	1.172	1.500	2.850	3.200	3.090	0
0.1	.441	.470	.430	.566	.715	1.093	1.500	2.610	3.074	2.749	0
0.2	.506	.506	.514	.607	.742	1.045	1.500	2.250	2.570	2.420	0
0.3	.573	.548	.590	.632	.775	1.079	1.500	1.980	2.179	2.104	0
0.4	.624	.598	.657	.708	.809	1.045	1.500	1.800	1.900	1.800	0
0.5	.677	.654	.716	.768	.849	1.093	1.500	1.710	1.734	1.509	0
0.6	.725	.716	.767	.834	.893	1.172	1.500	1.710	1.680	1.230	0
0.7	.782	.775	.825	.878	.932	1.197	1.488	1.672	1.592	1.072	0
0.8	.843	.834	.885	.910	.969	1.197	1.467	1.640	1.520	1.000	0
0.9	.896	.884	.944	.961	1.007	1.216	1.456	1.594	1.429	.889	0
1.0	.944	.927	1.003	1.020	1.045	1.239	1.450	1.540	1.330	.780	0
1.1	.999	.982	1.060	1.066	1.085	1.250	1.440	1.504	1.266	.743	0
1.2	1.054	1.039	1.114	1.115	1.128	1.268	1.433	1.472	1.213	.717	0
1.3	1.109	1.100	1.165	1.167	1.174	1.292	1.431	1.444	1.171	.703	0
1.4	1.163	1.163	1.214	1.222	1.222	1.323	1.433	1.420	1.140	.700	0
1.5	1.213	1.211	1.260	1.264	1.258	1.326	1.428	1.371	1.083	.656	0
1.6	1.264	1.264	1.306	1.306	1.298	1.340	1.424	1.323	1.028	.611	0
1.7	1.313	1.325	1.355	1.349	1.347	1.369	1.421	1.272	.969	.560	0
1.8	1.365	1.382	1.399	1.391	1.391	1.399	1.416	1.231	.922	.521	0
1.9	1.419	1.435	1.439	1.433	1.431	1.428	1.409	1.200	.886	.494	0
2.0	1.475	1.483	1.475	1.475	1.467	1.458	1.399	1.180	.860	.480	0
2.1	1.526	1.530	1.511	1.514	1.501	1.484	1.391	1.157	.832	.462	0
2.2	1.576	1.574	1.545	1.551	1.533	1.508	1.382	1.137	.808	.447	0
2.3	1.622	1.616	1.577	1.585	1.562	1.529	1.375	1.118	.786	.432	0

Flow conditions: Pe = 3.8, X_{A_o} = 0.5

Axial Position, ζ = z/R	Radial Position, ξ = r/R										
	0.0	0.1	0.2	0.3	0.4	0.5	0.6	0.7	0.8	0.9	1.0
2.4	1.666	1.656	1.608	1.617	1.589	1.548	1.367	1.100	.765	.419	0
2.5	1.707	1.694	1.638	1.647	1.614	1.565	1.359	1.084	.747	.407	0
2.6	1.745	1.729	1.666	1.675	1.636	1.579	1.352	1.070	.730	.396	0
2.7	1.781	1.762	1.693	1.700	1.655	1.591	1.346	1.056	.716	.387	0
2.8	1.814	1.792	1.718	1.723	1.673	1.600	1.339	1.044	.703	.379	0
2.9	1.845	1.821	1.743	1.744	1.688	1.607	1.333	1.034	.692	.371	0
3.0	1.872	1.846	1.765	1.763	1.700	1.611	1.327	1.025	.684	.366	0
3.1	1.897	1.870	1.786	1.780	1.710	1.613	1.321	1.017	.677	.361	0
3.2	1.920	1.891	1.806	1.794	1.718	1.613	1.316	1.011	.673	.357	0
3.3	1.939	1.911	1.824	1.806	1.723	1.610	1.311	1.007	.670	.355	0
3.4	1.956	1.927	1.841	1.815	1.726	1.605	1.306	1.003	.669	.354	0
3.5	1.971	1.942	1.857	1.823	1.727	1.597	1.301	1.001	.671	.354	0
3.6	1.982	1.954	1.871	1.828	1.725	1.587	1.297	1.001	.674	.355	0
3.7	1.991	1.964	1.884	1.831	1.721	1.574	1.293	1.002	.679	.358	0
3.8	1.997	1.971	1.895	1.831	1.714	1.559	1.289	1.004	.686	.362	0
3.9	2.001	1.976	1.905	1.830	1.705	1.542	1.286	1.008	.696	.367	0
4.0	2.000	1.980	1.920	1.820	1.680	1.500	1.280	1.020	.720	.380	0
4.1	2.000	1.980	1.920	1.820	1.680	1.500	1.280	1.020	.720	.380	0

Flow conditions: Pe = 3.8, X_{A_o} = 0.7

Temperatures in diffusion flow field, $(T - T_o)$, °C

where T_o is the reference temperature of the gases entering the diffusion tube.

T_o = 21.11°C R = 0.96 cm

NOTE: All values listed below are negative.

Axial Position, ζ = z/R	Radial Position, ξ = r/R										
	0.0	0.1	0.2	0.3	0.4	0.5	0.6	0.7	0.8	0.9	1.0
0.0	.59	.59	.57	.55	.52	.49	.44	.38	.30	.22	.12
0.1	1.54	1.53	1.50	1.46	1.39	1.30	1.17	1.02	.84	.64	.40
0.2	2.17	2.15	2.12	2.07	1.98	1.85	1.68	1.46	1.21	.90	.55
0.3	2.50	2.50	2.48	2.42	2.33	2.20	2.02	1.77	1.46	1.07	.66
0.4	2.58	2.57	2.56	2.49	2.41	2.28	2.10	1.84	1.51	1.11	.68
0.5	2.45	2.44	2.42	2.36	2.27	2.14	1.96	1.72	1.42	1.04	.64
0.6	2.19	2.17	2.15	2.09	2.00	1.87	1.70	1.49	1.23	.92	.56
0.7	1.90	1.89	1.86	1.81	1.72	1.61	1.46	1.28	1.05	.79	.49
0.8	1.60	1.59	1.56	1.52	1.44	1.35	1.22	1.07	.88	.67	.42
0.9	1.34	1.33	1.30	1.26	1.20	1.12	1.01	.88	.72	.54	.34
1.0	1.10	1.08	1.06	1.03	.97	.90	.81	.70	.57	.42	.26
1.1	.88	.87	.85	.83	.78	.73	.65	.56	.45	.34	.20
1.2	.68	.68	.66	.64	.61	.57	.51	.44	.35	.26	.15
1.3	.54	.53	.52	.50	.48	.45	.40	.34	.27	.20	.10
1.4	.42	.42	.41	.39	.37	.35	.31	.26	.21	.15	.07
1.5	.31	.31	.30	.29	.27	.25	.23	.19	.15	.11	.05
1.6	.22	.22	.22	.21	.20	.18	.17	.14	.11	.07	.03
1.7	.16	.16	.15	.15	.14	.13	.11	.09	.07	.05	.02
1.8	.10	.10	.10	.09	.09	.08	.07	.06	.04	.03	.00
1.9	.05	.05	.05	.05	.05	.04	.04	.03	.02	.01	.00
2.0	.02	.02	.02	.02	.01	.01	.01	.00	.00	.00	.00

Flow conditions: Pe = 3.8, X_{A_o} = 0.7

Mole fractions of nitrogen in diffusion flow field (based on data from Stock (1972))

R = 0.96 cm

Axial Position, ζ = z/R	Radial Position, ξ = r/R										
	0.0	0.1	0.2	0.3	0.4	0.5	0.6	0.7	0.8	0.9	1.0
0.0	.698	.698	.698	.698	.698	.698	.698	.698	.698	.698	.698
0.1	.755	.752	.750	.749	.749	.746	.745	.741	.740	.740	.741
0.2	.800	.795	.793	.792	.791	.788	.786	.780	.778	.778	.779
0.3	.827	.824	.824	.823	.823	.822	.820	.816	.813	.813	.814
0.4	.852	.851	.851	.851	.851	.851	.849	.846	.844	.843	.843
0.5	.875	.875	.875	.875	.875	.874	.872	.871	.870	.868	.866
0.6	.893	.893	.893	.893	.893	.893	.893	.892	.890	.887	.886
0.7	.910	.910	.910	.910	.910	.910	.911	.910	.908	.905	.905
0.8	.927	.926	.926	.926	.926	.926	.926	.925	.924	.923	.922
0.9	.940	.939	.939	.939	.939	.939	.938	.937	.937	.936	.935
1.0	.949	.949	.949	.949	.948	.948	.948	.947	.946	.945	.944
1.1	.957	.957	.957	.957	.956	.956	.956	.956	.954	.953	.952
1.2	.964	.964	.964	.964	.963	.963	.964	.963	.962	.960	.960
1.3	.969	.970	.970	.970	.969	.969	.969	.969	.968	.966	.966
1.4	.974	.974	.974	.974	.974	.974	.974	.974	.973	.972	.972
1.5	.979	.979	.979	.979	.978	.978	.978	.978	.977	.976	.976
1.6	.984	.984	.983	.983	.982	.982	.982	.981	.981	.980	.979
1.7	.987	.987	.986	.985	.985	.985	.985	.983	.984	.983	.982
1.8	.987	.987	.987	.986	.986	.986	.986	.985	.985	.984	.984
1.9	.989	.989	.989	.988	.988	.988	.988	.987	.987	.986	.986
2.0	.991	.991	.991	.991	.991	.991	.991	.990	.990	.989	.989
2.1	.993	.993	.993	.992	.992	.992	.992	.991	.991	.991	.991
2.2	.994	.994	.994	.993	.993	.993	.993	.993	.993	.992	.992
2.3	.995	.995	.995	.995	.994	.994	.994	.994	.994	.993	.993
2.4	.996	.996	.996	.995	.995	.995	.995	.995	.995	.994	.994
2.5	.997	.997	.996	.996	.996	.996	.996	.996	.996	.995	.995
2.6	.997	.997	.997	.997	.997	.997	.997	.996	.996	.996	.996
2.7	.998	.998	.997	.997	.997	.997	.997	.997	.997	.997	.996
2.8	.998	.998	.998	.998	.998	.998	.998	.997	.997	.997	.997
2.9	.998	.998	.998	.998	.998	.998	.998	.998	.998	.998	.997
3.0	.999	.999	.999	.998	.998	.998	.998	.998	.998	.998	.998
3.1	.999	.999	.999	.999	.999	.999	.999	.998	.998	.998	.998
3.2	.999	.999	.999	.999	.999	.999	.999	.999	.999	.998	.998
3.3	.999	.999	.999	.999	.999	.999	.999	.999	.999	.999	.999
3.4	.999	.999	.999	.999	.999	.999	.999	.999	.999	.999	.999
3.5	.999	.999	.999	.999	.999	.999	.999	.999	.999	.999	.999

Flow conditions: Pe = 3.8, X_{A_o} = 0.7

Axial Position, ζ = z/R	Radial Position, ξ = r/R										
	0.0	0.1	0.2	0.3	0.4	0.5	0.6	0.7	0.8	0.9	1.0
3.6	1.000	1.000	.999	.999	.999	.999	.999	.999	.999	.999	.999
3.7	1.000	1.000	1.000	1.000	.999	.999	.999	.999	.999	.999	.999
3.8	1.000	1.000	1.000	1.000	1.000	1.000	1.000	.999	.999	.999	.999
3.9	1.000	1.000	1.000	1.000	1.000	1.000	1.000	1.000	1.000	1.000	1.000

Flow conditions: Pe = 3.8, X_{A_o} = 0.7

Dimensionless mass average axial velocities in diffusion flow field (based on data from Stock (1972))

Values tabulated: $V(\xi,\zeta) = \frac{v(\xi,\zeta)}{\bar{V}_{A_o}}$

where $\bar{V}_{A_o}$ is the mass average velocity of nitrogen over flow cross sections far upstream of the helium injection plane.

$|\bar{V}_{A_o}|$ = 1.186 cm/sec for flow conditions under which the data listed below were taken.

R = 0.96 cm

Axial Position, ζ = z/R	Radial Position, ξ = r/R										
	0.0	0.1	0.2	0.3	0.4	0.5	0.6	0.7	0.8	0.9	1.0
0.0	.321	.377	.409	.425	.498	.658	1.003	1.920	2.180	2.220	0
0.1	.425	.433	.490	.490	.578	.722	1.027	1.722	2.040	2.100	0
0.2	.498	.506	.562	.570	.650	.787	1.043	1.557	1.940	2.000	0
0.3	.562	.562	.642	.642	.714	.819	1.059	1.429	1.837	1.862	0
0.4	.642	.642	.714	.714	.770	.875	1.075	1.338	1.670	1.660	0
0.5	.722	.722	.787	.787	.819	.915	1.091	1.317	1.578	1.529	0
0.6	.803	.803	.827	.851	.883	.971	1.116	1.296	1.490	1.406	0
0.7	.875	.875	.883	.915	.947	1.027	1.140	1.276	1.408	1.289	0
0.8	.939	.931	.947	.979	1.011	1.059	1.156	1.257	1.330	1.179	0
0.9	1.011	.971	.987	1.035	1.059	1.108	1.172	1.239	1.256	1.077	0
1.0	1.051	1.027	1.051	1.083	1.116	1.140	1.196	1.221	1.188	.981	0
1.1	1.124	1.100	1.108	1.140	1.164	1.188	1.204	1.205	1.124	.893	0
1.2	1.180	1.172	1.164	1.204	1.204	1.212	1.220	1.188	1.064	.812	0
1.3	1.220	1.220	1.212	1.236	1.236	1.252	1.228	1.173	1.008	.738	0
1.4	1.284	1.276	1.268	1.284	1.284	1.276	1.252	1.159	.956	.672	0
1.5	1.348	1.308	1.300	1.340	1.340	1.308	1.276	1.145	.909	.613	0
1.6	1.396	1.364	1.356	1.364	1.380	1.348	1.284	1.131	.867	.561	0
1.7	1.445	1.429	1.388	1.429	1.413	1.372	1.300	1.119	.831	.515	0
1.8	1.493	1.453	1.445	1.445	1.445	1.404	1.324	1.107	.799	.476	0
1.9	1.533	1.509	1.477	1.501	1.461	1.437	1.348	1.096	.772	.444	0
2.0	1.573	1.533	1.509	1.525	1.509	1.445	1.356	1.086	.751	.418	0
2.1	1.685	1.589	1.549	1.549	1.525	1.469	1.372	1.076	.735	.399	0
2.2	1.669	1.637	1.589	1.589	1.557	1.493	1.388	1.067	.725	.386	0
2.3	1.685	1.677	1.613	1.605	1.589	1.500	1.404	1.059	.720	.380	0

Flow conditions: Pe = 3.8, X_{A_o} = 0.7

Axial Position, ζ = z/R	Radial Position, ξ = r/R										
	0.0	0.1	0.2	0.3	0.4	0.5	0.6	0.7	0.8	0.9	1.0
2.4	1.709	1.701	1.653	1.621	1.605	1.500	1.437	1.051	.720	.380	0
2.5	1.734	1.726	1.685	1.653	1.621	1.500	1.445	1.043	.720	.380	0
2.6	1.758	1.758	1.717	1.685	1.637	1.500	1.453	1.043	.720	.380	0
2.7	1.774	1.774	1.742	1.701	1.653	1.500	1.469	1.035	.720	.380	0
2.8	1.790	1.782	1.758	1.734	1.669	1.500	1.501	1.035	.720	.380	0
2.9	1.806	1.798	1.766	1.750	1.669	1.500	1.517	1.035	.720	.380	0
3.0	1.814	1.814	1.782	1.766	1.680	1.500	1.525	1.027	.720	.380	0
3.1	1.830	1.838	1.790	1.774	1.680	1.500	1.541	1.027	.720	.380	0
3.2	1.846	1.854	1.814	1.782	1.680	1.500	1.589	1.020	.720	.380	0
3.3	1.862	1.862	1.830	1.798	1.680	1.500	1.597	1.020	.720	.380	0
3.4	1.886	1.886	1.846	1.806	1.680	1.500	1.605	1.020	.720	.380	0
3.5	1.910	1.910	1.854	1.814	1.680	1.500	1.605	1.020	.720	.380	0
3.6	1.918	1.918	1.862	1.820	1.680	1.500	1.605	1.020	.720	.380	0
3.7	1.934	1.926	1.894	1.820	1.680	1.500	1.597	1.020	.720	.380	0
3.8	1.958	1.934	1.902	1.820	1.680	1.500	1.589	1.020	.720	.380	0
3.9	1.974	1.950	1.910	1.820	1.680	1.500	1.581	1.020	.720	.380	0
4.0	1.982	1.958	1.910	1.820	1.680	1.500	1.565	1.020	.720	.380	0
4.1	1.990	1.966	1.920	1.820	1.680	1.500	1.541	1.020	.720	.380	0
4.2	1.990	1.980	1.920	1.820	1.680	1.500	1.525	1.020	.720	.380	0
4.3	2.000	1.980	1.920	1.820	1.680	1.500	1.509	1.020	.720	.380	0
4.4	2.000	1.980	1.920	1.820	1.680	1.500	1.461	1.020	.720	.380	0
4.5	2.000	1.980	1.920	1.820	1.680	1.500	1.437	1.020	.720	.380	0
4.6	2.000	1.980	1.920	1.820	1.680	1.500	1.396	1.020	.720	.380	0
4.7	2.000	1.980	1.920	1.820	1.680	1.500	1.372	1.020	.720	.380	0
4.8	2.000	1.980	1.920	1.820	1.680	1.500	1.356	1.020	.720	.380	0
4.9	2.000	1.980	1.920	1.820	1.680	1.500	1.348	1.020	.720	.380	0
5.0	2.000	1.980	1.920	1.820	1.680	1.500	1.324	1.020	.720	.380	0
5.1	2.000	1.980	1.920	1.820	1.680	1.500	1.308	1.020	.720	.380	0
5.2	2.000	1.980	1.920	1.820	1.680	1.500	1.292	1.020	.720	.380	0
5.3	2.000	1.980	1.920	1.820	1.680	1.500	1.284	1.020	.720	.380	0
5.4	2.000	1.980	1.920	1.820	1.680	1.500	1.280	1.020	.720	.380	0

Flow conditions: Pe = 5.9, X_{A_o} = 0.7

Temperatures in diffusion flow field, $(T - T_o)$, °C

where T_o is the reference temperature of the gases entering the diffusion tube.

T_o = 21.11°C R = 0.96 cm

NOTE: All values listed below are negative.

Axial Position, ζ = z/R	Radial Position, ξ = r/R										
	0.0	0.1	0.2	0.3	0.4	0.5	0.6	0.7	0.8	0.9	1.0
0.0	1.37	1.36	1.34	1.31	1.27	1.21	1.12	.99	.82	.62	.32
0.1	2.36	2.34	2.32	2.28	2.21	2.12	1.97	1.76	1.46	1.11	.60
0.2	2.86	2.85	2.82	2.78	2.71	2.60	2.42	2.15	1.80	1.35	.74
0.3	2.89	2.88	2.84	2.81	2.73	2.62	2.45	2.17	1.82	1.36	.75
0.4	2.54	2.52	2.50	2.47	2.39	2.31	2.14	1.92	1.60	1.21	.66
0.5	2.05	2.03	2.00	1.96	1.90	1.81	1.68	1.49	1.23	.93	.50
0.6	1.57	1.55	1.54	1.50	1.45	1.39	1.29	1.14	.94	.71	.37
0.7	1.12	1.12	1.11	1.08	1.05	1.00	.93	.81	.68	.51	.26
0.8	.80	.79	.78	.77	.75	.71	.66	.57	.47	.34	.15
0.9	.54	.54	.53	.53	.51	.49	.45	.39	.31	.22	.07
1.0	.37	.37	.36	.35	.35	.33	.30	.26	.20	.14	.04
1.1	.22	.22	.22	.22	.21	.20	.18	.16	.12	.08	.02
1.2	.12	.12	1.2	1.2	.11	.11	.10	.08	.06	.04	.00
1.3	.05	.05	.05	.05	.05	.04	.04	.03	.02	.01	.00

Flow conditions: Pe = 5.9, X_{A_o} = 0.7

Mole fractions of nitrogen in diffusion flow field (based on data from Stock (1972))

R = 0.96 cm

Axial Position, ζ = z/R	Radial Position, ξ = r/R										
	0.0	0.1	0.2	0.3	0.4	0.5	0.6	0.7	0.8	0.9	1.0
0.0	.700	.700	.700	.700	.700	.700	.700	.700	.700	.700	.700
0.1	.781	.771	.765	.763	.764	.762	.756	.748	.740	.742	.752
0.2	.839	.828	.821	.818	.819	.816	.808	.799	.789	.790	.799
0.3	.874	.870	.868	.866	.866	.863	.857	.852	.846	.843	.842
0.4	.903	.903	.902	.900	.897	.894	.891	.886	.881	.878	.877
0.5	.927	.928	.928	.926	.922	.919	.918	.913	.909	.907	.905
0.6	.945	.945	.945	.943	.941	.939	.937	.934	.931	.929	.927
0.7	.960	.960	.959	.958	.956	.955	.953	.951	.948	.947	.944
0.8	.971	.970	.969	.968	.967	.966	.965	.963	.961	.959	.957
0.9	.979	.978	.977	.976	.975	.975	.974	.972	.971	.969	.967
1.0	.984	.983	.983	.982	.981	.980	.979	.978	.977	.975	.974
1.1	.989	.988	.989	.988	.987	.986	.985	.984	.983	.981	.981
1.2	.993	.993	.993	.992	.991	.990	.989	.989	.989	.987	.987
1.3	.997	.996	.997	.996	.995	.994	.993	.993	.993	.991	.991
1.4	.999	.999	.999	.999	.998	.997	.996	.996	.996	.995	.995
1.5	.999	.999	.999	.999	.999	.999	.998	.998	.998	.997	.997
1.6	.999	.999	.999	.999	.999	.999	.999	.999	.999	.998	.998
1.7	.999	.999	.999	.999	.999	.999	.999	.999	.999	.998	.998
1.8	.999	.999	.999	.999	.999	.999	.999	.999	.998	.998	.999
1.9	.999	.999	.999	.999	.999	.999	.999	.999	.999	.999	.999
2.0	1.000	1.000	1.000	1.000	1.000	1.000	1.000	1.000	.999	.999	.999
2.1	1.000	1.000	1.000	1.000	1.000	1.000	1.000	1.000	1.000	1.000	1.000

Flow conditions: Pe = 5.9, X_{A_o} = 0.7

Dimensionless mass average axial velocities in diffusion flow field (based on data from Stock (1972))

Values tabulated: $V(\xi,\zeta) = \frac{v(\xi,\zeta)}{\bar{V}_{A_o}}$

where $\bar{V}_{A_o}$ is the mass average velocity of nitrogen over flow cross sections far upstream of the helium injection plane.

$|\bar{V}_{A_o}|$ = 1.863 cm/sec for flow conditions under which the data listed below were taken.

R = 0.96 cm

Axial Position, ζ = z/R	Radial Position, ξ = r/R										
	0.0	0.1	0.2	0.3	0.4	0.5	0.6	0.7	0.8	0.9	1.0
0.0	.295	.365	.429	.429	.429	.564	1.020	1.879	2.415	2.523	0
0.1	.403	.483	.564	.564	.564	.778	1.057	1.664	2.067	2.120	0
0.2	.537	.590	.671	.682	.698	.886	1.084	1.422	1.852	1.932	0
0.3	.698	.751	.805	.805	.832	.966	1.111	1.369	1.664	1.610	0
0.4	.859	.870	.913	.918	.955	1.047	1.138	1.315	1.476	1.396	0
0.5	.993	1.004	1.031	1.036	1.063	1.095	1.154	1.261	1.288	1.192	0
0.6	1.127	1.127	1.138	1.143	1.154	1.159	1.170	1.208	1.181	1.047	0
0.7	1.235	1.235	1.235	1.235	1.235	1.208	1.197	1.170	1.074	.913	0
0.8	1.342	1.363	1.326	1.320	1.315	1.278	1.218	1.138	1.020	.805	0
0.9	1.422	1.422	1.422	1.422	1.369	1.315	1.245	1.111	.955	.709	0
1.0	1.503	1.519	1.503	1.476	1.422	1.353	1.261	1.100	.913	.671	0
1.1	1.578	1.593	1.565	1.532	1.471	1.391	1.280	1.084	.870	.603	0
1.2	1.644	1.656	1.617	1.579	1.510	1.426	1.297	1.074	.837	.549	0
1.3	1.700	1.710	1.658	1.614	1.543	1.456	1.313	1.068	.816	.506	0
1.4	1.749	1.754	1.688	1.639	1.567	1.481	1.328	1.068	.811	.475	0
1.5	1.787	1.787	1.707	1.653	1.583	1.503	1.342	1.074	.805	.456	0
1.6	1.824	1.815	1.734	1.678	1.604	1.508	1.352	1.069	.790	.433	0
1.7	1.855	1.833	1.757	1.700	1.621	1.517	1.359	1.066	.777	.415	0
1.8	1.878	1.843	1.775	1.718	1.634	1.523	1.364	1.063	.767	.405	0
1.9	1.895	1.844	1.789	1.733	1.643	1.524	1.368	1.060	.758	.404	0
2.0	1.906	1.836	1.798	1.744	1.648	1.530	1.369	1.057	.751	.403	0
2.1	1.910	1.843	1.812	1.755	1.657	1.535	1.371	1.053	.749	.396	0
2.2	1.914	1.849	1.824	1.763	1.665	1.541	1.372	1.048	.747	.392	0
2.3	1.917	1.855	1.835	1.768	1.671	1.546	1.372	1.042	.745	.390	0

Flow conditions: Pe = 5.9, X_{A_o} = 0.7

Axial Position, ζ = z/R	Radial Position, ξ = r/R										
	0.0	0.1	0.2	0.3	0.4	0.5	0.6	0.7	0.8	0.9	1.0
2.4	1.919	1.858	1.843	1.770	1.675	1.553	1.374	1.035	.743	.389	0
2.5	1.922	1.863	1.852	1.771	1.680	1.557	1.369	1.031	.741	.386	0
2.6	1.924	1.867	1.859	1.779	1.684	1.559	1.361	1.027	.738	.384	0
2.7	1.926	1.870	1.866	1.786	1.687	1.560	1.351	1.024	.734	.383	0
2.8	1.929	1.873	1.871	1.795	1.689	1.560	1.338	1.022	.729	.382	0
2.9	1.931	1.877	1.875	1.805	1.690	1.559	1.323	1.021	.725	.381	0
3.0	1.932	1.879	1.879	1.814	1.691	1.557	1.304	1.020	.720	.381	0
3.1	1.938	1.884	1.887	1.814	1.691	1.551	1.299	1.020	.720	.381	0
3.2	1.943	1.889	1.896	1.814	1.691	1.546	1.294	1.020	.720	.381	0
3.3	1.948	1.895	1.904	1.814	1.691	1.541	1.288	1.020	.720	.381	0
3.4	1.954	1.900	1.904	1.814	1.691	1.535	1.288	1.020	.720	.381	0
3.5	1.959	1.906	1.905	1.814	1.691	1.530	1.288	1.020	.720	.380	0
3.6	1.967	1.921	1.906	1.816	1.689	1.524	1.288	1.020	.720	.380	0
3.7	1.974	1.936	1.908	1.817	1.687	1.516	1.288	1.020	.720	.380	0
3.8	1.982	1.951	1.908	1.818	1.684	1.511	1.288	1.020	.720	.380	0
3.9	1.989	1.966	1.914	1.819	1.682	1.506	1.288	1.020	.720	.380	0
4.0	2.000	1.980	1.920	1.820	1.680	1.500	1.280	1.020	.720	.380	0
4.1	2.000	1.980	1.920	1.820	1.680	1.500	1.280	1.020	.720	.380	0

Appendix J. MOLECULAR DIFFUSION COEFFICIENTS AND THERMAL DIFFUSION FACTORS COMPUTED FROM DATA TABULATED IN APPENDIX H

NOTE: All computed values listed in this appendix are average values over diffusion tube cross sections at axial locations upstream of and relative to the helium injection plane.

Flow conditions: Pe = 1.9, $X_{A_o} = 0.5$

Axial Position, $\zeta = z/R$	$\bar{X}_A$	$\bar{T}$, °K	$\bar{D}_{AB}$, 1 atm $m^2/sec \times 10^4$	α_T
0.3	.612	293.53	.764	
0.4	.645	293.27	.724	.232
0.5	.680	293.09	.691	
0.6	.707	292.96	.697	.232
0.7	.732	292.89	.704	
0.8	.756	292.86	.689	.224
0.9	.780	292.88	.683	
1.0	.800	292.93	.700	.218
1.1	.817	292.99	.753	
1.2	.832	293.06	.836	.209
1.3	.843	293.13	.886	
1.4	.852	293.20	.893	.192
1.5	.864	293.28	.804	
1.6	.875	293.36	.727	.180
1.7	.887	293.43	.705	
1.8	.897	293.51	.697	.173
1.9	.906	293.58	.704	
2.0	.914	293.64	.674	.166
2.1	.922	293.69	.701	
2.2	.931	293.76	.737	.158
2.3	.934	293.81	.814	
2.4	.940	293.87	.829	
2.5	.945	293.90	.750	
2.6	.950	293.95	.739	

Molecular diffusion coefficients and thermal diffusion factors

Flow conditions: Pe = 3.8, X_{A_o} = 0.5

Axial Position, ζ = z/R	$\bar{X}_A$	$\bar{T}$, °K	$\bar{D}_{AB}$, 1 atm $m^2/sec \times 10^4$	α_T
0.3	.674	292.04	.692	
0.4	.726	291.69	.691	.221
0.5	.772	291.57	.682	
0.6	.813	291.66	.676	.222
0.7	.844	291.90	.692	
0.8	.867	292.18	.717	.203
0.9	.889	292.46	.706	
1.0	.908	292.75	.678	.189
1.1	.924	293.01	.705	
1.2	.936	293.23	.773	.177
1.3	.945	293.40	.831	

Flow conditions: Pe = 3.8, X_{A_o} = 0.7

Axial Position, ζ = z/R	$\bar{X}_A$	$\bar{T}$, °K	$\bar{D}_{AB}$, 1 atm $m^2/sec \times 10^4$	α_T
0.3	.816	292.67	.730	
0.4	.846	292.58	.721	.209
0.5	.871	292.66	.722	
0.6	.890	292.84	.719	.187
0.7	.908	293.01	.702	
0.8	.925	293.20	.681	.176
0.9	.938	293.37	.692	
1.0	.947	293.54	.729	

Molecular diffusion coefficients and thermal diffusion factors

Flow conditions: Pe = 5.9, X_{A_o} = 0.7

Axial Position, ζ = z/R	$\bar{X}_A$	$\bar{T}$, °K	$\bar{D}_{AB}$, 1 atm $m^2/sec \times 10^4$	α_T
0.3	.852	292.26	.706	
0.4	.886	292.45	.679	.204
0.5	.914	292.81	.690	
0.6	.935	293.12	.677	.182